2022

Understanding Structure/Process-Property Relationships to Optimize Development Lifecycle in Yttria-Stabilized Zirconia Aerogels for Thermal Management

Rebecca C. Walker
Virginia Commonwealth University

Understanding Structure/Process-Property Relationships to Optimize Development Lifecycle in Yttria-Stabilized Zirconia Aerogels for Thermal Management

Rebecca Catherine Walker

Department of Chemical & Life Science Engineering, Virginia Commonwealth University, Richmond, VA

Approved: November 29th, 2022

A dissertation submitted in partial fulfillment of the requirements for the degree of Doctor of Philosophy in Chemical and Life Science Engineering at Virginia Commonwealth University.

Acknowledgements

The last 4.5 years have held many experiences and opportunities. Yet I know that looking back, it's the people who have helped me on this journey that I will remember the most.

First, I would like to thank my Ph.D. advisor, Dr. James Ferri. Your guidance, direction, and feedback have been instrumental during the last four years. I appreciate all of your encouragement and anecdotes. Thank you for helping me achieve this goal.

I would also like to thank the members of my dissertation committee - Dr. B. Frank Gupton, Dr. Christina Tang, Dr. Massimo Bertino, and Dr. Jamesa Stokes. Each of you have been influential in my undergraduate and graduate career in different ways and your suggestions during the last couple of years have helped bring my dissertation to completion.

To my lab mates, peers, and friends from VCU, the last four (and even the last eight) years have been memorable. I've enjoyed working with you all. A special thank you to Andres Hyer for your help with the aerogel information architecture and machine learning and to Kimberly Penzer for your help with the surfactant measurements.

To my advisors from NASA Glenn Research Center - Dr. Frances Hurwitz, Dr. Jamesa Stokes, and Dr. Haiquan (Heidi) Guo - thank you for the opportunity to work on this interesting project and to experience research at NASA Glenn. I'm grateful for your leadership and representation of this great organization. And to everyone at Glenn, thank you for making my two summers on center an exciting and engaging time. This research would not have been financially possible without the support of NASA Fellowship 80NSSC18K1697.

A special thank you to my parents, David and Stephanie, and my sister, Caroline. Your endless support and encouragement have helped me more than you know. Thank you for being my biggest cheerleaders, especially when I was in the thick of it. I love you.

All glory be to God, my Savior and the Creator and Sustainer of all things. *It is he who made the earth by his power, who established the world by his wisdom, and by his understanding stretched out the heavens.* (Jeremiah 10:12, ESV)

Table of Contents

List of Figures

List of Tables

Abstract

Aerogels are mesoporous materials with unique properties, including high specific surface area, high porosity, low thermal conductivity, and low density, increasing these materials' effectiveness in applications such as catalyst supports, sorption media, and electrodes in solid oxide fuel cells. Zirconia (ZrO_2) aerogels have special interest for high-temperature applications due to the high melting point of ZrO_2 (2715°C) and stability between 600°C and 1000°C, where other aerogel systems often begin to sinter and densify. These properties and unique pore structure make zirconia aerogels advantageous as thermal management systems, especially in aeronautics and aerospace applications. However, to be effective in high-temperature applications, the aerogel formulation must be optimized so that pore collapse and subsequent surface area decrease are mitigated following high-temperature exposure. By utilizing surfactant templates, it is anticipated that the mesoporous structure and high surface area of yttria-stabilized zirconia (YSZ) aerogels will be retained following exposure to high temperatures, increasing the thermal stability and efficiency of YSZ aerogels as thermal management systems. To experimentally consider the impact of synthetic variables on aerogels, surfactants are used as templating agents to influence the pore structure and surface area of YSZ aerogels. Additionally, due to the large number of parameters associated with aerogel synthesis and processing, a developed aerogel graph database and a machine learning predictive model are applied to examine the complex relationships between aerogel synthesis, processing, and final properties, specifically BET surface area. Subgraphs of the developed aerogel graph database are used to visually determine the impact of specific variables on the aerogel surface area, while the predictive model maps from aerogel synthetic and processing conditions to predict the final property, BET surface area, with precision. These digital design tools could reduce experimental dimensionality, time, and resources, enabling the successful synthesis of high surface area aerogels.

Chapter 1 Introduction

Aerogels are a unique class of mesoporous solid materials that exhibit a wide range of useful properties, including high surface area, low density, and low thermal conductivity. They are useful for a broad range of applications and have gained attention over the last several decades. Zirconia aerogels are used in an expansive variety of applications, including catalyst supports, sorption media, and electrodes in solid oxide fuel cells.[1,2] High porosity and high surface area aerogels have significance in a wide range of disciplines, including astrophysics, material science, high-energy physics, and chemical engineering.[3] Due to the extremely low thermal conductivity and high porosity of zirconia aerogels, these materials are often used in thermal management applications, such as high-temperature thermal insulation, especially in aeronautics and aerospace systems.[4] In comparison with silica aerogels, which display sintering and loss of mesoporous structure at high temperatures, zirconia aerogels are promising candidates for applications taking place at temperatures above 1000°C due to their high melting point of ZrO_2 at 2715°C, low thermal conductivity, and presence of both acid and base active centers. The high thermal stability of zirconia aerogels can be increased further by optimizing the aerogel formulation; for example, zirconia metal oxide aerogels stabilized by yttria, or other rare earth dopants, are especially thermally stable. This is due to the low thermal conductivity of yttria-stabilized zirconia (0.5 - 2.36 W/m·K), which is made even lower when used as an aerogel system (0.168 - 0.212 W/m·K).[5] Since the formulation of zirconia aerogels can directly influence the thermal stability of these materials, an understanding of the effects of synthesis and processing on the zirconia aerogel system is valuable.

The general aerogel synthesis process is outlined in Figure 2. First, to create the aerogel's sol, precursors are added to the solvent system, along with any dopants or templating agents that will be used. A gelation agent is then added and, following hydrolysis and condensation reactions, a gel is formed. After washing and aging steps, the gel is then dried, typically

with supercritical drying, to become an aerogel. As-dried aerogels are then heat-treated to determine the behavior of the aerogel following high-temperature exposure. The aerogels are then characterized using various techniques to determine the final properties of the aerogels, including surface area, pore volume, pore structure, crystallite size, and crystalline phase. Depending on the conditions chosen, it can take up to 2 - 3 weeks to fully synthesize, process, and characterize an aerogel. A comprehensive review of aerogel synthesis and processing is included first in this dissertation.

This dissertation sought to optimize the synthesis of aerogels to improve the thermal stability and effectiveness of these materials when used in high-temperature systems, specifically for aerospace and aeronautics applications. To achieve this, two objectives were outlined: to optimize the formulation of yttria-stabilized zirconia (YSZ) aerogels using surfactant templating and to enhance understanding of the relationships between aerogel synthetic pathways and final properties using information architecture and machine learning.

When exposed to high-temperature, aerogels begin to sinter and densify, collapsing the mesoporous structure and decreasing the surface area of the aerogels, as displayed in Figure 1. Yet, the mesoporous structure, high surface area, and high porosity of the aerogel is required to leverage the benefits of aerogel properties in thermal management systems. Therefore, the collapse of the pore structure and decrease of surface area diminishes the utility of the material as a thermal insulator. To use these materials effectively in high-temperature applications, the aerogel formulation must be further understood and optimized to mitigate the negative effects upon exposure to high temperatures.

Silica aerogels, which are well-known and well-studied, suffer from sintering and densification when exposed to temperatures above 700°C due to polycondensation reactions and structural rearrangement.[6,7] Therefore, to achieve use of aerogels at a higher temperature range, zirconia aerogels have been considered for thermal management systems.[8] Typically, zirconia aerogels have lower surface areas than silica aerogels, 200 – 900 m^2/g for zirconia aerogels versus 500 – 1200 m^2/g for silica aerogels, and higher thermal conductivities than

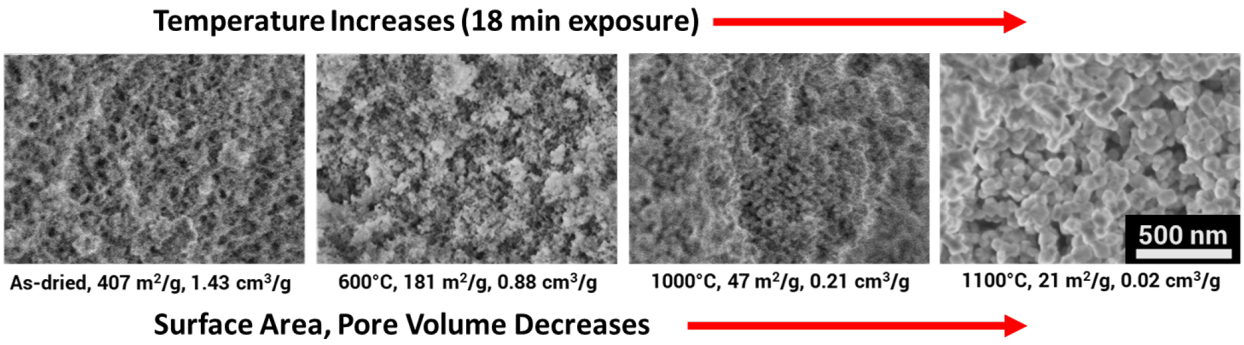

Figure 1: Sintering and densification of aerogels. Increasing temperature leads to sintering and densification of aerogels, decreasing surface area and pore volume, as displayed in the SEM micrographs. Exposure temperatures, BET specific surface areas, and BJH desorption cumulative pore volumes are displayed below each micrograph.

silica aerogels, 0.021 – 0.180 W/m·K for zirconia aerogels versus 0.012 – 0.020 W/m·K for silica aerogels.[9,10] These properties alone would make silica aerogels more favorable for use in thermal management systems than zirconia aerogels. However, because of the high melting point of zirconium dioxide, 2715°C, zirconia aerogels can remain stable at high temperatures between 600°C and 1000°C, while silica aerogels begin to sinter and densify around 700°C, collapsing the pore structure.[7,11] Adding yttrium as a dopant further stabilizes zirconia aerogels; yttrium stabilizes high temperature polymorphs of zirconia, preventing transformation to the monoclinic phase and decreasing the aerogel thermal conductivity (as low as 0.168 W/m·K).[5,12]

To influence the pore structure of aerogels, surfactants can be used as templating agents during aerogel synthesis. Surfactant templating was proposed within this dissertation as a way to optimize the mesoporous structure of YSZ aerogels. Surfactants are used in the synthesis of a variety of aerogels as these chemicals can be used as structure directing agents to influence pore structure in mesoporous materials due to electrostatic repulsion and steric hinderance effects.[10,13] Surfactants can template the aerogel structure during synthesis, enhancing surface area and pore size upon high-temperature exposure.[14–16] With a hydrophilic head and a hydrophobic tail, surfactants can also reduce interfacial energy, which causes surface tension in the aerogel system and leads to pore collapse and shrinkage during drying.[17,18]

Surfactants control nanoparticle and crystallite growth through a capping effect, which influences crystalline structure; they also prevent agglomeration, which increases aerogel surface area.

As the first objective of this dissertation, to understand the influence of surfactant on aerogels, the cationic surfactant cetrimonium bromide (CTAB), the anionic surfactant sodium dodecyl sulfate (SDS) and the nonionic surfactant Pluronic® P-123 were chosen as surfactant templating agents for 20 mol% YSZ aerogels. The chosen surfactants were added at concentrations of one-half, twice, and three-times the CMC of each surfactant. It was anticipated that the use of surfactant templates would enable the retention of mesoporous structure and high surface area in as-dried aerogels, while also mitigating crystallite growth and densification of aerogels exposed to high-temperatures.

Due to the lengthy development lifecycle of aerogels and since the formulation of aerogels can directly influence the thermal stability of these materials, knowledge of the effects of synthesis and processing on the aerogel system is valuable. Therefore, enhanced understanding of the synthesis and processing conditions of aerogels, and the influence of these conditions on the final properties of aerogels, should be achieved.

As the second objective of this dissertation, to further understand the complex relationships between aerogel synthesis, processing, and final properties, aerogel property graph databases and machine learning models were developed. As a test case, the aerogel property graph database was first applied to 600 zirconia aerogels.[1,4,5,11,13,18–51] The graph database was further expanded and applied to 1000 silica aerogels, which had a wider scope of available literature.[52–148] Visualization of the aerogel graph databases could be used to determine the impact of specific synthesis and processing conditions on the final properties of aerogels. Following the development of the silica aerogel graph database, machine learning models were used to map from aerogel synthesis and processing conditions to predict the final silica aerogel property, BET surface area, with precision. The BET surface area was chosen as it can be used to map to the thermal behavior of the aerogels and is a commonly reported aerogel

property. These digital design tools could be advantageous by decreasing the experimental dimensionality of aerogel synthesis, reducing experimental time and resources.

Further optimization of aerogel synthesis and an increased understanding of the complex relationships between aerogel synthesis, processing, and final properties would lead to increasingly efficient synthesis of aerogels with target properties, including high surface area, high pore volume, and mesoporous structure.

1.1 Aerogel-based technologies with review of aerogel properties

Aerogels are a unique class of mesoporous solid materials with high specific surface area, high porosity, and low density.[149] Aerogels are the lightest synthetic material in the world, composed of 95 - 99% air by volume. Aerogels also have low thermal conductivity and some can have high mechanical strength. Due to these extreme material properties, aerogels can be used for many different applications.[3,87,150–157] Here, the benefits of using aerogels, what properties make aerogels useful, and specific application examples are highlighted. In section 2.1, a more comprehensive review for the properties and applications of five different aerogel types, zirconia (ZrO_2), silica (SiO_2), alumina (Al_2O_3), aluminosilicate (Al_2O_3/SiO_2), and carbon aerogels, is presented.

The high porosity of aerogels lowers the thermal conductivity of these materials due to larger amounts of air, which has a low thermal conductivity, being present in the system. Because these materials are mesoporous, the small pore size inhibits the movement of air molecules, suppressing gas convection. Additionally, aerogels can be made of insulating solids such as yttria-stabilized zirconia and with such low amounts of solid present in the aerogel sample, as well as a tortuous path for heat transfer, the solid conduction of the material is decreased. Because of this extremely low thermal conductivity, and ultralightweight structure, as well as high surface area and high porosity, aerogels are excellent thermal insulating solids. Due to the thermal stability of aerogels, they are used in many different types of applications as thermal management systems. Insulating applications include architec-

tural (roofs, facades, windows, etc.), appliance (refrigerators, outdoor cooling boxes, etc.), aerospace, aeronautics, and pipeline insulation.[5,149,158–164]

Aerogels have lower thermal conductivity values than traditional insulation materials, leading to weight and space saved by using less material in construction and improved insulation performance. However, aerogel insulation remains more expensive than traditional insulation so efforts are in process to reduce the manufacturing cost so that aerogel insulation can become more widespread. As a specific example, aerogel-based slurries consisting of silica aerogels and yttria-stabilized zirconia have been utilized in thermal spray-drying to obtain a thermally resistant coating; this spray coating could be useful in aerospace applications where space is constrained for large insulating materials.[165,166] Aerogels have also been used as reinforcing material in firefighters' protective clothing and blankets, enhancing both comfort and thermal protection; the aerogel nonwoven material could provide up to eight times the thermal resistance of traditional thermal batting material.[167]

Aerogels have high sensitivity and selectivity, as well as fast response and recovery times, when used in sensing applications, such as in biosensors, gas sensors, or strain and pressure sensors.[168–170] Due to the fact that all constituting elements are nanoscale and that the pore size of aerogels is extremely small, these materials are useful as electrodes in solid oxide fuel cells, catalyst supports, thermoresistors, piezoelectrics, and templating materials.[13,171,172] Mixed oxide materials, e.g., ZrO_2/SiO_2, ZrO_2/TiO_2, that are highly porous are useful in a variety of applications, including biomaterials and heterogeneous catalysis.[1] High-surface area zirconia aerogels were used to catalyze the ketonization of hexanoic acid, leading to high conversion and high selectivity.[173]

The porosity, low density, and high surface area of aerogels give these materials very high sorption capabilities, making them beneficial for chemical absorption or adsorption applications, such as oil absorption.[174,175] Aerogels are useful for many environmental applications, such as the adsorption of heavy metal ions or organic pollutants in wastewater, the adsorption of organic molecules in air, hydrogen production, and carbon dioxide capture.[176–179]

For instance, zirconia aerogels have been explored as reactive sorbents and decomposers of chemical warfare agents.[2] Aerogels have also been used in a variety of separation processes, such as oil/water separation or pollutant removal, as well as in filtration through the removal of airborne nanoparticles.[178,180–183] As an example of aerogel filtration, zirconium-crosslinked graphene oxide/alginate aerogel beads were used in phosphate removal from polluted water with good phosphate sorption capacity and easy separation advantage.

While several main applications of aerogels have been discussed above, there are a wide range of other applications in which aerogels are useful. Due to their stiffness and mechanical strength, some aerogels are used in construction materials and as ballistic protection.[149] The excellent acoustic properties of aerogels make them useful for sound insulation.[159,160,184] Aerogels with higher porosities and lower bulk densities demonstrate the best sound absorption performance.[185] The mesoporous structure and high surface area of aerogels make them useful for drug delivery, biosensing applications, and medical implants.[186–189] Aerogel materials can have high drug loading capacities and are capable of controlled drug release, which can be influenced by the sol-gel processing of the materials. However, toxicity and biocompatibility studies of aerogels are rare, which occasionally hinder commercialization. The future of aerogels in biomedicine may be in the field of regenerative medicine, such as wound care and tissue engineering.

1.2 Importance of understanding aerogel structure/process-property relationships

There are an extensive number of synthetic variables and processing conditions for aerogels. Depictions of the general synthesis and processing pathways of aerogels are found in Figure 2; a more comprehensive review of aerogel synthesis and processing is included in section 2. Prior to formation of the gel, the aerogel's sol must be formulated using a variety of precursors, dopants, solvent systems, templating agents, and gelation agents. Following formulation of the sol, the sol-gel method is most commonly used to initiate gelation;

however, hydrothermal, sonochemical, electrolysis, solution heating, chemical precipitation, and microwave irradiation methods can also be used. Aging and washing are then typically conducted to strengthen the gel network and prepare for the drying process. After aging and washing, the gel can be dried using a variety of drying methods, such as freeze drying, ambient pressure drying, oven drying, atmospheric drying, and most frequently for aerogels, supercritical drying. Dried aerogels are often heat-treated, causing sintering and densification of the pore structure, at a variety of temperatures and times to determine behavior of the system upon high-temperature exposure. As-dried and heat-treated aerogel samples are then characterized using a variety of characterization techniques, including scanning electron microscopy, nitrogen adsorption/desorption, x-ray diffraction, and thermogravimetric analysis, some of which can be time-consuming.

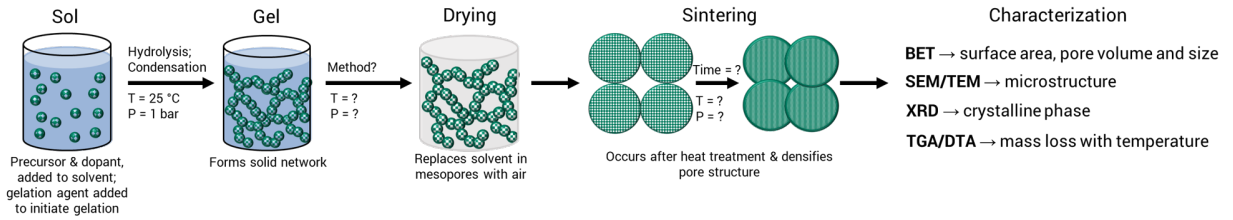

Figure 2: General synthesis, processing, and characterization methods of aerogels. Following gelation of the precursor via the sol-gel technique, a variety of drying methods and sintering parameters can be used in the processing of the final aerogel. As-dried and heat-treated aerogels are then characterized using several techniques.

The number of synthetic pathways can be determined using the relationship m^n where n is the number of synthetic variables considered and m is the number of distinct options possible for each variable. Looking at the sol formation alone, there are at least five distinct synthetic variables to be considered: precursor, rare earth dopant stabilizer, solvent system, templating agent, and gelation agent. If there were only two distinct options for each of these five variables ($m = 2$, $n = 5$), there would be 32 synthetic pathways; if there were three distinct options ($m = 3$, $n = 5$), 243 synthetic pathways would be feasible. Typically, m is much greater than two or three, as there are many more potential options for each synthetic variable; for example, m is greater than 17 for the gelation agent variable when considering

zirconia aerogel synthesis. The concentrations of each of the five synthetic variables added to the sol also need to be considered, further increasing the value of m. Following the formulation of the sol, variables included in the gelation method, aging method, washing method, drying method, and sintering method need to also be examined, increasing the value of n. The large number of synthetic variables shows an exponential increase as each processing step is evaluated.

In addition to the extensive amount of synthesis and processing variables that must be considered, the development lifecycle of aerogels from initial sol formulation to characterized product can take as long as one to three weeks, with some reported synthetic pathways requiring even longer times, up to two months.

During a comprehensive review of zirconia aerogel synthesis and processing, it was established that, on average, aging occurred in 37 hours, washing occurred in 80 hours, drying occurred in 6 hours, and sintering occurred in 1 hour. However, some reported synthetic pathways were much longer, as washing occurred for up to 9 days, drying occurred for up to 3 days, and sintering occurred for up to 24 hours; one synthesis reported aging the zirconia gels for one to two months prior to drying. Additionally, when considering characterization, the BET surface area measurement takes approximately 48 hours to complete both degassing and analysis and can typically only be done with one to a few samples at a time per instrument. Overall, it was reported that zirconia aerogel synthesis took 6 to 12 days, with some reported synthetic pathways taking much longer, even up to approximately two months.

Following a review of silica aerogel synthesis and processing, it was determined that, on average, silica sols stirred for 1 hour, sols were left for 15 hours prior to gelation, gelation occurred in 10 hours, aging occurred in 40 hours, washing occurred in 48 hours, and drying occurred in 10 hours. However, a number of silica aerogel synthetic pathways reported much longer synthesis and processing times, with aging occurring for up to 7 days, washing occurring for up to 8 days, and drying occurring for up to 8 days. In total, including

BET characterization time, from initial sol formulation to final characterized material, the silica aerogel synthetic process on average took approximately 7 days. The maximum time reviewed for silica aerogel synthesis was 20 days.

Due to the lengthy experimental time between initial formulation and final characterized product, as well as cost of materials and methods, arbitrary investigation of the synthetic pathways of aerogels should be avoided. An optimized synthetic pathway, creating aerogels with high surface area and mesoporous structure, should be determined prior to experimentation. Yet, the sheer number of synthetic and processing variables of aerogels can make the optimization of these materials difficult and can hinder potential development. To mitigate the number of synthesis and processing variables used in the creation of aerogels, tools that can optimize aerogel synthesis, such as a property graph database or machine learning models, were developed and utilized in this dissertation. Here, data science was utilized in a way that could clarify structure-property relationships in colloidal chemistry, providing a more efficient way to evaluate the synthesis and processing of materials with high experimental dimensionality.

Chapter 2 Review of aerogel synthesis and processing

An extensive review of aerogel synthetic and processing conditions was conducted as part of this dissertation. Following an introduction to five aerogel systems, zirconia (ZrO_2), silica (SiO_2), alumina (Al_2O_3), aluminosilicate (Al_2O_3/SiO_2), and carbon, an overview of synthesis and processing conditions of aerogels will be presented, with a primary focus of the synthesis and processing of zirconia aerogels and silica aerogels, as these two aerogel systems were predominately considered in this work.

2.1 Various aerogel systems: Properties and applications

While many precursor systems are used in the synthesis of aerogels, zirconia (ZrO_2), silica (SiO_2), alumina (Al_2O_3), aluminosilicate (Al_2O_3/SiO_2), and carbon aerogels are among some of the most prevalent. Here, we discuss the synthesis methods, properties, and applications, which are summarized in Table 1, specific to each of these aerogel systems. Figure 3 depicts a selection of the potential applications for each aerogel system.

Table 1: Review of various aerogel types. Several precursors, averaged aerogel properties, and potential applications for five different aerogel types: zirconia, silica, alumina, aluminosilicate, and carbon.

Aerogel	**Precursors**	**Surface Area (m^2/g)**	**Density (g/cm^3)**	**Thermal Conductivity (W/m·K)**
Zirconia (ZrO_2)	zirconyl chloride octahydrate, zirconium(IV) propoxide, zirconium(IV) chloride	200 - 900	0.050 - 0.450	0.021 - 0.180
Silica (SiO_2)	tetraethyl orthosilicate, tetramethyl orthosilicate, methyltriethoxysilane, sodium metasilicate	600 - 1000	0.030 - 0.350	0.012 - 0.020
Alumina (Al_2O_3)	aluminum isopropoxide, aluminum sec-butoxide, aluminun chloride hexahydrate	350 - 700	0.035 - 0.400	0.028
Aluminosilciate (Al_2O_3/SiO_2)	tetraethyl orthosilicate, sodium metasilicate, aluminum chloride hexahydrate	150 - 905	0.050 - 0.630	0.023 - 0.081
Carbon	graphene, carbon nanotubes, resorcinol, biomass	500 - 900	0.003	0.018 - 0.350

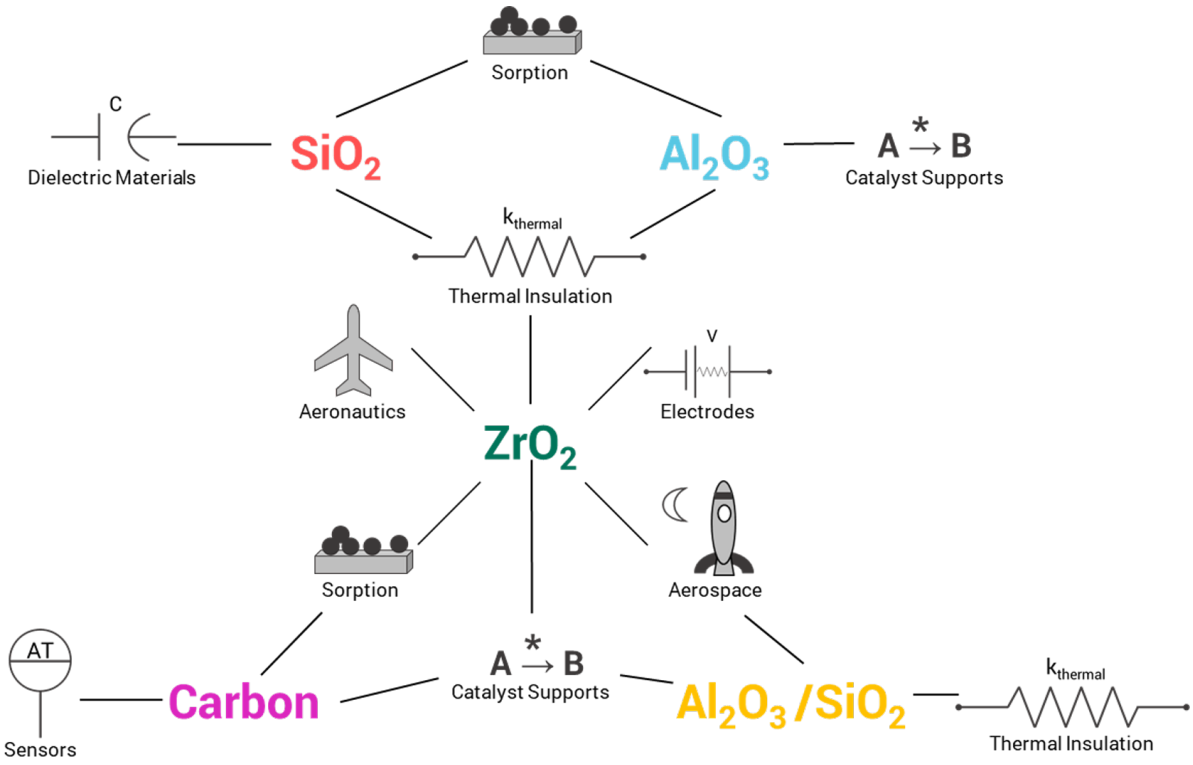

Figure 3: Aerogel applications. Applications for various aerogel types, including zirconia (ZrO_2), silica (SiO_2), alumina (Al_2O_3), aluminosilicate (Al_2O_3/SiO_2), and carbon aerogels. Applications for zirconia aerogels include thermal insulation, aeronautics, aerospace, sorption media, catalysis, and electrode material. Silica, alumina, aluminosilicate, and carbon aerogels can be used in applications such as catalysis, concentration sensors, and dielectric materials.

2.1.1 Zirconia (ZrO_2) aerogels

Zirconia (ZrO_2) aerogels were first synthesized in 1976 by Teichner et al. using the sol-gel method, with a zirconium alkoxide precursor in organic solvent, and supercritical drying.[190] These materials have recently become further investigated for high-temperature applications due to their low thermal conductivity and increased thermal stability.[1] Zirconia aerogels have thermal conductivities as low as 0.021 W/m·K and up to 0.180 W/m·K. As-dried zirconia aerogels have specific surface area values ranging between 200 and 900 m^2/g. They also have high porosities of up to 97% and densities between 0.05 - 0.45 g/cm^3.

Zirconia aerogels are synthesized using a variety of precursors, including zirconyl chloride

octahydrate, zirconium(IV) propoxide, zirconium(IV) chloride, and zirconium(IV) oxynitrate hydrate.[37,49,191–193] The choice of precursor can have an effect on the final properties of the aerogel, including surface area, pore volume, and density. Drying techniques, including supercritical drying and ambient pressure drying, are used to create zirconia aerogels.[32,35]

The microstructure and resulting properties of zirconia aerogels are beneficial when used in a variety of applications. Selected zirconia aerogel applications are displayed in Figure 3. The high melting point of ZrO_2, 2715°C, allows zirconia aerogels to be used at high temperatures where other aerogel systems, such as silica, begin to sinter.[1] This makes zirconia aerogels useful in a wide range of thermal management systems, including high-temperature thermal insulation. In addition, zirconia aerogels can be used in a variety of aerospace and aeronautics applications. Specifically, zirconia aerogels have been formulated for use as thermal barrier coatings in gas turbines and aero-engines, as well as hypervelocity particle capture systems for space applications.[5,162,165] Zirconia aerogels are also used as heterogeneous catalyst supports, sorption media, and electrodes in solid oxide fuel cells.[1,2,4,23]

2.1.2 Silica (SiO_2) aerogels

Silica (SiO_2) aerogels are widely studied and used due to their vast range of exceptional properties. Silica aerogels have low thermal conductivity (0.012 - 0.020 W/m·K), high specific surface area (600 - 1000 m^2/g), low density (0.03 - 0.35 g/cm^3) and excellent porosity (approx. 99%) with a mean pore diameter of 20 nm.[9,152,194,195] Silica aerogels also have low dielectric constant (1.0 - 2.0), refractive index (1.00 - 1.08), and sound velocity (100 m/s). However, silica aerogels are known to sinter and densify when exposed to temperatures between 600°C and 700°C, which makes them not as suitable for high-temperature applications, due to thin structural links and a melting temperature of 1713°C for silicon dioxide.[7,196] Silica aerogels are also fragile and can be sensitive to relatively low stresses.

Silica aerogels are synthesized using precursors such as tetraethyl orthosilicate (TEOS), tetramethyl orthosilicate (TMOS), methyltriethoxysilane (MTES), or sodium metasilicate

(water glass), which tend to be less expensive than precursors typically used for other aerogel systems.[152,194,195] Whether a silica precursor is hydrophilic or hydrophobic has an effect on the optical transmission, density, hardness, and elasticity of silica aerogels. Additives, for example polyethylene glycol (PEG) to influence pore size or glycerol to prevent further reaction of water, can also be added to the silica sols prior to gelation to tailor the process for specific properties or to stabilize gels, especially during drying. As additional examples, He et al.'s work utilized a drying control chemical agent, N,N-Dimethylacetamide (DMA), to minimize shrinkage during drying and Zhu et al. used graphene to aid in the thermal stability and conductivity of graphene-doped silica aerogel products.[90,123] Transition metal complexes, containing metals such as nickel, copper, or cobalt, and compounds such as graphene can be used as dopants in silica aerogels.[90,197] Acid catalysts, including hydrochloric acid or sulfuric acid, or base catalysts, namely ammonia, are typically added to the silica sol to increase hydrolysis and condensation rates and induce gelation, completing the sol-gel transition.[57,66,67,143] Silica aerogels are dried using supercritical drying, ambient pressure drying, and freeze drying.

Silica aerogels have a wide range of potential applications because of their unique properties. A few select silica aerogel applications are depicted in Figure 3. Due to their low thermal conductivity, silica aerogels can be used as insulators in building construction, blankets, solar devices, and thermal insulation on space craft and in space suits.[194,198] Superhydrophobic silica aerogels can be effective, reusable absorbents of oils and organic liquids, with high uptake capacity and rate.[199] Silica aerogels can also be used as photoanodes for dye sensitized solar cells because of their high surface area and mesoporosity.[200] Due to the low dielectric constant of silica aerogels, these materials can be used for intermetal dielectric materials in microelectronic devices.[201]

2.1.3 Alumina (Al_2O_3) aerogels

Similar to silica aerogels, alumina (Al_2O_3) aerogels have low density (0.035 - 0.400 g/cm^3), high porosity (> 98%), high surface area (350 - 700 m^2/g), and low thermal conductivity (0.028 W/m·K).[9,202,203] Alumina aerogels are typically more thermally and chemically stable than silica aerogels due to a network microstructure that is crystalline and fibrous, as well as aluminum oxide's higher melting point of 2072°C.[204] Alumina aerogels are very fragile and can have poor mechanical properties, limiting their application; however, the optimization of synthesis method often strengthens alumina aerogels.[205]

Alumina aerogels can be synthesized using aluminum alkoxides (aluminum isopropoxide or aluminum sec-butoxide), aluminum salts (aluminum chloride hexahydrate or aluminum nitrate nonahydrate), or aluminum oxyhydroxides (boehmite).[9,202,206] Alumina aerogels synthesized using aluminum alkoxides have high thermal stability and are mechanically strong due to a polycrystalline aerogel microstructure.[207] However, using aluminum salts in conjunction with an epoxide proton scavenger synthesizes high surface area and low density alumina aerogels, without the use of highly reactive alkoxide precursors. A variety of dopants can be added to stabilize alumina aerogels, including yttrium oxide, titanium dioxide, and silicon dioxide.[208–210] Acid catalysts, such as acetic acid, or epoxides, such as propylene oxide, can be used as gelation initiators in alumina aerogels. Alumina aerogels are dried using typical aerogel drying methods, including supercritical drying, freeze drying, and ambient pressure drying.

There are many diverse applications for alumina aerogels, a few of which are represented in Figure 3. Due to their thermal stability, alumina aerogels are useful in thermal management applications, such as high-temperature thermal superinsulators and heat-storage systems. Alumina aerogels tend to be better insulating materials than silica aerogels because of increased thermal stability.[203,207] Alumina aerogels can be used as high-temperature catalyst supports and adsorption material for separations due to their high surface area.[202,205,206]

2.1.4 Aluminosilicate (Al_2O_3/SiO_2) aerogels

Aluminosilicate (Al_2O_3/SiO_2) aerogels, made from both silicon and aluminum precursors, have become increasingly popular. The addition of silica to alumina aerogels can inhibit the crystalline phase transition of alumina aerogels at 1000°C, which can deform the porous structure.[211] Aluminosilicate aerogels show increased resistance to high temperatures than pure silica aerogels and better thermal stability than pure alumina aerogels.[212] Aluminosilicate compounds can have melting points greater than 1810°C, which is higher than the melting point of silicon dioxide alone (1713°C).[213] Aluminosilicate aerogels have low density (0.05 - 0.63 g/cm^3), low thermal conductivity (0.023 - 0.081 W/m·K), small pore size (0.5 - 50 nm), and high surface area (150 - 905 m^2/g).[9] However, aluminosilicate aerogels are very fragile and can lack mechanical strength without the proper formulation.

Aluminosilicate aerogels are synthesized with a combination of silica and alumina sols that are used in the synthesis of pure silica and pure alumina aerogels. For silicon precursors, tetraethyl orthosilicate or sodium metasilicate are frequently used. For aluminum precursors, aluminum chloride hexahydrate or boehmite powders are often used.[7,9,212] To initiate gelation, epoxides, for example propylene oxide, acid catalysts, or base catalysts are added to the sol. Aluminosilicate aerogels are dried using methods typical to most aerogel synthesis - supercritical drying, freeze drying, or ambient pressure drying.

There are many potential applications that aluminosilicate aerogels can be used in. Select applications of aluminosilicate aerogels are shown in Figure 3. Due to their high-temperature resistance, aluminosilicate aerogels can be used in thermal protection systems, such as building insulation and aerospace applications, including use as particle collectors, cryogenic fluid containers, and re-entry vehicles.[7,9] Aluminosilicate aerogels are also used in catalytic applications because of their large surface area, high pore volume, and high acid site concentration.[214] Aluminosilicate aerogels can also be used in environmental applications, such as water vapor or nickel adsorbents, due to high surface area.[215]

2.1.5 Carbon aerogels

Carbon aerogels, with excellent chemical and mechanical properties, are a current topic of research interest. Carbon aerogels have low density (0.003 g/cm^3), low thermal conductivity (0.018 - 0.350 W/m·K), high specific surface area (500 - 900 m^2/g), and high pore volume (0.4 - 2.6 cm^3/g) with porosities of up to 98%.[216–218] Carbon aerogels can be very brittle, depending on formulation, which can limit use in certain applications, such as stretchable electronics and smart manufacturing.[219] However, carbon aerogels have excellent thermal stability and can maintain a mesoporous structure up to 2800°C. This high thermal stability is in part due to the high melting temperature of carbon, as some forms of carbon, such as graphite, can have a melting temperature greater than 4000°C.[196]

Carbon aerogels are synthesized using precursors such as graphene, carbon nanotubes (CNTs), biomass, resorcinol, and formaldehyde.[217] Each precursor has unique benefits, as discussed below. Graphene aerogels can be synthesized using a variety of methods, including sol-gel, templating, self-support, and substrate-based methods.[216] Aerogels derived from carbon nanotubes are electrically conductive; however, CNT aerogels that are formed directly can have poorly formed structures and can be mechanically unstable. Biomass is a promising precursor for carbon aerogels as it is inexpensive and abundant. To initiate polymerization and gelation of carbon aerogels, a variety of catalysts are used, including alkali catalysts and acid catalysts. A range of dopants can be used in carbon aerogels, such as copper, sulfur, nitrogen, and silver nanoparticles.[220–222] Highly porous carbon aerogels are typically dried using freeze-drying; however, supercritical drying and ambient pressure drying can also be used. Carbon aerogels can be used in a variety of applications because of their advantageous properties. Carbon aerogels are used as dampening components, electromagnetic metamaterials, and sensors.[219] Due to the large pore volume and high surface area of carbon aerogels, these materials can be used in supercapacitors, with ultrafast energy conversion and charging.[223] Carbon aerogels can also be used in catalytic applications, such as electrode material for lithium-ion batteries and solar photocatalysts.[224] These aerogels have high rate capability

and recyclable photocatalytic activity. Multiwall carbon nanotube-graphene hybrid aerogels, with superhydrophobicity, superoleophilicity, large pore volume, and high compressibility, can be used in oil sorption with large sorption capacity and excellent recyclability.[225] Due to low thermal conductivity, carbon aerogels can also be used in high-temperature thermal insulation applications.[217] A selection of applications used with carbon aerogels are displayed in Figure 3.

2.2 Aerogel synthesis

Prior to drying and processing to synthesize aerogels, wet gels must first be prepared. Here, several different routes for colloidal dispersion and gel formation, along with a variety of precursors, dopants, gelation agents, modifying agents, and surfactant templates that are added to the system prior to gelation are reviewed. The technique chosen influences the properties of as-dried and heat-treated aerogels, including pore structure, surface area, crystalline phase, and sintering or grain growth upon high-temperature exposure. Tuning the final aerogel properties can affect the way that they are used for various applications, including use as thermal management, catalytic, and sorption systems. Many of the reviewed synthetic and processing techniques are used for a variety of aerogel systems; however, examples referring specifically to zirconia aerogels and silica aerogels are highlighted as these aerogel systems were specifically considered as part of this dissertation.

2.2.1 Dispersion & Gel Formation

A dispersion of colloidal particles can be used to form a variety of products, including nanocrystals, powders, gels, and aerogels.[226–231] Here, methods are discussed for dispersing particles, forming sols and gels, which can then be transformed to aerogels following further processing. Figure 4 depicts seven different methods used for gels: sol-gel, hydrothermal treatment, sonochemical, electrolysis, solution heating, chemical precipitation, and microwave irradiation.

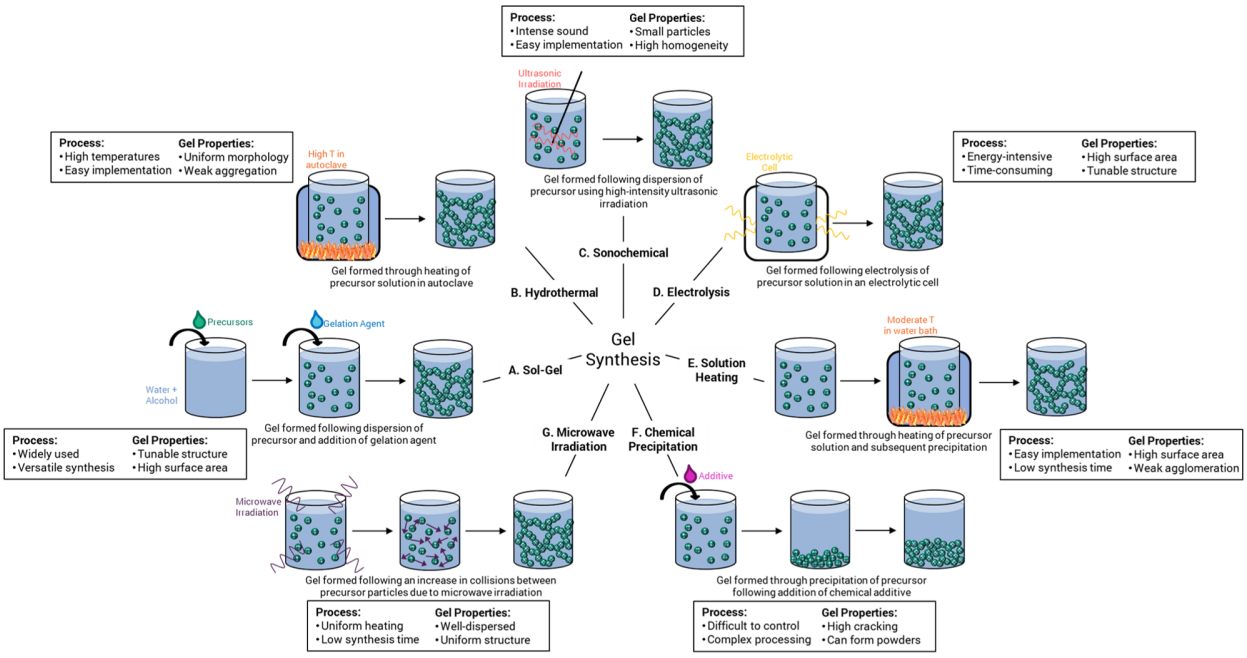

Figure 4: Gel synthesis methods. Gels can be synthesized using a variety of methods, including A) sol-gel, B) hydrothermal, C) sonochemical, D) electrolysis, E) solution heating, F) chemical precipitation, and G) microwave irradiation methods. Each method can be used for a variety of aerogel systems and has different process parameters and resulting gel properties associated with it.

The conventional method to form aerogels is through sol-gel synthesis, which uses inorganic polymerization to form gels through hydrolysis and condensation reactions.[8,10,32,192,232–235] A depiction of the sol-gel method is shown in Figure 4A. The sol-gel method can effectively synthesize aerogels with high surface areas, tunable pore size distributions, controllable properties, and stable crystalline phase. Advantages of using the sol-gel method to synthesize solid materials are low processing temperatures, increased tunability of microstructure and morphology, inexpensive design, convenient processing (completed under room conditions with general lab equipment), process safety, and versatility of synthesized materials. To form aerogels using the sol-gel method, precursors or colloidal particles are first dispersed in an aqueous and alcoholic, most commonly ethanol, mixture to create a sol of particles with nanoscale dimensions. Once a gelation agent is added, the sol can form a gel, which, with continued processing such as drying and densification, can form an aerogel or other type of solid material, e.g., ceramic powder. The precursors, alcoholic or aqueous solvents, dopants, dispersants, gelation agents, or overall chemical procedure can have an influence on the gelation time, mechanical strength, morphology, pore structure and size, surface area, and thermal stability of the aerogels synthesized through the sol-gel method.[236,237] As an example, Bedilo et al. synthesized zirconia aerogels by a sol-gel method and subsequent high-temperature supercritical drying.[233] The zirconia aerogels had high surface areas of greater than 500 m^2/g, which remained above 100 m^2/g after 2 hours of calcination at 500°C. In a similar case, Sun et al. determined that ultrafine zirconia aerogels, with high thermal stability, surface area, and pore volume, could be prepared through a sol-gel supercritical fluid drying method.[234] Additionally, Chervin et al. synthesized yttria-stabilized zirconia (YSZ) aerogels through a non-alkoxide sol-gel method using Zr^{4+} and Y^{3+} chlorides as precursors and propylene oxide as the gelation agent.[8] The wet gels were dried using supercritical CO_2, transforming into aerogels, which were then crystallized into stable ZrO_2 upon 500°C exposure. The resulting aerogels had high surface areas, particle diameters below 10 nm, and cubic-tetragonal crystalline structure.

Through the sol-gel hydrolysis of a mixture of aqueous solutions and alcoholic zirconium alkoxide solutions, zirconium oxides can be prepared.[232,236] To slow down condensation by decreasing reactivity and prevent aggregation of zirconia nanoparticles, a complexing agent, such as acetylacetone, can be added to the sol; this increases the stability of the colloidal oxide particles. The sol-gel method produces stable zirconia solid solutions, as well as zirconia solid solutions with high dopant content, that have high thermal resistance, which is difficult to achieve using other synthesis methods, such as coprecipitation. As another example of the sol-gel method, using zirconyl chloride octahydrate and yttrium nitrate hexahydrate precursors dissolved in a water-ethanol mixture, with polyethylene glycol (PEG) used as a dispersant, yttria-stabilized zirconia (YSZ) gel powders were formed by Kuo et al. following pH adjustment.[237] The presence of residual ions caused agglomeration of YSZ nanopowders with high thermal stability, high ionic conductivity, and exceptional mechanical properties. While examples relating specifically to zirconia systems were presented, these sol-gel methods can be applied to many different candidate systems.

In the hydrothermal treatment method, shown in Figure 4B, an aqueous solution of precursor is heated to form a colloidal dispersion or sol.[238,239] Prior to heating, the pH of the solution is usually adjusted. Following heat-treatment in an autoclave, generally around 150°C to 280°C for anywhere from 2 hours to 3 days, the solution is cooled, centrifuged, washed, and dried to form the solid product. This hydrothermal treatment method forms colloidal suspensions, which consist of small colloids that do not aggregate. This method is generally low-energy, safe, controlled, and high yielding.[240] Using microwave hydrothermal methods, which utilize microwave irradiation in addition to hydrothermal treatment, can also be beneficial in synthesizing highly crystallized products. As an example of hydrothermal treatment, Chang et al. used a sol-gel-hydrothermal method to synthesize zirconia single crystal nanoparticles containing pores.[241] The pores were directly resulting from the gel's structure and hydrothermal treatment. Similarly, Wang et al. utilized a modified hydrothermal-assisted sol-gel method to synthesize Y_2O_3-stabilized tetragonal ZrO_2 poly-

crystal composites.[242] The precursor solution was heated at 180°C for 2 hours, followed by freeze drying and calcination. The powders had high crystallinity, as well as uniform size and near-spherical morphology. Additionally, Lee et al. formed zirconia sols from solutions of zirconium acetate, zirconium nitrate, and zirconium chloride using hydrothermal methods at 150, 200, and 300°C, respectively.[243] The sols produced via hydrothermal methods could be further processed to achieve a number of final products, including thin films, nanopowders, gels, and aerogels. As an example relating specifically to aerogels, Cao et al. used an alcohothermal method, similar to hydrothermal methods but with alcoholic solvents, to synthesize thermally stable zirconia aerogels with high surface area.[244] To create the zirconia gels prior to supercritical drying, an alcoholic solution of $Zr(NO_3)_4 \cdot 5\,H_2O$ was placed in an autoclave at 110°C for 1 hour, which is a slightly lower temperature and time than typically used for hydrothermal treatment.

Sonochemical methods can be used to transform precursor solutions into colloidal sols, and therefore, aerogels or nanopowders.[227,231,245–247] Sonochemical methods, as depicted in Figure 4C, utilize sound at high-frequency through an ultrasonic probe and high-intensity ultrasound irradiation (approx. power 500 - 600 W, approx. frequency 20 - 35 kHz) to aid in the homogeneous dispersion of colloidal particles. Ultrasonic irradiation creates waves of pressure that form cavities that are capable of violent collapse; the induced stress of this collapse creates smaller particles, typically in the 1 - 300 nm size-range, and breaks up powder agglomerates. Because of the formation of smaller particles, the use of ultrasound irradiation can form particles with higher surface areas, which decrease negligibly after calcination at 500°C, than those produced with other methods.[246–248] Ultrasonic parameters such as applied ultrasonic power, frequency, and processing time, have effects on the structure of the resulting particles as well as the final aerogel properties. As an example of using this technique, Jodłowski et al. used a sonochemical sol-gel method to produce zirconium dioxide dip-coatings.[249] The formed gel nanoparticles had high homogeneity and small molecular size, both of which were controlled by the ultrasound irradiation. Gubanova et al. synthesized

amorphous zirconia gels from zirconium(IV) propoxide using the sonochemical approach.[250] The zirconia gels synthesized using sonication exhibited a more structured surface and higher specific surface area as compared to gels made without ultrasonic irradiation. As another example, Jiayi Zhu et al. created graphene and silica hybrid aerogels where the initial silica sols underwent ultrasonic irradiation treatment after the addition of graphene in order to ensure thorough dispersion of the graphene particles in the sols.[90]

Aerogels can also be synthesized using an electrolysis method (see Figure 4D). For example, Zhao et al. synthesized high-surface area (640 m^2/g) zirconia aerogels by electrolyzing zirconium oxychloride solution.[251] The electrolysis method converts a metal chloride solution to a wet gel, which can then be transformed to an aerogel via supercritical drying or freeze drying. The resulting zirconia aerogels were mesoporous with a mixture of monoclinic and tetragonal ZrO_2 crystalline structure. The electrolysis route has also been used to produce fibers, suggesting that the resulting morphology and properties are highly dependent on the sol precursors used. The electrolysis method is capable of scale-up and is a green process, making it advantageous to the production of aerogels. However, the electrolysis method has high energy consumption in comparison to other synthesis methods.[32]

As an example of the solution heating method, Wu et al. synthesized aerogels by heating a zirconyl dihydrate solution with an alcohol-aqueous mixture, followed by supercritical drying.[252] The solution heating method, which can be easily implemented in the lab, formed zirconia aerogels with weak agglomeration and high specific surface area of 676 m^2/g. This synthesis method leverages the significant decrease of the dielectric constant and solvent energy upon heating in a water bath at 80°C for approximately one hour, which results in precipitation leading to gels. Solution heating typically occurs at lower temperatures for shorter times compared to the hydrothermal treatment method, which uses temperatures ranging from 150°C to 280°C for anywhere from 2 hours to 3 days. As an additional distinction between the two methods, solution heating takes place in a water bath, while the hydrothermal treatment method is conducted in an autoclave. The solution heating method

is displayed in Figure 4E.

The chemical precipitation method can be used to synthesize aerogels, powders, or nanoparticles from a solution of colloidal particles.[236,253,254] One of the most widely used methods of zirconia powder synthesis is the precipitation of zirconia-based ceramics via sol-gel technique.[255] This method permits the synthesis of high purity and quality powders by providing regulation of chemical homogeneity and particle size. Precipitation occurs when a basic additive, such as an ammonium zirconium carbonate solution, sodium hydroxide, or aqueous ammonia, is added to the zirconium solution and solid particles precipitate out of solution. The solid precipitate is then further processed, which can include filtering, rinsing, or drying, to create nanoparticles or powder; upon exposure to high temperature, the solid can be crystallized. Figure 4F depicts the chemical precipitation method. Parameters such as precursors, solvents, pH, temperature, and additives, e.g., surfactants, can affect the chemical precipitation reaction, thus influencing the final properties, including structure, surface, and texture of the solid material. However, when precipitation is used to synthesize aerogels, the method can be uncontrollable and complicated; aerogels synthesized using precipitation are typically powders or greatly cracked, which limits and shortens use.[32]

Colloidal sols can be formed using microwave irradiation, displayed in Figure 4G.[256,257] This technique uses microwave irradiation to increase the speed and number of collisions between nanoparticles. An apparatus capable of producing microwave irradiation allows for uniform heating of the sol and reduced synthesis time. This technique allows the colloidal solution to be well-dispersed, well-crystallized, and uniform. Aerogels can be formed by combining sol-gel methods with microwave irradiation, which would be utilized during the hydrolysis and condensation reactions taking place throughout the sol-gel transition. To illustrate the benefits of microwave irradiation, Fetter et al. found that, in zirconia aerogels, a tetragonal crystalline phase was formed at nearly any pH level using microwave irradiation, while conventional sol-gel methods only formed the tetragonal phase at pH 3 - 4 or pH 13 - 14.[258]

2.2.2 Precursors

Precursors, the starting material of the aerogel system, are necessary for aerogel synthesis, regardless of dispersion or gel formation methods. Here, precursors that are often used for zirconia aerogels and silica aerogels, the aerogel systems predominately studied in this dissertation, are reviewed.

In the synthesis of zirconia aerogels, many different types of zirconium precursors - such as oxychlorides, chlorides, nitrates, hydroxides, oxyhydroxides and alkoxides - can be used.[32] Zirconium oxyhydroxides and hydroxides can be used as precursors in zirconia aerogel synthesis. For example, Gossard et al. used $Zr_4(OH)_{16}$ hydroxides as the zirconium precursor.[193] These hydroxides are not stable in solution and, thus, undergo dehydration via oxolation to form the oxyhydroxide $ZrO(OH)_2$. Conversely, Baklanova et al. synthesized $ZrO(OH)_2$ from an ion exchange reaction in aqueous acetic acid solution from Li_2ZrO_3.[259] This $ZrO(OH)_2$ oxyhydroxide spontaneously precipitated out of solution; however, following the addition of the chelating agent, acetylacetone, the oxyhydroxide could be stabilized. A zirconia gel was formed once the pH of the system was increased and the system was destabilized.

Alkoxide precursors are commonly used in zirconia aerogels. As an example, Livage et al. synthesized stable tetragonal zirconia sols using zirconium alkoxides.[232] Due to the electrophilicity of Zr^{4+}, zirconium alkoxides tend to react violently towards hydrolysis and condensation reactions upon the addition of water, inhibiting the development of a well-established gel structure and causing precipitation.[37] Complexing agents are typically added to stabilize the zirconium alkoxide solutions in order to control the formation of the resulting metal oxide. Using zirconium(IV) propoxide and yttrium(III) isopropoxide as the alkoxide precursors, Peshev et al. synthesized yttria-stabilized zirconia amorphous gel coatings using the sol-gel method.[191] Similarly, Rezaee et al. synthesized zirconia ceramic powders using the sol-gel method and zirconium alkoxide solution.[260] The synthesized nanopowders had reduced thermal conductivity and high porosity. As another example, Zu et al. synthesized zirconia/silica composite aerogels via supercritical deposition using zirconium(IV) butoxide

as the zirconium precursor; the aerogels retained high specific surface area of 172 m^2/g and large pore volume 0.97 cm^3/g after exposure to 1000°C.[45]

Inorganic salts, such as nitrates or chlorides, can also be used as precursors for zirconia aerogel synthesis. Using a non-alkoxide synthesis route, such as inorganic salts as zirconium precursor with epoxides as proton scavenger, is advantageous as alkoxides can be difficult to handle and sensitive during the sol-gel process.[43] Zirconyl chloride octahydrate ($ZrOCl_2 \cdot 8\,H_2O$) is a frequently used zirconium precursor in zirconia aerogel synthesis, resulting in aerogels with high surface area, low density, and large pore volume.[37,49] As an example of a different chloride precursor, using zirconium(IV) chloride ($ZrCl_4$), Gash et al. synthesized zirconium dioxide (ZrO_2) metal oxide aerogels with the epoxide addition method.[192] Demonstrating nitrates used in synthesis, Gossard et al. used an inorganic zirconium salt, zirconium(IV) oxynitrate hydrate ($ZrO(NO_3)_2$), to form a colloidal nitrate zirconyl solution and subsequent gels.[193] The nitrate counter ions of nitrate zirconium salts are neutral for cluster complexation, especially compared to other counter ions, such as chloride ions.

Regarding silica aerogel synthesis, the four most commonly used precursors are tetraethyl orthosilicate (TEOS), tetramethyl orthosilicate (TMOS), sodium silicate (water glass), and methyltrimethoxysilane (MTMS).[87] Less common silica aerogels can also be used, such as silicic acid derived from organic waste; in Garram Ban et al.'s work, rice husk ash was used as the silica precursor.[86]

The silicon alkoxide tetraethyl orthosilicate (TEOS) is frequently used, as it is less expensive and less toxic than the precursor used before it, tetramethyl orthosilicate (TMOS).[107,194] Silica aerogels from TEOS precursors were created by Tiemin Li et al. by varying the aging and washing times of the wet gels. The aged and washed silica aerogels had densities ranging from 0.086 g/cm^3 to 0.108 g/cm^3 and good optical transmittance with low refractive indices. Gels produced in this study that were not washed or aged had a bulk density of 0.172 g/cm^3 and the highest refractive index.[107]

Researchers looking for an alternative to TEOS have studied another hydrophilic pre-

cursor, sodium silicate (water glass), as it can be less expensive, more abundant, and more environmentally friendly than TEOS.[54,58] The main difference between using water glass and using TEOS is that water glass must undergo strong cation exchange in order to replace the sodium ions with hydrogen ions and create silicic acid for use in the silica gel sols. An example of this process is seen in the work by Yujin Wang et al. where water glass was first ion exchanged using strong acid styrene cation exchange resin before gelation and drying to form silica aerogels with surface areas as high as 772 m^2/g.[58]

Silica aerogels synthesized from hydrophilic precursors, such as TEOS or water glass, must be supercritically dried or modified prior to ambient pressure drying. The hydroxyl groups in these wet gels undergo condensation reactions, leading to moisture absorption. This moisture absorption can result in sharp shrinkages, increased thermal conductivities, low compressive strengths, and poor flexibilities of the aerogels.

A benefit of using a hydrophobic precursor, such as methyltrimethoxysilane (MTMS), is that it leads to hydrophobic silica aerogels without surface modification since the methyl groups on MTMS replace the hydroxyl groups on the surface of the wet silica gels.[72,194,261,262] These methyl groups reduce moisture absorption and subsequent shrinkage during drying. For example, Song He et al. created silica aerogels with MTMS as a precursor using ambient pressure drying without the surface modification necessary for ambient pressure dried TEOS or water glass gels. The samples created in this manner yielded surface areas in the range of 325 m^2/g to 543 m^2/g and densities of 0.116 g/cm^3 to 0.413 g/cm^3.[121] Properties of MTMS based silica aerogels can be improved with the addition of other precursors such as in the work of Hongyi Gao et al. which synthesized silica aerogels with surface areas ranging from 424 m^2/g to 937 m^2/g from combinations of MTMS and and additional silica precursors and ambient pressure drying without surface modification.[72] The disadvantage of MTMS aerogels is that the surface areas are not as high as seen with hydrophilic precursors. MTMS aerogels, as with most hydrophobic aerogels, are also fully opaque and tend to have densities greater than 0.1 g/cm^3.[262] Due to increased elasticities, hydrophobic precursors and their

resultant gels are soft and flexible in comparison to the hard and brittle aerogels created with hydrophilic precursors.[194,261]

Surfactants are particularly useful in aerogel synthesis when a hydrophobic precursor is chosen. Hydrophobic precursors do not dissolve in water making surfactants such as the cationic surfactant cetrimonium bromide (CTAB) key additions to the initial sols.[263] Typically, an alcoholic solvent is used to dissolve the silica precursor, however in cases with hydrophobic precursors this is often not ideal due to the difference in polarities between alcohols and the hydrophobic silica precursor.

It should also be noted that sometimes hybrid aerogels, such as zirconia/silica hybrid aerogels, are synthesized. In this case, the ZrO_2 sol containing Zr precursors and the SiO_2 sol containing Si precursors are usually mixed together to prepare a homogeneous sol prior to gelation. The addition of SiO_2 into the ZrO_2 aerogel is shown to improve the structural stability of the aerogels following thermal exposure.[4,21,45] SiO_2 is shown to form a shell-like layer around zirconia particles, inhibiting crystalline growth at high temperatures. For silica aerogels, precursors such as silver nitrate ($AgNO_3$), aluminum nitrate ($Al(NO_3)_3$), or titanium tetrachloride ($TiCl_4$) can be combined with a silica precursor to make a silver-silica, aluminosilicate, or titanium-silica aerogel respectively.[77,93] These combinations of precursors can lead to a wider range of applications as well as beneficial properties such as mechanically stronger aerogels, higher surface areas, or lower thermal conductivities according to the hybrid precursor used. Many hybrid silica aerogels have much greater thermal stability at higher temperatures than silica aerogels. However, these benefits often come at the expense of another property as shown in the work of Shalygin et al.. Aluminum isopropoxide was used as a precursor along with TEOS to form aluminosilicate aerogels with high thermal stability but with low surface areas only ranging from 143 m^2/g to 517 m^2/g.[116]

2.2.3 Dopants

Aerogels are often stabilized by a variety of dopants. Each dopant has various effects on the aerogel properties; these different effects are caused by various intrinsic characteristics of the dopants, such as the ionic radius or electronic properties of the dopant.[8] As an example relating to dopant stabilization of zirconia aerogels, zirconia is a polymorphic oxide, capable of several different crystalline phases. At room temperature, zirconia is monoclinic; zirconia transforms to tetragonal phase at approximately 1172°C and cubic phase at approximately 2370°C. To stabilize the tetragonal and cubic phases of zirconia, Zr^{4+} can be substituted using rare earth or alkali earth cation dopants. To balance charge compensation, oxygen vacancies are formed, which are critical for thermally activated conduction processes. The following is a review of some rare earth dopants that have been used in stabilizing zirconia aerogels, including yttrium, ytterbium, cerium, and gadolinium. Following this review, a few select non-rare earth dopants are briefly discussed. While sometimes observed, the use of dopants to stabilize silica aerogels is not as common.

Rare earth oxyhydroxides and rare earth hydroxides, can be used as rare earth precursors for rare earth doped zirconia aerogels.[264] Rare earth oxyhydroxides (REOOH) are known to form tetragonal crystalline structure at high temperature and pressure, while a monoclinic structure is formed at ambient pressure. As an example of use, Yang et al. utilized REOOH (RE = Eu to Lu) as synthetic and thermodynamic intermediates in rare earth oxide - water systems.[265] Using thermal conversion of REOOH, rare earth oxides (RE_2O_3) can be achieved as dehydration products. Thermodynamically, oxyhydroxides are more energetically stable than oxides plus water in the rare earth series; these oxyhydroxides act as intermediates between hydroxides and oxides.

The rare earth metal, yttrium (Y), is commonly used to stabilize zirconia aerogels.[8] Yttria-stabilized zirconia (YSZ) has been used as a thermal barrier coating with high thermal stability and low thermal conductivity.[266] YSZ has an extremely low thermal conductivity; a YSZ aerogel would have an even lower thermal conductivity due to the nature of aerogel

properties, including small pore size and low amounts of solid material. To demonstrate using yttria, Chervin et al. synthesized YSZ aerogels using yttrium(III) chloride hexahydrate; the aerogels had high surface area and thermal conductivity measurements that were similar to that of YSZ reported previously.[8] Depending on the temperature, above 8 mol% Y_2O_3, it is known that cubic stabilization occurs; below this concentration, a mixture of tetragonal and cubic phases exists. At approximately 8 mol% Y_2O_3, the optimal ionic conductivity occurs; electrolyte applications of YSZ use 8 - 10 mol% Y_2O_3. Yttria-stabilized zirconia has high ionic conductivity, high thermal stability, and outstanding mechanical strength, making YSZ useful in a wide variety of high-temperature applications.[237] For example, Chao et al. proved the improvement of zirconia aerogel thermal stability by doping with yttrium(III) nitrate hexahydrate.[48] The YSZ aerogels maintained a stable tetragonal phase after 1200°C exposure for 2 hours. Zirconia aerogels without yttrium are shown to transform from tetragonal to monoclinic after 600°C exposure, which causes a volume increase and limits use of the aerogels as structural materials due to cracking. Additionally, Angle et al. demonstrated that the addition of alumina in 8 mol% YSZ increases the thermal shock resistance, reducing crack propagation during thermal stress.[267] As another example of using yttria, Tsay et al. utilized yttrium oxide (Y_2O_3) precursor solution to synthesize gels, and subsequent thin films, via the sol-gel method.[268]

While yttria-stabilized zirconia aerogels are widely studied, other rare earth dopants are used to stabilize the zirconia aerogel systems. Since the rare earth metal, ytterbium (Yb), has a smaller ionic radius than yttrium, 3 - 10 mol% ytterbia-doped zirconia has a lower thermal conductivity than YSZ. Using ytterbium(III) chloride hexahydrate, Hurwitz et al. synthesized ytterbia-stabilized zirconia (YbSZ) aerogels, which retained a higher porosity, predicted to decrease thermal conductivity, when exposed to temperatures of 1100°C - 1200°C when compared to YSZ aerogels.[22] The rare earth metal, cerium (Ce), is also doped into the zirconia aerogel system as a stabilizer. Ceria-stabilized zirconia (CeSZ) draws attention due to its high oxygen storage capacity and catalytic activity. Ceria-stabilized zirconia can

be synthesized using a variety of methods, including sol-gel, co-precipitation, and template-assisted approaches.[269] For example, Mejri et al. synthesized ceria-doped sulfated zirconia aerogels that had excellent catalytic activity due to retention of specific surface area upon exposure of temperatures up to 600°C.[270] Likewise, Lamas et al. synthesized compositionally homogeneous ZrO_2-CeO_2 solid solutions which had high specific surface areas and retained the tetragonal phase with cerium oxide content up to 70 mol%.[228] As another example, Sun et al. synthesized CeSZ aerogels, as well as zirconia aerogels stabilized using lanthanum (La), via the sol-gel method which were shown to have greater thermal stability, surface area, and mesoporosity than the pristine zirconia aerogels.[271] Using the rare earth metal gadolinium (Gd), Montoya et al. synthesized gadolinium-doped ZrO_2 nanoparticles via the sol-gel method which were monodisperse and had high crystallinity.[272]

To demonstrate the use of a variety of rare earth elements, Torres-Rodriguez et al. synthesized rare earth zirconate ($Ln_2Zr_2O_7$ where Ln is La (lanthanum), Nd (neodymium), Gd (gadolinium), and Dy (dysprosium)) monolithic aerogels via the sol-gel method and supercritical drying.[35] The aerogels had high specific surface areas following calcination at 1000°C and a mixture of cubic and tetragonal zirconia phases.[34]

In addition to rare earth metals, non-rare earth metals can also be used as stabilizing dopants in zirconia aerogel synthesis. As an example, Wu et al. synthesized monolithic microporous zirconia gels using magnesium chloride hexahydrate.[39] The addition of Mg^{2+} led to gels with high surface area and stabilized cubic zirconia phase after heat-treatment at 800°C. As another example of non-rare earth dopants, Boyse et al. synthesized zirconia aerogels that were doped with either tungstate or sulfate, as well as a combination of the two.[273] It was determined that having both dopants led to aerogels that had increased thermal stability, as compared to aerogels which only had either tungstate or sulfate. Similarly, Chakhari et al. doped zirconia aerogels with either sulfates or heteropolytungstic acid (HPW).[274] The aerogels doped with sulfate groups had higher resulting surface area and average pore diameter than the aerogels doped with HPW.

2.2.4 Solvents

In a typical sol-gel process, a solvent system of water and alcohol, commonly ethanol or isopropanol, is used. This solvent system is used to dissolve the precursor material, which is not usually soluble in water.[275] The amount of water added to the solution must be controlled because if too little water is added, hydrolysis does not go to completion; if too much water is added, the aerogel is likely to have narrower pores, leading to higher density.[276] He et al. created aerogels from methyltriethoxysilane (MTES) precursor, ethanol, water, and ammonia base catalyst by varying the volume ratio of water/ethanol from 0.7 to 1.5.[110] As the ratio increased from 0.7 to 1.5 average pore diameters of the resultant aerogels decreased from 6.1 nm to 3.4 nm.

2.2.5 Gelation agents

Gelation agents, or gelators, are used to transform solutions of colloidal precursors into a gel, a weakly organized internal structure.[277] Alternatively, complexing agents or chelating agents can be added to the system in order to influence gelation.[278,279] Chelating agents can be used to modify alkoxide precursors, slowing down rapid hydrolysis and premature precipitation during the sol-gel process. The measurement of gelation time, defined as the time it takes for the sol to stand without flowing, typically starts after the addition of the gelation agent and ends once a wet gel has formed.[73,105] The gelation time can be slowed down or sped up by changing many variables in the sol-gel process including precursor, hydrolysis time, acid and base catalyst concentrations, process temperature, and solvent to precursor ratio.[280] Gelation time for wet gels can range from mere seconds to many days depending on the sol contents and processing conditions.

The gelation agent that is selected has impacts on the final synthesized aerogel, including its pore structure, surface area, crystalline phase stability, and sintering behavior. While a variety can be used for aerogels, four select gelation agents are considered in this dissertation: propylene oxide, acetylacetone, water glass, and acids. Base catalysts can also be used to

initiate gelation in aerogels, specifically in silica aerogels.

Epoxides are frequently used as gelation agents during the sol-gel process as they are able to synthesize wet gels from a variety of initial precursors, including oxynitrates, oxychlorides, and chlorides.[37] Propylene oxide (CH_3CHCH_2O) is a widely used gelation agent for all types of sol-gel materials, providing consistent and quick gelation times.[66,143] As an example, Schäfer et al. synthesized yttria-stabilized zirconia (YSZ) and pure zirconia aerogels starting from zirconium(IV) chloride and using propylene oxide.[281] Similarly, Chervin et al. synthesized YSZ aerogels, using propylene oxide, with retained high surface areas and nanostructure following 500°C exposure.[8]

The role of propylene oxide (PO) as a gelation agent is to promote metal ions to undergo hydrolysis and condensation reactions.[281] PO accomplishes this by consuming acid as a proton scavenger, raising the pH of the solution through an irreversible ring-opening reaction.[51] In metal oxide aerogel synthesis, the gelation time varies with the molar ratio of PO to total metals; increasing amounts of PO lead to faster gelation times.[8]

While propylene oxide is a widely used gelation agent, PO is a hazardous substance, with high toxicity, flammability, explosiveness, and irritancy.[37] The safety hazards associated with propylene oxide make it problematic for use as a gelation agent, especially when considering the potential scale-up of the metal oxide aerogel synthesis process. As alternatives to propylene oxide, Gash et al. demonstrated that other epoxides, such as 1,2-epoxybutane, 1,2-epoxypentane, 2,3-epoxy(propyl)benzene, trimethylene oxide, glycidol, epichlorohydrin, and epibromohydrin, can be used to synthesize metal oxide aerogels by inducing gelation.[192]

Acetylacetone ($CH_3COCH_2COCH_3$), the conjugate acid of acetylacetonate, is another gelation agent that is used in sol-gel reactions. For instance, Gossard et al. synthesized zirconia gels using zirconyl nitrate salt as the precursor and acetylacetone as the complexing agent via a colloidal sol-gel method.[193] Furthermore, Schäfer et al. synthesized zirconia gels using acetylacetone as a gelation agent and found that the addition of acetylacetone was required for the formation of the gel.[281] Acetylacetone is used to inhibit dehydration

reactions via oxolation and to prevent precipitation of the Zr precursor. Acetylacetone also acts as a chelating agent by creating a steric barrier and stabilizing the Zr-based colloids, which facilitates the formation of the nanoparticles and subsequent zirconia gel. Along with the concentration of the precursor and the pH of the sol, the concentration of acetylacetone, specifically the concentration ratio of acetylacetone to precursor, influences the gelation time of the system. Gelation time is known to increase with the concentration of acetylacetone.[281,282] As an example, Gossard et al. set the value of the [acetylacetone]/[Zr] ratio at a value of 0.5 for the best optimization of gelation time and avoiding powder precipitation.[283]

Sodium silicate (Na_2SiO_3), also known as "water glass", can be used as a gelation agent in sol-gel reactions. For example, Gao et al. synthesized high-temperature resistant zirconia aerogels via an environmentally friendly, co-hydrolysis method using water glass as the gel initiator.[49] Water glass was used to control the hydrolysis of the Zr^{4+} ions and to accelerate gelation. Water glass also acted as a modifier and was used to introduce SiO_2 in-situ as a shell around ZrO_2 nanoparticles, reinforcing the nanoparticles and inhibiting crystal growth, which improved the thermal stability and preserved the high surface area of the aerogel upon high-temperature exposure. To demonstrate the use of water glass, Schäfer et al. attempted to synthesize silica-zirconia mixed oxide aerogels using zirconium(IV) chloride as precursor and water glass as a crosslinking agent; non-stable wet gels resulted.[284] However, the group was able to synthesize stable silica aerogels starting from silicon tetrachloride and water glass. As another example, water glass in combination with the base catalyst, NH_4OH, formed silica aerogels in the work of Eskandari et al.[128] Base catalysts are rarely used without acid catalysts; however, in this case, using water glass as a precursor allows for the use of a base and not an acid catalyst. The results were surface areas ranging from 447 m^2/g to 764 m^2/g and densities from 0.08 g/cm^3 to 0.19 g/cm^3 but with porosities as low as 84%.

A variety of acids, such as citric acid ($C_6H_8O_7$), nitric acid (HNO_3) and mercaptosuccinic acid ($C_4H_6O_4S$), are also used as gelation agents, or acid catalysts, in the synthesis of aero-

gels. The hydrolysis and condensation reactions of the sol-gel method are easily influenced by the solution pH; therefore, it is often necessary to use acid, or base catalysts as later discussed, to control the rate at which hydrolysis and condensation occur.[132,194,262,285] For example, Wang et al. used citric acid to initiate the sol-gel transition during the synthesis of monolithic zirconia aerogels.[37] The interactions between the hydroxyl groups of citric acid were critical in crosslinking the metal ions to produce the gel network. Citric acid also prevents precipitation by creating an acidic environment, which slows down hydrolysis. As another example, Zhang et al. synthesized yttria-stabilized zirconia aerogels using citric acid as the gelation accelerator.[42] By adjusting the ratio of citric acid to Zr^{4+}, the gelation time, density, and specific surface area of the aerogels could be influenced. In addition to synthesizing high surface area, mesoporous aerogels, citric acid is cost-effective and non-toxic, which leads to a safer synthesis route than using traditional gelation agents that can be harmful, such as propylene oxide.

In addition to using citric acid as a gelation agent, Wang et al. synthesized aerogels with high surface area and large pore volume using various other organic acids.[37] Zirconia aerogels were formed using L-malic acid, L-aspartic acid, and mercaptosuccinic acid, which each have identical main chain structures with carboxylic acid ends but different side groups (-OH, -NH_2, and -SH, respectively). Interactions between the organic acid and the Zr^{4+} ions, due to the presence of the side group, could form coordination bonds, which were critical in inducing gelation. The resulting zirconia aerogels showed negligible differences when each acid was used in the synthesis, as most of the organic material was removed during the supercritical drying process.

Using highly concentrated acids can cause loss of control over the rate of hydrolysis, speeding up the reaction due to its exothermic nature. However, when done carefully, successful aerogels can result. For example, Ming Li et al. used the acid catalyst HCl to create aerogels from TEOS with a range of pore volumes from 2.628 cm^3/g to 3.875 cm^3/g.[132]

To demonstrate the use of an inorganic acid, Torres-Rodriguez et al. synthesized zirconia

and yttria-stabilized zirconia aerogels via a nitric acid-catalyzed sol-gel method.[34] Nitric acid was used to hydrolyze the zirconium and yttrium precursors, forming thermally stable wet gels and subsequent aerogels. Additionally, Southon et al. synthesized zirconia gels via the controlled hydrolysis of zirconium carbonate in nitric acid.[229] When the Zr:NO_3 ratio was 1:1, the solution gelled reversibly following either water evaporation or an increase in pH or irreversibly following removal of nitrate anions.

Acid catalysts are often used with base catalysts, especially for silica aerogels. Sols that are only acid catalyzed, if the pH is too low, may create weak gels due to randomly branched or entangled linear polymer chain structures, which will lead to high density aerogels with small pore volumes.[194,285] Therefore, base catalysts are an important addition to initiate and aid condensation reactions.

Base catalysts, such as ammonium hydroxide (NH_4OH) or ammonium fluoride (NH_4F), increase the branching of sol particles and strengthen the gel network with cross-linking between polymer chains, leading to a stronger gel structure with larger pore volume and lower density.[128] Base catalysts also typically decrease gelation time when used in combination with acid catalysts by raising pH levels of the silica sol.[114,275] For example, Zhi Li et al. triggered gelation with the addition of ammonium hydroxide.[57] A method by Deng Yiyi et al. using both the acid catalyst HCl and the base catalyst NH_4OH displayed aerogels from TEOS with pore volumes from 1.04 cm^3/g to 2.02 cm^3/g.[114]

2.2.6 Gel modification

Synthesizing aerogels with a core-shell nanostructure or with surface modification can increase the strength and thermal stability of the aerogels, as well as inhibit crystalline transformation and minimize shrinkage. Recent applications of several techniques used for each modification method, relating specifically to zirconia aerogels, are described below.

The presence of a core-shell nanostructure provides many benefits when aerogels are used in applications such as thermal superinsulators, catalysts, and adsorbents.[32,44] There

are four main types of core-shell aerogels: 1) inorganic/inorganic, 2) organic/organic, 3) organic/inorganic, and 4) inorganic/organic, with the last two types considered as core/shell hybrids.[286] Many different compounds are used to form the shell of core-shell aerogels, including metal oxides, silica, and polymers.[32,44,286–288]

As an example of inorganic/inorganic core-shell nanostructures, Zu et al. synthesized core-shell aerogels with metal oxide-silica shells using an alkoxide chemical liquid deposition (ACLD) technique; the metal oxide cores used were ZrO_2, Al_2O_3, and TiO_2.[44] First, the metal oxide was deposited onto the surface nanoparticles of the metal oxide wet gel. Next, a metal oxide and silica composite was deposited onto the metal oxide surface formed in the first step. Finally, silica was deposited onto the metal oxide/silica surface. The group found that metal oxide aerogels made using core-shell synthesis have increased specific surface areas, larger pore volumes, lower thermal conductivities, and minimized shrinkages with heat-treatment as compared to aerogels made without a core-shell nanostructure. The core-shell structure enhances the mechanical strength, prevents transformation of the crystalline structure, and improves thermal stability of the aerogel. As another example, Ren et al. synthesized ZrO_2/SiO_2 core-shell aerogels, via immersion in tetraethyl orthosilicate (TEOS), that demonstrated uniform pore structure, low bulk density, and high specific surface area.[32] High surface area was retained because of the resistance to capillary stress caused by deposited SiO_2 nanoparticles on the ZrO_2 aerogel primary particle surface. Due to TEOS modification, the dried aerogel was amorphous and transformed to tetragonal ZrO_2 following high-temperature exposure at 1000°C; crystalline growth following heat-treatment was inhibited. Additionally, Wang et al. synthesized monolithic ZrO_2 aerogels that inhibited cracking and had low thermal conductivity by modifying with SiO_2.[36] ZrO_2 gels were aged in tetraethyl orthosilicate solution and supercritically dried. The layer of SiO_2 on the aerogels reinforced the solid skeleton that was formed during the sol-gel process, increasing the compressive strength of the aerogel and improving the ability to withstand aging and drying stresses of the aerogel.

For core-shell aerogel nanostructures that consist of an organic and an inorganic component, typical nanoparticles have an inorganic solid core and a polymer shell. Polymer coatings are compatible with a wide range of cores, including zirconia, silica, iron oxide, and noble metals, as the surface hydroxyls of the aerogel core can interact with the polymer to form a shell.[286,287] Particularly, Leventis et al. synthesized rare earth aerogels with a polymer shell of polyurethane/polyurea.[288] The presence of the polymer shell retained the mesoporous structure and surface area of the aerogel. Additionally, Leventis synthesized zirconia aerogels with a polymer shell coating that had high mechanical strength. The group determined that inorganic core-polymer shell aerogel nanostructures should be achievable for all sol-gel materials.

The introduction of deactivating functional groups used to inhibit the surface hydroxyls of aerogels is another way to increase the thermal stability. To demonstrate, Hu et al. improved the stability of ZrO_2-SiO_2 aerogels exposed to high temperature using surface modification.[21] To create Fe modified aerogels, inorganic ions (Fe(III) ions) that were thermally stable were introduced into the ZrO_2-SiO_2 gel skeleton prior to drying. To generate inert silyl surface groups, the Fe modified aerogels were treated with hexamethyldisilazane (HMDZ) gas phase. The functional groups replaced the hydroxyl groups on the aerogel surface, which was confirmed by fourier-transform infrared spectroscopy (FTIR). Upon heat-treatment at 1000°C, the uniform pore structure of the surface modified aerogels was retained due to the inhibition of particle growth caused by hydroxyl group condensation; in addition, the surface modified aerogels demonstrated a lower degree of particle agglomeration. A high specific surface area was maintained in the aerogels following calcination, as well as high pore volume. Surface modification was shown to not affect the mesoporous structure of the ZrO_2-SiO_2 aerogels. Both the addition of Fe modifiers and HMDZ gas phase treatment were shown to inhibit crystalline transformation of ZrO_2-SiO_2 aerogels at high temperatures. It is anticipated that surface modification of aerogels could lead to ultrahigh-temperature applications.

2.2.7 Templating methods

The use of surfactants as templating agents for aerogels is discussed in detail in section 3, therefore it will not be elaborated on here. However, there are several other ways to template aerogels and control their porosity and surface area. This includes superfine powders, emulsion templating and foam insertion, to name a few. For instance, Duan et al. templated tetragonal phase mesoporous zirconia with poly(methyl methacrylate) superfine powders using the sol-gel method.[289] The synthesized mesoporous zirconia had a small particle size of 3.7 nm and a narrow pore size distribution. Alternatively, Teo et al. synthesized aerogel foams using an oil-in-oil emulsion templating method; the emulsion was stabilized using block copolymer surfactant.[290] The resulting aerogel foams had an increased pore volume following emulsion templating, which lead to an increased capacity for oil absorption. Porous materials can also be templated using direct foaming methods, which insert air bubbles into the solution prior to gelation or setting.[14] The porosity of the final material is directly related to the amount of gas inserted during the foaming process; the pore size is dependent on the stability of the wet foam prior to gelation. To stabilize the incorporated air bubbles, surfactants or solid particles can be used.

2.2.8 Gel aging & washing

Final gel processing, including aging and washing, is performed prior to drying for most aerogel systems. Following gelation, gels are usually aged at elevated temperature and/or washed in solvent to prepare the wet gels for the drying process. During aging, gels are submerged typically in an alcohol, such as ethanol, to strengthen the gel skeleton in order to minimize shrinkage and cracking. The aging process allows the composition, structure, and properties of the gel to continue to evolve over time.[18,74,291] The chemical reactions during the gelation period are known to occur long after the initial gelation of the solution; the aging process allows for the reactions to continue prior to drying, enhancing the aerogel backbone.[292] The aging process increases the modulus of rupture of the aerogel, as well

as enhances stiffness.[293] As an example, Bedilo et al. showed that longer aging times (up to 52 hours) resulted in zirconia aerogels with higher surface areas (111 m^2/g) following supercritical drying and heat treatment.[233] It was also shown that aging had negligible effect on the pore structure of the aerogels.

Washing of the gels typically occurs in a solution that is compatible with the drying process for several hours to several days.[10,37,43] Subsequent washes are generally used to exchange the water and potential byproducts contained in the gels' pores prior to drying.[49] Alcohols, such as ethanol and isopropanol, are often chosen for gels intended for supercritical drying because these solvents have high solubility in supercritical CO_2 which is necessary in order for the solvent to be extracted from the pores efficiently during the drying process.[294] When the drying process is ambient pressure drying, n-hexane is one of the most used wash solvents due to its reactivity with common surface modifiers such as trimethylsilyl chloride (TMCS).[295]

Modifying washes are an important step for gels using ambient pressure drying as the modification preserves pore structure and protects against the high capillary pressure that occurs when solvent evaporates from the pores.[21,40] When using hydrophillic precursors in silica aerogels, such as tetraethyl orthosilicate (TEOS) and sodium silicate (water glass), if not modified, silanol groups on the surface of wet gels undergo condensation reactions. These condensation reactions can lead to densification and shrinkage during the ambient pressure drying process.[53] Chemical modification of the gel surface replaces the hydrogen on the hydroxyl group of silanol in order to create hydrophobic surfaces on the gel.[194] One common modifier used in silica aerogel creation is TMCS, as mentioned above. In the work of Hyeonjung Kim et al., TMCS modified water glass aerogels are compared with unmodified silica aerogels after ambient pressure drying. The results of this study show that the modified silica aerogels could reach surface areas as high as 473 m^2/g with a pore volume of 4.15 cm^3/g while the unmodified aerogel had a surface area of only 98 m^2/g and a pore volume of 0.08cm^3/g.[67] A hydrophobic precursor, such as methyltrimethoxysilane (MTMS), can be

advantageous as methyl groups on MTMS replace hydroxyl groups on the wet gel surface, synthesizing hydrophobic silica aerogels without modification.

2.3 Aerogel post-synthesis processing

Following synthesis, gels are further processed to form aerogels. Here, different drying techniques, sintering parameters, and characterization methods that are used in the processing of aerogels are discussed. It should be noted that the majority of these processing techniques are generally used for a wide range of aerogel systems; however, select examples relating to zirconia aerogels and silica aerogels are presented.

2.3.1 Drying techniques

Many techniques are used to dry a wet gel, transforming it into an aerogel. Depending on choice of drying technique and conditions, aerogel properties, such as pore structure, surface area, sintering behavior, or crystalline phase transformation, can be controlled or enhanced. Five selected drying techniques are discussed below and are displayed in Figure 5: supercritical drying, ambient pressure drying, freeze drying, atmospheric drying, and oven drying. These general drying techniques can be used for a variety of aerogel systems.

Supercritical fluid drying is a widely used technique for drying aerogels. Supercritical drying transforms wet gels into aerogels by extracting the solvent in the pores of the gel via a supercritical fluid, as shown in Figure 5A.[10,294] Supercritical fluids, fluids that have been heated and compressed above the critical temperature and pressure of the fluid, have high diffusion coefficients and gas-like viscosities, allowing for greater mass transfer than traditional liquid solvents. Supercritical drying results in aerogels that have high pore volumes, high porosities, high surface areas, and low shrinkages; these properties are generally greater than those in aerogels that are dried using ambient pressure drying or freeze drying. An example of supercritical drying used to produce silica aerogels can be seen in the work of Duan et al. where an unmodified TEOS based silica gel was supercritically dried with CO_2

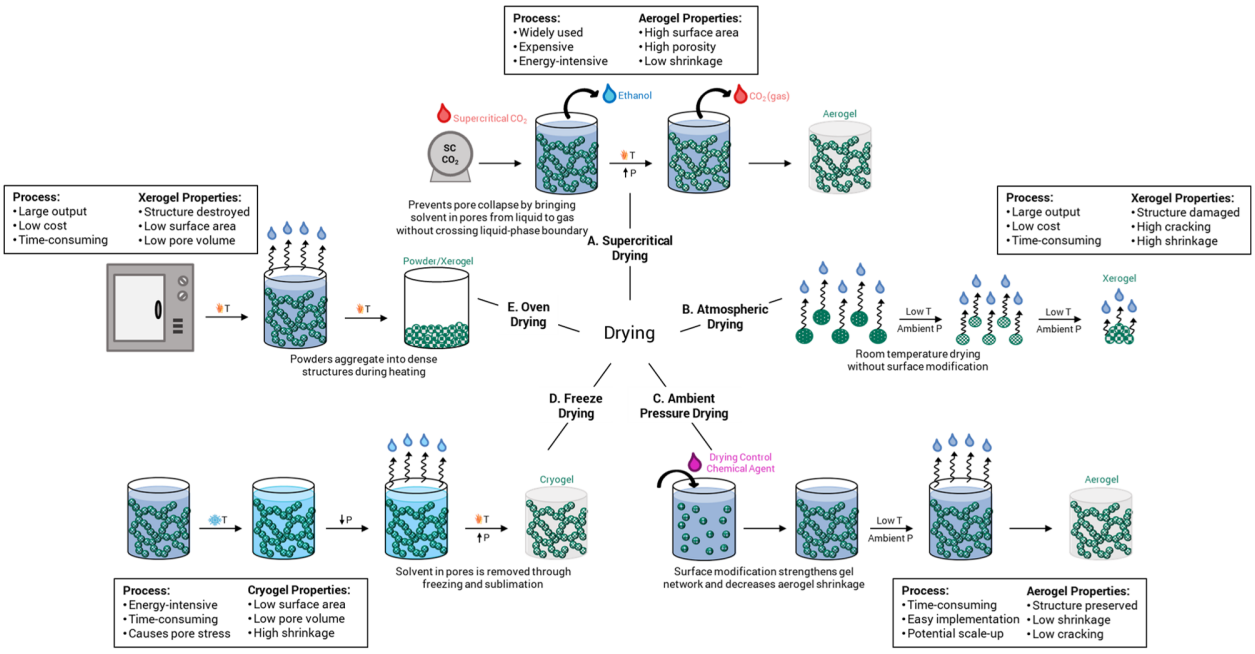

Figure 5: Drying techniques for aerogels. An overview of five drying techniques, resulting in different materials, including A) supercritical drying for aerogels, B) atmospheric drying for xerogels, C) ambient pressure drying for aerogels, D) freeze drying for cryogels, and E) oven drying for xerogels. Each drying technique has different process parameters and results in materials with varying properties.

solvent for a high surface area of 805 m^2/g.[139]

Supercritical drying is advantageous as it allows the solvent within the pores to be brought from the liquid phase to the gas phase without crossing the liquid-phase boundary, which often causes cracking or shrinkage of the sample. Supercritical fluids can accomplish this by crossing through the supercritical region, where there is no distinction between gas and liquid.[296] Carbon dioxide is the most frequently used solvent for supercritical fluid drying, with a mild critical temperature of 31.1°C and mild critical pressure of 7.39 MPa.[297] Supercritical CO_2 ($scCO_2$) is a safer (non-toxic, non-flammable) and greener (natural, plentiful) alternative to solvents with higher critical temperatures used in nanotechnology. Advantages to using $scCO_2$ are tunable solvent strength, high diffusivity, and exceptional wetting of the complex surfaces of nanostructures. The extremely low surface tension of $scCO_2$ provides the capability to synthesize mesoporous materials via supercritical drying.[235]

In the supercritical drying process, any residual water in the gels is first washed away with alcohol, which is then washed away using high pressure liquid carbon dioxide.[296] Once the liquid CO_2 has been heated beyond the critical point, the pressure is increased until the supercritical solvent replaces any fluid in the gel pores. When the pressure is released, the supercritical solvent drains from the pores leaving behind a dried aerogel.[10,139,298] The resulting product is a dried aerogel, with high surface area, porosity, and pore volume.

It should be noted that ethanol is also a widely used supercritical drying solvent, yet it has a critical temperature of 240.8°C , much higher than carbon dioxide, which can pose a higher safety risk.[299] In addition, ammonia can be a useful supercritical solvent due to its mild critical point of 132.5°C and 11.28 MPa; however ammonia is caustic and hazardous, which can lead to unsafe operability.[297]

While aerogels are often synthesized under supercritical conditions, which can be an energy-intensive, expensive, and, sometimes, dangerous process, aerogels can also be synthesized through ambient pressure drying.[300] Ambient pressure drying, depicted in Figure 5C, results in aerogels through the evaporation of the liquid in the pores of the wet gel

at ambient pressures and temperatures ranging from room temperature to 200°C.[294] This drying method is attractive as it does not require any complicated instruments, has easy implementation, and can be scaled-up for use in industry.[301] Ambient pressure drying also consumes less energy than supercritical drying. Generally, in order to combat the negative effects of capillary tension, such as shrinkage or cracking, during ambient pressure drying, surface modification is applied to the gels through solvent-exchange with low surface tension solvents prior to drying.[294,300,302] This method causes the hydrophobization of the wet gel, decreasing the capillary tension forces on the surface, and strengthens the network of the gel skeleton. This results in a spring-back action, as the shrunken elastic gel network returns to its porous state as the liquid-vapor withdraws into the interior of the gel. To ensure the spring-back effect, drying control agents are often incorporated into the sol-gel reactions prior to drying.[303] Due to high thermal stability and low vapor pressure, ionic liquids don't evaporate over a long period of time, allowing them to be used to yield a stable gel network and inhibit pore structure collapse. It should be noted that if ambient pressure drying does not maintain the original gel structure in the sample, xerogels are obtained instead of aerogels.[304] For silica aerogels made with hydrophilic precursors like TEOS and water glass, surface modification is necessary for successful aerogel production from ambient pressure drying as surface modification is necessary to increase the surface tension of the gels to allow them to withstand the heightened capillary pressure with minimal shrinkage and cracking.[53] If surface modification is not completed, ambient pressure drying of silica gels with hydrophilic precursors can result in xerogels. For example, in the work of Maria de Fátima Júlio and Laura M. Ilharco, hexamethyldisilazane (HMDZ) was used to modify TEOS based silica aerogels.[120] It was found that the reaction between HMDZ and silanol produced trimethylsilyls instead of silanol surface groups. This replacement meant the gel had become hydrophobic and was ready to be dried with ambient pressure drying without collapsing the gel network. The final aerogels prepared with TEOS, HMDZ modifications, and ambient pressure drying displayed surface areas of 379 m^2/g to 783 m^2/g with respective

pore volumes of 0.79 cm^3/g and 1.76 cm^3/g. When a hydrophobic precursor such as MTMS is used, often surface modification is not necessary for the creation of an aerogel from ambient pressure drying. This is because of the methyl groups on MTMS which do not undergo the condensation reactions that adjacent silanol groups do.[194] This can be seen in the work of Mahani et al. where MTMS based silica aerogels were prepared without surface modification through ambient pressure drying.[103] The resulting aerogels maintained porosities as high as 94% with a surface area of 712 m^2/g.

Surfactants can be used to aid in the formation of high surface area aerogels via ambient pressure drying. As an example, Perissinotto et al. used the surfactant sodium dodecyl sulfate (SDS) in the synthesis of ambient pressure dried silica aerogels; it was determined that higher amounts of SDS led to aerogels with larger pore volume and mean pore size.[141] In the work of Chen et al., surfactants allowed for the ambient pressure drying of gels without further surface modification and with minimal shrinkage of the final aerogel product.[88]

Ambient pressure drying and subsequent surface modification can be a lengthy process, taking up to several days or weeks.[298] The ambient pressure drying process involves several water or ethanol washing steps, as well as multiple solvents used in surface modification, leading to large solvent consumption and possible environmental pollution. However, recent industrial developments have led to the economic and large-scale ambient pressure drying of aerogels and the production time has been reduced to approximately one day.[302]

Similar to supercritical drying, freeze drying is a method of drying gels that seeks to avoid the liquid-phase boundary. Freeze drying consists of subjecting a sample to temperatures below freezing, generally -50 to -85°C, by either placing it in a freezer, a freeze-dryer, or a solution of liquid nitrogen in order to remove the solvent from the gel.[251,305] Freeze drying is displayed in Figure 5D. In a typical freeze drying process, the solvent inside of the pores of the gel is frozen, followed by sublimation of the solvent directly into the gas phase by reducing the pressure via pulling vacuum on the system, which removes approximately 95% the solvent from the pores without forming a liquid-vapor interface.[125,141,294,306] This is the

primary drying step of the freeze drying process and is typically the most time-consuming. After full removal of the solvent (any unfrozen water is removed during the secondary drying step by raising the temperature of the system), the sample is brought to room temperature by pressurization of the system. At the end of the drying process, the residual water content in the sample should be only 1 to 4%. Freeze drying of aerogels previously resulted in powder-like materials, however, more recently, freeze drying has been used to produce monolithic aerogel pieces.[301] The final product of freeze drying is often called a cryogel and is usually in powder form due to the cracking of the gel structure during the initial crystallization of the solvent in the pores.

There are quite a few disadvantages to freeze drying, such as that it is an energy-intensive process, which can have long processing times, including aging, sublimation, and drying times, and low potential for scale-up.[294,305] Freeze drying can also cause crystal growth or stress development inside of the gel's pores, which could lead to damage of the nanostructure or fracture of the matrix. One way to decrease the effects of solvent crystallization on final gel structure is to increase the aging time of the gel in order to strengthen the network structure. Salts can also be added to lower freezing temperatures.[194,262,307] In freeze drying, choice of solvent must be carefully considered as it is important to choose a solvent with a low expansion coefficient and high sublimation pressure. If water is used as the solvent, water can expand within the pores during the freezing process, further destroying the pore structure. If an alcohol is used as the solvent, the freezing temperature can be hard to achieve and maintain; for instance, ethanol freezes at -113.15°C. Aerogels that are freeze dried also tend to shrink and have low surface areas or pore volumes. Methods of improving freeze dried gels can be seen in the work of Pan et al.[125] In this work, tert-Butanol, with a high freezing point, was used as the solvent in a MTMS based silica aerogel. The gel was also aged for two days for gel network stabilization. The resulting cryogels achieved surface areas and pore volumes ranging from 485 m^2/g to 867 m^2/g and 3.26 cm^3/g to 1.34 cm^3/g, respectively. To compare drying methods, Zhao et al. prepared zirconia aerogels by both

supercritical CO_2 drying and freeze drying.[251] Zirconia aerogels that were synthesized using freeze drying had a microporous structure with low surface area (400 m^2/g) and pore size (0.6 nm), while zirconia aerogels synthesized using supercritical drying had a mesoporous structure with high surface area (640 m^2/g) and pore size (9.7 nm). However, Simón-Herrero et al. demonstrated that aerogels with higher porosity were synthesized using a freeze drying process with higher freezing time, vacuum pressure, and freezing temperature.[306]

In addition to traditional freeze drying, directional freeze drying and spray freeze drying can also be used to dry aerogels. In directional freeze drying, a sol is frozen in one x-y-z direction in a controlled manner; the pores are templated by the areas that were not occupied by the solution.[308,309] The porosity of the aerogel is influenced by the temperature gradient that occurs during the freezing process, the morphology of the ice crystals, and the solute concentration. Directional freeze drying is easily operable, free of by-products, and environmentally friendly.[310] Aerogels that are synthesized using directional freeze-drying exhibit minimized shrinkage upon heat-treatment, high surface area, high compressive strength, and special anisotropic aligned porous structure.[174] In spray freeze drying, the sol is atomized, guided into a mold that is soaked in liquid nitrogen, and then dried in a freeze dryer. The sol droplets, typically with a diameter of a few micrometers, make up thin layers of the gel. To improve upon spray freeze drying, Pan et al. demonstrated that the addition of a solvent with a high freezing point, such as tert-Butanol with a freezing point of 25.7°C, allows fast freezing, rapid cooling, and the formation of smaller ice crystals than traditional freeze drying.[311] Aerogels synthesized using spray freeze drying are monolithic in shape and have high thermal stability and low thermal conductivity.

Atmospheric drying, oven drying, and evaporative drying typically result in xerogels.[35,303,312] Xerogels are distinguished from aerogels since they are unable to retain the original nanostructure of the wet gel following drying in the same way that an aerogel can.[304] Xerogels can be used in a range of applications, including use as sensors, sorption media, and catalysts.[313–316]

Atmospheric drying, or direct air drying, is similar to ambient pressure drying except that there is no surface modification taking place and the gels are dried at room temperature or atmospheric conditions leading to evaporation of solvent from pores, as shown in Figure 5B.[85,115,312] Atmospheric drying usually leads to cracking and shrinking of the pore structure due to the high capillary pressure gradient generated by the surface tension of the liquid within the pores that is present during solvent removal.[304]

Oven drying is typically conducted in laboratory and uses increased temperatures to remove the liquid solvent from the pores of the gel. This drying method can also be called evaporative drying and can be useful for drying large quantities of sample at low cost.[317] Oven drying, depicted in Figure 5E, typically produces large amounts of capillary pressure, which can lead to agglomeration, and causes the sample to dry rapidly and crack due to the different thermal expansion coefficients between gels and liquid solvents. According to Wang et al., the rate of drying must be controlled to be as low as possible to reduce cracking of the sample; low-rate oven drying can be very time-consuming, sometimes taking as long as one year.[318] Oven drying is very similar to ambient pressure drying where gels are dried in ovens at various heightened temperatures but not necessarily ambient pressure and typically without surface modification, thus oven drying typically yields xerogels or aerogel powders, which have lower surface areas and pore volumes than aerogels dried using supercritical or freeze drying.[10,35,128,319] Similar to oven drying, microwave drying is most commonly used in the food and ceramics industry; in recent years, it has been considered as a potential method of silica aerogel drying. The work of Guo et al. used microwave drying for MTMS based aerogels to improve production efficiency without pore collapse.[82] The work showed that microwave drying at 700W for 32 minutes produced an aerogel with a surface area of 796 m^2/g while drying at 200W for 55 minutes produced an aerogel with a surface area of 783 m^2/g. The same aerogel when dried with evaporation for over 48 hours had a surface area of 795 m^2/g.

2.3.2 Sintering

Sintering, or calcination, is a process technique in which a solid material is heated below its melting point; this technique promotes mobility of the surface and the bulk and generally leads to a reduction in surface area of the sample. When studying sintering, both surface energies and grain-boundary energies need to be considered. Both of these energies can be significantly changed by modification of the sample composition, specifically when dopants are added to the system.[320] Aerogels are sintered in order to determine the influence of heat treatment temperature on the microstructure, morphology, and thermal properties of the aerogels.[321] Thermal treatment causes aerogels to densify, decrease in surface area, and to show a collapse in pore volume and structure.[322] However, sintering also causes an enhancement of the elastic and mechanical properties of aerogels.[10] Sintering is a multifaceted evolution on the microstructure of aerogels via several mass transport mechanisms.[320]

Heat treatment of aerogels also leads to the crystalline transformation of the system. Pertaining specifically to zirconia aerogels, zirconia exhibits many different crystalline structures. Monoclinic zirconia is thermodynamically stable at temperatures below 1172°C; tetragonal is stable at temperatures between 1172°C and 2347°C; cubic zirconia is stable above a temperature of approximately 2347°C; orthorhombic zirconia is thermodynamically stable at high pressure.[227] A stable crystalline phase is desirable as the crystalline phase of zirconia affects its structural and textural properties, including surface area, porosity, and density.[34] For example, the stabilized tetragonal phase of zirconia is shown to have high strength and wear resistance; under optimized synthetic conditions, tetragonal zirconia can be stabilized at temperatures outside of its normal stabilization range. The addition of Y_2O_3 dopant in zirconia aerogels, for example, can stabilize the tetragonal crystalline phase up to higher temperatures.[48]

In sintering experiments, typically the effect of heat-treatment temperature, time, and heating rate are studied.[321] To identify the independent variables of the sintering process, a brief list of typical sintering parameters for zirconia aerogels is shown in Table 2.

Table 2: Aerogel sintering parameters. Reported sintering parameters, including temperature, time, ramp rate, and atmosphere, used for selected zirconia aerogels.

Reference	Temperature (°C)	Time (hrs)	Rate (°C/min)	Atmosphere
Bangi, 2018[13]	500	1	10	Air
Hu, 2017[21]	120	6	-	-
Hurwitz, 2020[22]	600/1000/1100/1200	0.3	5	Argon
Jung, 2017[18]	40	4	-	-
Jung, 2018[23]	400/800	1	5	-
Ren, 2015	1000	2	5	-
Torres-Rodríguez, 2019[35]	1000	5	-	-
Torres-Rodríguez, 2019[34]	300/500/1200	3/2/2	10	Atmospheric
Yoon, 2019[5]	500	2	-	-

The majority of silica aerogels do not undergo heat treatment. Silica aerogels have a melting point of around 1700°C, but they begin densifying and cracking at around 650°C, making heat treatment at high temperatures generally not viable.[298] In some cases, such as in Song He et al.'s work, heat treatment is carried out at lower temperatures, 600°C or below, creating silica aerogels with surface areas that decrease from 734 m^2/g when as-dried to 448 m^2/g when heat-treated at 600°C.[123] Studies that choose to sinter silica aerogels at temperatures above 650°C often obtain final aerogels with significantly lower surface areas such as in Cai et al.'s study where aerogels were heat treated with temperatures ranging from 600°C to 1300°C, with surface areas as low as 99 m^2/g when treated at 1100°C for four hours and even lower at 0.0018 m^2/g when treated at 1300°C for just 30 minutes.[62]

2.3.3 Characterization techniques

The most frequently used characterization methods for aerogels are scanning electron microscopy (SEM), transmission electron microscopy (TEM), nitrogen physisorption, x-ray diffraction (XRD), fourier-transform infrared spectroscopy (FTIR), thermogravimetric analysis (TGA), differential thermal analysis (DTA), and Raman spectroscopy. Each of these techniques is used to determine different properties of the final aerogel materials. These

characterization techniques are relevant to a variety of aerogel systems. The following paragraphs include a brief review on the different characterization techniques and a description of the aerogel property that is determined using each technique.

Typically, scanning electron microscopy (SEM) is used to determine the morphology and microstructure of aerogels qualitatively.[323] Image analysis is used to extract quantitative feature size. SEM could be used to help determine whether the aerogel sample is mesoporous or microporous, the effectiveness of certain surfactants as pore templates, or the extent of sample densification following heat-treatment. SEM can also be paired with energy-dispersive X-ray spectroscopy (EDX or EDS) to determine the elemental composition of aerogel samples.[23,44] SEM imaging works best with conductive samples. Transmission electron microscopy (TEM) is also used to determine the morphology and formation of the network pore structure in aerogel samples. In TEM, an electron beam passes through and interacts with a conductive sample.[324] Due to the interaction between the transmitted electrons and the sample, an image is formed, which can be magnified and detected by a camera. In addition to further determining the morphology and microstructure of aerogels seen in SEM, TEM can be used to determine the average crystallite size (Å) of particles within the aerogel.[37,45]

Powder x-ray diffraction (XRD) is performed to determine crystalline structure and phase composition of aerogel samples. The average crystallite size (Å) can be determined using XRD and further confirmed by TEM. The crystalline phase of aerogels can also be determined through analysis of XRD spectra. Cu Kα radiation, with a wavelength of 1.541 Å, is often used over a 2θ range of approximately 10° to 90°.[21,49] Typical current values range between 30 and 45 mA, while typical voltage values range between 40 and 45 kV.[35,48] To better distinguish between phases and mixtures of phases, Raman spectroscopy can be used to determine different polymorphs of metal oxides, due to its sensitivity to the polarizability of oxygen ions.[43] Specifically, Raman can easily distinguish between various crystalline phases due to different Raman active modes. Raman can also be used to quantify the incorporation

of modifiers into the aerogel structure.[50]

Nitrogen physisorption is used to determine the surface area of aerogels using the Brunauer, Emmett, and Teller (BET) method of analysis and the pore size distribution of aerogels using the Barrett, Joyner, and Halenda (BJH) method of analysis for pores up to 100 nm in size.[325,326] The sample must be properly equilibrated during analysis to ensure that the full pore volume is determined in aerogels with high porosity.[327] Nitrogen physisorption is useful in determining values for surface area (m^2/g), pore diameter (nm), and pore volume (cm^3/g) for zirconia aerogels. The different adsorption isotherms can be used to determine the pore structure of the aerogel: microporous (pores < 2 nm), mesoporous (pores between 2 and 50 nm), or macroporous (pores > 50 nm).[328] Aerogels are typically mesoporous materials with high surface areas.

Fourier-transform infrared spectroscopy (FTIR) is performed on aerogel samples to establish information on chemical bonds and surface functional groups. FTIR spectra are useful in determining whether aerogels have been properly modified by functional groups through the presence of chemical bonds represented by absorption peaks.[40,50] The mechanism of gelation can also be studied using FTIR.[37]

Thermogravimetric analysis (TGA), differential thermal analysis (DTA), and differential scanning calorimetry (DSC) are run to determine the amount of mass lost (%) by aerogel samples as a function of temperature. Thermal analysis is typically run up to temperatures between 1000°C and 1400°C.[29,38] The thermal analysis techniques are useful in determining the thermal stability of aerogels during high-temperature exposure. Endothermic and exothermic effects are also observed during thermal analysis.

X-ray photoelectron spectroscopy (XPS) is used to determine the surface concentrations and the chemical states of oxygen atoms within the aerogel samples.[25,44] XPS can also be used to show interactions that occur during the formation of wet gels.[37] Inductively coupled plasma mass spectrometry (ICP) is used to determine the ratio of elemental species in aerogels.[21] ICP can be useful in determining whether modifiers or dopants have been

successfully incorporated into aerogel samples. Using atomic force microscopy (AFM), force-distance curves can be used to determine the strength of the gel network.[23] The thermal conductivity (W/m·K) of aerogel samples can be determined using a transient hot-wire technique or a hot disk thermal analyzer.[49] Aerogel samples are sometimes incorporated into a fibrous material, such as ZrO_2 fibrofelt, to determine the thermal conductivity.[41] Physical measurement can be used to obtain as-dried shrinkage (%) and bulk density (g/cm^3) information of aerogels.[22]

Chapter 3 Understanding structure/property-process relationships in aerogels through surfactant templating

This dissertation experimentally considered yttria-stabilized zirconia (YSZ) aerogels, which have high surface area and low thermal conductivity and are expected to be used for temperatures between 600°C and 1000°C. Specifically, the use of surfactants as templating agents for YSZ aerogels was considered. The cationic surfactant cetrimonium bromide (CTAB), the anionic surfactant sodium dodecyl sulfate (SDS), and the nonionic surfactant Pluronic® P-123 (P-123) were utilized as surfactant templates. It was anticipated that surfactant templating would yield YSZ aerogels that exhibited retained mesoporous structure, increased surface area, and minimized shrinkage upon exposure to higher temperatures in the expected use range.

3.1 Introduction to surfactant templating methods

The extreme material properties of aerogels make them useful for many applications, including thermoresisters, sensors, catalysis, sorption media, drug delivery, and electrodes in solid oxide fuel cells.[1,13,171,173,177,186,188] Due to having low thermal conductivities and an overall mesoporous and lightweight structure, the use of aerogels in thermal management systems is also promising, with applications including insulation, fire suits or blankets, aerospace, and aeronautics.[5,149,162,165–167] However, aerogels often suffer from sintering and densification when exposed to high-temperatures due to polycondensation reactions and structural rearrangement.[6,7] The pore structure and high surface area of the aerogel upon high-temperature exposure is required to leverage the benefits of aerogel properties in thermal management systems. Therefore, the collapse of the pore structure and decrease of surface area diminishes the utility of the material as a thermal insulator.

One of the ways that densification and surface area reduction of aerogels can be mitigated

during high-temperature exposure is by using surfactants to template the aerogels during sol-gel synthesis. Surfactants can be used as structure directing agents to control the pore structure of materials in the mesopore range, from 2 to 50 nm.[13] Surfactants are used in the synthesis of a variety of aerogels to template the mesoporous structure of aerogels during gelation and drying, optimizing pore size, surface area, and crystalline structure upon heat-treatment of the aerogel.[13–18] These optimized properties are due to the electrostatic repulsion and steric hinderance effect resulting from the presence of the surfactants.[17]

Surfactants, composed of a hydrophilic head and hydrophobic tail, are known to assemble at interfaces and in the bulk solution; this assembly is dependent on the surfactants' molecular structure and concentration in solution.[17] Within the aerogel system, surfactants provide a saturated absorption layer on the solvent surfaces which reduces interfacial energy, a major cause of surface tension leading to pore collapse and cracking during the drying process.[18] The surfactants are also used to control the size of the aerogel nanoparticles and crystalline growth via a capping effect to prevent overgrowth and agglomeration, leading to enhanced surface area. Surfactants can be used to support initial gel structure and improve mechanical properties by reducing phase separation in the sols through facilitation of thorough mixing.[88,104,263] For example, in the work of Ehgartner et al., the addition of cetrimonium bromide (CTAB) was found to be necessary to synthesize monoliths with homogeneous gelation in aerogels that were synthesized using MTMS and an organofunctional trialkoxysilane with a reactive functional group due to the polarity difference of these functional groups and the polar solvents used.[119]

Due to the amphiphilic nature of surfactants, certain types of surfactants are known to form micelles, either spherical or rod-shape, at or above the critical micelle concentration (CMC) of the surfactant.[329] When surfactants are used to form pores, the formation and integration of micelles in sols is extremely important. By adding surfactants to the aerogel solution prior to gelation, surfactants act as structure directing agents as the gel forms around the micelles.[13] The precursor particles will aggregate around the micelles and, following the

addition of the gelation agent, the precursor particles form a solid network around the micelles. The presence of the surfactants typically does not impede the formation of the solid gel matrix.[330] The surfactants are removed from the aerogel system following washing or high-temperature exposure; when the gels are exposed to temperatures above 350°C, either through drying to form aerogels or post-processing heat-treatment, the surfactant micelles are oxidized and burned off, leaving behind tunable, uniform pores within the aerogel.[18,331] The surfactant templating process is depicted in Figure 6. It was anticipated that by templating aerogel pores with surfactants, pore structure and high surface area would be maintained when aerogels were exposed to high temperatures as the resulting pore structure of the aerogel was influenced by the type and concentration of the surfactant used during synthesis. It should be noted that while surfactants aid in templating aerogel pores, not all pores are templated from surfactant micelles and instead result from the aggregation of solid precursor particles and the subsequent formation of the gel network. Surfactants are not required for the synthesis of aerogels; however, surfactant templating can be used to influence the aerogel pore structure.

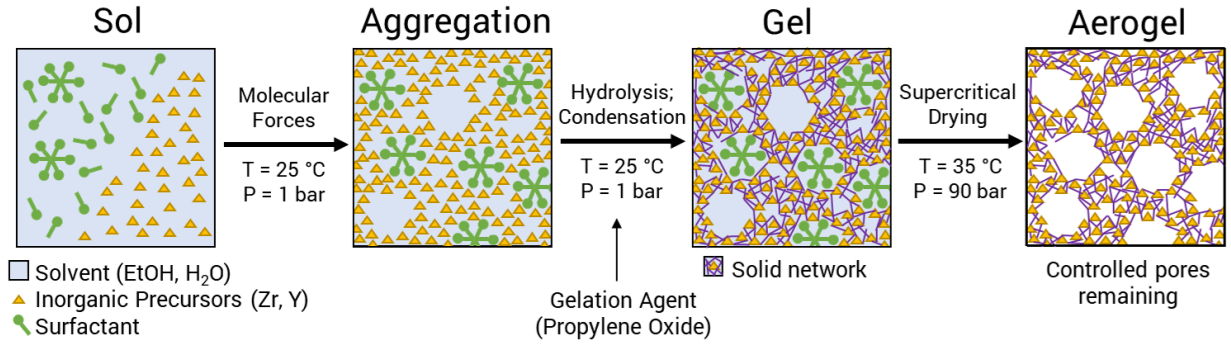

Figure 6: Surfactant templating during sol-gel synthesis of aerogels. Following formulation of the sol, precursors aggregate surrounding surfactant micelles, forming a solid gel network; surfactants are removed from the aerogel network through washing, supercritical drying and/or heat-treatment, leaving behind tunable, uniform pores.

As an example of surfactant templating, Chen et al. compared the usage of the cationic surfactant cetrimonium bromide (CTAB), the anionic surfactant surfactant sodium dodecyl sulfate (SDS), and the amphoteric surfactant surfactant lauramidopropyl betaine (Ralufon

414) in silica hydrosol based aerogels.[88] The hydrophilic heads of a cationic surfactant hold a positive charge, anionic surfactant heads hold a negative charge, and amphoteric, also called zwitterionic, surfactant heads hold both positive and negative charges. This study determined that the cationic surfactant, CTAB, and the anionic surfactant, SDS, produced more thermally stable, higher surface area aerogels than the amphoteric surfactant, Ralufon 414, at higher temperatures. This was due to pore structure collapse and coarsening of the solid network at 600°C of the aerogel synthesized with Ralufon 414. Sai et al. determined that CTAB and polyethylene glycol (PEG) inhibited cracking and increased monolithicity in silica aerogels that were produced via ambient pressure drying.[15] It was also found that the optical transmission of the surfactant-templated aerogels decreased when the surfactant concentration increased. While small amounts of CTAB increased the pore size and volume of the aerogels, large amounts of CTAB caused a decrease in pore size and volume due to large shrinkages following drying as CTAB decreased the skeleton strength of the aerogels. In addition, PEG was found to increase the pore size and pore volume of the aerogels; however, the pores were reduced when the amount of PEG was increased.

As an example pertaining to zirconia aerogels, Jung et al. used the cationic surfactant, CTAB, and the non-ionic surfactants, Brij® S10 and Pluronic® P-123 (P-123), in the sol-gel process of ambient pressure dried zirconia aerogels.[18] It was determined that each of these surfactants increased the specific surface areas of the aerogels; CTAB was shown to increase the specific surface area by up to 89% due to the electrostatic attractive force between CTAB and the zirconia matrix. The surfactants were also shown to enhance the thermal stability of the aerogels because of the retention of large specific surface areas following high-temperature exposure at 400°C. The addition of surfactants during the sol-gel process inhibited pore structure collapse of the aerogels. The cationic surfactant, CTAB, exhibited the highest effectiveness in preventing pore collapse due to the steric effects of the larger molecular weight surfactant. Additionally, Bangi et al. synthesized zirconia aerogel powders using Brij®-76; the aerogel powders demonstrated a well-ordered mesoporous structure and

amorphous morphology without any heat-treatment.[13]

In this dissertation, we explored the use of surfactant templating agents to control the porosity of yttria-stabilized zirconia (YSZ) aerogels following high-temperature exposure. Zirconia aerogels were first known to be synthesized by a non-alkoxide, epoxide addition sol-gel route by Chervin et al. in 2005.[8] The zirconia aerogel system was chosen because, although zirconia aerogels on average have lower surface areas and higher thermal conductivities than silica aerogels, the higher melting point of zirconium dioxide (2715°C) allows zirconia aerogels to remain thermally stable between 600°C and 1000°C where silica aerogels begin to sinter and densify.[7,9–11] Adding yttrium to the zirconia system also makes these materials advantageous as, even when not in aerogel form, the YSZ system is thermally stable; the addition of yttrium stabilizes the tetragonal zirconia phase, which prevents transformation to the monoclinic phase, thereby lowering the thermal conductivity of the system (2.2 - 2.9 W/m·K).[5,12] By making YSZ into aerogels, this thermal conductivity is further decreased to be as low as 0.168 W/m·K by leveraging the high porosity and high surface area properties of the aerogels. We anticipated that by adding surfactant to the formulation of the aerogels during sol-gel synthesis, we could control the pore structure of the aerogels and we could attenuate the negative effects, such as densification and decrease of surface area, due to heat-treatment.

3.2 Experimental methods: Yttria-stabilized zirconia aerogels with surfactant templates

A wide variety of surfactants (cationic, anionic, and non-ionic surfactants) can be used as templating agents for aerogels, including cetrimonium bromide (CTAB), sodium dodecyl sulfate (SDS), polyethylene glycol (PEG), Brij® S10, Brij®-76, and Pluronic® P-123 (P-123).[32,88,237,332] In this dissertation, the cationic surfactant cetrimonium bromide (CTAB), the anionic surfactant sodium dodecyl sulfate (SDS), and the nonionic surfactant Pluronic® P-123 (P-123) were used as templating agents for yttria-stabilized zirconia aerogels. Follow-

ing gelation, drying, and heat-treatment, the aerogels were characterized using a variety of techniques to determine the influence of surfactant on the pore structure, surface area, and crystallite size.

Yttria-stabilized zirconia (YSZ) aerogels were synthesized, as depicted in Figure 6, using a similar sol-gel procedure to the one used by Hurwitz et al.[22] Zirconyl chloride octahydrate, $ZrOCl_2 \cdot 8\,H_2O$, and yttrium(III) chloride hexahydrate, $YCl_3 \cdot 6\,H_2O$, were used as the zirconium and yttrium precursors, respectively. The precursors were mixed at room temperature with the solvents, ethanol and deionized water, to create the sol. To minimize experimental variables, a value of 20 mol% for yttria content was chosen because this mole ratio retained mesoporous structure and smaller particle size after high-temperature exposure compared with lower dopant levels in prior work completed by Hurwitz et al.[22] Higher yttria content was also shown to increase the thermal stability of YSZ aerogels.[333] Regarding water content, twice the stoichiometric amount (2x water) was chosen, as this water level was shown to synthesize aerogels with higher surface area and pore volume at high temperature than higher water levels following experimentation.

Prior to gelation, the surfactants chosen for this study, cetrimonium bromide (CTAB), sodium dodecyl sulfate (SDS), or Pluronic® P-123 were added to the sol as a multiple of the surfactant's critical micelle concentration (CMC), the determination of which is discussed in section 4.2, section 5.2, and section 6.2, respectively. To determine the influence of surfactant on the aerogel pore structure, 0.5x and 2x the CMC of CTAB, 0.5x, 2x,and 3x the CMC of SDS, and 0.5x, 2x,and 3x the CMC of P-123 were added to the formulations. Aerogels without surfactant were also synthesized for comparison. The molar ratios of surfactant to inorganic precursors used for each surfactant in the sol is further discussed in the following sections. For CTAB aerogels, the sols were mixed for a couple of hours, while for SDS and P-123 aerogels, the sols were mixed overnight to allow for complete dissolution of the surfactants and precursors.

Following further mixing of the sol in an ice bath, the gelation agent, propylene oxide,

was added to the chilled sol. Immediately after the addition of propylene oxide, the sol was poured into the aerogel molds; gelation typically occurred within 10 minutes. After 24 hours of aging, the gel was washed in 200 proof ethanol for 5 - 8 days. The gel was then supercritically dried using carbon dioxide. The supercritical drying process exchanged the solvent in the gel's pores with air, transforming the gel into an aerogel. Following drying, a selection of the aerogels were heat-treated in high-purity alumina boats under flowing argon at temperatures of 600°C, 1000°C, and 1100°C for 18 minutes. The ramp rate of the tube furnace was 5°C/min.

3.3 Characterization methods: Yttria-stabilized zirconia aerogels with surfactant templates

Following synthesis, as-dried and heat-treated aerogels were characterized using a variety of techniques. As-dried shrinkage and density were determined through physical measurement using a digital caliper. Scanning electron microscopy (SEM) was performed using a Hitachi SU-70 FE-SEM (CTAB) and a Hitachi S-4700 FE-SEM (CTAB, SDS, and P-123) to show, qualitatively, the effects of surfactant on microstructure. The SEM samples were uncoated and imaged at 1 - 2 kV with a working distance of 4.5 - 9.0 mm. Nitrogen adsorption/desorption was conducted on a Micromeritics ASAP 2020 Plus instrument (CTAB), a Micromeritics ASAP 2020 instrument (CTAB), and a Tristar II 3020 (Micrometrics Instrument Corporation) instrument (SDS and P-123) following degas at 80°C overnight; the surface area of the aerogels was determined using the Brunauer–Emmett–Teller (BET) method and the pore size distribution was determined from the desorption isotherm using the Barrett-Joyner-Halenda (BJH) method, which accounts for open pores less than 100 nm in size only.[325,326] Following the measurement, pore size distributions of the aerogel samples were determined by plotting the pore volume (cm^3/g) as a function of the pore diameter (nm). An Empyrean Multipurpose X-ray diffractometer (CTAB) and a Bruker D8 Advance X-ray diffractometer (SDS and P-123) were used to determine surfactant effects

on crystalline phase transformation and average crystallite size for heat-treated aerogels. Cu Kα (1.54059 Å) radiation was used from 10°to 90° 2θ. Profile fitting in HighScore Plus by Malvern Panalytical and the cubic phase YSZ powder diffraction file (PDF) reference card were used to analyze the aerogel samples. To determine the average crystallite size for each sample, the Scherrer equation, the Monshi-Scherrer (M-S) method, the Williamson-Hall (W-H) method, and the Size-Strain-Plot (SSP) method were used.[334] Transmission electron microscopy (TEM) was conducted using a JEOL JEM-F200 Cold FEG Electron Microscope (CTAB) and a FEI Talos TEM (SDS and P-123) with an accelerating voltage of 200 kV to confirm the effects of surfactant on crystallite size.

Chapter 4 Yttria-stabilized zirconia aerogels with surfactant templates, part I: Cationic surfactant templating

The cationic surfactant, with a positively charged hydrophilic head, cetrimonium bromide (CTAB), was used as a surfactant template in this dissertation. It was anticipated that surfactant templating with CTAB would enable the retention of the pore structure and high surface area of yttria-stabilized zirconia (YSZ) aerogels upon high-temperature exposure so that the benefits of aerogel properties could be leveraged for use in thermal management systems. We predicted that the addition of CTAB would increase the surface area, pore volume, and pore size of as-dried YSZ aerogels. In addition, it was anticipated that CTAB would attenuate the decrease of the surface area and pore volume accompanying heat-treatment of the aerogels. The mesoporous structure of YSZ aerogels suppresses gas convection due to the small pore size, but the retention of open pore volume is critical for reducing solid conduction through the material. Successful surfactant templating of YSZ aerogels would improve the effectiveness of these materials when used in the expected use range of 600°C to 1000°C.

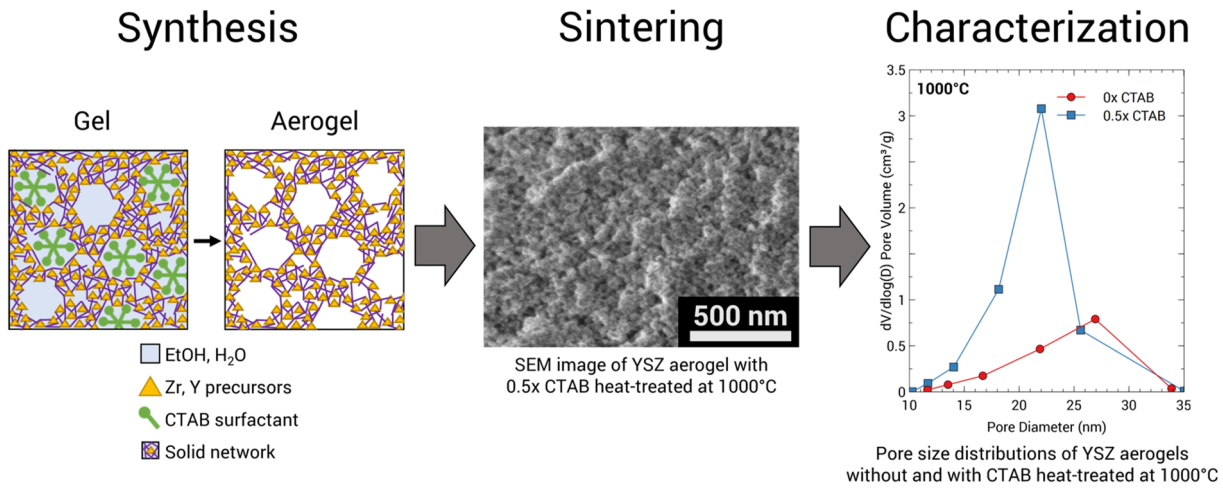

Figure 7: Surfactant templating with CTAB. Surfactant templating of YSZ aerogels with the cationic surfactant cetrimonium bromide (CTAB) to mitigate surface area decrease and pore volume collapse following high-temperature exposure.

4.1 Cationic surfactant templating: CTAB templating

As an example of using CTAB as a surfactant template in zirconia aerogels, Jung et al. found that in the synthesis of ambient pressure dried zirconia aerogels, the addition of CTAB increased the specific surface area of the aerogels by up to 89%.[18] High surface area was retained after annealing at 400°C, indicative of an enhanced thermal stability of the aerogels synthesized with CTAB. In the sol-gel synthesis of alumina-zirconia nanopowders, Rezaee et al. determined that the addition of CTAB synthesized smaller nanoparticles with narrow size distribution and higher surface areas as compared to nanoparticles synthesized with nonionic surfactants.[17] When dissolved in solvent, CTAB is known to release cations that can interact with the zirconia matrix. The cationic charges lead to an induced repulsive force between collections of zirconia during the drying process, which can prevent shrinkage of the pore system caused by capillary forces. The repulsive forces between the cation and the zirconia matrix are ultimately the cause of increased surface area in zirconia aerogels templated with CTAB. The addition of CTAB also improves the emulsification of the sol, leading to a more homogeneous resulting material. Additionally, CTAB discourages agglomeration and controls particle geometry by adsorbing onto the surface of precursor particles.

However, the adsorption of CTAB on the aerogel matrix by electrostatic attraction has been known to decrease the skeleton strength of the aerogel, which can lead to shrinkage during drying. Interestingly, Sai et al. determined that small amounts of CTAB increased pore size and volume of silica aerogels, while larger amounts of CTAB reduced pore size and volume.[15] Huang et al. demonstrated a similar result where larger concentrations of CTAB led to smaller pores and weakened skeletons in silica aerogels.[335] Therefore, in this work, the amount of CTAB needed to be optimized to mitigate pore shrinkage, surface area loss, densification, and sintering, which would enhance the mesoporous structure of the aerogel.

Here, it was determined that adding one-half times the critical micelle concentration of CTAB increased the surface area of the aerogels by 72% and 41% and increased the pore volume following exposure to 600°C and 1000°C, respectively. This level of CTAB had the

greatest increase in surface area and pore volume as compared to aerogels without CTAB or with twice the critical micelle concentration of CTAB. By optimizing the concentration of CTAB, the thermal stability of YSZ aerogels can be enhanced to make these materials more efficient when used as thermal management systems, specifically for aeronautics and aerospace applications. The optimization of aerogels used in these applications will lead to increased effectiveness and thermal stability of the systems up to temperatures of 1000°C.

4.2 Cationic surfactant templating: CTAB concentrations

Prior to gelation, the chosen surfactant, cetrimonium bromide, CTAB, was added to the sol as a multiple of the surfactant's critical micelle concentration (CMC). The CMC of CTAB varied when ethanol was added to the solution; the CMC increased as the ethanol volume fraction increased. This change in CMC was taken into account in the YSZ aerogel formulations, as CMC values of CTAB at varying ethanol fractions were estimated from a thermodynamic model.[336] For the aerogel formulation used in this work, the CMC of CTAB was estimated to be 0.230 M. The addition of the inorganic salts $ZrOCl_2 \cdot 8\,H_2O$ and $YCl_3 \cdot 6\,H_2O$ was determined to have a negligible effect on the CMC of CTAB, as the decrease in CMC due to the salt addition was shielded by the large increase of the CMC due to the ethanol addition. For these experiments, the effect of ethanol on the CMC values of CTAB was considered only. To determine the influence of different concentrations of CTAB on the aerogel pore structure, 0.5x the CMC of CTAB and 2x the CMC of CTAB were added to the formulations. The molar ratio of CTAB to inorganic precursors was 0.13 for 0.5x CTAB and 0.50 for 2x CTAB, summarized in Table 3.

Table 3: Molar ratios of surfactant CTAB to inorganic precursors. Molar ratios of the surfactant cetrimonium bromide (CTAB) to the inorganic precursors, zirconia and yttria, in the aerogel formulations at concentrations of 0.5x and 2x the CMC. The CMC of CTAB used in the formulations is also included.

		Molar Ratios	
Surfactant	**CMC (M)**	**0.5x**	**2x**
CTAB	0.230	0.13	0.50

4.3 Cationic surfactant templating: Results and discussion

Physical measurements taken after supercritical drying were used to determine the as-dried shrinkage and density, displayed in Table 4 of the YSZ aerogels. The as-dried shrinkage was the percent change of the as-dried aerogel monolith diameter with respect to the original diameter of the gelation mold. It was determined that the as-dried shrinkage increased as the CTAB level was increased. The shrinkage was 17 ± 1.1% for aerogels without CTAB, 20 ± 1.1% for 0.5x CTAB aerogels, and 25 ± 1.1% for 2x CTAB aerogels. While added CTAB increased the as-dried shrinkage, 2x CTAB was shown to have the greater increase. This effect could have been the result of a reduction in the skeleton strength of the aerogel at higher CTAB amounts, which is further elaborated below. The density remained approximately constant when the amount of CTAB was changed: 0.261 ± 0.012 g/cm^3 at 0x CTAB, 0.251 ± 0.012 g/cm^3 at 0.5x CTAB, and 0.252 ± 0.012 g/cm^3 at 2x CTAB.

Table 4: Shrinkage and density of YSZ aerogels with varying CTAB levels. As-dried shrinkage for YSZ aerogels with varying levels of CTAB determined through physical measurement.

CTAB	**Shrinkage (%)**	**Density (g/cm^3)**
0x	17 ± 1.1	0.261 ± 0.012
0.5x	20 ± 1.1	0.251 ± 0.012
2x	25 ± 1.1	0.252 ± 0.012

Figure 8 displays the pore size distributions of the YSZ aerogels at different levels of CTAB. Figure 8A is the pore size distribution for as-dried aerogels, Figure 8B is the pore

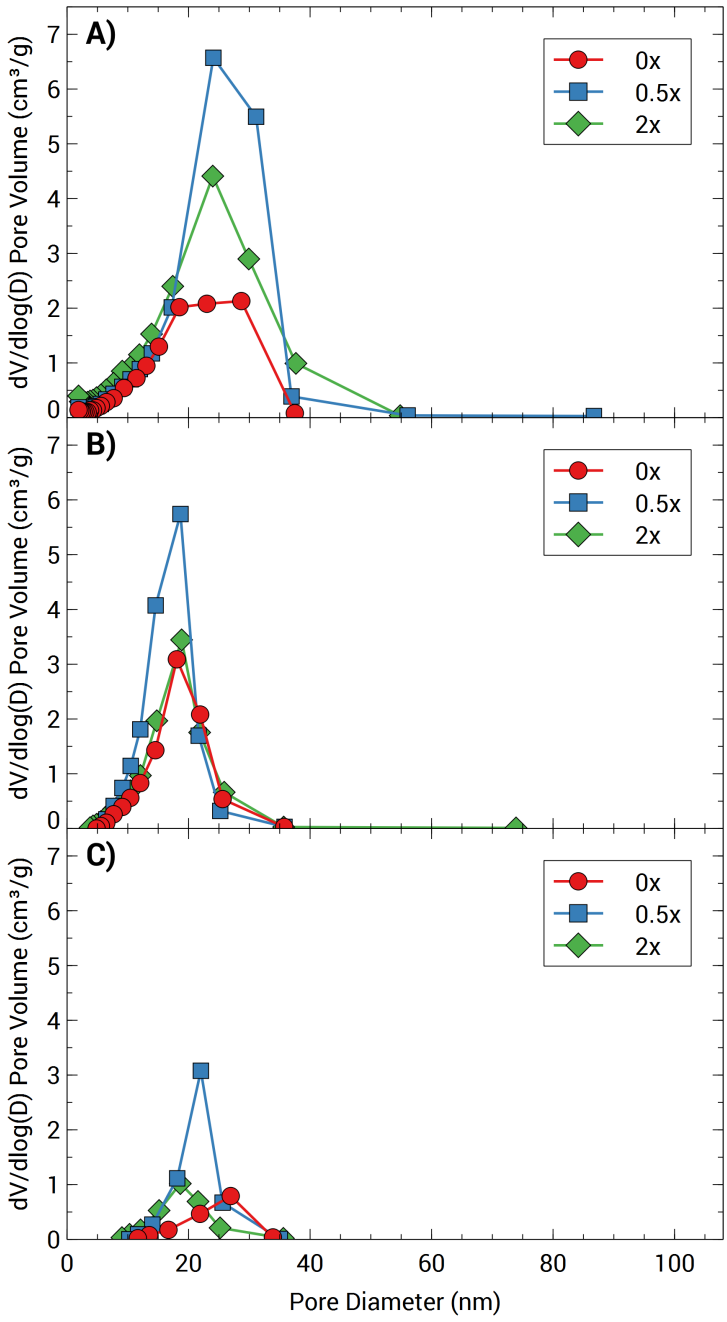

Figure 8: Pore size distributions of YSZ aerogels with varying CTAB levels and heat-treatment. Pore size distributions of YSZ aerogels at 0x CTAB, 0.5x CTAB, and 2x CTAB at heat-treatment conditions of A) as-dried, B) 600°C, and C) 1000°C.

size distribution at 600°C, and Figure 8C is the pore size distribution at 1000°C. Three different concentrations of CTAB are displayed on each plot and represented as different marker shapes: 0x CTAB (circle), 0.5x CTAB (square), and 2x CTAB (diamond). Considering the as-dried aerogel samples, the aerogel without CTAB had a pore size distribution between 0 nm and 40 nm, while the aerogels with 0.5x CTAB and 2x CTAB had wider pore size distributions within 0 nm and 80 nm and within 0 nm and 55 nm, respectively. Figure 8 showed that aerogels heat-treated at 600°C had similar pore sizes, regardless of CTAB content. At 600°C, the pore size distributions ranged from 5 to 35 nm with major distributions at 18 nm. For aerogels heat-treated at 1000°C, the pore size distributions ranged from 10 to 35 nm with the major pore size distributions shifting to smaller pore sizes with increasing CTAB amount, from 28 nm (0x CTAB) to 22 nm (0.5x CTAB) and 18 nm (2x CTAB). As a templating agent, the micelle size of CTAB can be affected by many factors, such as concentration, temperature, and pH.[337] CTAB forms micelles with diameters of 2 to 3 nm in water. In this study, the precursor solution, prior to the addition of CTAB, had a pH of 1. At this pH, it was estimated according to the work reported by Patel et al. describing the influence of solution pH on the size of CTAB micelles that the hydrodynamic diameter of CTAB was approximately 25 nm, which was closer to the measured pore size distribution of the aerogels.[338] It should be noted that, since nitrogen physisorption only measures pores less than 100 nm, the actual distribution could have included pores that were greater than 100 nm but were not measured by nitrogen physisorption. No macroporosity was observed in the SEM images of the as-dried samples, which are not displayed here. Because of this, it was determined that the distribution seen in nitrogen physisorption was representative of the range of pore sizes in the sample.

The BET surface area (m^2/g) and BJH desorption cumulative pore volume (cm^3/g) values of YSZ aerogels without and with CTAB are displayed in Figure 9A and Figure 9B, respectively. The addition of CTAB was shown to increase the surface area of the as-dried YSZ aerogels, with 0.5x CTAB increasing the surface area by 53% to 403 m^2/g and 2x

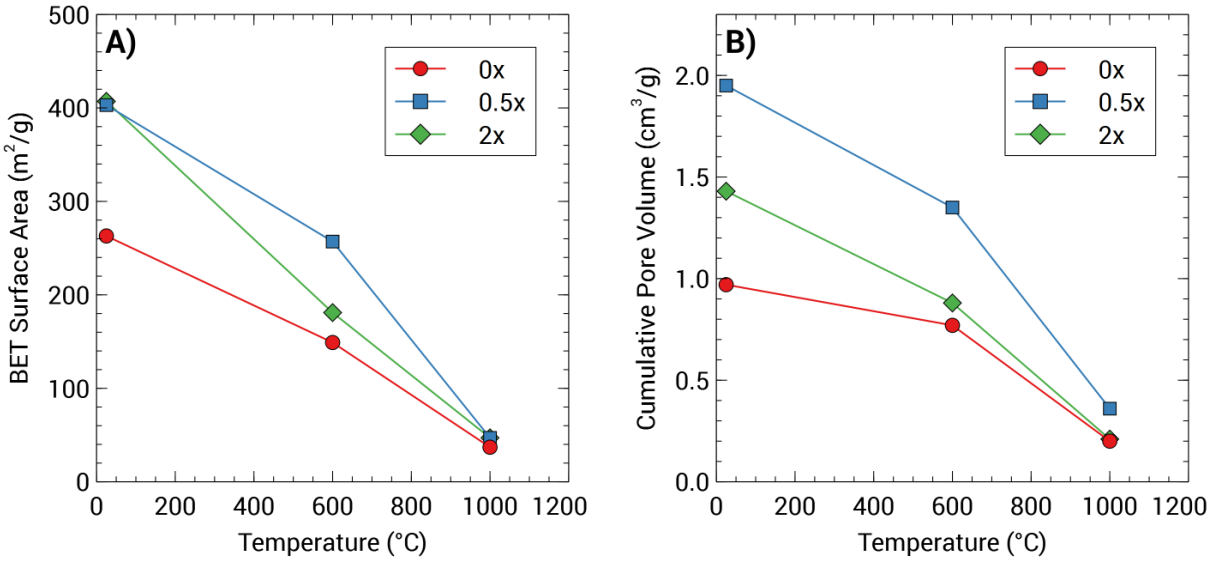

Figure 9: BET surface area and BJH desorption cumulative pore volume of YSZ aerogels with varying CTAB levels and heat-treatment. A) BET surface area (m^2/g) and B) BJH desorption cumulative pore volume (cm^3/g) for YSZ aerogels with varying concentrations of CTAB at as-dried, 600°C, 1000°C, and 1100°C heat-treatment conditions.

CTAB increasing the surface area by 55% to 407 m^2/g, as compared to the aerogel without CTAB at 263 m^2/g. Once the aerogels were heat-treated, the surface areas were shown to decrease, which was indicative of sintering following high-temperature exposure. However, the addition of CTAB was shown to increase the surface area of the aerogels at 600°C and 1000°C. At 600°C, the addition of 0.5x CTAB and 2x CTAB increased the surface area by 72% to 257 m^2/g and by 21% to 181 m^2/g, respectively, as compared to the aerogel without CTAB at 149 m^2/g. At 1000°C, the surface area increased by 41% to 52 m^2/g with 0.5x CTAB and by 27% to 47 m^2/g with 2x CTAB as compared to the aerogel without CTAB at 37 m^2/g.

Regarding cumulative pore volume, for the as-dried aerogels, the aerogel with 0.5x CTAB had the highest pore volume of 1.95 cm^3/g, while the aerogel with 2x CTAB had a pore volume of 1.43 cm^3/g. Compared to the aerogel without CTAB, with a pore volume of 0.97 cm^3/g, the addition of CTAB was shown to increase pore volume. Aerogels with 0.5x CTAB and 2x CTAB displayed a decrease in pore volume as heat-treatment temperature

increased, which was expected due to sintering and densification. However, the aerogels with 0.5x CTAB had larger pore volumes at 600°C and 1000°C (1.35 cm^3/g and 0.36 cm^3/g, respectively) than the aerogels without CTAB (0.77 cm^3/g and 0.20 cm^3/g) and with 2x CTAB (0.88 cm^3/g and 0.21 cm^3/g). Specifically, the addition of 0.5x CTAB was shown to enable the retention of a measurably larger total pore volume following heat-treatment at 600°C and 1000°C than the aerogels without CTAB or with 2x CTAB.

The addition of 0.5x CTAB was shown to be more effective at inhibiting surface area decrease and pore collapse following high-temperature exposure as aerogels with 0.5x CTAB showed the overall highest surface area and pore volume following heat-treatment. The larger pore volume would most likely lower the solid conduction of the aerogel, enhancing the use of the aerogel as a thermal insulator. This result was surprising, as it was predicted that a larger amount of CTAB would more effectively template the aerogel pores. This result could have been influenced by the estimation of the critical micelle concentration of CTAB. The effect of ethanol was considered when estimating the CMC values; however, other factors, including the inorganic salt concentration, could have influenced the CMC, but were not considered in the estimate. The pore size distribution in Figure 8 was narrower at 0.5x CTAB than at 2x CTAB for as-dried aerogels, pointing to a more homogeneous pore structure during synthesis, and suggesting that 0.5x CTAB may have been closer to the actual CMC.

Alternatively, the addition of 2x CTAB could have had a negative effect on the surface area and pore volume of the heat-treated aerogels because a larger amount of surfactant was detrimental to the aerogel structure. This was supported by the study conducted by Sai et al. which determined that, at higher amounts, the polar head groups of CTAB may have interacted with the zirconia domains, adsorbing onto the aerogel backbone by electrostatic attraction.[15,18] The steric hindrance caused by this adsorption could have constrained the gelation reaction, causing a reduction of the skeleton strength of the gel and leading to increased shrinkage during drying.

Scanning electron microscopy (SEM) was used to determine how the pore structure of

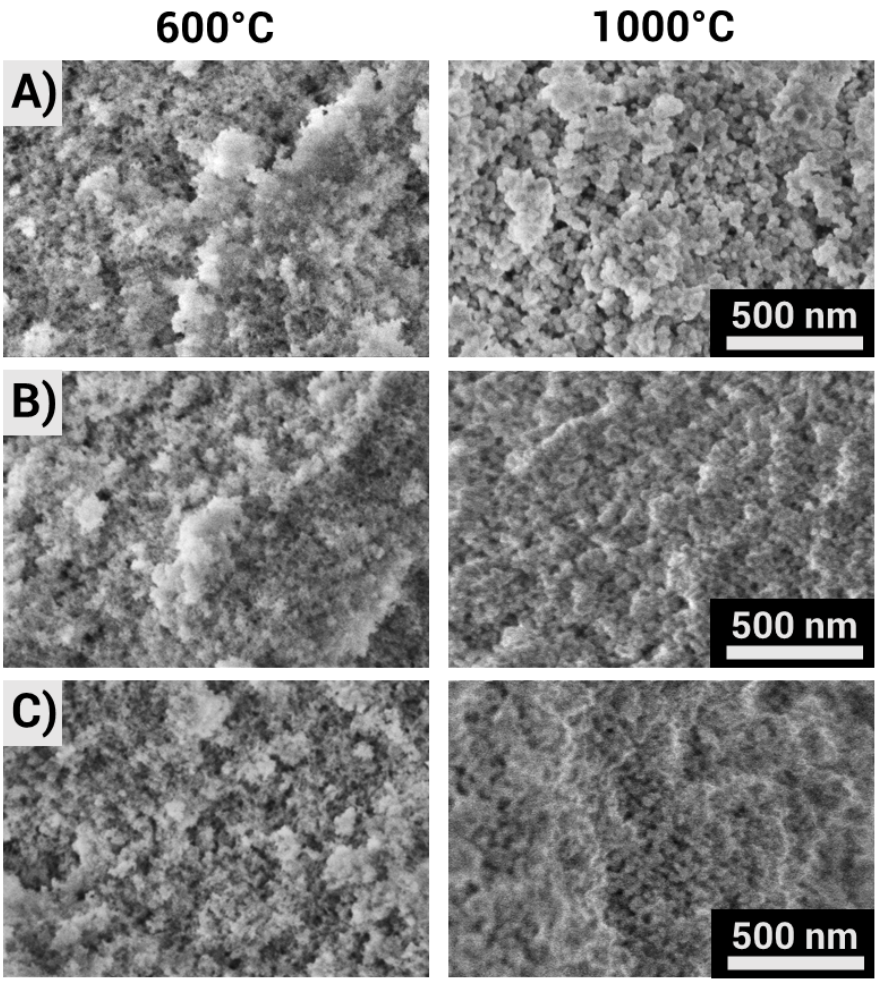

Figure 10: SEM images of YSZ aerogels with varying CTAB levels and heat-treatment. SEM images of YSZ aerogels at two different heat-treatment conditions, 600°C (left) and 1000°C (right), for aerogels with A) 0x CTAB, B) 0.5x CTAB, and C) 2x CTAB.

the YSZ aerogels was affected by high-temperature exposure. Figure 10 displays SEM images of YSZ aerogels with 0x CTAB (Figure 10A, 0.5x CTAB (Figure 10B), and 2x CTAB (Figure 10C) following heat-treatment at 600°C for 18 min (left) and at 1000°C for 18 min (right). Sintering and densification of the aerogels without CTAB were evident following high-temperature exposure, especially noticeable at 1000°C. This behavior was anticipated and is typical for metal oxide materials exposed to high temperatures. With the addition of CTAB, the aerogel structures were less dense or coarse than those without, especially at 1000°C. It was predicted that the addition of CTAB would template distinct pores within the aerogel structure, even after exposure to 1000°C. However, while a slight shift in pore size could be observed, it was difficult to assign statistical significance to the difference.

X-ray diffraction (XRD) was used to determine the crystalline phase transformation and crystallite size following heat-treatment of YSZ aerogels with different amounts of CTAB. Figure 11 displays the XRD patterns of YSZ aerogels at different surfactant levels and heat-treatment conditions. The aerogel that was not heat-treated was non-crystalline or amorphous; this was true for all as-dried samples, regardless of CTAB loading. The aerogel samples that were heat-treated at 600°C and 1000°C were all crystalline, regardless of CTAB content. The XRD patterns in Figure 11 for the YSZ aerogels without CTAB showed increased crystallinity with heat-treatment. The as-dried sample had very broad peaks, indicative of an amorphous structure, while the sample heat-treated at 600°C displayed sharper, more defined peaks, exhibiting some crystallization of the material. It was determined from these patterns that the YSZ aerogel transformed from an amorphous structure to a crystalline structure by 600°C. When comparing to the sample at 600°C, the 0x CTAB sample that was heat-treated at 1000°C displayed even sharper and more defined peaks, possibly indicative of increased crystallite size following exposure to increased temperatures. When considering Figure 9, it was determined that increasing crystallite size was accompanied by a decrease of surface area and pore volume.

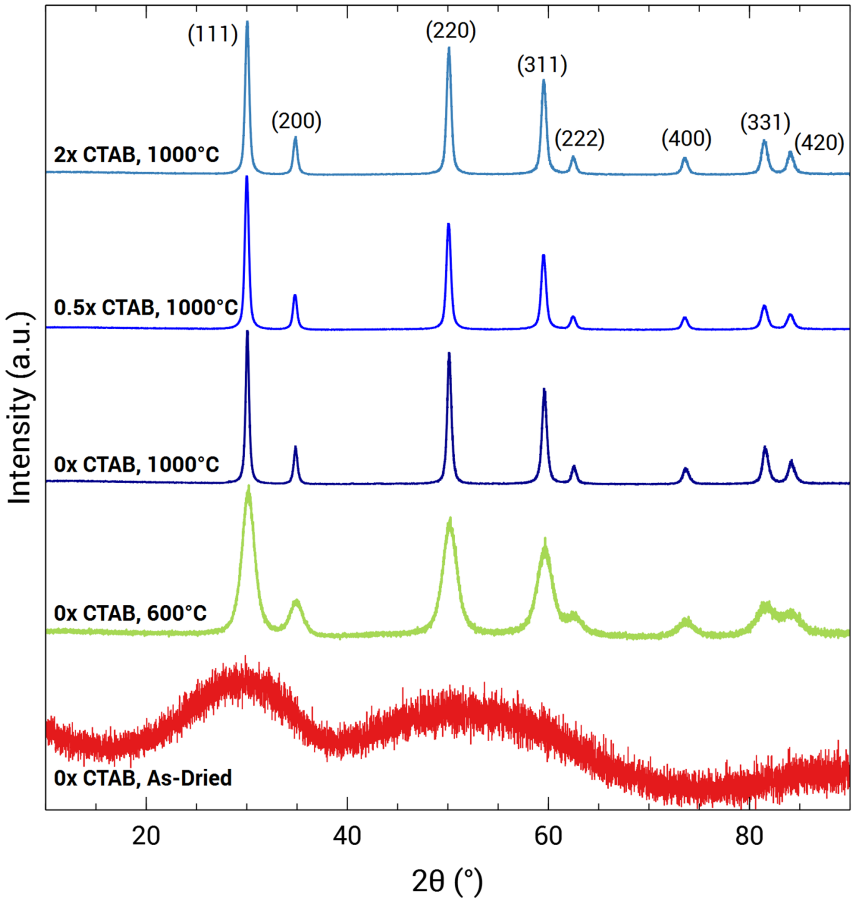

Figure 11: XRD patterns of YSZ aerogels with varying CTAB levels and heat-treatment. XRD patterns for YSZ aerogels with 0x CTAB, 0.5x CTAB, and 2x CTAB at various heat-treatment conditions of as-dried, 600°C, and 1000°C. The Miller indices (hkl values) are displayed at the top of the figure.

Table 5: Average crystallite size of YSZ aerogels with varying CTAB levels and heat-treatment. Average crystallite size values (Å) for 0x CTAB, 0.5x CTAB, and 2x CTAB YSZ aerogels at 600°C and 1000°C determined through XRD and TEM analysis. Four different equations were used to determine the crystallite size following XRD analysis.

CTAB Concentration	**Temperature (°C)**	**Crystallite Size via XRD (Å)**	**Crystallite Size via TEM (Å)**
0x	600	62 ± 5	61 ± 13
	1000	239 ± 37	270 ± 63
0.5x	600	61 ± 4	73 ± 14
	1000	209 ± 13	216 ± 54
2x	600	59 ± 4	76 ± 17
	1000	200 ± 6	214 ± 55

Following analysis, it was determined that the peaks for all the heat-treated samples were indicative of the cubic YSZ crystalline phase. This was expected as, based on the YSZ phase diagram, the cubic phase should be the primary phase for samples with 20 mol% Y at temperatures up to 2500°C.[339] There may have been small amounts of the tetragonal YSZ phase mixed with the cubic phase; however, the cubic peaks overlapped with the tetragonal peaks on the pattern, which made the presence of the tetragonal phase hard to determine. The addition of CTAB was shown to have no effect on the crystalline phase of the YSZ aerogels. Table 5 displays the average crystallite size of the YSZ aerogel samples in this study. The Scherrer equation, the conventional method for determining the crystallite size of particles, can only be utilized for crystallite sizes up to 1000 Å and often has error associated with it due to the instrument signal and noise. Therefore, as a way to compare the results of the Scherrer equation, the Monshi-Scherrer (M-S) method, the Williamson-Hall (W-H) method, and the Size-Strain-Plot (SSP) method were also utilized.[334] In Table 5, the XRD analysis values for the average crystallite size are the average and standard deviation of these four equations. At 600°C, the average crystallite size was smaller for each level of CTAB than the crystallite size at 1000°C. At 1000°C, the crystallite size was the smallest in YSZ aerogels with CTAB, as compared to the aerogel without CTAB.

Due to certain limitations and error associated with the XRD equations, TEM was con-

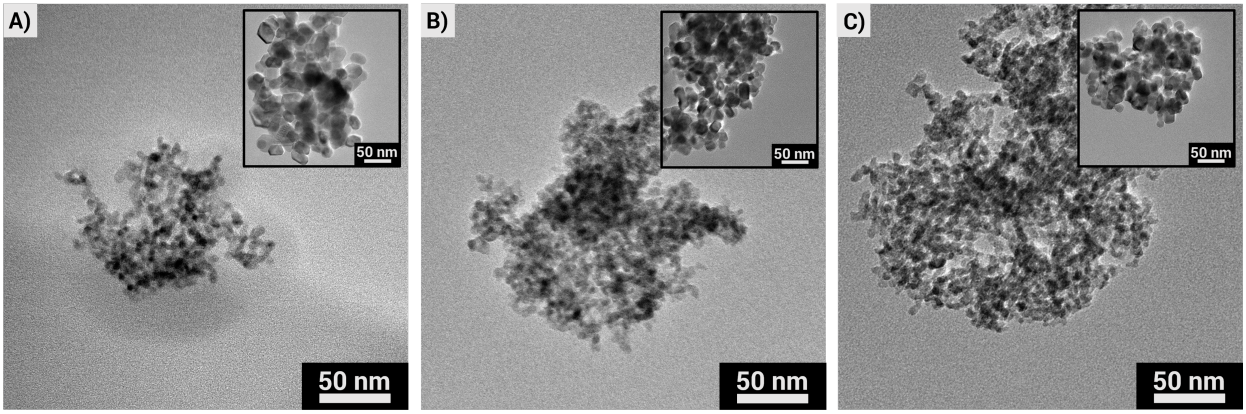

Figure 12: TEM images of YSZ aerogels with varying CTAB levels and heat-treatment. TEM images at 100k magnification of YSZ aerogels with A) 0x CTAB, B) 0.5x CTAB, and C) 2x CTAB that have been heat-treated at 600°C and 1000°C (inset).

ducted to confirm the values estimated from the XRD analysis. Figure 12 displays the TEM images of YSZ aerogels with 0x CTAB (Figure 12A), 0.5x CTAB (Figure 12B), and 2x CTAB (Figure 12C) that were heat-treated at two different conditions: 600°C and 1000°C (inset). The aerogels heat-treated at 600°C and 1000°C all appeared to display some crystallization, with the aerogels at 1000°C displaying larger crystallites than the aerogels at 600°C. Analysis of the TEM images determined that the average size of the crystallite particles, displayed in Table 5, increased by 343% at 0x CTAB, 196% at 0.5x CTAB, and 182% at 2x CTAB when the temperature was increased from 600°C to 1000°C, which further indicated that exposure to higher temperatures increased the crystallite size. This behavior was expected as heat-treatment is known to promote crystallization of the YSZ aerogels and to increase growth of the crystallite particles. Additionally, in Figure 12, the aerogel without CTAB appeared to have crystallites larger than the aerogels with CTAB at 1000°C. The TEM analysis confirmed the XRD results, which determined that the average crystallite size was smaller at 600°C than at 1000°C, as well as smaller in aerogels with CTAB than the aerogel without CTAB at 1000°C. It was determined that the addition of CTAB to the YSZ aerogels inhibited crystallite growth at 1000°C, which may have hindered surface area and pore volume decrease, as well as shrinkage, at high temperatures. YSZ aerogels with CTAB may show increased effectiveness when used at high-temperature if crystallite growth, and

accompanying surface area and pore volume decrease, can be impeded.

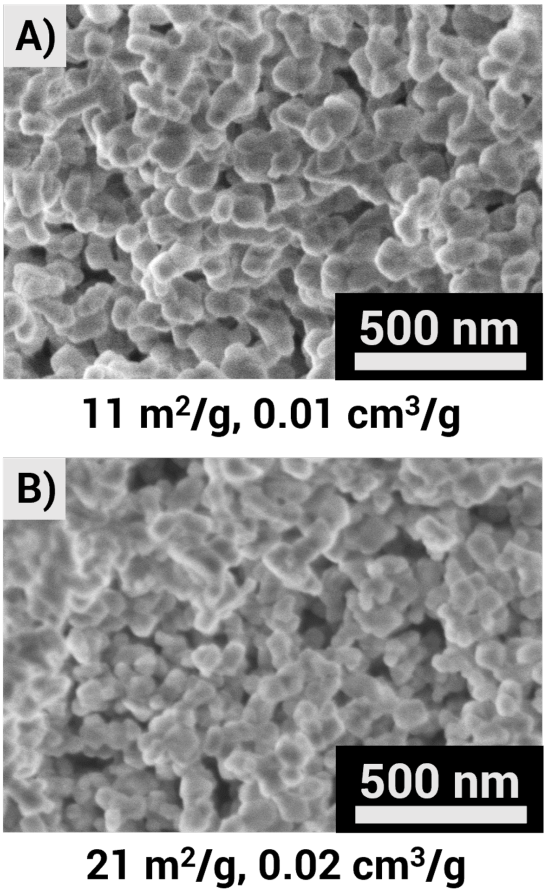

Figure 13: SEM images of YSZ aerogels at 1100°C with varying CTAB levels. SEM images of YSZ aerogels with A) 0x CTAB and B) 2x CTAB that were heat-treated at 1100°C. BET surface area and BJH desorption cumulative pore volume values are also displayed.

To further determine the effect of high-temperature exposure on aerogels without and with CTAB, selected aerogel samples were heat-treated at 1100°C for 18 min. Figure 13 displays the SEM images of YSZ aerogel samples with 0x CTAB (Figure 13A) and 2x CTAB (Figure 13B) that were heat-treated at 1100°C. The BET surface area and BJH desorption cumulative pore volume values are displayed below each sample. Heat-treatment at 1100°C was shown to cause further sintering and densification, in addition to larger particle growth, of the aerogels, as compared to the heat-treatment at 600°C and 1000°C displayed in Figure 10. The effect of CTAB was not distinctly apparent in the SEM images of the 0x CTAB and 2x CTAB aerogels. The YSZ aerogels without CTAB had a surface area and pore volume

of 11 m^2/g and 0.01 cm^3/g, respectively, following exposure to 1100°C. For aerogels exposed to the same temperature with 2x CTAB, the surface area and pore volume were 21 m^2/g and 0.02 cm^3/g, respectively. These results demonstrate that there was significant collapse of the pore structure at 1100°C. In order to extend the use range for these materials, it was determined that the formulation must be further optimized so that pore collapse and subsequent densification are mitigated. This optimization included investigating different surfactant types and concentrations to extend the use range of these materials above 1000°C.

Based on the study of the cationic surfactant CTAB, it was determined that 0.5x CTAB was an effective amount of CTAB to use as a surfactant template in YSZ aerogels as compared to 2x CTAB. This was in agreement with the study conducted by Sai et al. with silica aerogels which determined that smaller amounts of CTAB increased the pore size and pore volume of the aerogels.[15] The surface area of aerogels with 0.5x CTAB was higher following exposure to 600°C and 1000°C than aerogels without CTAB or with 2x CTAB. In addition, the pore volume at 0.5x CTAB was larger for both as-dried and heat-treated (600°C and 1000°C) aerogels than the pore volume of aerogels without CTAB and with 2x CTAB. The addition of CTAB releases cations, which attach to the zirconia aerogel network, inducing a repulsive force and effectively reducing shrinkage of the pore structure during drying.[18] The mitigation of shrinkage overall increases the surface area and pore volume of the aerogels following high-temperature exposure, allowing these materials to be used as effective thermal insulators.

However, following this investigation, it was believed that at the increased level of 2x CTAB, the higher concentration of cationic surfactant may have been negatively influencing the pore structure, which could have included a reduction in surface area and pore volume.[15] Cationic surfactants are known to adsorb onto the negatively charged surface sites of minerals through electrostatic attractions, often forming a dense electrical double layer at the solid-liquid interface.[340] When the concentration of surfactant increases, the hydrocarbon chains of the surfactants begin to aggregate and form two-dimensional structures called hemicelles.

We hypothesized that at the higher concentration of CTAB, the strength of the gelled matrix was decreased, making it more susceptible to shrinkage during drying and heat-treatment and reducing the surface area and pore volume of the aerogels. Similar interactions have been known to occur between CTAB and silica aerogels through settling of the polar head groups of CTAB towards the silica domain.[341,342] Additionally, CTAB was known to interact with negatively charged copper(II) hydroxide during the templating of cuprite nano-whiskers; this interaction influenced the structure and morphology of the final nano-materials.[343] YSZ aerogels with 2x CTAB exhibited decreased surface area and pore volume following high-temperature exposure as compared to aerogels with 0.5x CTAB; this surprising behavior may have been a result of the adsorption of CTAB, which may have impeded the extent of the gelled network.

4.4 Cationic surfactant templating: Conclusions

The addition of the cationic surfactant, cetrimonium bromide (CTAB), was shown to influence the mesoporous structure and surface area of 20 mol% Y, 2x H_2O yttria-stabilized zirconia (YSZ) aerogels. However, it was critical that the amount of CTAB used was optimized so that it was used at an amount that was low enough to inhibit interactions with the zirconia aerogel matrix that may have caused a reduction in surface area and pore volume yet high enough to be advantageous for surfactant templating. It was established following this study that 0.5x the critical micelle concentration (CMC) of CTAB was an ideal concentration for effective surfactant templating. The addition of 0.5x CTAB synthesized aerogels with higher surface area and pore volume following exposure to 600°C and 1000°C, as compared to aerogels without CTAB or with 2x the CMC of CTAB. It was anticipated that optimized surfactant templating would lead to the synthesis of YSZ aerogels with increased thermal stability. These materials would then be more efficient when used in thermal management systems in the expected use range of 600°C to 1000°C for a variety of applications, including aeronautics and aerospace applications.

Chapter 5 Yttria-stabilized zirconia aerogels with surfactant templates, part II: Anionic surfactant templating

Anionic surfactants, with a negatively charged hydrophilic head, were also studied as part of this dissertation. The anionic surfactants sodium dodecyl sulfate (SDS) was chosen as a nonionic surfactant template for 20 mol% YSZ aerogels. SDS has been previously used in silica aerogels and was shown to maintain high surface area and pore size in aerogels heat-treated at 600°C.[88] SDS has also been shown to lower the bulk density and thermal conductivity of silica aerogels.[330]

5.1 Anionic surfactant templating: SDS templating

The anionic surfactant, sodium dodecyl sulfate (SDS), is an organic sodium salt that has a wide scope of available literature, especially regarding the use of SDS as a detergent or protein denaturant. Additionally, SDS has been reported for use as a surfactant template in aerogels. At or above the critical micelle concentration (CMC) of SDS, the amphiphilic surfactant molecule forms micelles in solution with a hydrophobic core and hydrophillic shell; the micelles become embedded in the aerogel network through reactions involving hydroxyl groups.[88] The embedded SDS micelles influence the aerogel pore structure through steric hinderance effects, as well as through electrostatic interactions between the metal ions of the aerogel network and the negatively charged surfactant head groups. Similar to a cationic surfactant, anionic surfactants also release ions when dissolved in solution that interact with the zirconia aerogel matrix. The release of anions and subsequent induced repulsive force between the zirconia particles influence the aerogel pore structure, reducing the shrinkage and pore collapse of the aerogel caused by capillary forces during drying.[331] As mentioned previously, as a surfactant template, SDS also reduces the interfacial energy of the aerogel system, which reduces shrinkage and pore collapse during drying, and controls nanoparticle

growth, which inhibits agglomeration and increases surface area. As an example of SDS templating aerogels, SDS was used in ambient-pressure dried silica aerogels and resulted in larger pore volume and mean pore size.[141] SDS was also used to increase the thermal stability and surface area of silica aerogels exposed to 600 °C.[88] Additionally, SDS was shown to decrease density and thermal conductivity of silica aerogels.[330] SDS was used with a zirconia system in the synthesis of highly porous ceramic zirconia foams with low thermal conductivity; increasing concentrations of SDS resulted in foams with increasing porosity.[344]

5.2 Anionic surfactant templating: SDS concentrations through hydrodynamic radius measurements

Prior to the synthesis of the YSZ aerogels with SDS, the concentration of SDS that would be added to the aerogel formulations was determined. SDS was to be added as multiples (0.5x, 2x, and 3x) of the surfactant's critical micelle concentration (CMC) value in the YSZ sol. The CMC value was determined using a series of experiments where the surfactant was added to the base sol, which was the 20 mol% yttria, 2x water YSZ sol formulation used for all of the aerogels, at different concentrations prior to gelation. The surface tension and hydrodynamic radius of the surfactant at each concentration was then determined.

The surface tension of each solution was determined using a Sinterface Profile Analysis Tensiometer PAT1M. For SDS, there was determined to be no correlation between surfactant concentration and surface tension value. Surface tension was determined to be too sensitive of a measurement to see changes at the SDS concentrations analyzed.

The hydrodynamic radius of each solution was determined using dynamic light scattering on an ALV/CGS-3 Compact Goniometer from ALV-GmbH utilizing a vertically polarized 633 nm 22 mW laser. There was a correlation between hydrodynamic radius value and SDS concentration as seen in Figure 14. The hydrodynamic radius values were between 3.7 and 4.6 nm for SDS concentrations between 1 x 10^{-5} M and 1 x 10^{-2} M in the base sol. SDS concentrations above 1 x 10^{-2} M were not measured as SDS would not dissolve into the base

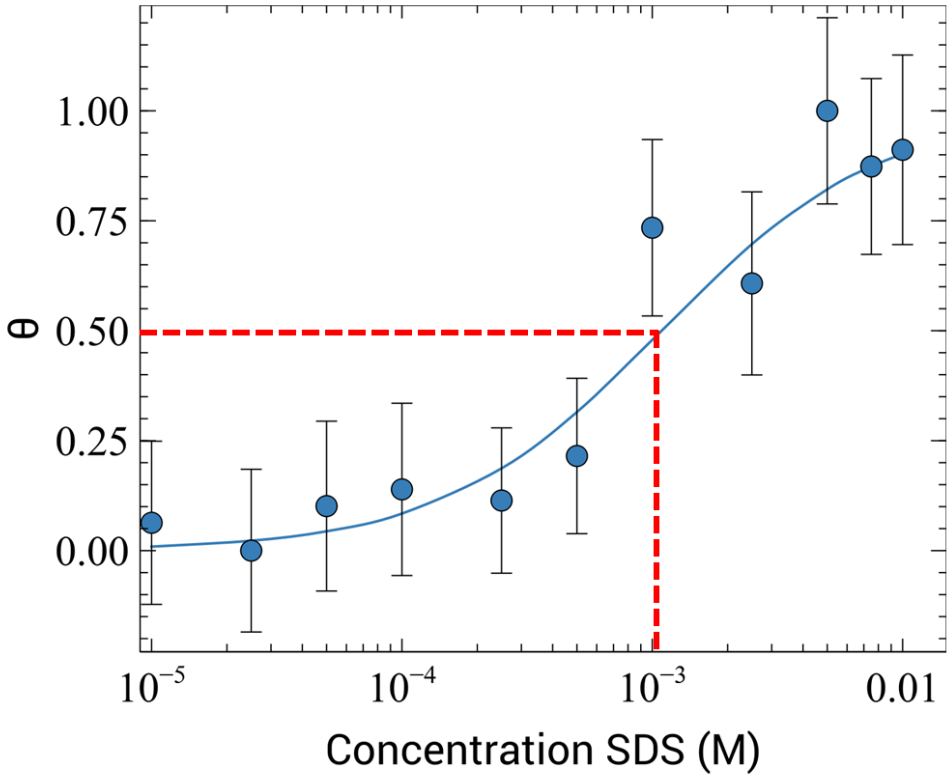

Figure 14: Theta (θ) as a function of surfactant concentration to determine the CMC of SDS. θ values, defined as (R - R_{min})/(R_{max} - R_{min}) where R is the hydrodynamic radius, for concentrations (M) of the surfactant SDS. The critical micelle concentration (CMC) of SDS in the aerogel base sol was estimated from 50% θ (red dashed line) to be 1 x 10^{-3} M.

sol, even with extended mixing times (> 3 days). Theta (θ), defined as (R - R_{min})/(R_{max} - R_{min}) where R is the hydrodynamic radius, was plotted as a function of the concentration of SDS in the aerogel base sol solution. By convention, the CMC of SDS was determined to be 50% of the θ value; therefore, the CMC was determined to be 1 x 10^{-3} M in the aerogel base sol, denoted by the red dashed line in Figure 14. This estimated value of the SDS CMC in the aerogel base sol (an ethanol-water solvent system) was reasonable, as the CMC of SDS in water at 25°C is 8 x 10^{-3}; the CMC is known to increase with the addition of ethanol, but decrease with the addition of salts, such as the inorganic zirconium and yttrium precursors.[345,346] For the aerogel formulations discussed in section 3.2, at 0x, 0.5x, 2x, and 3x the CMC of SDS, the CMC value of 1 x 10^{-3} M SDS was used; the molar ratios of SDS to inorganic precursors in the aerogel formulations are given in Table 6.

Table 6: Molar ratios of surfactant SDS to inorganic precursors. Molar ratios of the surfactant sodium dodecyl sulfate (SDS) to the inorganic precursors, zirconia and yttria, in the aerogel formulations at concentrations of 0.5x, 2x, and 3x the CMC. The CMC of SDS used in the formulations is also included.

		Molar Ratios		
Surfactant	**CMC (M)**	**0.5x**	**2x**	**3x**
SDS	1 x 10^{-3}	6 x 10^{-4}	2 x 10^{-3}	3 x 10^{-3}

We mapped a predictive measurement, surfactant hydrodynamic radius, in the sol to final properties of the synthesized aerogels. It was anticipated that a predictive measurement that can be made in the sol, prior to gelation, drying, heat-treatment and characterization, could save experimental time and resources by providing insight into final aerogel properties before completion of the full aerogel synthetic pathway.

5.3 Anionic surfactant templating: Results and discussion

In the following paragraphs, YSZ aerogels with sodium dodecyl sulfate (SDS) at different concentrations are compared following heat-treatment at 600°C, 1000°C, and 1100°C for 18 min. The SDS concentrations were determined through a predictive measurement of

the sol; mapping this predictive sol measurement to aerogel properties may save valuable experimental time in the future as insights into the final aerogel could be gained through a sol measurement prior the completion of the full aerogel development lifecycle. It was anticipated that the use of a surfactant template would retain the mesoporous structure and high surface area of YSZ aerogels.

Table 7: Shrinkage and density of YSZ aerogels with varying SDS levels. As-dried shrinkage for YSZ aerogels with varying levels of SDS determined through physical measurement.

SDS	**Shrinkage (%)**	**Density (g/cm^3)**
0x	17 ± 0.30	0.254 ± 0.003
0.5x	17 ± 0.29	0.253 ± 0.005
2x	18 ± 0.41	0.237 ± 0.005
2.5x	17 ± 0.48	0.237 ± 0.011
3x	17 ± 0.50	0.254 ± 0.002

Following supercritical drying, physical measurements were taken to determine the as-dried shrinkage (%) and density (g/cm^3) for the synthesized YSZ aerogels. The as-dried shrinkage was a measure of the percent change between the aerogel monolith following supercritical drying and the syringe mold used during synthesis. For aerogels without surfactant, the as-dried shrinkage was 17% and the density was 0.254 g/cm^3. For aerogels with SDS, the as-dried shrinkage and density remained approximately constant for the various amounts of SDS at 17% and 0.248 g/cm^3, respectively. The addition of SDS as a templating agent had a negligible effect on the as-dried shrinkage and density, as compared to aerogels without SDS.

Figure 15 shows scanning electron microscopy (SEM) images at 80kx magnification for YSZ aerogels at various heat-treatment conditions, both with and without SDS. SEM was used to qualitatively determine the influence of surfactant type and heat-treatment condition on the aerogel pore structure. The SEM images represent aerogels with no templating agent (Figure 15A) and with 3x SDS (Figure 15B) at four different heat-treatment conditions.

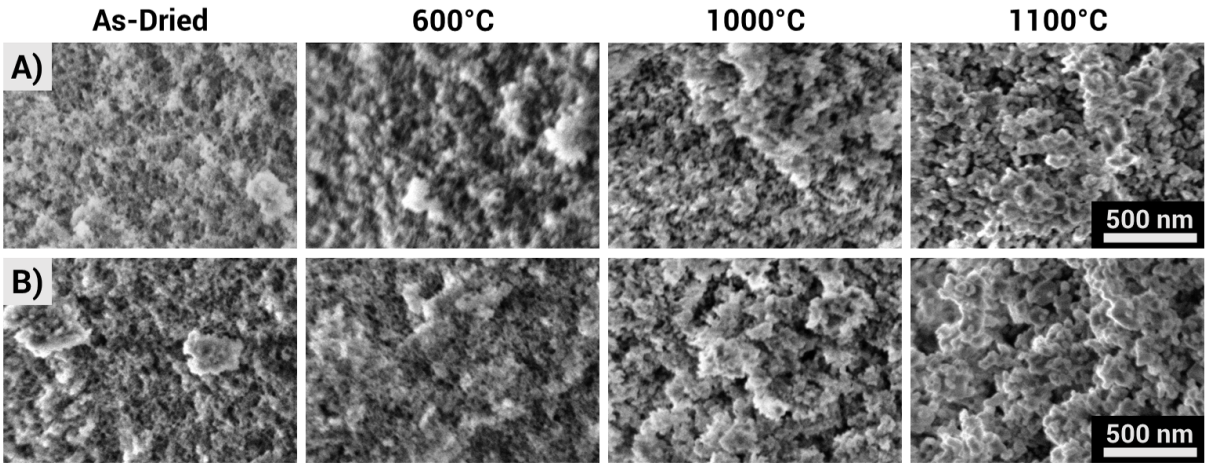

Figure 15: SEM images of YSZ aerogels with varying SDS levels and heat-treatment. SEM images (80kx magnification) of YSZ aerogels with A) no templating agent and B) 3x SDS at four different heat-treatment conditions, left to right, as-dried, 600°C, 1000°C, and 1100°C.

As mentioned previously, sintering was expected following high-temperature exposure due to polycondensation reactions and structural rearrangement; sintering often leads to pore collapse and densification of the pore structure. In Figure 15, the aerogels kept the mesoporous structure at 1000°C, however densification of the aerogel pore structure was evident following exposure to 1100°C. Exposure to 1100°C resulted in larger voids present in the SDS templated aerogel sample, which was visible in the SEM micrograph.

Regarding surfactant influence on the aerogel pore structure, differences in the aerogel pore structure between aerogels without a templating agent (Figure 15A) and aerogels with SDS (Figure 15B) were difficult to distinguish from SEM micrographs. The as-dried aerogel with SDS (Figure 15B) did display a few larger voids that were not present in the as-dried aerogel without a surfactant template. However, there was difficulty in assigning statistical significance to the shifts in pore size that were observed in the SEM micrographs.

The pore size distributions for YSZ aerogels with SDS are displayed in Figure 16 for concentrations of 0x (circle), 0.5x (square), 2x (diamond), and 3x (pentagon) the CMC of SDS. Four different heat-treatment conditions are represented: as-dried (Figure 16A) , 600°C (Figure 16B), 1000°C (Figure 16C), and 1100°C (Figure 16D).

It should be noted that, in the aerogels with SDS, the measured pore sizes were larger

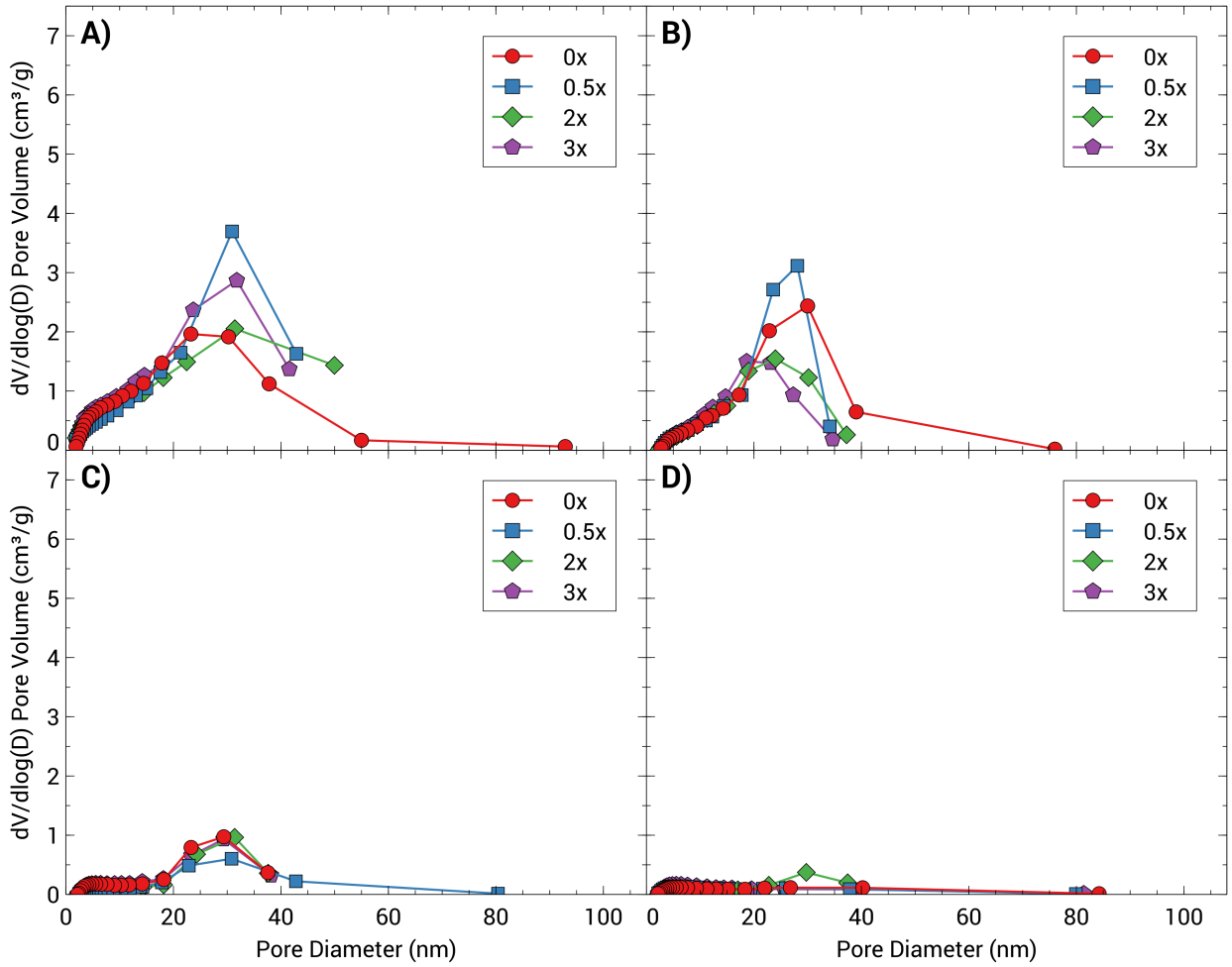

Figure 16: Pore size distributions of YSZ aerogels with varying SDS levels and heat-treatment. Pore size distributions of YSZ aerogels at 0x SDS, 0.5x SDS, 2x SDS, and 3x SDS at heat-treatment conditions of A) as-dried, B) 600°C, C) 1000°C, and D) 1100°C.

than the average diameter of the SDS micelles measured in the YSZ sol. However, the pores were not all directly formed by the surfactant micelles as the surfactant only aided in pore templating. The primary mechanism for the formation of aerogel pores was the aggregation of the solid precursor and the resultant arrangement of the gel network.

The major pore size distributions were centered around 32 nm for all SDS concentrations in the as-dried aerogels. These pore sizes were slightly larger compared to the as-dried aerogel without SDS (0x SDS), which had a major pore size distribution centered around 28 nm. The addition of SDS promoted slightly larger pore sizes and volumes in as-dried aerogels, possibly indicating that SDS was an effective surfactant template. The aerogel without templating agent had the widest pore size distribution, from 0 nm to 93 nm, as compared to the aerogels with SDS, which had pore size distributions from 0 to 45 nm (0.5x SDS), 0 to 52 nm (2x SDS), and 0 to 42 nm (3x SDS). Surfactants are known to increase the emulsification of the sol and prevent particle agglomeration, leading to a more homogeneous aerogel.[18] The addition of SDS led to a narrower pore size distribution for the aerogels by potentially increasing the homogeneity of the pores. The presence of macropores (pores > 50 nm) was not evident in the as-dried pore size distribution for the aerogels with SDS; primarily mesopores (pores between 2 and 50 nm) were formed. Larger pores were present in the aerogel without a surfactant template, which could have potentially encouraged the collision of air molecules, ultimately increasing the thermal conductivity of the as-dried aerogel without SDS.

To maintain effectiveness as a thermal insulator, the formation of large pores should be mitigated. Small mesopores inhibit gas convection as the pore diameter is small compared to the mean free gas path, which can hinder the collision of air molecules. The large volume of mesopores in the as-dried aerogels with SDS would have potentially lowered the thermal conductivity of these aerogels as compared to the aerogel without SDS due to suppression of gas convection. Enhanced control of the mesopore range in aerogels with SDS may have resulted from increased electrostatic interactions present in the aerogels with the anionic

surfactant template.

For the aerogels at 600°C, the aerogel without SDS had a wider pore size distribution with a slightly larger major pore size as compared to the aerogels with SDS. Macropores were also present in the aerogel without SDS. For the aerogels with SDS at 600°C, the pore size distributions were similar, with 0.5x SDS having a slightly larger major pore size at 28 nm. The major pore size distributions were slightly less in the aerogels at 600°C than the as-dried aerogels, except for the aerogel without SDS, which had a slightly larger major pore size distribution at 600°C.

For the aerogels at 1000°C, the pore size distributions were very similar in aerogels with SDS and the aerogel without SDS; the major pore size distribution was centered around 30 nm. However, the aerogel at 0.5x SDS displayed macropores. For the aerogels at 1100°C, the aerogel with 2x SDS had a major pore size distribution centered around 30 nm, while the aerogels with 0.5x SDS and 3x SDS, as well as the aerogel without SDS, displayed macropore formation with very low pore volume.

It is important to note that nitrogen physisorption was only capable of measuring pores less than 100 nm. Therefore, pores with diameters greater than 100 nm could have been present in the synthesized aerogels. As an example, a few larger voids were observed in the as-dried aerogel with 3x SDS (Figure 15B). For this sample, while a significant volume of pores with diameters less than 50 nm were observed in the as-dried pore size distribution (Figure 16A), the aerogel could have had pores greater than 100 nm that were not measured through nitrogen physisorption.

The BET surface area (m^2/g) and BJH desorption cumulative pore volume (cm^3/g) values are represented in Figure 17A and Figure 17B, respectively, for aerogels with SDS. The surfactant concentrations 0x (circle), 0.5x (square), 2x (diamond), and 3x (pentagon) are displayed for temperatures of as-dried, 600°C, 1000°C, and 1100°C.

For aerogels with SDS and aerogels without a surfactant template, there was a large decrease in both surface area and pore volume following high-temperature exposure. A de-

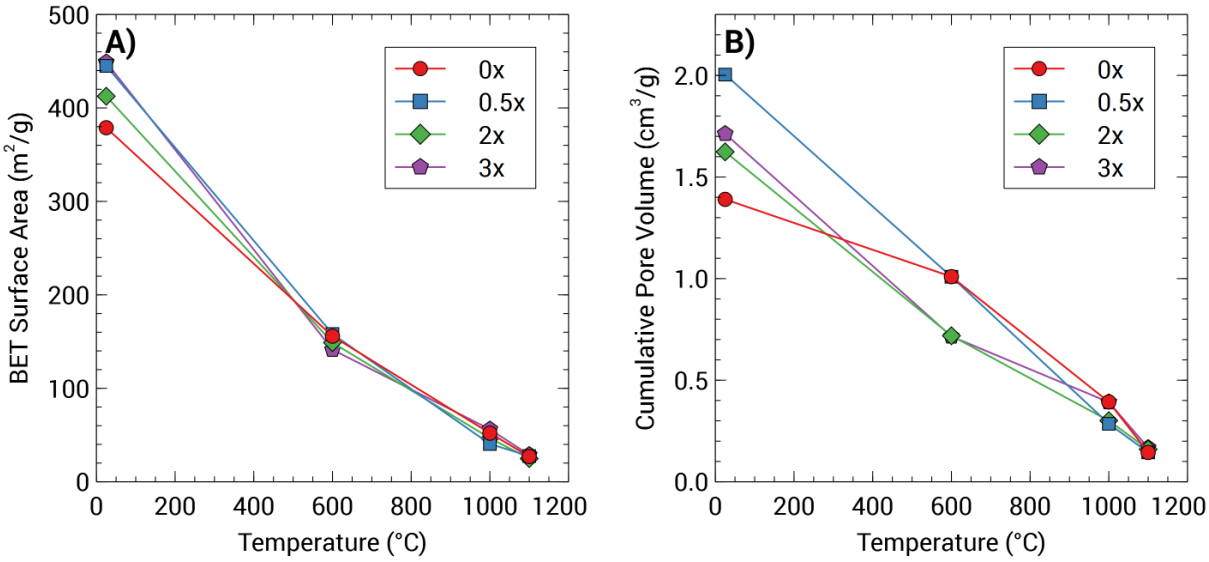

Figure 17: BET surface area and BJH desorption cumulative pore volume of YSZ aerogels with varying SDS levels and heat-treatment. A) BET surface area (m^2/g) and B) BJH desorption cumulative pore volume (cm^3/g) for YSZ aerogels with varying concentrations of SDS at as-dried, 600°C, 1000°C, and 1100°C heat-treatment conditions.

crease in surface area and pore volume was anticipated due to the sintering and densification of the aerogel pore structure at high-temperatures, seen in Figure 15. Larger voids were not included in the measurement of the surface area and pore volume values displayed in Figure 17 since nitrogen physisorption was only capable of measuring pores less than 100 nm. However, the surface area and pore volume values at high-temperature, while much lower than the as-dried values, indicated the retention of mesoporosity following high-temperature exposure. The pore size distributions at high-temperature in Figure 16 also displayed this retained mesoporosity.

For as-dried aerogels with SDS, 0.5x SDS and 3x SDS had higher BET surface area values (in Figure 17A), at 445 m^2/g and 449 m^2/g, respectively than 2x SDS at 413 m^2/g. All concentrations of SDS had higher surface areas than the aerogel without a surfactant template, with a surface area of 379 m^2/g. For the heat-treated aerogels, the aerogels with SDS and the aerogels without SDS all had approximately the same surface area value, with a difference of 17 m^2/g between the aerogels with or without SDS at 600°C, a difference of

16 m^2/g between the aerogels at 1000°C, and a negligible difference of 4 m^2/g between the aerogels at 1100°C.

The BET surface area of as-dried aerogels demonstrated an increase when using SDS as a surfactant template at various concentrations, indicating that SDS potentially was an effective templates for YSZ aerogels, as compared to the aerogel without a surfactant template. It was determined that, following high-temperature exposure, the use of SDS did not have a strong impact on aerogel surface area, as the differences in surface areas between aerogels without a surfactant template and aerogels with SDS were negligible.

Regarding the BJH desorption cumulative pore volume values in Figure 17B, the as-dried aerogels using SDS as a surfactant template had a higher pore volume, at 2.00 cm^3/g, 1.62 cm^3/g, and 1.71 cm^3/g for 0.5x SDS, 2x SDS, and 3x SDS, respectively, as compared to the aerogel without a surfactant template at 1.39 cm^3/g. As was the case with BET surface area, the larger pore volume in as-dried aerogels with SDS indicated that SDS potentially was an effective surfactant template. At 600°C, the aerogel without SDS and the aerogel with 0.5x SDS both had higher pore volume, both at 1.01 cm^3/g, than the aerogels with higher surfactant content (2x SDS and 3x SDS) with pore volumes at 0.72 cm^3/g. Following heat-treatment at 1000°C and 1100°C, the pore volumes were approximately the same for aerogels without a surfactant template and aerogels with SDS with a variation of 0.1 cm^3/g and 0.03 cm^3/g, respectively.

The increased electrostatic interactions of the anionic surfactant with the aerogel matrix may have increased the as-dried pore volume of the aerogels with SDS as compared to the aerogels without a surfactant template. However, similar to the results for BET surface area, following high-temperature exposure, the addition of SDS did not significantly enhance the aerogel pore volume as compared to the aerogels without a surfactant template.

X-ray diffraction (XRD) was used to determine the effect of concentrations of SDS on the crystalline structure of YSZ aerogels. The resulting XRD patterns from 10°to 80° 2θ are displayed in Figure 18. For aerogels without a templating agent, patterns are displayed for

the aerogel heat-treated at 600°C, 1000°C, and 1100°C. For aerogels at 0.5x SDS, 2x SDS, and 3x SDS, patterns at 1100°C only are displayed.

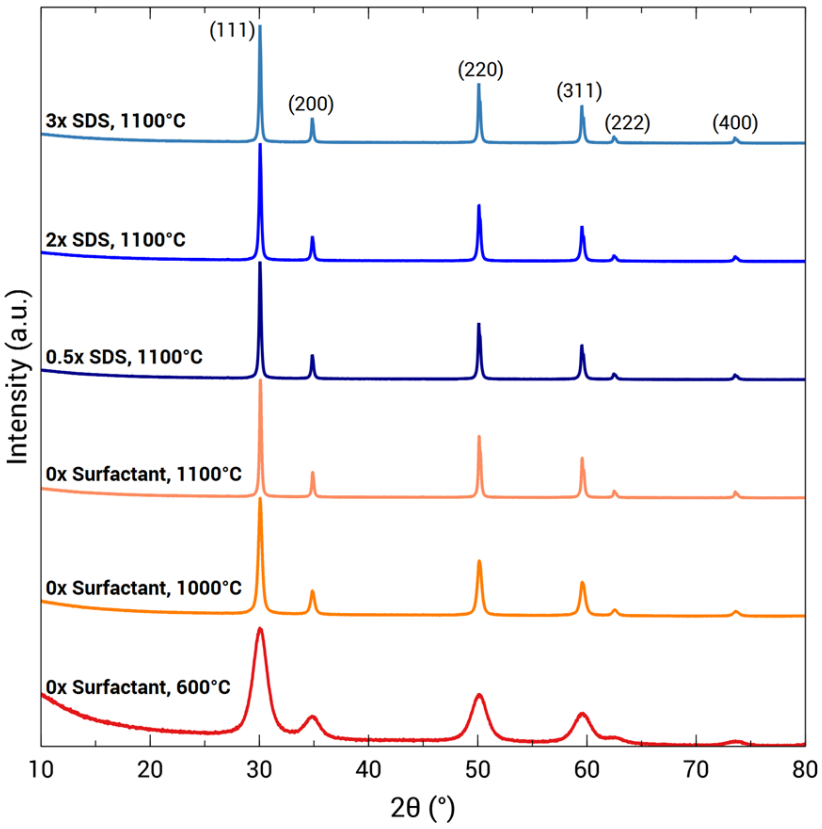

Figure 18: XRD patterns of YSZ aerogels with varying SDS levels and heat-treatment. XRD patterns from 10°to 80° 2θ for YSZ aerogels without surfactant and aerogels with SDS at various heat-treatment conditions of 600°C, 1000°C, and, primarily, 1100°C. The Miller indices (hkl values) are displayed at the top of the figure.

All synthesized as-dried aerogels, regardless of the presence or absence of SDS surfactant templates, were non-crystalline or amorphous. However, all heat-treated aerogels exhibited crystallinity, which increased with increasing heat-treatment temperature from 600°C to 1100°C, indicated by the presence of well-defined peaks in the XRD pattern. Following analysis, it was determined that all heat-treated YSZ aerogels exhibited the cubic fluorite crystalline phase, regardless of SDS concentration; the cubic phase is expected in 20 mol% yttria YSZ aerogels up to 2500°C.[339] The use of SDS a as surfactant template was found to have no effect on the resulting crystalline structure of the YSZ aerogels.

Table 8 displays the average crystallite size (Å) values for each aerogel sample at 600°C, 1000°C, and 1100°C. For the XRD analysis, the crystallite size values resulting from four different equations, the Scherrer equation, the Monshi-Scherrer (M-S) method, the Williamson-Hall (W-H) method, and the Size-Strain-Plot (SSP) method were averaged.[334] These four equations were used together, as the Scherrer equation, traditionally used to determine crystallite size, has restrictions above 1000 Å and often has error due to noise and instrument signal. Due to the limitations and errors associated with the XRD equations, analysis of images from transmission electron microscopy (TEM) was also used to confirm the average crystallite size.

Table 8: Average crystallite size of YSZ aerogels with varying levels of SDS and heat-treatment. Average crystallite size values (Å) for YSZ aerogels with varying levels of SDS at 600°C, 1000°C, and 1100°C determined through XRD and TEM analysis. Four different equations were used to determine the crystallite size following XRD analysis.[334]

SDS Concentration	**Temperature (°C)**	**Crystallite Size via XRD (Å)**	**Crystallite Size via TEM (Å)**
0x	600	55 ± 19	-
	1000	246 ± 20	-
	1100	529 ± 39	364 ± 161
0.5x	600	58 ± 1	-
	1000	237 ± 23	-
	1100	535 ± 19	411 ± 176
2x	600	54 ± 14	-
	1000	197 ± 11	-
	1100	605 ± 9	-
3x	600	56 ± 22	-
	1000	244 ± 9	-
	1100	535 ± 19	355 ± 128

Crystallite growth was evident following high-temperature exposure, especially at 1000°C and 1100°C. This was expected as high-temperature is known to increase growth of crystallite particles, promoting crystallization. At 1000°C, the average crystallite size determined via XRD analysis was slightly lower in all aerogels with SDS than the aerogel without a surfactant template; 2x SDS exhibited the lowest average crystallite size for aerogels with SDS at 197

± 11 Å. At 1100°C, there was a different behavior as the aerogel without the surfactant template had a slightly smaller average crystallite size of 529 ± 39 Å than the aerogels with SDS, which had average crystallite sizes ranging from 535 Å to 605 Å.

At 1000°C, the presence of SDS was shown to decrease the average crystallite size compared to the aerogel without a surfactant template. Due to a capping effect, surfactants are known to control crystallite growth; the lower average crystallite size at 1000°C potentially indicated that SDS was an effective surfactant template, inhibiting crystallite growth at this high-temperature. At 1100°C, the SEM micrographs (Figure 15) displayed significant densification, which was even more pronounced than in the aerogels heat-treated at 1000°C. Increased densification was potentially indicative of a decrease in the effectiveness of SDS as a surfactant template, which was further evidenced by a negligible impact of the surfactant on the surface area and pore volume of the aerogels at 1100°C. The greater extent of densification and the insignificant impact on the crystallite size at 1100°C may have indicated that SDS was a more effective surfactant template at 1000°C than at 1100°C.

The TEM images are displayed for aerogels with no templating agent (Figure 19A), aerogels at 0.5x SDS (Figure 19B), and aerogels at 3x SDS (Figure 19C) that were heat-treated at 1100°C. The TEM images are displayed at 58k magnification.

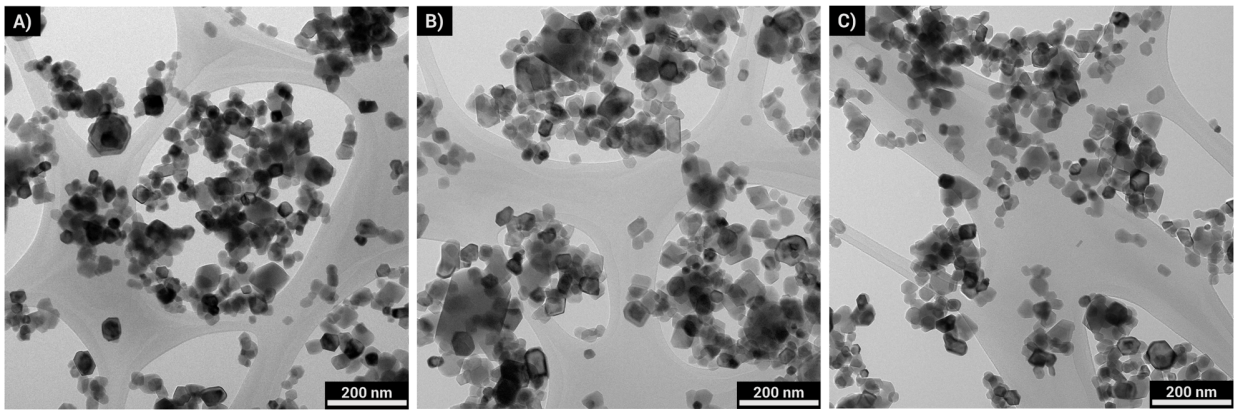

Figure 19: TEM images of YSZ aerogels with varying SDS levels. TEM images at 58k magnification for YSZ aerogels at 1100°C with A) no templating agent, B) 0.5x SDS, and C) 3x SDS.

In Figure 19, it could be seen that crystallite particles with a distribution of sizes were present in the aerogel samples. This was true for aerogels with SDS at varying concentrations, as well as the aerogel without a surfactant template; differences in the TEM images were difficult to distinguish. Crystallinity of the YSZ aerogels was evident following exposure to high-temperature, 1100°C.

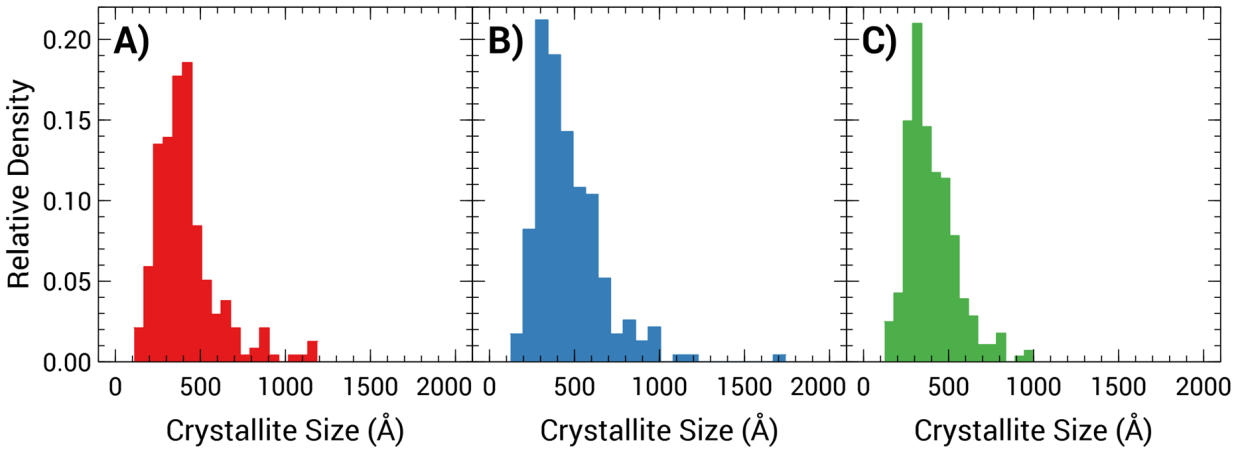

Figure 20: Distribution of crystallite sizes (Å) from TEM images of YSZ aerogels with varying SDS levels. Histograms displaying the distribution of average particle sizes (Å) analyzed via TEM for aerogels at 1100°C with A) no templating agent, B) 0.5x SDS, and C) 3x SDS. The Freedman-Diaconis rule was used to determine the bin width. The average crystallite size and standard deviation determined from each sample are displayed in Table 8.

The crystallite size values at 1100°C determined via TEM analysis in Table 8 for the aerogel without a surfactant template and the aerogel at 3x SDS were similar at 364 Åand 355 Å, respectively. The aerogel with 0.5x SDS was higher at 411 Å. The average crystallite size values determined via TEM were lower than the crystallite size values determined via XRD. However, the standard deviations were large, between 128 Åand 176 Å. These large standard deviations resulted from the wide variations in size of the crystallite particles in the TEM images (Figure 19). Figure 20 includes the distribution of crystallite sizes displayed in the TEM images. The size distribution was very broad for all of the samples. The larger particles in Figure 19 could have been agglomerates of multiple crystallites, attributing to the broad size distribution. It should be noted that for the aerogels with SDS, both at 0.5x and

3x, the major crystallite size distributions were slightly smaller than for the aerogel without a surfactant template, potentially demonstrating that adding SDS may have suppressed crystallite growth even at 1100°C.

5.4 Anionic surfactant templating: Conclusions

For as-dried aerogels, it was determined that the anionic surfactant sodium dodecyl sulfate, SDS, was an effective surfactant template, increasing the surface area, pore volume, and pore size of YSZ aerogels, as compared to aerogels without a surfactant template. The addition of SDS led to primarily mesopores in as-dried aerogels. This may have been due to increased electrostatic interactions between the ions of SDS and the zirconia aerogel matrix, leading to more control over pore formation. Aerogels with SDS also had narrow pore size distributions, which could have indicated that SDS increased the homogeneity of the aerogel pore structure. Following high-temperature exposure, the use of SDS as a surfactant template did not have an influence on the aerogel surface area, pore volume, or crystalline phase. However, at 1000°C, aerogels with SDS had smaller average crystallite sizes than the aerogel without a surfactant template, indicative of the control of crystallite growth by the surfactants via a capping effect. At 1100°C, the addition of SDS did not decrease crystallite size; this may have indicated that SDS was more a effective surfactant template at 1000°C than 1100°C, further evidenced by increased densification of the pore structure at 1100°C. At higher temperatures, the advantages of SDS as a surfactant template may have diminished.

Chapter 6 Yttria-stabilized zirconia aerogels with surfactant templates, part III: Nonionic surfactant templating

Nonionic surfactants, without charge, were also studied as part of this dissertation. Pluronic® P-123 was chosen as the nonionic surfactant template. P-123 has been used as a surfactant template in ambient-pressure dried silica aerogels and ambient-pressure dried zirconia aerogels, leading to surface area and thermal stability enhancement. The large molecular weight (approximately 5800 g/mol) of P-123 has been known to improve the pore volume of aerogels.

6.1 Nonionic surfactant templating: P-123 templating

Pluronic copolymers are linear tri-block-copolymers of poly (ethylene oxide)-poly (propylene oxide)-poly (ethylene oxide) (PEO-PPO-PEO). These copolymers form core-shell micelles at or above the CMC. The hydrophobic PPO makes up the micelle core, with a corona of hydrophilic PEO on the outside.[347] In comparison to templating with CTAB or SDS, there are differences between surfactant templating with surfactants with charge (ionic) and nonionic surfactants. For example, charged surfactant micelles often embed into the aerogel matrix through electrostatic interactions to influence pore formation, while nonionic surfactants form hydrogen bonds between the zirconia aerogel matrix and the ether oxygens of the surfactant.[18,341,348] Additionally, while cationic and anionic surfactants release ions in solution once dissolved, nonionic surfactants do not release ions. With nonionic surfactant templating, the pore structure is primarily influenced by the hydrogen bonding and steric hinderance effects of the surfactant micelles. The surfactant templating process with a nonionic block copolymer is depicted in Figure 21.

In this dissertation, the nonionic copolymer Pluronic® P-123 was used as a surfactant template of YSZ aerogels. P-123 is poly(ethylene glycol)-block-poly(propylene glycol)-block-poly(ethylene glycol) with a number average molecular weight of 5800 g/mol. As an exam-

ple, Sarawade et al. used P-123 as a structure directing agent during surface modification of ambient pressure dried silica aerogels; the aerogels with P-123 exhibited increased surface areas in both as-dried aerogels and aerogels following exposure to 600°C.[349] Cao et al. synthesized titania-silica aerogels with larger, ordered mesopores following the addition of P-123.[350] Additionally, Jung et al. used P-123 in the synthesis of ambient pressure dried zirconia aerogels.[18] The aerogels with P-123 exhibited increased surface area (by 35%), improved thermal stability, and mitigation of pore collapse. Additionally, the large molecular size of P-123 overall increased the pore volume of the resulting aerogels due to steric effects.

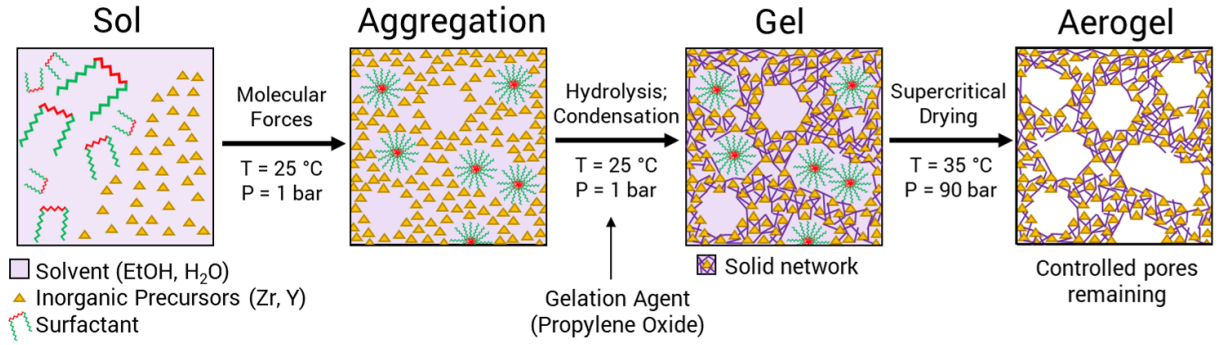

Figure 21: Surfactant templating with a nonionic block copolymer during aerogel synthesis. The block copolymer is added to the sol and precursor particles aggregate around the surfactant micelles, gelling to form a solid network. Surfactants are removed from the aerogel, either through washing, supercritical drying, or heat-treatment, leaving behind controllable, uniform pores.

6.2 Nonionic surfactant templating: P-123 concentrations through hydrodynamic radius measurements

The concentration of P-123 added to the aerogel formulations was determined prior to the synthesis of the aerogels. P-123 was added as multiples (0.5x, 2x, and 3x) of the surfactant's critical micelle concentration (CMC) value in the 20 mol% YSZ sol. To determine the CMC value, a series of experiments were conducted where P-123 was added to the base sol (the 20 mol% yttria, 2x water YSZ sol formulation used for all of the aerogels) at several different concentrations. The surface tension and hydrodynamic radius of the surfactant was then

determined.

A Sinterface Profile Analysis Tensiometer PAT1M was used to determine the surface tension of each solution. For P-123, similar to SDS, there was determined to be no correlation between surfactant concentration and surface tension, as surface tension was determined to be too sensitive of a measurement.

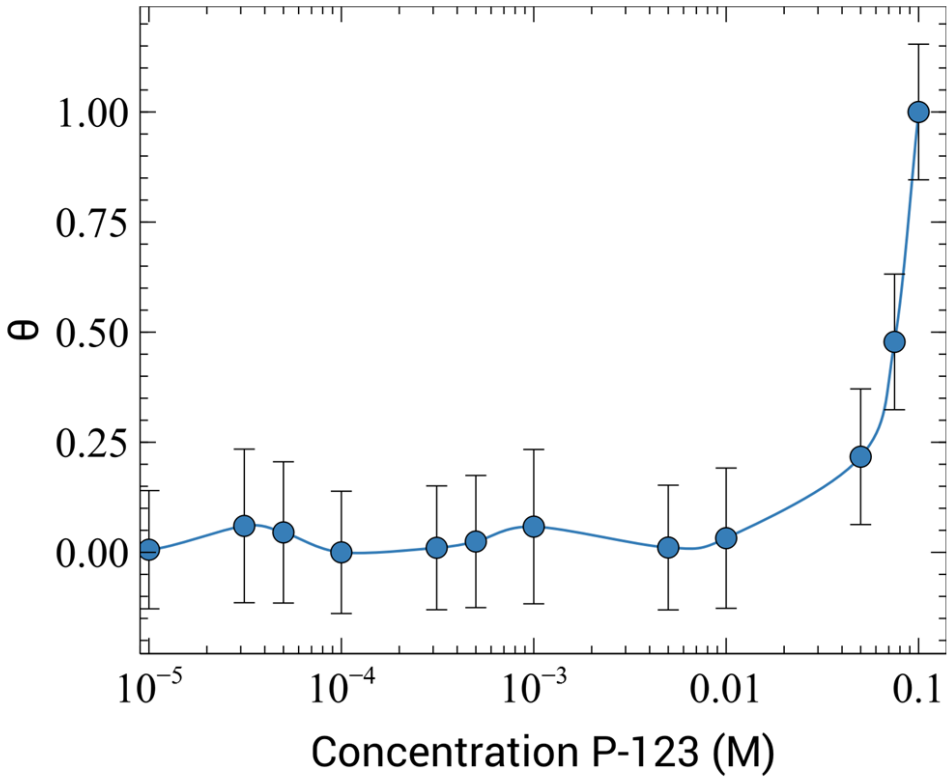

Figure 22: Theta (θ) as a function of surfactant concentration to determine the CMC of P-123. θ values, defined as (R - R_{min})/(R_{max} - R_{min}) where R is the hydrodynamic radius, for concentrations (M) of the surfactant P-123. The critical micelle concentration (CMC) of P-123 used in aerogel formulations was the value for P-123 in water, 3 x 10^{-4} M, as there was not a correlation between hydrodynamic radius and P-123 concentration in this sol.

The hydrodynamic radius of each solution was determined using dynamic light scattering on an ALV/CGS-3 Compact Goniometer from ALV-GmbH utilizing a vertically polarized 633 nm 22 mW laser. For P-123, the hydrodynamic radius values ranged from 3.6 nm to 4.8 nm for P-123 concentrations between 5 x 10^{-6} and 1 x 10^{-2} M P-123 in the base sol. However, there was no correlation between θ and surfactant concentration, as seen in Figure

22. Therefore, as a benchmark, the CMC of P-123 in water, a value of 3 x 10^{-4} M, was used for the aerogel formulations discussed in section 3.2, at 0x, 0.5x, 2x, and 3x the CMC of P-123.[351] The molar ratios of P-123 to inorganic precursors in the aerogel formulations are given in Table 9. It should be noted that, between 5 x 10^{-2} M P-123 and 1 x 10^{-1} M P-123, there was a large increase seen in hydrodynamic radius value from 7.67 nm to 22.02 nm. YSZ aerogels were made with a concentration of 1 x 10^{-1} M P-123, equaling approximately 320x the CMC of P-123. However, the surface area of the as-dried aerogel at this concentration was relatively low, 244 m^2/g, compared to the other aerogels synthesized with P-123. Therefore, this P-123 concentration was not included in the following discussion of surfactant influence on aerogels.

Table 9: Molar ratios of P-123 surfactant to inorganic precursors. Molar ratios of the surfactant Pluronic® P-123 to the inorganic precursors, zirconia and yttria, in the aerogel formulations at concentrations of 0.5x, 2x, and 3x the CMC. The CMC of P-123 used in the formulations is also included.

		Molar Ratios		
Surfactant	**CMC (M)**	**0.5x**	**2x**	**3x**
P-123	3 x 10^{-4}	2 x 10^{-4}	7 x 10^{-4}	1 x 10^{-3}

In doing this, a predictive measurement, surfactant hydrodynamic radius, in the sol was mapped to properties of the YSZ aerogels. This could provide insight into final aerogel properties before completing the full aerogel lifecycle, saving time and resources.

6.3 Nonionic surfactant templating: Results and discussion

YSZ aerogels with Pluronic® P-123 (P-123) at different concentrations are compared in the following paragraphs following heat-treatment at 600°C, 1000°C, and 1100°C for 18 min. We anticipated that the use of surfactant templates would retain the high surface area and high porosity of the YSZ aerogels.

Table 10: Shrinkage and density of YSZ aerogels with varying P-123 levels. As-dried shrinkage for YSZ aerogels with varying levels of P-123 determined through physical measurement.

P-123	**Shrinkage (%)**	**Density (g/cm^3)**
0x	17 ± 0.30	0.254 ± 0.003
0.5x	16 ± 0.25	0.226 ± 0.002
2x	16 ± 0.26	0.228 ± 0.002
3x	17 ± 0.24	0.233 ± 0.006

The as-dried shrinkage (%) and density (g/cm^3) for the synthesized YSZ aerogels were determined following supercritical drying. For aerogels without P-123, the as-dried shrinkage was 17% and the density was 0.254 g/cm^3. For aerogels with P-123, the as-dried shrinkage and density remained approximately constant at 16% and at 0.229 g/cm^3 for varying surfactant levels. The as-dried shrinkage and density were slightly lower for aerogels synthesized using P-123 than for aerogels synthesized without a templating agent. The density was shown to decrease by 10% for aerogels with P-123 as compared to aerogels without templating agent. This decrease in density may have been due to the high molecular weight of P-123, approximately 5800 g/mol. As some of the surfactant was likely removed from the aerogel system during drying due to washing via the supercritical solvents, aerogels synthesized with the high molecular weight surfactant P-123 may have resulted in a lower density as-dried aerogel as compared to the aerogel without a templating agent.

Figure 23 displays scanning electron microscopy (SEM) images at 80kx magnification for YSZ aerogels, with and without P-123, at various heat-treatment conditions. SEM qualitatively determines the influence of surfactant and heat-treatment on the aerogel pore structure. The SEM images represent aerogels with no templating agent (Figure 23A) and with 3x P-123 (Figure 23B) at four different heat-treatment conditions of as-dried, 600°C, 1000°C, and 1100°C.

In Figure 23, mesoporosity was retained at 1000°C; however, densification was evident following exposure to 1100°C, which was expected due to polycondensation reactions and

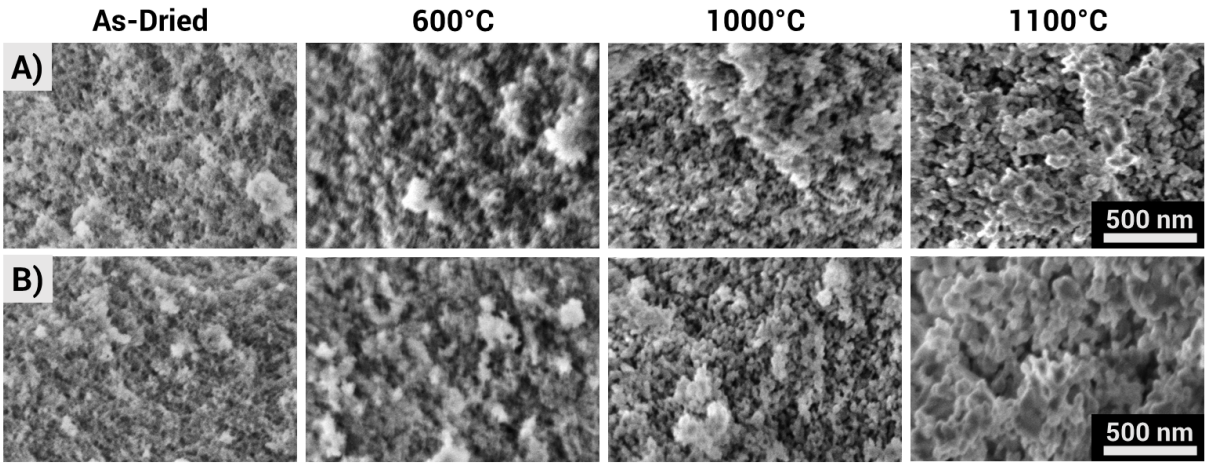

Figure 23: SEM images of YSZ aerogels with varying P-123 levels and heat-treatment. SEM images (80kx magnification) of YSZ aerogels with A) no templating agent and B) 3x P-123 at four different heat-treatment conditions, left to right, as-dried, 600°C, 1000°C, and 1100°C.

structural rearrangement following high-temperature exposure. Large voids were visible in the SEM micrograph of the sample with P-123 at 1100°C. However, statistical significance to the slight shifts in pore size that were observed in the SEM micrographs was difficult to determine from SEM micrographs.

Figure 24 displays the pore size distributions for YSZ aerogels with P-123. Various concentrations of 0x (circle), 0.5x (square), 2x (diamond), and 3x (pentagon) are represented. Four different heat-treatment conditions are also displayed: as-dried (Figure 24A), 600°C (Figure 24B), 1000°C (Figure 24C), and 1100°C (Figure 24D). Since the aerogel pores were not only formed by the surfactant template, the measured pore sizes were larger than the average diameters of the P-123 micelles that were measured in the sol prior to gelation.

The addition of higher concentrations of P-123 appeared to shift the as-dried major pore size distribution to slightly larger pore sizes. In the as-dried aerogel without P-123 (0x P-123), the major pore size distribution was centered around 28 nm, which shifted to slightly higher pore sizes centered around 40 nm at 2x P-123 and 35 nm at 3x P-123. However, at a smaller concentration of P-123 (0.5x P-123), the major pore size was slightly smaller at 18 nm than in the aerogel without a templating agent. Larger pore sizes occurred only

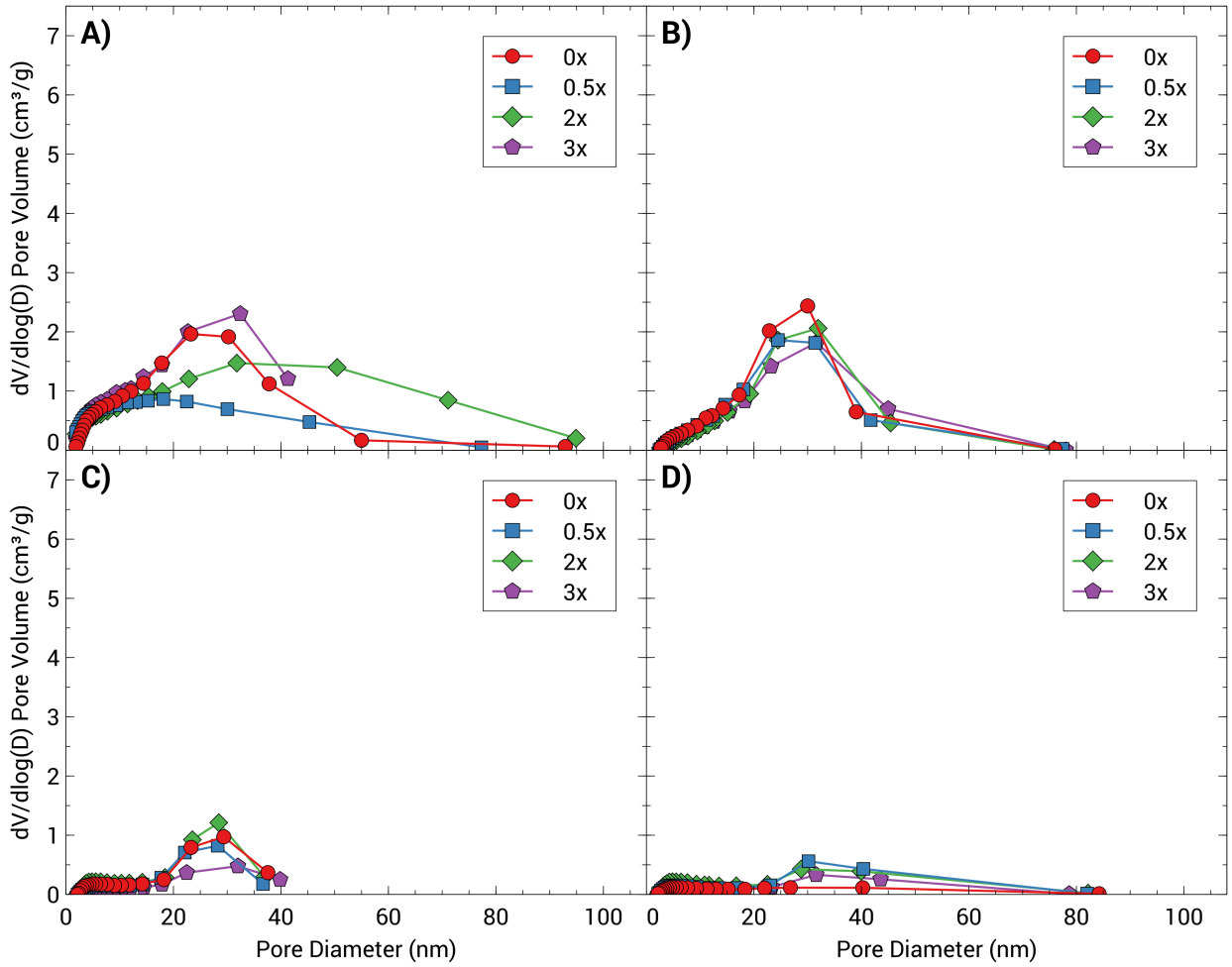

Figure 24: Pore size distributions of YSZ aerogels with varying P-123 levels and heat-treatment. Pore size distributions of YSZ aerogels at 0x P-123, 0.5x P-123, 2x P-123, and 3x P-123 at heat-treatment conditions of A) as-dried, B) 600°C, C) 1000°C, and D) 1100°C.

above the critical micelle concentration (CMC) of P-123, potentially indicating that only the presence of micelles led to larger pores in the as-dried aerogels with P-123 surfactant templates. As-dried aerogels with P-123 had overall wide pore size distributions, from 0 nm to 78 nm at 0.5x P-123 and from 0 nm to 95 nm at 2x P-123, which were approximately equal to the as-dried pore size distribution in the aerogel without templating agent (0x P-123) at 0 nm to 93 nm. The large pore size distribution may have resulted from the large size of the P-123 surfactant template. For the as-dried aerogel with 3x P-123, the pore size distribution was narrower from 0 nm to 42 nm, which indicated the presence of mesopores only.

The as-dried aerogels with P-123 did contain macropores (pores $>$ 50 nm) at 0.5x P-123 and 2x P-123. The presence of pores greater than 50 nm and wide pore size distribution may have resulted in increased gas convection due to increased opportunity for air molecule collision. The formation of large pores in P-123 could have been potentially caused by the lack of electrostatic interactions that enhanced pore control in the aerogels templated with cationic and anionic surfactants that were not prevalent in the aerogels templated with P-123. Additionally, due to a wide pore size distribution, P-123 may have not been effective in emulsification of the sol, leading to aerogels with non-homogeneous pore structure. The as-dried aerogels with P-123 may have had a wide pore size distribution due to the large size of the P-123 surfactant templates.

For all of the heat-treated aerogels, at each temperature (600°C, 1000°C, and 1100°C), all of the pore size distributions were very similar for all P-123 concentrations as well as the aerogels without P-123. At 600°C, the major pore size distributions were centered around 32 nm and macropores were present. At 1000°C, the major pore size distributions were centered around 28 nm; no macropores were present. At 1100°C, the major pore size distributions were centered around 30 nm with very low pore volume. Macropores were present in the aerogels heat-treated at 1100°C. The addition of various concentrations of P-123 did not seem to have much effect on the pore size distributions of the heat-treated aerogels.

Figure 25A and Figure 25B display the BET surface area (m^2/g) values and the BJH

desorption cumulative pore volume (cm^3/g) values, respectively, for aerogels templated using P-123. For heat-treatment conditions of as-dried, 600°C, 1000°C, and 1100°C, the P-123 concentrations 0x (circle), 0.5x (square), 2x (diamond), and 3x (pentagon) are represented .

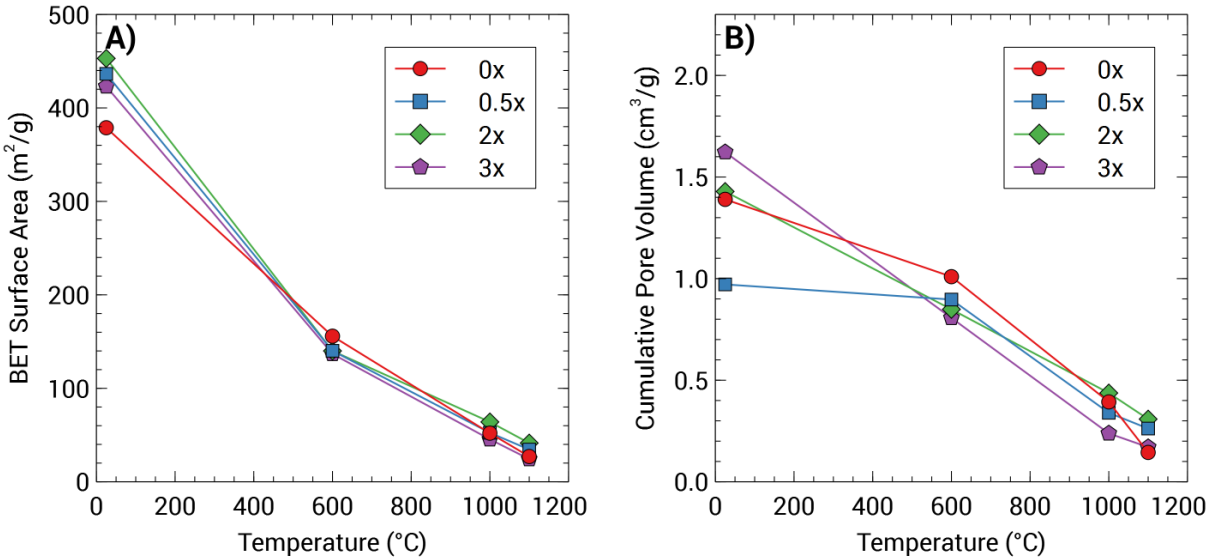

Figure 25: BET surface area and BJH desorption cumulative pore volume of YSZ aerogels with varying P-123 levels and heat-treatment. A) BET surface area (m^2/g) and B) BJH desorption cumulative pore volume (cm^3/g) for YSZ aerogels with varying concentrations of P-123 at as-dried, 600°C, 1000°C, and 1100°C heat-treatment conditions.

There was a large decrease in surface area and pore volume following exposure up to 1100°C for the aerogels with and without P-123. This behavior was expected as sintering and densification of the aerogel pore structure often occurs at high-temperatures. Large voids and densification were observed in the SEM micrographs (Figure 23) for the aerogels exposed to high temperatures. As nitrogen physisorption was only capable of measuring pores less than 100 nm, the larger voids were not measured and are thus not taken into account in the values in Figure 25. However, the surface area and pore volume values, as well as the pore size distributions in Figure 24, did indicate the retention of some mesoporosity following exposure up to 1100°C.

The as-dried aerogels with P-123 in Figure 25A all had higher surface areas, at 436 m^2/g, 453 m^2/g, and 423 m^2/g for 0.5x P-123, 2x P-123, and 3x P-123, respectively, than

the aerogel without a surfactant template at 379 m^2/g. For the heat-treated aerogels, the aerogels with P-123 and the aerogels without P-123 all had approximately the same surface area value, with a difference of 19 m^2/g between the aerogels with or without P-123 at 600°C, a difference of 19 m^2/g between the aerogels at 1000°C, and a difference of 17 m^2/g between the aerogels at 1100°C. A similar behavior was seen in the aerogels templated with SDS discussed in section 5. It should be noted that at 600°C, the aerogel without P-123 had a higher surface area of 156 m^2/g than the surface areas at 140 m^2/g, 140 m^2/g, and 137 m^2/g of the aerogels at 0.5x P-123, 2x P-123, and 3x P-123, respectively. The increase in as-dried surface area for the aerogels with P-123, as compared to the aerogels without a surfactant template, may indicate that P-123 was an effective templating agent; however, there was no influence on the surface area of heat-treated aerogels following the addition of the P-123 surfactant templates.

Considering the BJH desorption cumulative pore volume values (Figure 25B), the aerogel with the lowest surfactant concentration, 0.5x P-123, had the lowest pore volume at 0.97 cm^3/g, while the aerogel with the highest surfactant concentration, 3x P-123, had the highest pore volume at 1.62 cm^3/g. At 600°C, the aerogel without a surfactant template had the highest pore volume at 1.01 cm^3/g, as compared to the aerogels with 0.5x P-123, 2x P-123, and 3x P-123 at 0.90 cm^3/g, 0.85 cm^3/g, and 0.81 cm^3/g, respectively. For aerogels heat-treated at 1000°C and 1100°C, the pore volumes were approximately the same in aerogels without a surfactant template and aerogels with P-123; the variation of pore volume was 0.20 cm^3/g at 1000°C and 0.17 cm^3/g at 1100°C.

Concentrations of 2x and 3x P-123 increased the as-dried pore volume as compared to the aerogel without a surfactant template. The pore volume at 0.5x P-123 was much lower as compared to the other aerogels, both with or without P-123. This may have potentially indicated that P-123 was an effective template only above the CMC. Additionally, due to the high molecular weight of P-123, residual amounts of P-123 surfactant may have been retained in the aerogel pore structure following the washing and drying processes. This

may have resulted in the smaller pore volume for the as-dried aerogel with 0.5x P-123x, as well as the overall lesser increase in pore volume following templating with P-123 as compared to the anionic or cationic surfactants. Additionally, as with the BET surface area, following exposure to high-temperature, P-123 did not increase pore volume as compared to the aerogels without P-123.

To determine the influence of P-123 on the crystalline phase and crystallite size of YSZ aerogels, X-ray diffraction (XRD) was used. Figure 26 displays the XRD patterns from 10°to 80° 2θ.

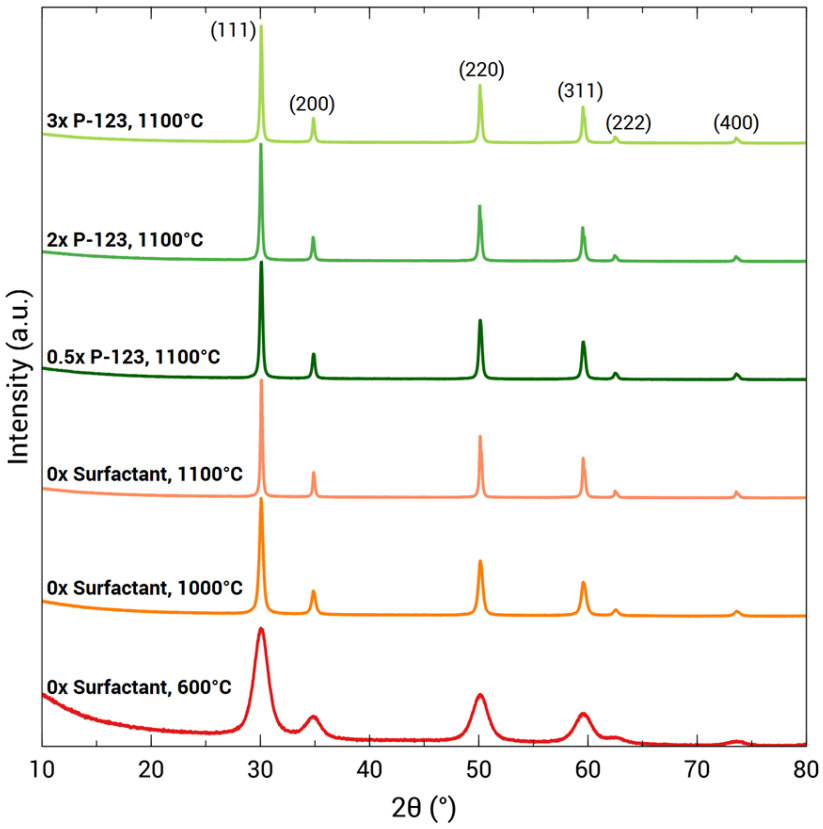

Figure 26: XRD patterns of YSZ aerogels with varying P-123 levels and heat-treatment. XRD patterns from 10°to 80° 2θ for YSZ aerogels without surfactant and aerogels with P-123 at various heat-treatment conditions of 600°C, 1000°C, and, primarily, 1100°C. The Miller indices (hkl values) are displayed at the top of the figure.

The as-dried aerogels, with or without P-123, were amorphous or non-crystalline, while all of the heat-treated aerogels displayed crystallinity. The crystallinity, indicated by sharp

peaks on the XRD pattern, increased with increasing temperature up to 1100°C. All heat-treated YSZ aerogels exhibited the cubic fluorite crystalline phase, which was expected in 20 mol% YSZ aerogels.[339] Using P-123 as a surfactant template did not influence the crystalline phase of the YSZ aerogels.

The average crystallite size (Å) values for aerogels with P-123 heat-treated at 600°C, 1000°C, and 1100°C are displayed in Table 11. The XRD analysis utilized four different equations to determine the average crystallite size: the Scherrer equation, the Monshi-Scherrer (M-S) method, the Williamson-Hall (W-H) method, and the Size-Strain-Plot (SSP) method; these equations were chosen due to certain restrictions and error associated with the conventional Scherrer equation.[334] Transmission electron microscopy (TEM) was used in addition to the XRD analysis to support the determined crystallite sizes.

Table 11: Average crystallite size of YSZ aerogels with varying P-123 levels and heat-treatment. Average crystallite size values (Å) for YSZ aerogels with varying levels of P-123 at 600°C, 1000°C, and 1100°C determined through XRD and TEM analysis. Four different equations were used to determine the crystallite size following XRD analysis.[334]

P-123 Concentration	**Temperature (°C)**	**Crystallite Size via XRD (Å)**	**Crystallite Size via TEM (Å)**
0x	600	55 ± 19	-
	1000	246 ± 20	-
	1100	529 ± 39	364 ± 161
0.5x	600	58 ± 25	-
	1000	202 ± 7	-
	1100	349 ± 3	355 ± 135
2x	600	54 ± 13	-
	1000	200 ± 16	-
	1100	579 ± 18	-
3x	600	57 ± 24	-
	1000	198 ± 5	-
	1100	517 ± 32	347 ± 173

Exposure to high-temperature is known to promote crystallite growth, which was evident at 1000°C and 1100°C. The aerogels with P-123 at 1000°C all exhibited a lower average crystallite size than the aerogel without a surfactant template, with 3x P-123 having the

lowest crystallite size at 198 ± 5 Å. At 1100°C, the average crystallite size in the aerogels with 0.5x and 3x P-123 was lower than the crystallite size in the aerogel without a surfactant template at 349 ± 3 and 517± 32, respectively. At 2x P-123, the average crystallite size was larger at 579 ± 18. The presence of P-123 mitigated crystallite growth at 0.5x P-123 and 3x P-123; however, for the aerogel at 2x P-123, the crystallite size exhibited an increase as compared to the aerogel without P-123. Surfactants can control crystallite growth due to particle capping; the smaller crystallites at 1000°C and 1100°C potentially indicated that P-123 was an effective surfactant template.

Figure 27A, Figure 27B, and Figure 27C display the TEM images for aerogels with no templating agent, aerogels at 0.5x P-123, and aerogels at 3x P-123, respectively, that were heat-treated at 1100°C. The TEM images were taken at 58k magnification. There was a distribution of sizes for the crystallite particles in the TEM images, which was true for the aerogel without a surfactant template and with aerogels with P-123.

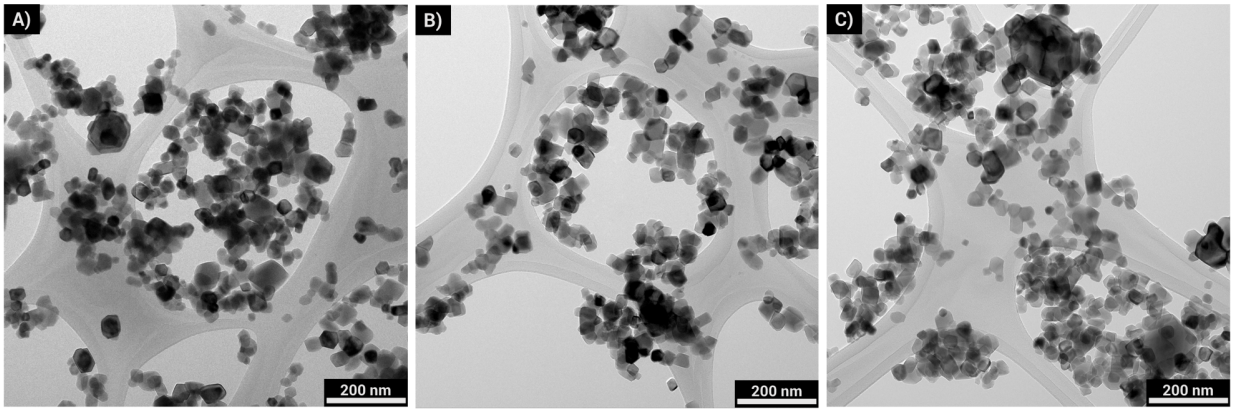

Figure 27: TEM images of YSZ aerogels with varying P-123 levels. TEM images at 58k magnification for YSZ aerogels at 1100°C with A) no templating agent, B) 0.5x P-123, and C) 3x P-123.

In Table 11, at 1100°C, the crystallite sizes determined via TEM were all approximately the same, ranging from 347 Å to 364 Å; the values determined via TEM were on average lower than the crystallite sizes determined via XRD. Very large standard deviations were present, however, between 135 Å and 173 Å, resulting from the large distributions in size

of the crystallite particles in the TEM images in Figure 27. The distribution of crystallite sizes of the TEM images is displayed in Figure 28. The aerogels show a wide distribution of crystallite sizes, which most likely attributed to the standard deviations. The larger particles could have been indicative of agglomerates of multiple crystallites. The major crystallite size distributions were slightly smaller for the aerogels with 0.5x and 3x P-123 as compared to the aerogel without P-123. This potentially indicates that using P-123 as a surfactant template may have suppressed crystallite growth at 1100°C.

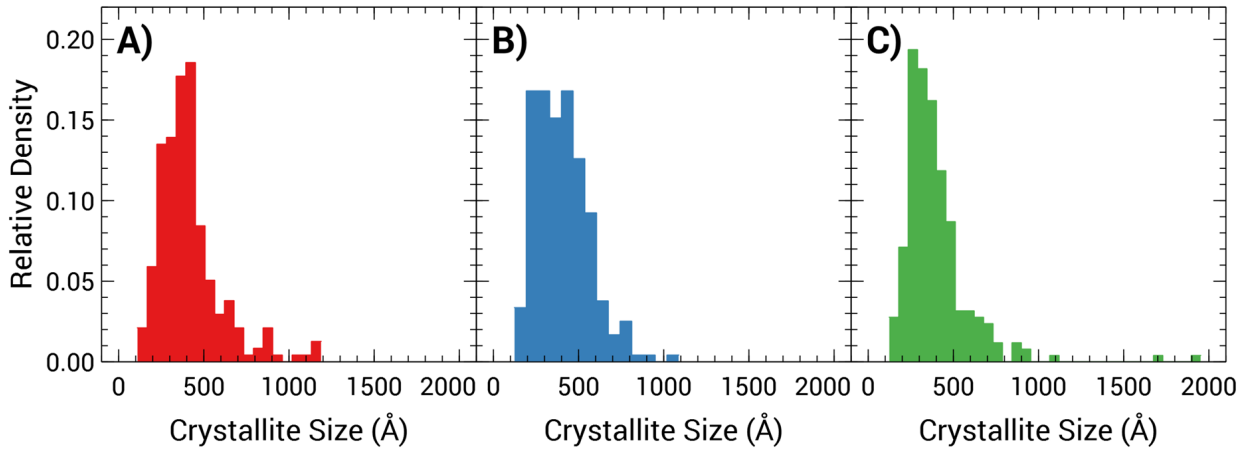

Figure 28: Distribution of crystallite sizes (Å) from TEM images of YSZ aerogels with varying P-123 levels. Histograms displaying the distribution of average particle sizes (Å) analyzed via TEM for aerogels at 1100°C with A) no templating agent, B) 0.5x P-123, and C) 3x P-123. The Freedman-Diaconis rule was used to determine the bin width. The average crystallite size and standard deviation determined from each sample are displayed in Table 11.

6.4 Nonionic surfactant templating: Conclusions

Using the nonionic surfactant Pluronic® P-123 did result in increased surface area, pore volume, and pore size of as-dried YSZ aerogels; however, certain concentrations of the non-ionic surfactant P-123 led to the formation of macropores, which may have been due to a lack of electrostatic interactions. Following high-temperature exposure P-123 did not impact the aerogel surface area, pore volume, or crystalline phase, although the resulting average crystallite size at 1000°C and 1100°C was lowered using P-123.

Chapter 7 Yttria-stabilized zirconia aerogels with surfactant templates, part IV: Comparison of surfactant types

In this dissertation, three different surfactant templates were studied: the cationic surfactant cetrimonium bromide (CTAB), the anionic surfactant sodium dodecyl sulfate (SDS) and the nonionic surfactant Pluronic® P-123. The influence of each surfactant on the pore structure, surface area, pore volume, and crystalline structure of 20 mol% YSZ aerogels was evaluated for both as-dried and heat-treated aerogels.

The aerogels templated with CTAB and SDS had electrostatic interactions between the positively and negatively charged surfactant head groups, respectively, as well as the released ions in solution, and the zirconia aerogel matrix. These electrostatic interactions, while not the only means of ionic surfactant templating, were a significant influence on aerogel pore formation. In the aerogels with the nonionic P-123, electrostatic interactions were not prevalent, as the pore structure was primarily influenced by the hydrogen bonding and steric hinderance resulting from the nonionic surfactant interaction with the zirconia aerogel matrix. The increased electrostatic interactions may have been the driving force behind the enhanced pore structure control in the aerogels with CTAB and SDS, evidenced by the formation of primarily mesopores with narrower size distributions and increased surface areas and cumulative pore volumes in as-dried aerogels.

Both SDS and P-123 increased the surface area of as-dried aerogels as compared to the aerogel without a surfactant template, as displayed in Figure 17A and Figure 25A, respectively. The increase in surface area for the as-dried aerogels may have been indicative of higher threshold operating limits for the surfactant-templated aerogels. However, increased surface area was not demonstrated following high-temperature exposure at 600°C, 1000°C, and 1100°C, as there was a negligible change in the surface area of aerogels with surfactant and those without surfactant. Above temperatures of 350°C, the surfactants were most likely

oxidized and removed from the aerogel system.[331] Since the maximum temperature for the supercritical drying process stayed below 100°C in this work, remnants of surfactant not removed during the washing process were most likely still present in the as-dried aerogels; however, during the heat-treatment process, well above 350°C, any remaining surfactant was removed.[22] The presence of remaining surfactant in the as-dried aerogels templated with SDS and P-123 may have influenced the higher as-dried surface area, and the overall higher pore volume in the case of SDS templated aerogels. However, following exposure to temperatures above 600°C and full removal of surfactant from the aerogel system, the surface area and pore volume of the aerogels with SDS and P-123 showed negligible differences when compared to the aerogels without surfactant template. The advantages, reduction of pore collapse and mitigation of densification, of the anionic and nonionic surfactant templates were mostly eliminated following the removal of the surfactants. This was further evidenced by the inhibition of crystallite growth at 1000°C, which was not apparent at 1100°C. At higher temperatures, the advantages of the surfactant templates were diminished.

The behavior of surfactant-templated aerogels was much different for the aerogels templated with SDS (anionic surfactant) and P-123 (nonionic surfactant) as compared to when using cetrimonium bromide, CTAB (cationic surfactant), as a template. A concentration of 0.5x CTAB increased the surface area (Figure 9) of YSZ aerogels by 72% and 41% following exposure to 600°C and 1000°C, respectively, as compared to aerogels without CTAB.[331] Pore volume was also shown to increase at 0.5x CTAB by 75% and 80% at 600°C and 1000°C, respectively. CTAB was shown to increase surface area and pore volume in heat-treated aerogels, however, at 0.5x CTAB, the as-dried surface area was 403 m^2/g, lower than any of the as-dried aerogels using SDS and P-123 surfactant templates. Therefore, while SDS and P-123 increased the as-dried surface area as compared to CTAB, there was not an enhancement of surface area and pore volume at high-temperature for these surfactants as there was for CTAB.

We hypothesized two reasons for the different behavior in the cationic surfactant tem-

plated aerogels: the estimation of the critical micelle concentration (CMC) value for CTAB and the strong interaction of the CTAB surfactant with the zirconia aerogel matrix. First, prior to the gelation of the YSZ aerogels, CTAB was added in multiples of 0.5x and 2x the CMC of CTAB. Unlike with the anionic and nonionic surfactants, where the CMC was estimated from experimental measurements (Figure 14) or a literature value (Figure 22), the value of CTAB used in the aerogel formulations was estimated from a thermodynamic model.[336] This thermodynamic model only considered the water and ethanol volumes in the sol and did not take into account other factors, including the inorganic salt concentration. Due to this estimation, the molar ratios of CTAB and the inorganic precursors in the aerogel formulation were much higher (Table 3) compared to the molar ratios of SDS and P-123 (Table 6 and Table 9, respectively). While there may have been problems with the estimation of the CTAB CMC, the larger amount of CTAB in the YSZ aerogels may have had a larger influence of the aerogel pore structure, in both as-dried and heat-treated aerogel samples, as compared to the SDS and P-123 templated aerogels.

However, the larger amount of CTAB potentially had negative effects on the aerogel pore structure. As discussed previously, larger amounts of CTAB (2x the CMC as compared to 0.5x the CMC) resulted in lower surface areas and pore volumes of as-dried and heat-treated aerogels. It was hypothesized that the higher concentration of CTAB led to increased adsorption and a potential build-up of the surfactant onto the zirconia aerogel matrix, which could have impeded the gelation reaction and caused subsequent shrinkage and pore collapse during drying and heat-treatment. Therefore, while higher amounts of CTAB may have positively influenced the surface area and pore volume of aerogels as compared to the lower amounts of SDS and P-123, too much CTAB was shown to have a negative impact.

Regarding aerogels with SDS and P-123, larger amounts of both surfactants may have positively impacted the surface area and pore volume of surfactant templated aerogels at high-temperature. Larger concentrations of micelles, as well as increased electrostatic interactions in aerogels with SDS, could have further decreased surface tension and prevented

agglomeration, leading to reduced pore collapse and higher surface area. However, increased amounts of surfactants may have potentially led to an excess of surfactant, causing gelation impediment due to matrix adsorption in the case of SDS or due to steric effects in the case of P-123 that could have resulted in negative impacts to surface area and pore volume.

Chapter 8 Understanding structure/property-process relationships in aerogels through information architecture

Aerogels are mesoporous, high surface area materials with extensive synthetic and processing conditions, as reviewed in section 2. To effectively synthesize aerogels, the impact of synthetic pathways on resulting aerogel properties must be understood prior to experimental investigation. To examine these relationships, we have developed two information architectures: the zirconia aerogel graph database (600 aerogels) and the silica aerogel graph database (1000 aerogels). These property graph databases enabled rapid queries and visualization of the impact of synthesis and processing conditions on final aerogel properties. Both in current form and with further expansion, these developed graph databases could reduce experimental dimensionality, time, and resources, enabling the successful synthesis of high surface area aerogels, which are advantageous for applications including thermal insulation, sorption media, and catalysis.

8.1 Information architecture metamodel

A property graph database can be a powerful tool as connections, such as those representing the varied relationships between structures, properties, and processes in materials exploration, can be easily seen.[352] Visualization of graph databases is often used when there are large amounts of variables with many complex possible connections, as is the case in the different synthetic and processing conditions of aerogels and the relationship of those conditions to aerogel properties, including surface area. To understand the influence of aerogel synthetic and processing variables, we developed the zirconia aerogel graph database (ZrAGDB) and the silica aerogel graph database (SiAGDB). A visualization tool was used to display queries of the graph databases as sets of nodes and edges that represented variables and the relationships between them.[353] Aerogel synthetic processes have a multitude of vari-

ables that are hyper-connected; the graph databases represented the relationships between aerogel synthesis, processing, and the final properties.

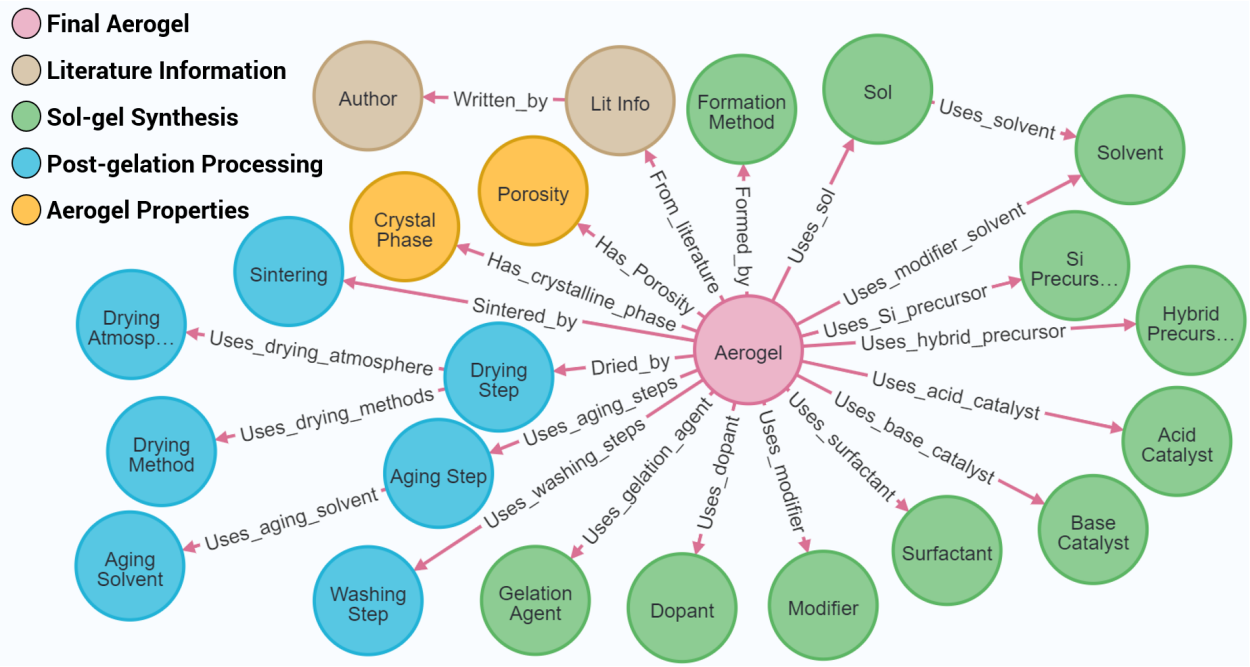

Figure 29: Metamodel of the silica aerogel graph database (SiAGDB). Synthetic and processing variables are connected to the aerogel through edges representing the influence of each variable on the final aerogel.

Here, the architecture of the metamodel for the SiAGDB (Figure 29) will be specifically considered, although the metamodel for the ZrAGDB followed very similar conventions. Each node, representing a feature of silica aerogel sol-gel synthesis or post-gelation processing, connected to the central silica aerogel node through edges. Information stored on separate nodes was useful for framing graph queries. For example, the central silica aerogel node was connected to two nodes representing two final aerogel properties, crystalline phase and porosity; these properties were represented as separate nodes as they resulted in 6 - 9 common values and could be used to group aerogels together through queries. The central silica aerogel node had attributes representing additional final aerogel properties, including surface area, density, average pore size, pore volume, and thermal conductivity; these properties were stored as node attributes as they resulted in unique values for each aerogel. While the design of information architecture is subjective, these design decisions were made based on

the utility of the SiAGDB for this work.

The graph database management system, Neo4j (`https://neo4j.com/`), was used to represent the vast set of information contained in the aerogel graph databases. Neo4j's data visualization tool, Neo4j Bloom, displayed queries of the aerogel graph databases as sets of nodes and edges that represented variables and the relationships between them.

8.2 Information architecture use case, part I: Zirconia aerogels

An objective of this dissertation was to optimize aerogel synthesis by creating and utilizing tools such as property graph databases and machine learning models. It was anticipated that these tools could improve the understanding of synthetic and processing variables and increase the effectiveness of experimentation in aerogel synthesis by reducing experimental time.

There are an extensive number of compositional and process variables that must be considered in the synthesis and processing of zirconia aerogels. Each of these synthetic pathways can influence the final properties of the zirconia aerogels, specifically the surface area, mesoporous structure, density, thermal conductivity, and crystalline phase.

Here, we used an architected information structure to begin to mitigate the volume of synthetic variables, which would aid in the understanding and enhancement of these materials. It was anticipated that this information architecture could lead to a greater knowledge of zirconia aerogels and a future optimized synthetic pathway of these materials. In a broader aspect, this dissertation provides an example for ways in which data science can be used to enhance colloidal chemistry, providing more efficient experimentation and development of materials, specifically those with high experimental dimensionality. The synthesis, processing, and characterization of 600 zirconia aerogel materials reported since 2014 was the focus of the information structure.[1,4,5,11,13,18–51] Information from these sources was organized in Python and Neo4j and the ZrAGDB was constructed.[354] This zirconia aerogel graph database (ZrAGDB) visually and dynamically connected the synthesis and

processing of zirconia aerogels with the properties resulting from each synthetic pathway. The ZrAGDB constructed contained 3,783 nodes, which represented unique variables describing the synthesis and processing of each zirconia aerogel. In addition, the ZrAGDB contained 10,326 relationships connecting nodes together. The complete ZrAGDB, along with a color legend for the most represented nodes, is displayed in Figure 30. The ZrAGDB was useful for understanding the scope of zirconia aerogel synthesis.

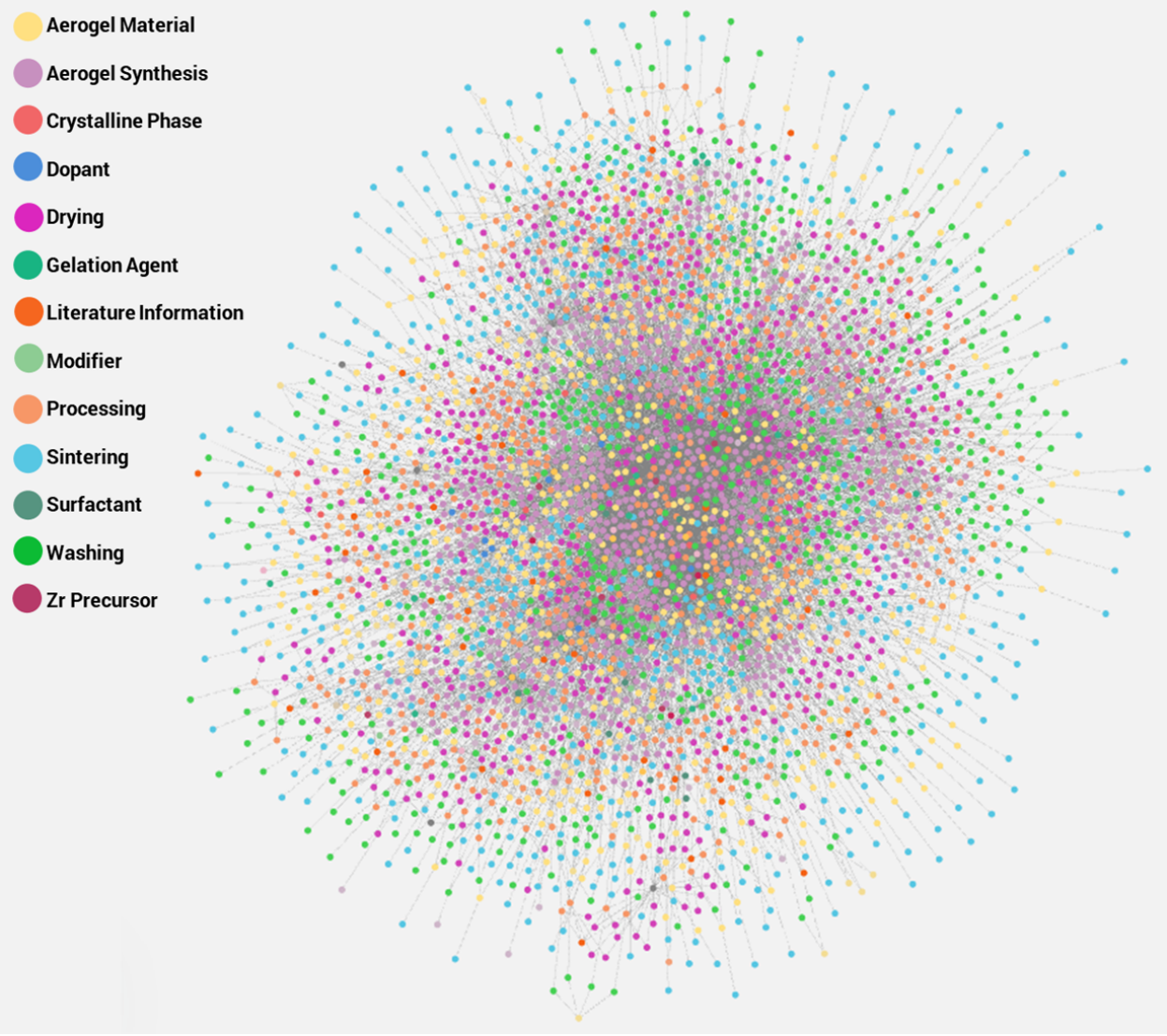

Figure 30: Full zirconia aerogel graph database (ZrAGDB). The complete zirconia aerogel graph database (ZrAGDB) showing the connection between aerogel properties and the synthesis pathways used to produce them.

Here, the utility of the ZrAGDB using simple queries is demonstrated. First, rare earth

dopants used in the synthesis of zirconia aerogels were considered. By querying the complete ZrAGDB, Figure 31 displays the sub-graph which describes the synthesis of 214 zirconia aerogels (Figure 31A) using nine various dopants (Figure 31B). The size of the zirconia aerogel nodes compared the surface area values exhibited by the aerogels; the larger nodes corresponded to higher surface area values, while the smaller nodes corresponded to smaller surface area values or aerogels with unreported surface area values. A color gradient was added to the zirconia aerogel nodes; purple nodes corresponded to as-dried aerogels without heat-treatment and red nodes corresponded to aerogels heat-treated at 1200°C. By observing the sub-graph, it could be seen that yttrium(III) chloride hexahydrate and yttrium(III) nitrate hexahydrate were the most frequently used rare earth dopants in zirconia aerogel synthesis. Gadolinium(III) nitrate hexahydrate, neodymium(III) nitrate hexahydrate, and dysprosium(III) nitrate hydrate were seldom used in zirconia aerogel synthesis. It could also be seen that yttrium(III) chloride hexahydrate and ytterbium(III) chloride hexahydrate were often used in conjunction with one another, as were yttrium(III) nitrate hexahydrate and cerium(III) nitrate hexahydrate. Select surface area values are also displayed in Figure 31. Yttrium(III) nitrate hexahydrate, in combination with cerium(III) nitrate hexahydrate, was shown to synthesize as-dried aerogels with the highest surface areas. It could also be seen that heat-treatment was related to decreasing surface area of the zirconia aerogels. However, the addition of dopant attenuated the extent of decrease in surface area and each dopant had a different extent of decrease. This sub-graph allowed us to see immediately the most frequently used dopants in the synthesis of zirconia aerogels as well as the effect of dopant on the final surface area of the aerogels.

The second preliminary query of the ZrAGDB resulted in Figure 32, which displays the sub-graph depicting the synthesis of 559 zirconia aerogels (Figure 32A) using 17 various gelation agents (Figure 32). Similar to Figure 31, the sizes of the zirconia aerogel nodes compared the surface area values, with larger nodes corresponding to aerogels with higher surface areas. The purple to red color gradient was also present, with purple nodes rep-

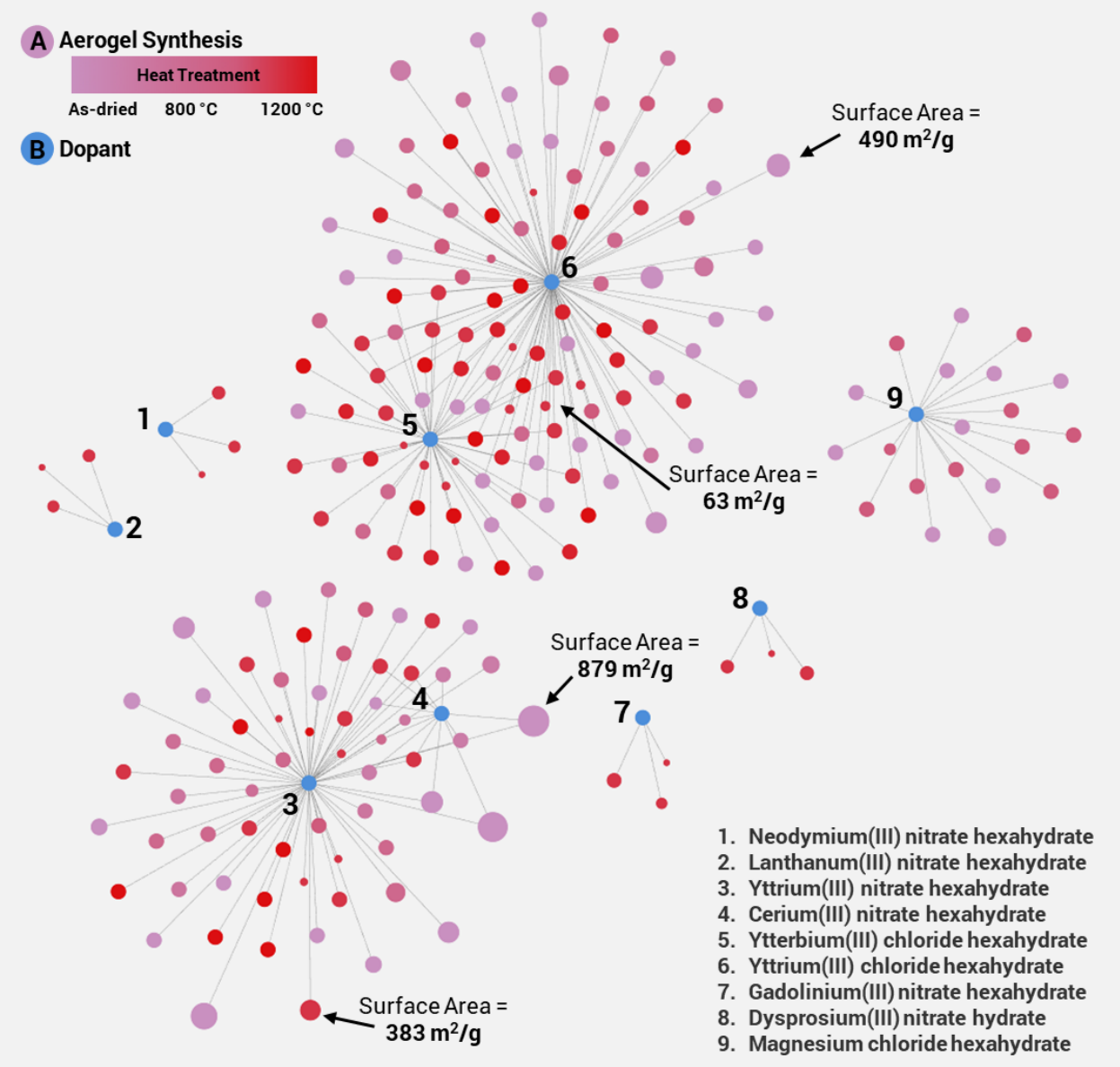

Figure 31: Dopant sub-graph of the zirconia aerogel graph database (ZrAGDB). Sub-graph of the ZrAGDB examining A) zirconia aerogel synthesis using B) dopants. The purple to red color gradient corresponds to the heat-treatment temperature of the aerogels from as-dried to 1200°C. The larger nodes correspond to aerogels with higher resulting surface areas.

resenting as-dried aerogels and red nodes representing aerogels heat-treated at 1200°C. By observing the sub-graph, it could be determined that propylene oxide was the most frequently used gelation agent in zirconia aerogel synthesis, synthesizing as-dried aerogels with both high and low surface areas. This sub-graph also showed gelation agents that were used in combination with one another, such as water glass and ammonia or mercaptosuccinic acid, 2,2-dimethoxy-2-phenylacetophenone, triethoxyvinylsilane, and ethanol. To view the effect of gelation agent on surface area in a quantitative way, Table 12 is displayed, which shows the gelation agent used in the synthesis of as-dried aerogels with surface areas that were in the top 10th percentile in the ZrAGDB. Additionally, select surface area values are displayed in Figure 32.

Table 12: Gelation agents for zirconia aerogels. Gelation agents used in the synthesis of zirconia aerogels that had surface areas in the top 10th percentile in the zirconia aerogel graph database (ZrAGDB).

Reference	**Gelation Agent**	**Surface Area (m^2/g)**
Koval'ko, 2017[27]	propylene oxide	878.5
Koval'ko, 2017[27]	propylene oxide	815.5
Hu, 2017[21]	propylene oxide	772.2
Benad, 2018[46]	propylene oxide	709.0
Benad, 2018[46]	propylene oxide	696.0
Xiong, 2014[40]	propylene oxide	672.9
Liu, 2019[4]	propylene oxide	651.0
Gao, 2018[49]	water glass + ammonia	650.0
Xiong, 2014[40]	propylene oxide	644.3
Liu, 2018[1]	ammonium hydroxide	630.7
Ren, 2015[32]	propylene oxide	619.0
He, 2016[19]	propylene oxide	616.4
Liu, 2019[4]	propylene oxide	603.0
Benad, 2018; Ren, 2015[32,46]	propylene oxide	602.0
Liu, 2019[4]	ammonium hydroxide	600.0
Benad, 2018[46]	propylene oxide	599.0

The sub-graph also exhibited potentially unexplored synthesis pathways for zirconia aerogels with high surface areas. It could be observed that, although citric acid and ammonium

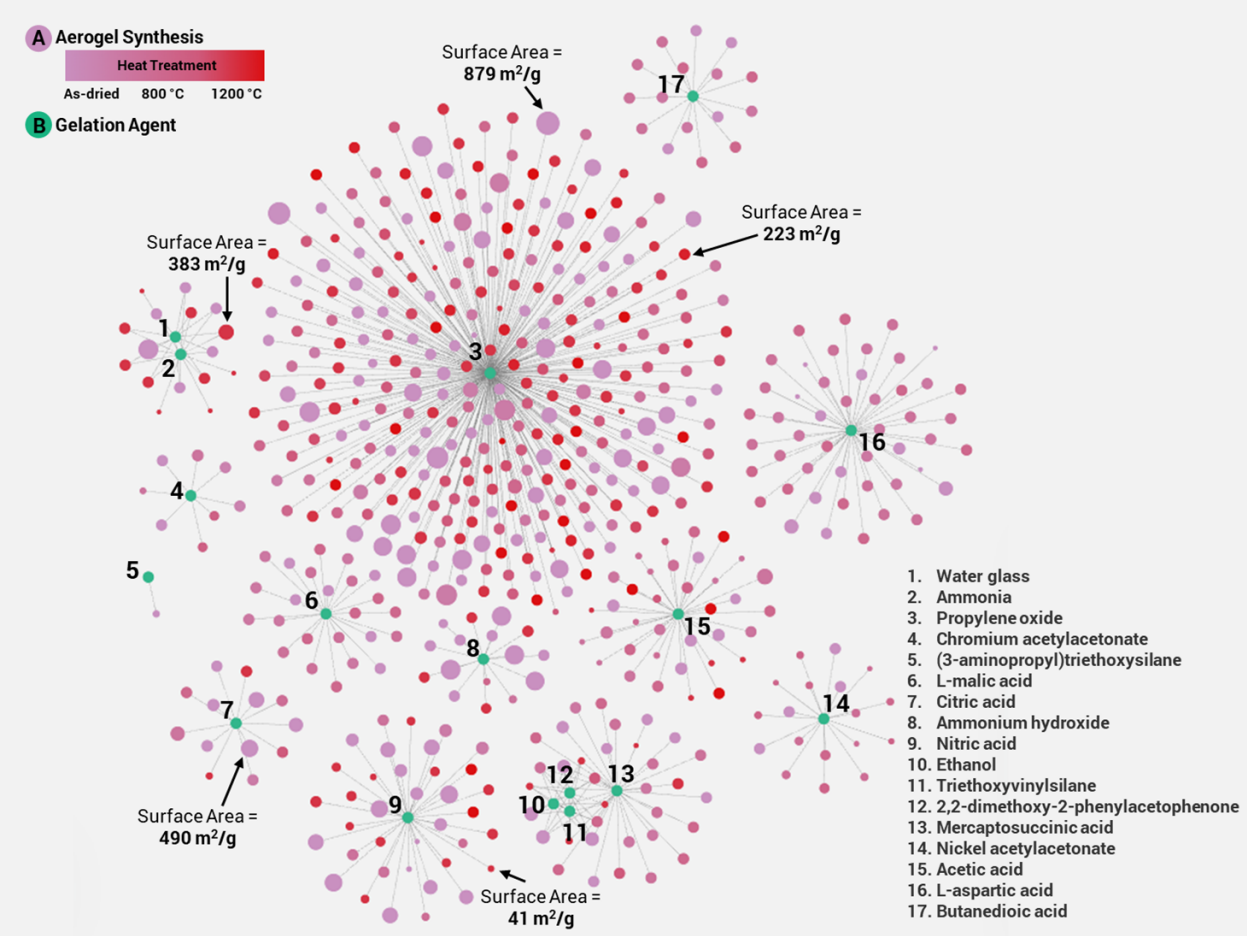

Figure 32: Gelation agent sub-graph of the zirconia aerogel graph database (ZrAGDB). Sub-graph of the ZrAGDB examining A) zirconia aerogel synthesis and B) the gelation agent used. The purple to red color gradient corresponds to the heat-treatment temperature of the aerogels from as-dried to 1200°C. The larger nodes correspond to aerogels with higher resulting surface areas.

hydroxide were not commonly used, these gelation agents synthesized as-dried aerogels with high surface areas. In addition, while heat-treatment seemed to decrease aerogel surface area with most of the gelation agents, the combination of water glass and ammonia was shown to be used in the synthesis of heat-treated aerogels with high surface areas. While water glass and ammonia were not frequently used, the use of this solvent system as a gelation agent may be beneficial when synthesizing zirconia aerogels for thermal management applications. These examples showed ways in which the ZrAGDB could be useful in enhancing the understanding and efficiency of zirconia aerogel synthesis prior to experiment.

Zirconia aerogels, unique mesoporous materials with high specific surface areas and low thermal conductivities, can be useful in a wide range of thermal management systems, including high-temperature applications in aerospace and aeronautics. However, it is important to optimize the synthesis methods and processing conditions of these materials so that the mesoporous structure is retained when the aerogel is exposed to temperatures above 1000°C. Due to the large number of synthetic variables, this dissertation utilized an architected information structure to begin to analyze the synthesis, processing, and properties of zirconia aerogels. The connection between the final properties of the zirconia aerogels and the synthesis pathways used to produce them was displayed in the zirconia aerogel graph database (ZrAGDB) in a visual and dynamic way. It was anticipated that the ZrAGDB would be useful in the optimization of these materials, enhancing the understanding and efficiency of zirconia aerogel synthesis. While the preliminary queries observed synthetic effects on surface area, properties such as crystalline phase, pore structure, density, and thermal conductivity could also be investigated. The influence of the combination of multiple synthesis and processing parameters could also be explored. This information could be further extended for assisting in the synthesis of various other highly dimensional materials, leading to improved elucidation in structure-properties-performance relationships.

8.3 Information architecture use case, part II: Silica aerogels

While preliminary work was done in the development of the zirconia aerogel graph database, this process was taken one step further in the development of the silica aerogel graph database (SiAGDB). While zirconia aerogels were not synthesized until 1976, silica aerogels were discovered by Samuel S. Kistler in 1931.[190,355] Because they preceded zirconia aerogels by over 40 years, the availability of literature documenting silica aerogels was much greater.

The SiAGDB included the synthesis and processing variables of approximately 1000 silica aerogel materials.[52–148] The SiAGDB was created from 97 manuscripts detailing the synthesis of 997 silica aerogel materials. The manuscripts were selected based on a balance of research impact and contemporary work. Using Web of Science, all journal articles resulting from the topic search of "silica aerogel(s)" and published between 2016 and 2020 were reviewed for relevance. All applicable information detailing the synthesis and properties of silica aerogels was added to the SiAGDB. Following this initial manuscript screening, an additional search was completed in Web of Science for the topic of "silica aerogel(s)", which was sorted by highest citation. The results were reviewed for relevance and all applicable manuscripts with over 350 citations were included in the SiAGDB.

Each unique material in the SiAGDB had as many as 100 synthetic or processing variables associated with its lifecycle, as well as final aerogel properties reported. These variables included elements of the sol-gel synthesis, such as silica precursor, solvents, dopants, surfactants, and acid or base catalysts, along with the concentration of each material added to the sol. Sol-gel synthesis variables also included hydrolysis times, stir times, and pHs. The SiAGDB included information on post-gelation processing, such as aging, washing, and modification solvents and soak times. Drying and sintering parameters were also included, such as temperatures, times, pressures, and cycles. Additionally, the SiAGDB included the final properties reported for the aerogel samples, such as surface area, pore volume, average pore size, average pore diameter, bulk density, crystalline phase, Young's modulus and thermal conductivity. We primarily focused on the property of resulting surface area as high surface

area is one of the key features of silica aerogels. In most cases, as previously described, surface area is characterized by the method of Brunauer, Emmett and Teller (BET).[325]

The final silica aerogel graph database (SiAGDB) curated more than 1000 aerogel instances with more than 7500 nodes and 20,000 edges. The full SiAGDB is displayed in Figure 33, with Figure 33A,B showing the influence of surfactant and base catalyst on the aerogel surface area, respectively.

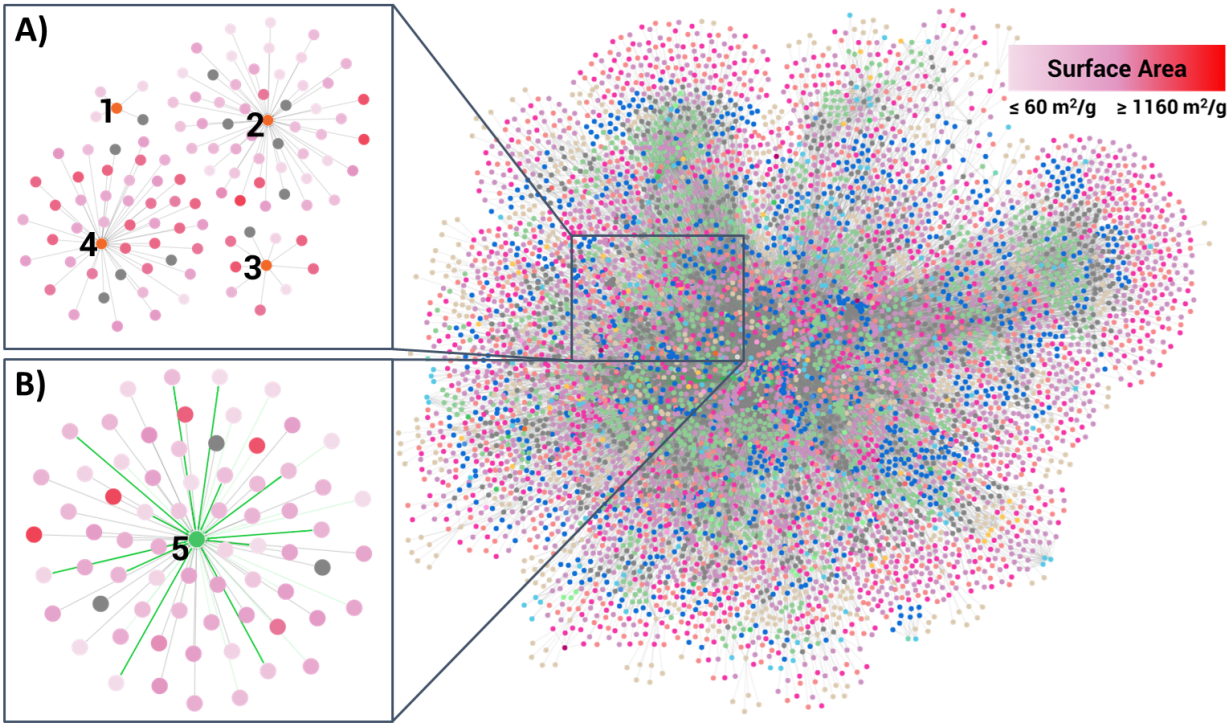

Figure 33: Sub-graphs of the silica aerogel graph database (SiAGDB). Influence of A) surfactant and B) base catalyst on aerogel surface area. Surfactant nodes and base catalyst node represent 1) Ralufon 414, 2) Cetrimonium Bromide, 3) Sodium Dodecyl Sulfate, 4) Cetyltrimethylammonium Chloride, and 5)Ammonium Hydroxide.

In Figure 33, the graph was reduced to amplify the impact of specific synthesis or processing conditions on silica aerogel properties. The surface area reported for each aerogel was represented by a gradient (Figure 33A,B) and the initial concentration of the base catalyst was represented by thicker edges for higher concentrations (Figure 33B). The utility of node and edge manipulations as well as the necessity of performing smaller queries is evident in Figure 33. The central figure shows the entire collection of data from all 1000 aerogels, while

the sub-graphs provide examples of how the SiAGDB can be queried for smaller groups of samples for easier visualization. Consider Figure 33A, which shows all aerogels with a surfactant template. The resulting figure is far more manageable than the entire SiAGDB and gives information upon observation about which surfactants were used in aerogels with higher surface areas. For example, cetyltrimethylammonium chloride led to more aerogels with higher surface areas as compared to cetrimonium bromide. In Figure 33B, each aerogel was synthesized using a surfactant and the base catalyst ammonium hydroxide, NH_4OH. This figure displays which surfactant used in combination with NH_4OH might yield the largest surface area as the aerogels with the top five highest surface areas were synthesized using cetrimonium bromide, determined when further expanding the aerogel node properties. The line thickness in Figure 33B also gives insight into which initial concentrations of NH_4OH to use as high surface area aerogels were synthesized using NH_4OH with an initial concentration of 0.5 M. Both sub-graphs show the product of queries to the SiAGDB resulting in useful insights into surfactant and base catalyst selection as it influenced aerogel surface area.

Chapter 9 Understanding structure/property-process relationships in aerogels through machine learning

The complex synthetic pathways to aerogels result in a large number of synthetic and processing variables, making effective aerogel synthesis often time-consuming and difficult. The synthetic and processing variables used in aerogel synthesis must be understood and carefully determined, as each variable can influence the final properties of the aerogel including surface area, porosity, and density.[10,152] However, each synthetic and processing variable has a certain level of uncertainty attributed to it due to variations in experimental precision. Therefore, to reduce experimental dimensionality within synthetic and processing conditions of aerogels, we have developed a supervised machine learning neural network regression model.

We focused on the final surface area of the aerogels, as surface area is a commonly reported property and aerogels with high surface area are effective for many applications. Following the development of the SiAGDB, discussed previously in section 8.3, and data cleaning methods, we used a neural network model to predict the surface area of silica aerogels from synthetic and processing conditions, as shown in Figure 34. Machine learning models have been used in tandem with experimental results as a way to screen and validate choices of synthetic and processing parameters, as well as to accurately predict adsorption isotherms in nanoporous materials.[356–359]

We explored the neural network regression model through a variety of silica aerogel sub-regions contained in the SiAGDB, including silica precursor, base catalyst, and drying method. We demonstrated that predictive relationships between synthesis and processing of silica aerogels and the resulting properties, specifically surface areas, could be established. This increased understanding could be used to reduce experimental dimensional complexity and to recommend synthesis and processing conditions to achieve a silica aerogel target.

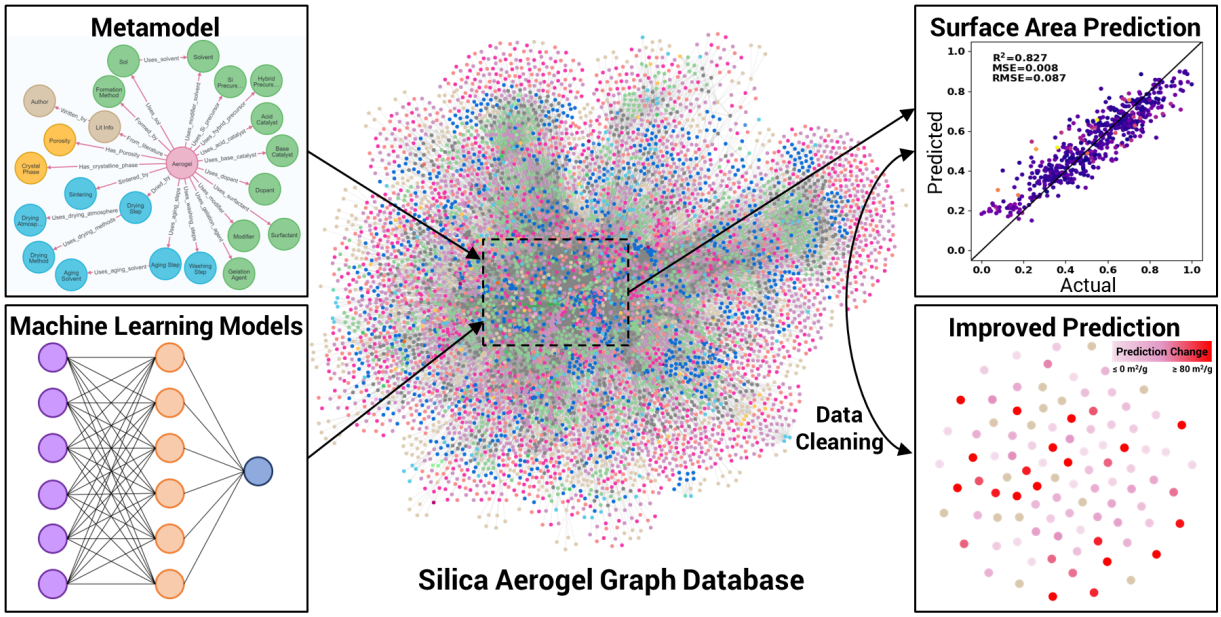

Figure 34: Utilization of the silica aerogel graph database (SiAGDB) and machine learning. Machine learning models are used with the SiAGDB to predict the BET surface area of silica aerogels from synthetic and processing conditions.

9.1 Machine learning by neural network for prediction of aerogel surface area

Machine learning models have been used to screen choices of synthetic and processing parameters, determining candidate materials that should be investigated experimentally following an initial computational analysis.[356,357] Figure 35 is a summary of the modeling and data cleaning workflow. The machine learning algorithm was a Keras Sequential Neural Network.[360] Several parameters could be modified to improve the model, including number of layers, number of nodes in each layer, etc. Hypertuning was used to find the best parameters for a given model and split. The process outlined below was applied to all the splits in this dissertation.

The Random Search method was used to randomly select values for each parameter. Parameters were randomly selected 15 times (15 trials). In each trial, following the selection of random parameters, the model was trained and it was observed how well the model

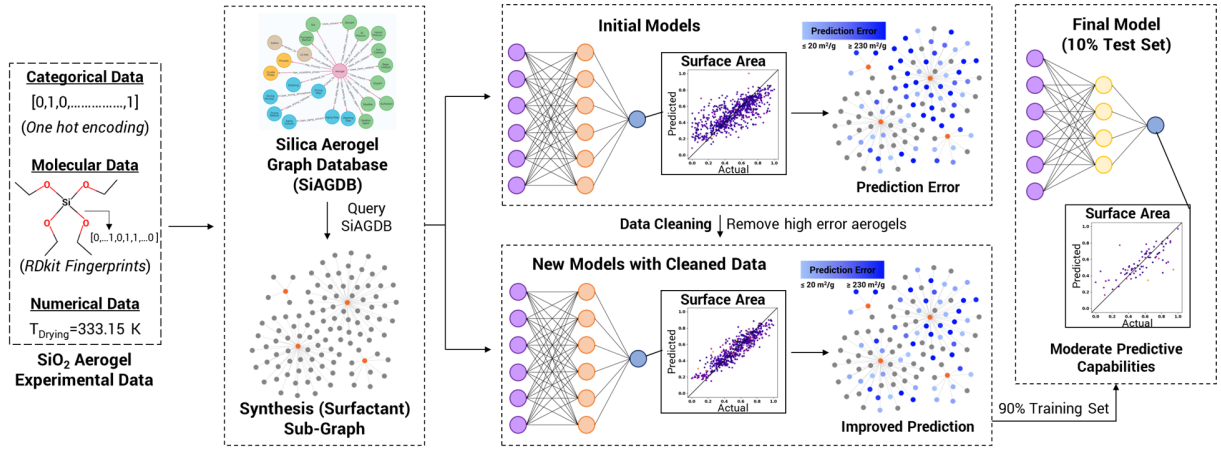

Figure 35: Modeling workflow. The utilization of machine learning models, with the silica aerogel graph database (SiAGDB), to clean silica aerogel experimental data prior to the development of the final neural network regression model, which uses a 10% test set and a 90% training set.

predicted on the validation set. The trial with the lowest value of mean squared error (MSE) was the trial that the final parameters were pulled from. In these models, there were [0, 9] hidden layers between the input and output layers. There were [10, 200] neurons in each hidden layer with a step of 10. The dropout for each hidden layer was [0.15, 0.4] with a step of 0.02. Dropout represents the odds of a given neuron being forced to zero in each layer during training; this parameter reduces overfitting and trades training accuracy for validation accuracy. There were 100 epochs, number of times that the entire dataset was cycled through the algorithm. In this hypertuning pipeline, no early stopping was used.

Prior to model training and validation, it was ensured that all of the data within the SiAGDB was machine-readable and that samples contained in the SiAGDB that were classified as xerogels or did not have a reported surface area were removed. Of the 997 samples contained in the SiAGDB, 119 were classified as xerogels and 94 did not have a reported surface area value; these samples were dropped prior to training any of the machine learning models. Attribute values in the model included both numerical data, such as sol concentrations, aging, or drying temperatures, and non-numerical data, such as precursors, solvents, or surfactants. For use in the neural network, non-numerical molecular data was converted to a

feature representation using RDKit; RDkit fingerprints contain information about molecules in a 1D bit-vector array and can be used to compare different synthetic compounds.[361] Additionally, categorical data was encoded to a one-hot numeric array.[362] Numerical data describing the synthesis and processing of silica aerogels contained in the SiAGDB was then used by initial models, utilizing K-fold cross-validation, to predict the resulting aerogel surface area. The results of the models were quantified using the absolute error of the predicted surface area value and the actual surface area value, which was found to be a better metric when quantifying the results as compared to percent error. Data cleaning, further described in section 9.2, was conducted to enhance the prediction capabilities of the models.

Following data cleaning by the removal of aerogels with high prediction error, a supervised machine learning neural network regression model was developed for the whole range of cleaned data, using 10% of the aerogels as a test set and 90% of the aerogels as a training set. The resulting model had an average surface area predicted error of 109 ± 84 m^2/g. The PVA graph (Figure 36) had an R^2 value of 0.731, with MSE and RMSE values of 0.014 and 0.118, respectively, demonstrating moderate predictive capabilities for aerogel surface area. This neural network model was used to map synthetic and processing conditions of SiAGDB sub-regions to the aerogel BET surface area, establishing predictive relationships between synthetic variables and a final aerogel property.

In the SiAGDB, a link to the model that predicted the surface area for each aerogel was stored as a node property for each aerogel contained in the test set. The raw silica aerogel data, the code to create the SiAGDB, and the code used to train and test the models have been included in the following GitHub repository: `https://github.com/jameskferri/Aerogel_ML_Neo4j.git`.

9.2 Machine learning by neural network for data cleaning

Prior to the development of the neural network regression model, data cleaning was conducted to decide which data sets should be included to aid in prediction. As an example,

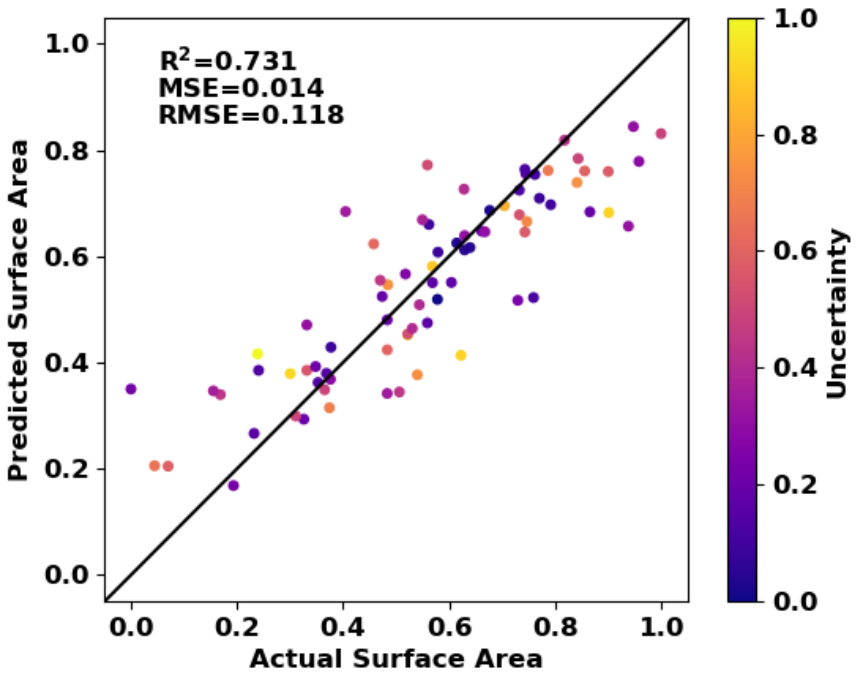

Figure 36: Results of the final neural network regression model. Normalized predicted versus actual (PVA) graph for the surface areas of all aerogels in the model.

Zhang et al. utilized data cleaning to improve predictions of structural properties and adsorption isotherms of carbide-derived carbons which concurred with experimental results.[363] Data cleaning was also utilized by Kojima et al. in the modeling of adsorption isotherms in nanoporous adsorbents to determine deviations between experimental and simulated data.[364] Reproducibility of experimental data is known to be an issue in materials chemistry research.[365] While the number of replicate measurements was often lacking, meta-analyses have described the inconsistency with replicate measurements of approximately 20% of reported adsorption isotherms for porous materials.[366–369] Additionally, considering the reproducibility of the BET measurement of surface area, a possible spread of at least 300 m^2/g for identical materials was reported by Osterrieth et al.[370] The reasoning behind deviations was not always directly identified; however, outliers may have pointed to the reproducibility of experimental conditions and results, low experimental precision, or inconsistency in measurement calculations.

Similarly, due to experiments with high error or results with low precision, not all reported

synthesis and processing conditions of silica aerogels may be reliable or reproducible. By using the developed models to identify aerogels with high prediction error, data cleaning was beneficial for determining unreliable experimental data that may have been difficult to classify a priori. We anticipated that, following data cleaning methods, the developed neural network regression model could be used to predict aerogel surface area from synthesis and processing conditions with precision. However, we recognized that high prediction error may also have pointed to unique or unconventional processes reported in the SiAGDB, previously unseen by the model.

Prior to data cleaning, a control set of models was considered; the aerogels had an average surface area predicted error of 135 ± 119 m^2/g. As a benchmark, a simple data cleaning protocol of removing statistical outliers only, aerogels with a reported surface area above or below two standard deviations of the mean surface area, was used. Following data cleaning by statistical outliers, the aerogels had an average predicted error of 125 ± 106 m^2/g. Compared to the control models, removing statistical outliers decreased the average error by 7%.

Data cleaning by statistical outliers is a primitive method, as there were still persistent low-resolution experiments that were being used in the models; therefore, a second method of data cleaning was utilized to improve the models. Data cleaning by prediction error removed statistical outliers and removed aerogels with a resulting prediction error greater than one standard deviation from the average absolute error following the previous models. Using data cleaning by prediction error, the aerogels had an average surface area prediction error of 76 ± 55 m^2/g. By removing high error samples, the average error decreased by 39% as compared to just removing statistical outliers. Dropping aerogels with high prediction error overall improved the models and kept the prediction error relatively constant across samples. Data cleaning by prediction error was determined to be the most effective method, as further seen in Figure 37 and Figure 38.

Predicted versus actual (PVA) graphs, normalized using min-max scaling, are displayed

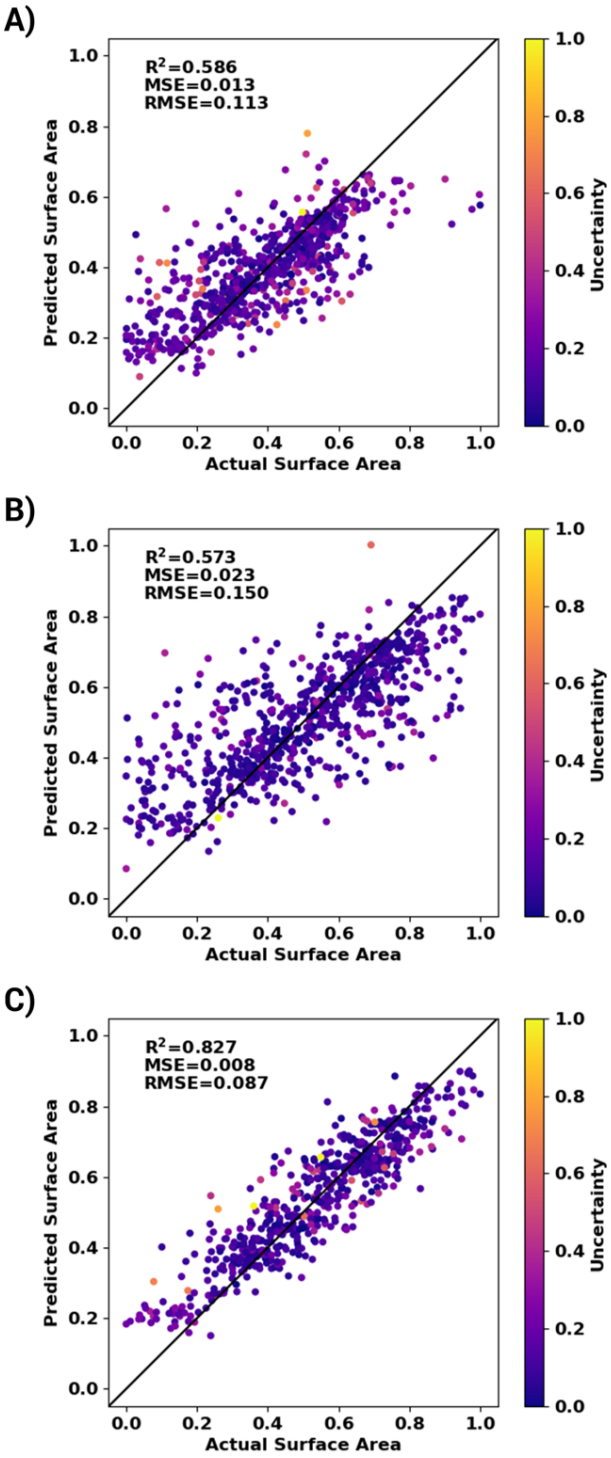

Figure 37: Normalized predicted versus actual (PVA) graphs for all aerogels using K-fold cross-validation. The PVA graphs represent A) control models, B) data cleaning by statistical outliers, and C) data cleaning by machine learning prediction error.

for the surface areas of all aerogels used in the control models (Figure 37A), the models in which statistical outliers were removed (Figure 37B), and the models in which high error samples were removed (Figure 37C). The uncertainty of each sample represents the standard deviation of the predicted surface area values. The R-squared (R^2), mean squared error (MSE), and root mean squared error (RMSE) values described the goodness of fit between the predicted and actual surface area values. An increasing R^2 value and deceasing MSE and RMSE values, as well as a closer fit to the y = x line, indicated that a model was predicting surface area more accurately. A priori removal of statistical outliers alone (Figure 37B) resulted in negligible improvement of model prediction as compared to control models (Figure 37A). However, successive, serial removal of aerogels with high prediction error (Figure 37C) resulted in significant improvement of model prediction.

Figure 38 displays the average surface area prediction error for all aerogels across a manuscript following data cleaning by statistical outliers (Figure 38A) and following data cleaning by prediction error (Figure 38B). The average surface area prediction error was represented with a gradient, while tan nodes indicated manuscripts that were not included in the models, as they either contained aerogels with unreported surface areas, contained information only relating to xerogels, or contained only aerogels with surface area values that were statistical outliers. It could be seen from Figure 38 that prediction error decreased following data cleaning by prediction error for most of the manuscripts; additionally, a few manuscripts were removed from the model due to data cleaning. The change in prediction error is represented in Figure 38C. A large average change in prediction error indicated that data cleaning by prediction error decreased the average prediction error significantly as compared to data cleaning by statistical outliers. A minimal change between data cleaning by statistical outliers and data cleaning by prediction error or, in a few cases, a negative change in prediction error indicated that the error increased in data cleaning by prediction error as compared to data cleaning by statistical outliers. For these manuscripts, dropping the high error samples did not overall decrease the prediction error; this may have been due to the

prediction capabilities of the models, which may have struggled predicting the surface areas of certain aerogels either based on unique experimental conditions, experimental precision, or experimental uncertainty. Figure 38 shows that data cleaning by prediction error resulted in a lower prediction error overall.

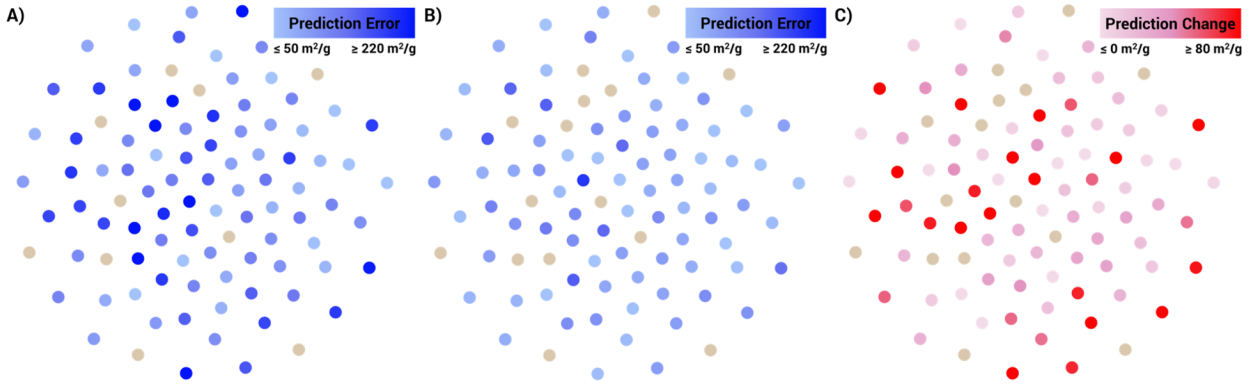

Figure 38: Surface area prediction error by manuscript. The sub-graphs represent A) data cleaning by statistical outliers, B) data cleaning by prediction error, and C) prediction change between data cleaning methods.

Samples with higher error were harder for the model to accurately predict surface area. This could potentially have been caused by a number of reasons, including experimental precision and reproducibility or unique experimental conditions previously unseen by the model. As an example, one sample with high error following data cleaning by statistical outliers was reported with only two other samples, and while it was dried via ambient pressure drying, the other samples were dried via autoclave and classified as xerogels; therefore, this sample was the only sample to be included in the model from this manuscript. This particular sample was also sintered, which is relatively infrequent for silica aerogels, as only about 20% of samples in the SiAGDB had reported sintering conditions. This sample was dropped from the model due to high prediction error. As another example, the sample with the highest uncertainty following data cleaning by statistical outliers was reported in a manuscript that detailed an unconventional formation method for the sols; 95% of the SiAGDB reported the sol-gel method as the primary formation method, while this manuscript detailed laser exposure of the sols as the formation method. This sample was not dropped from the models,

as the resulting error was not within the high error values that were dropped during data cleaning, and the sample's prediction error decreased in subsequent models.

Following data cleaning by machine learning prediction error, the supervised machine learning neural network regression model was developed using a 10% test set; the model had an average surface area predicted error of 109 ± 84 m^2/g, demonstrating moderate predictive capabilities for aerogel surface area.

9.3 Synthesis optimization by machine learning with the silica aerogel graph database

We considered machine learning methods to predict thermophysical properties, such as surface area, of silica aerogels in this dissertation due to the sheer number of synthetic and processing variables. We anticipated that machine learning could be used as a guide to find valuable experiments, saving time and resources by avoiding arbitrary experimentation.

As discussed previously, base catalysts are an important component of the silica aerogel sol and should be chosen deliberately. We used the developed silica aerogel graph database (SiAGDB) and predictive neural network model to further investigate the base catalyst sub-region of silica aerogel synthesis (Figure 39). The model mapped the synthetic condition of base catalyst to the final aerogel property of surface area.

Utilization of the SiAGDB with the base catalyst sub-region is displayed in Figure 39A,B, showing the influence of base catalyst on aerogel surface area and surface area prediction error, respectively. In Figure 39A and Figure 39B, the surface area and surface area prediction error, respectively, were represented by a gradient; gray nodes represented unreported surface areas in Figure 39A and aerogels dropped from the models in Figure 39B. Figure 39A also shows the relationship between initial base catalyst concentration and surface area; edges with reported initial concentrations were thicker for larger concentrations. The remaining sub-graphs followed the same formatting.

From Figure 39A, observations on which base catalyst and initial concentrations led

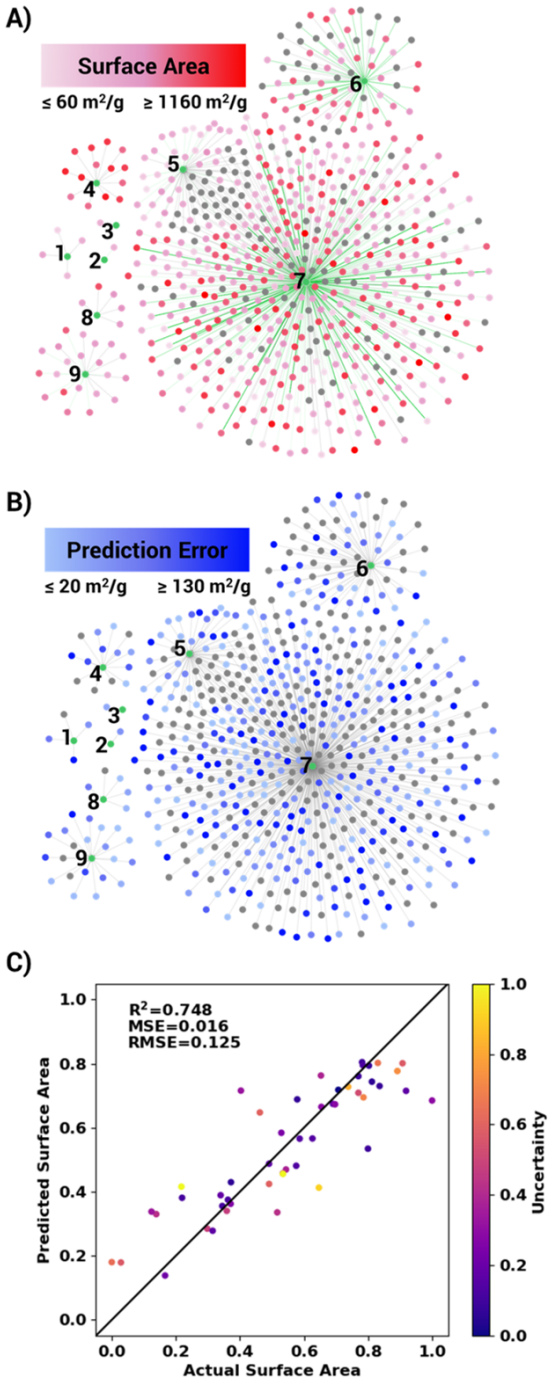

Figure 39: Influence of base catalyst on BET surface area of silica aerogels. Synthesis condition (base catalyst) sub-graphs of the silica aerogel graph database (SiAGDB) displaying the influence of base catalyst on A) surface area and B) surface area prediction error following machine learning. Base catalyst nodes represent 1) Amine, 2) Potassium Hydroxide, 3) Lithium Hydroxide, 4) Tetramethylammonium Hydroxide, 5) Ammonium Fluoride, 6) Ammonia, 7) Ammonium Hydroxide, 8) Water Glass, and 9) Sodium Hydroxide. C) Normalized PVA graph of the base catalyst sub-region.

to higher surface areas can be seen. For example, ammonium hydroxide was the most commonly used base catalyst and created aerogels with both low and high surface areas; however, tetramethylammonium hydroxide was less widely used but led to high surface area. Sodium hydroxide was also a less frequently used base catalyst but led to mid-range surface area values. Determination of base catalyst initial concentration influence on surface area was more difficult, potentially since base catalyst concentration had less of an impact on surface area than other synthetic variables. For example, when using ammonium hydroxide and when using ammonia, high initial concentrations (10 M) led to both low and high surface areas.

In Figure 39B, it did appear that the base catalyst had an effect on the prediction error following data cleaning. For example, the aerogels using sodium hydroxide and tetramethylammonium hydroxide had a lower prediction error than the aerogels with ammonium hydroxide and amine. However, this could have been due to other factors such as the wide variety of reported experimental conditions in the case of ammonium hydroxide or due to the sparseness of available data in the case of amine.

The normalized predicted versus actual (PVA) graph for the surface area values of aerogels using a base catalyst in the model (10% test set) is displayed in Figure 39C. The model was shown to have moderate surface area predictive capabilities on the base-catalyst subregion. A few samples were still difficult for the model to predict on; this could have been attributed to a number of different factors, including unique experimental techniques previously unseen by the models and varying levels of uncertainty in the experimental conditions or reported final properties.

9.4 Processing optimization by machine learning with the silica aerogel graph database

Drying is an important step in silica aerogel processing, transforming wet gels into aerogels. We utilized the developed SiAGDB and predictive neural network model for the supercriti-

cal drying sub-region and the ambient pressure drying sub-region, the two most used drying methods in the SiAGDB (Figure 40 and Figure 41, respectively). The model mapped processing condition, drying method, to the final aerogel property, surface area. The sub-graphs, grouped by the ten most frequently used silica precursors for each drying method, provided insight into which silica precursors were commonly used with each drying method as well as which precursors led to higher surface area and lower prediction error. The normalized PVA graphs for each drying method are also displayed, which show that the model had moderate predictive capabilities following data cleaning by prediction error.

Figure 40A,B display sub-graphs of the influence of precursor on the surface area and prediction error, respectively, of supercritically dried silica aerogels. Tetramethyl orthosilicate (TMOS) and tetraethyl orthosilicate (TEOS) were the most commonly used precursors for supercritically dried silica aerogels, leading to aerogels with both low and high surface areas. There were several common precursors that were used in combination with one another, such as TMOS and (3-aminopropyl)triethoxysilane (APTES). (3-aminopropyl) trimethoxysilane (APTMS) and vinylmethyldimethoxysilane (VMDMS) were used in combination and, while not used frequently, led to high surface area aerogels. In Figure 40B, it can be seen that the majority of the silica precursors, specifically the most commonly used precursors, TMOS and TEOS, had aerogels with both low and high prediction errors. This was most likely due to the larger number of samples and the spread of synthetic and processing variables reported. However, the precursor polyethoxydisiloxane (PEDS) was used in aerogels with relatively low prediction error, indicating that the models did better predicting the surface area values for aerogels using PEDS than for aerogels using other silica precursors.

The normalized PVA graph for the surface area values of aerogels used in the model (10% test set) that were dried using supercritical drying is displayed in Figure 40C.

Figure 41A,B display sub-graphs of the SiAGDB with ambient pressure dried silica aerogels. The most commonly used silica precursors for ambient pressure dried aerogels were tetraethyl orthosilicate (TEOS), polyethoxydisiloxane (PEDS), and water glass. Regarding

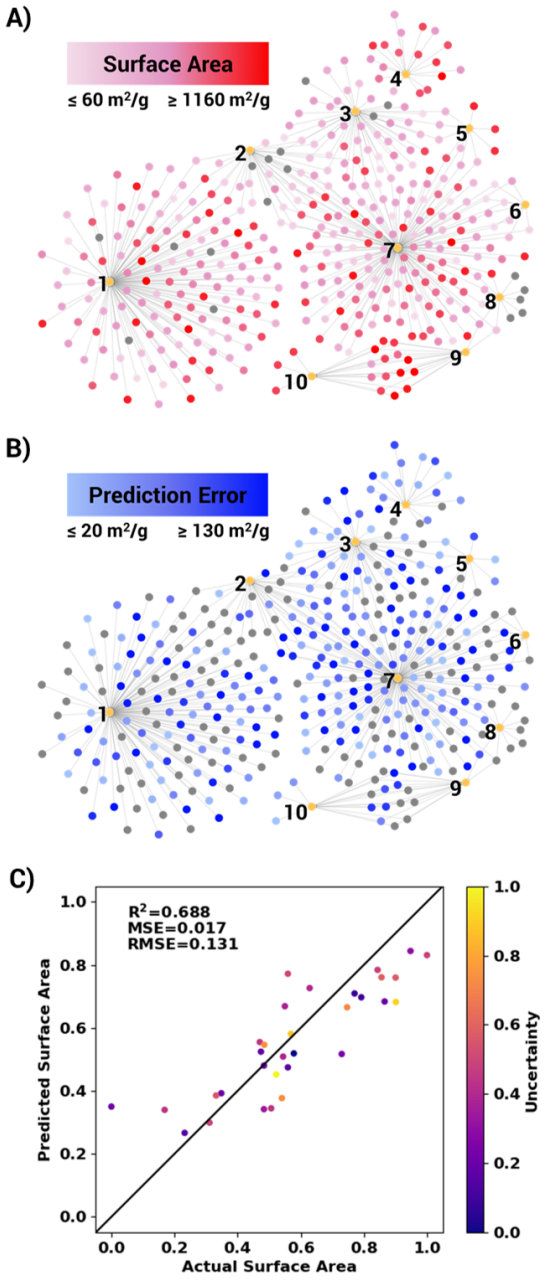

Figure 40: Influence of silica precursor and supercritical drying on BET surface area of silica aerogels. Processing condition (supercritical drying) sub-graphs of the silica aerogel graph database (SiAGDB) displaying the influence of silica precursor and drying method on A) surface area and B) surface area prediction error following machine learning. Silica precursor nodes represent 1) Tetramethyl Orthosilicate, 2) (3-aminopropyl)triethoxysilane, 3) Methyltrimethoxysilane, 4) Polyethoxydisiloxne, 5) Vinyltrimethoxysilane, 6) Vinyltriethoxysilane, 7) Tetraethyl Orthosilicate, 8) Methyltriethoxysilane, 9) (3-aminopropyl)trimethoxysilane, and 10) Vinylmethyldimethoxysilane. C) Normalized PVA graph of the supercritical drying sub-region.

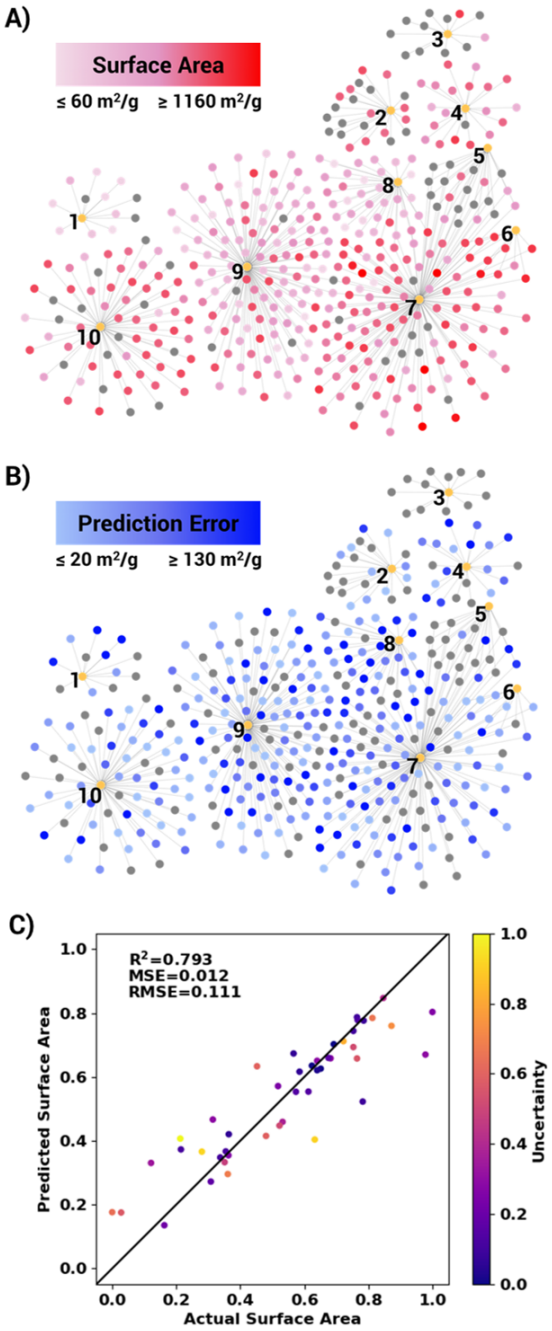

Figure 41: Influence of silica precursor and ambient pressure drying on BET surface area of silica aerogels. Processing condition (ambient pressure drying) sub-graphs of the silica aerogel graph database (SiAGDB) displaying the influence of silica precursor and drying method on A) surface area and B) prediction error following machine learning. Silica precursor nodes represent 1) Silica Hydrosol, 2) Methyltriethoxysilane, 3) Tetrapropoxysilane, 4) Rice Husk Ash, 5) Vinyltrimethoxysilane, 6) Hexamethyldisilazane, 7) Tetraethyl Orthosilicate, 8) Methyltrimethoxysilane, 9) Water Glass, and 10) Polyethoxydisiloxane. C) Normalized PVA graph of the ambient pressure drying sub-region.

the influence of silica precursor on the BET surface area, the precursor TEOS led to higher surface area than water glass. The precursors rice husk ash and methyltrimethoxysilane (MTMS), while not commonly used, often led to aerogels with low surface areas. When hexamethyldisilazane (HMDZ) was used with TEOS, high surface area aerogels resulted. In Figure 41B, it can be seen that the commonly used silica precursors, water glass and TEOS, led to aerogels with both low and high prediction error. This was most likely due to the large number of synthetic processes reported. The silica precursor polyethoxydisiloxane (PEDS) overall led to aerogels with low prediction error, which was also true for supercritically dried aerogels.

The normalized PVA graph for the surface area values of aerogels used in the model that were dried using the ambient pressure drying method is displayed in Figure 41C. The model had moderate predictive capabilities for resulting surface areas in both the supercritical drying and the ambient pressure drying sub-region. It was anticipated that expansion of the SiAGDB may potentially aid in further understanding of the relationships between synthetic and processing conditions and final properties of silica aerogels.

9.5 Experimental application of machine learning with the silica aerogel graph database

When considering an experimentalist, the developed SiAGDB and predictive neural network model described in this work could be highly useful. An experimental chemist, creating silica aerogels with target properties such as high surface area, is faced with a vast set of experimental synthesis and processing conditions, which exponentially increase as the synthetic pathway proceeds. The developed SiAGDB contained approximately 100 unique synthetic and processing variables for each aerogel. Silica aerogels also have a long development life-cycle; aerogel synthesis, from initial sol formulation to final characterized product, takes on average 7 days, with a maximum of 20 days reported in the SiAGDB.

Due to the lengthy experimental time required for aerogel synthesis, arbitrary experi-

mentation or tedious replicate experiments are not feasible. Therefore, understanding the influence of each synthetic pathway on final surface area, and additional properties, of the silica aerogels would be advantageous prior to experimentation. This is where the utility of the developed SiAGDB and neural network regression model is made evident, as these tools represent a new methodology for an experimentalist to digitally design silica aerogels.

Following preliminary considerations of initial starting materials and processing methods that are readily available, an experimentalist would use sub-graphs of the SiAGDB to visually see the relationships between the selected starting materials and processing methods and the final silica aerogel surface area, or another target property, reducing the experimental dimensionality of aerogel synthesis. The experimentalist could then utilize the neural network regression model to further refine the experimental variables by determining if the chosen synthetic pathway can be easily predicted on. Synthesis and processing variables that lead to the model having difficulty in prediction may point to experimental conditions that should be further scrutinized or novel experimental techniques previously unseen by the model.

The new methodology detailed in this work would be useful to an experimentalist by reducing experimental dimensionality through increased understanding of the influence of synthetic and processing variables on the surface area of silica aerogels or other target properties. Increased understanding of these relationships would begin to reduce experimental time and resources, allowing for additional synthesis trials or replicate experiments.

Chapter 10 Conclusions and perspectives

Aerogels are unique, highly porous materials with a wide variety of extreme material properties, including high specific surface area, low density, and low thermal conductivity. Aerogels, first introduced in 1932, are gels which have been isolated from their liquid component, as a gas replaces all of the gel's liquid through a drying process.[371] Aerogels are composed of 95 - 99% air by volume and are the lightest solid material in the world.[149] Due to their material properties, aerogels can be useful in a range of applications, such as catalysis, thermoresisters, sorption media, sensors, electrodes in solid oxide fuel cells, and drug delivery.[1,13,171,173,177,186,188] The high specific surface area and low thermal conductivity enables the effective use of aerogels as thermal management systems, including in aerospace and aeronautics applications.[158–161]

Zirconia (ZrO_2) aerogels have special interest for high-temperature applications due to the high melting point of ZrO_2 (2715°C) and stability between 600°C and 1000°C, where other aerogel systems, such as silica, often begin to sinter and densify. To further increase the thermal stability of zirconia aerogels, yttria-stabilized zirconia (YSZ) aerogels are often used as the addition of yttrium to the zirconia system stabilizes the tetragonal zirconia phase.

However, exposure of YSZ aerogels to high-temperature often leads to pore structure collapse and surface area decrease due to structural rearrangement and polycondensation reactions.[6,7] Pore structure collapse increases thermal conductivity of the aerogels, inhibiting their use at high-temperature; therefore, to effectively use aerogels in thermal management systems, collapse of pore structure and decrease of surface area must be mitigated. Surfactant templates are known to influence the pore structure of aerogels, increasing surface area and reducing pore collapse following high-temperature exposure.

To determine the effect of surfactants with different charges on the pore structure of aerogels, we considered cationic (positively charged), anionic (negatively charged) and non-ionic (without charge) surfactants as templates for 20 mol% YSZ aerogels in this work. The

cationic surfactant cetrimonium bromide (CTAB), the anionic surfactant sodium dodecyl sulfate (SDS) and the nonionic surfactant Pluronic® P-123 were chosen as templating agents for YSZ aerogels. The aerogels were heat-treated at temperatures up to 1100°C to determine the effect of the surfactants on the thermal stability of the aerogels. Further optimization of the aerogel formulation using surfactant templates may enable the effective use of YSZ aerogels at temperatures up to 1100°C.

We used the cationic (positively charged) surfactant cetrimonium bromide, CTAB, as a templating agent for 20 mol% yttria-stabilized zirconia (YSZ) aerogels.[331] As compared to aerogels without CTAB, it was determined that 0.5x the CMC of CTAB increased the surface area of YSZ aerogels by 72% and 41% following high-temperature exposure to 600°C and 1000°C, respectively. Additionally, at 0.5x CTAB, the aerogel pore volume was shown to increase by 75% and 80% at 600°C and 1000°C, respectively. When compared to a concentration of 2x the CMC of CTAB, the concentration of 0.5x had a greater increase in surface area and pore volume. We hypothesized that the higher concentration of CTAB may have negatively influenced gelation of the YSZ sol due to adsorption of the cationic surfactant onto the charged surface sites of the zirconia matrix and subsequent impediment to gelation. This may have decreased the strength of the YSZ gel, leading to increased shrinkage during drying and heat-treatment, and ultimately causing pore collapse and surface area reduction.

Following surfactant templating with CTAB, the anionic surfactant SDS was used as a surfactant template. It was determined that the addition of SDS increased the surface area and pore volume of as-dried aerogels and suppressed crystallite growth at high temperatures. SDS also lead to the formation of a larger volume of mesopores in as-dried aerogels. However, the impact of SDS on the surface area and pore volume of heat-treated aerogels was negligible, potentially due to low concentrations of surfactant and the removal of the surfactant following high-temperature exposure.

The nonionic surfactant, Pluronic® P-123, was then used as a templating agent. Similar to SDS, P-123 surfactant templating resulted in higher surface areas and pore volumes for

as-dried YSZ aerogels. Macropores were formed in the as-dried aerogels, which may have potentially increased the thermal conductivity of the aerogels due to larger pore size. Unlike the cationic and anionic surfactants, electrostatic interactions were not prevalent when the nonionic surfactant P-123 was used, which may have led to less control over pore formation than when using CTAB or SDS. At high-temperature, P-123 did not enhance the surface area and pore volume of the aerogels; however, the average crystallite size of the aerogels was lowered with the addition of P-123 at 1000°C and 1100°C.

Additionally, we demonstrated the use of a predictive measurement, surfactant hydrodynamic radius, to map the behavior of surfactants in the sol prior to gelation to the final properties of YSZ aerogels. By synthesizing aerogels at surfactant concentrations determined through this measurement, the influence of these surfactant concentrations on the final aerogel properties, including surface area, pore volume, and crystallite size, was seen. The use of this predictive measurement could potentially save experimental time as insights into the final properties of aerogels could be gained from measurements of the sol, prior to the completion of the full aerogel development lifecycle.

High surface area aerogels are experimentally favored; however, the abundance of synthetic and processing conditions for aerogels, and the high level of experimental uncertainty associated with these variables, often makes successful synthesis difficult and time-consuming. In this work, we applied an information architecture and a machine learning neural network regression model to enhance knowledge of aerogel synthesis by further understanding the relationships between chosen synthetic variables and final surface area.

A zirconia aerogel graph database (ZrAGDB) and a silica aerogel graph database (SiAGDB) were used to visually display the connections between aerogel properties, such as surface area, and the synthesis and processing pathways used to produce them. While purely a visualization tool, sub-graphs of the ZrAGDB and SiAGDB began to show which conditions may be optimal for aerogel synthesis. This work resulted in a queriable database that enabled search and retrieval in a highly efficient way. Machine learning models were then used to

further understand the influence of synthetic and processing conditions on silica aerogel surface area. The developed model mapped from synthetic and processing conditions to predict the aerogel property, BET surface area, with precision. Removing statistical outliers and aerogels with high prediction error enhanced the model, leading to the prediction of aerogel surface area with an average error of 109 $\pm$ 84 m^2/g. The utilization of these digital design tools by an experimentalist could reduce experimental dimensionality, ultimately reducing time and resource consumption. With further expansion of the SiAGDB, the model could be improved for potential optimization of silica aerogel synthesis, efficiently creating aerogels with high surface area, which are advantageous in applications including thermal insulation, sorption media, drug delivery, and catalysis.[87,154,156,157,163,164,169,170,175,179,189]

References

(1) Liu, B.; Gao, M.; Liu, X.; Xie, Y.; Yi, X.; Zhu, L.; Wang, X.; Shen, X. Monolithic zirconia aerogel from polyacetylacetonatozirconium precursor and ammonia hydroxide gel initiator: formation mechanism, mechanical strength and thermal properties. *RSC Advances* **2018**, *8*, 41603–41611.

(2) Long, J. W.; Chervin, C. N.; Balow, R. B.; Jeon, S.; Miller, J. B.; Helms, M. E.; Owrutsky, J. C.; Rolison, D. R.; Fears, K. P. Zirconia-based aerogels for sorption and degradation of dimethyl methylphosphonate. *Industrial and Engineering Chemistry Research* **2020**, *59*, 19584–19592.

(3) Pollanen, J.; Shirer, K. R.; Blinstein, S.; Davis, J. P.; Choi, H. C.; Lippman, T. M.; Lurio, L. B.; Halperin, W. P. Globally anisotropic high porosity silica aerogels. *Journal of Non-Crystalline Solids* **2008**, *354*, 4668–4674.

(4) Liu, B.; Gao, M.; Liu, X.; Zhao, X.; Zhang, J.; Yi, X. Thermally stable nanoporous ZrO2/SiO2 hybrid aerogels for thermal insulation. *ACS Applied Nano Materials* **2019**, *2*, 7299–7310.

(5) Yoon, S.; Han, G. D.; Jang, D. Y.; Kim, J. W.; Kim, D. H.; Shim, J. H. Fabrication of yttria-stabilized zirconia aerogel for high-performance thermal barrier coating. *Journal of Alloys and Compounds* **2019**, *806*, 1430–1434.

(6) Folgar, C.; Folz, D.; Suchicital, C.; Clark, D. Microstructural evolution in silica aerogel. *Journal of Non-Crystalline Solids* **2007**, *353*, 1483–1490.

(7) Hurwitz, F. I.; Gallagher, M.; Olin, T. C.; Shave, M. K.; Ittes, M. A.; Olafson, K. N.; Fields, M. G.; Guo, H.; Rogers, R. B. Optimization of alumina and aluminosilicate aerogel structure for high-temperature performance. *International Journal of Applied Glass Science* **2014**, *5*, 276–286.

(8) Chervin, C. N.; Clapsaddle, B. J.; Chiu, H. W.; Gash, A. E.; Satcher, J. H.; Kauzlarich, S. M. Aerogel synthesis of yttria-stabilized zirconia by a non-alkoxide sol-gel route. *Chemistry of Materials* **2005**, *17*, 3345–3351.

(9) Almeida, C. M.; Ghica, M. E.; Durães, L. An overview on alumina-silica-based aerogels. *Advances in Colloid and Interface Science* **2020**, *282*.

(10) Walker, R. C.; Potochniak, A. E.; Hyer, A. P.; Ferri, J. K. Zirconia aerogels for thermal management: Review of synthesis, processing, and properties information architecture. *Advances in Colloid and Interface Science* **2021**, *295*, 102464.

(11) Liu, B.; Liu, X.; Zhao, X.; Fan, H.; Zhang, J.; Yi, X.; Gao, M.; Zhu, L.; Wang, X. High-strength, thermal-stable ZrO2 aerogel from polyacetylacetonatozirconium. *Chemical Physics Letters* **2019**, *715*, 109–114.

(12) Chevalier, J.; Gremillard, L.; Virkar, A. V.; Clarke, D. R. The tetragonal-monoclinic transformation in zirconia: Lessons learned and future trends. *Journal of the American Ceramic Society* **2009**, *92*, 1901–1920.

(13) Bangi, U. K. H.; Park, H.-H. Evolution of textural characteristics of surfactant-mediated mesoporous zirconia aerogel powders prepared via ambient pressure drying route. *International Nano Letters* **2018**, *8*, 221–228.

(14) Studart, A. R.; Gonzenbach, U. T.; Tervoort, E.; Gauckler, L. J. Processing routes to macroporous ceramics: A review. *Journal of the American Ceramic Society* **2006**, *89*, 1771–1789.

(15) Sai, H.; Xing, L.; Xiang, J.; Zhang, F.; Cui, L.; Liang, X.; Song, B.; Zhao, C.; Li, Z. Effects of surfactants on the synthesis of silica aerogels prepared by ambient pressure drying. *Key Engineering Materials* **2012**, *512-515*, 1625–1630.

(16) Zarzycki, J.; Prassas, M.; Phalippou, J. Synthesis of glasses from gels: The problem of monolithic gels. *Journal of Materials Science* **1982**, *17*, 3371–3379.

(17) Rezaee, S.; Ranjbar, K.; Kiasat, A. R. The effect of surfactant on the sol–gel synthesis of alumina-zirconia nanopowders. *Ceramics International* **2018**, *44*, 19963–19969.

(18) Jung, H. N. R.; Han, W.; Cho, H. H.; Park, H. H. Effect of cationic and non-ionic surfactants on the microstructure of ambient pressure dried zirconia aerogel. *Materials Express* **2017**, *7*, 291–298.

(19) He, J.; Li, X.; Su, D.; Ji, H.; Zhang, X.; Zhang, W. Super-hydrophobic hexamethyldisilazane modified ZrO2-SiO2 aerogels with excellent thermal stability. *Journal of Materials Chemistry A* **2016**, *4*, 5632–5638.

(20) He, J.; Zhao, H.; Li, X.; Su, D.; Ji, H.; Yu, H.; Hu, Z. Large-scale and ultra-low thermal conductivity of ZrO2 fibrofelt/ZrO2-SiO2 aerogels composites for thermal insulation. *Ceramics International* **2018**, *44*, 8742–8748.

(21) Hu, Z.; He, J.; Li, X.; Ji, H.; Su, D.; Qiao, Y. Improvement of thermal stability of ZrO2–SiO2 aerogels by an inorganic–organic synergetic surface modification. *Journal of Porous Materials* **2017**, *24*, 657–665.

(22) Hurwitz, F. I.; Rogers, R. B.; Guo, H.; Garg, A.; Olson, N. S.; Phan, D.; Cashman, J. L. Phase development and pore stability of yttria- and ytterbia-stabilized zirconia aerogels. *Journal of the American Ceramic Society* **2020**,

(23) Jung, H. N. R.; Parale, V. G.; Kim, T.; Cho, H. H.; Park, H. H. Zirconia-based alumina compound aerogels with enhanced mesopore structure. *Ceramics International* **2018**, *44*, 10579–10584.

(24) Kamoun, N.; Younes, M.; Ghorbel, A.; Mamede, A.; Rives, A. Effect the solvent evacuation mode on the catalytic properties of nickel-modified sulfated zirconia catalysts: n-hexane isomerization. *Reaction Kinetics, Mechanisms and Catalysis* **2014**, *111*, 199–213.

(25) Kamoun, N.; Younes, M.; Ghorbel, A.; Mamede, A.; Rives, A. Comparative study of aerogels nanostructured catalysts: Ni/ZrO2-SO42- and Ni/ZrO2-Al2O3-SO42-. *Ionics* **2015**, *21*, 221–229.

(26) Kong, Y.; Shen, X.; Cui, S. Amine hybrid zirconia/silica composite aerogel for low-concentration CO2 capture. *Microporous and Mesoporous Materials* **2016**, *236*, 269–276.

(27) Koval'ko, N. Y.; Kalinina, M. V.; Malkova, A. N.; Lermontov, S. A.; Morozova, L. V.; Polyakova, I. G.; Shilova, O. A. Synthesis and comparative studies of xerogels, aerogels, and powders based on the ZrO2–Y2O3–CeO2 system. *Glass Physics and Chemistry* **2017**, *43*, 368–375.

(28) Lermontov, S. A.; Malkova, A. N.; Yurkova, L. L.; Straumal, E. A.; Gubanova, N. N.; Baranchikov, A. Y.; Ivanov, V. K. Diethyl and methyl-tert-buthyl ethers as new solvents for aerogels preparation. *Materials Letters* **2014**, *116*, 116–119.

(29) Lermontov, S.; Malkova, A.; Yurkova, L.; Straumal, E.; Gubanova, N.; Baranchikov, A.; Smirnov, M.; Tarasov, V.; Buznik, V.; Ivanov, V. Hexafluoroisopropyl alcohol as a new solvent for aerogels preparation. *Journal of Supercritical Fluids* **2014**, *89*, 28–32.

(30) Matějová, L.; Matěj, Z. Nanostructured ZrO2 synthesized by using pressurized and supercritical fluids—Its structural and microstructural evolution and thermal stability. *Journal of Supercritical Fluids* **2017**, *128*, 182–193.

(31) Raissi, S.; Kamoun, N.; Younes, M. K.; Ghorbel, A. Effect of drying conditions on the textural, structural and catalytic properties of Cr/ZrO2-SO4: N-hexane conversion. *Reaction Kinetics, Mechanisms and Catalysis* **2015**, *115*, 499–512.

(32) Ren, J.; Cai, X.; Yang, H.; Guo, X. Preparation and characterization of high surface area ZrO2 aerogel modified by SiO2. *Journal of Porous Materials* **2015**, *22*, 973–978.

(33) Shi, Z.; Gao, H.; Wang, X.; Li, C.; Wang, W.; Hong, Z.; Zhi, M. One-step synthesis of monolithic micro-nano yttria stabilized ZrO2-Al2O3 composite aerogel. *Microporous and Mesoporous Materials* **2018**, *259*, 26–32.

(34) Torres-Rodríguez, J.; Kalmár, J.; Menelaou, M.; Čelko, L.; Dvořak, K.; Cihlář, J.; Cihlař, J.; Kaiser, J.; Győri, E.; Veres, P.; Fábián, I.; Lázár, I. Heat treatment induced phase transformations in zirconia and yttria-stabilized zirconia monolithic aerogels. *Journal of Supercritical Fluids* **2019**, *149*, 54–63.

(35) Torres-Rodriguez, J.; Gutierrez-Cano, V.; Menelaou, M.; Kaštyl, J.; Cihlář, J.; Tkachenko, S.; González, J. A.; Kalmár, J.; Fábián, I.; Lázár, I.; Čelko, L.; Kaiser, J. Rare-earth zirconate Ln2Zr2O7 (Ln: La, Nd, Gd, and Dy) powders, xerogels, and aerogels: preparation, structure, and properties. *Inorganic Chemistry* **2019**, *58*, 14467–14477.

(36) Wang, Q.; Li, X.; Fen, W.; Ji, H.; Sun, X.; Xiong, R. Synthesis of crack-free monolithic ZrO2 aerogel modified by SiO2. *Journal of Porous Materials* **2014**, *21*, 127–130.

(37) Wang, X.; Li, C.; Shi, Z.; Zhi, M.; Hong, Z. The investigation of an organic acid assisted sol-gel method for preparing monolithic zirconia aerogels. *RSC Advances* **2018**, *8*, 8011–8020.

(38) Wang, X.; Wu, Z.; Zhi, M.; Hong, Z. Synthesis of high temperature resistant ZrO2-SiO2 composite aerogels via "thiol-ene" click reaction. *Journal of Sol-Gel Science and Technology* **2018**, *87*, 734–742.

(39) Wu, L.-a.; Jiang, X.; Wu, S.; Yao, R.; Qiao, X.; Fan, X. Synthesis of monolithic zirconia with macroporous bicontinuous structure via epoxide-driven sol-gel process accompanied by phase separation. *Journal of Sol-Gel Science and Technology* **2014**, *69*, 1–8.

(40) Xiong, R.; Li, X.; Ji, H.; Sun, X.; He, J. Thermal stability of ZrO2 SiO2 aerogel modified by Fe(III) ion. *Journal of Sol-Gel Science and Technology* **2014**, *72*, 496–501.

(41) Yu, H.; Tong, Z.; Qiao, Y.; Yang, Z.; Yue, S.; Li, X.; Su, D.; Ji, H. High thermal stability of SiO2–ZrO2 aerogels using solvent-thermal aging. *Journal of Solid State Chemistry* **2020**, *291*.

(42) Zhang, Z.; Gao, Q.; Liu, Y.; Zhou, C.; Zhi, M.; Hong, Z.; Zhang, F.; Liu, B. A facile citric acid assisted sol-gel method for preparing monolithic yttria-stabilized zirconia aerogel. *RSC Advances* **2015**, *5*, 84280–84283.

(43) Zhong, L.; Chen, X.; Song, H.; Guo, K.; Hu, Z. Synthesis of monolithic zirconia aerogel via a nitric acid assisted epoxide addition method. *RSC Advances* **2014**, *4*, 31666–31671.

(44) Zu, G.; Shen, J.; Wang, W.; Zou, L.; Lian, Y.; Zhang, Z.; Liu, B.; Zhang, F. Robust, highly thermally stable, core-shell nanostructured metal oxide aerogels as high-temperature thermal superinsulators, adsorbents, and catalysts. *Chemistry of Materials* **2014**, *26*, 5761–5772.

(45) Zu, G.; Shen, J.; Zou, L.; Zou, W.; Guan, D.; Wu, Y.; Zhang, Y. Highly thermally stable zirconia/silica composite aerogels prepared by supercritical deposition. *Microporous and Mesoporous Materials* **2017**, *238*, 90–96.

(46) Benad, A.; Jürries, F.; Vetter, B.; Klemmed, B.; Hübner, R.; Leyens, C.; Eychmüller, A. Mechanical properties of metal oxide aerogels. *Chemistry of Materials* **2018**, *30*, 145–152.

(47) Cahill, J. T.; Turner, S.; Ye, J.; Shevitski, B.; Aloni, S.; Baumann, T. F.; Zettl, A.; Kuntz, J. D.; Worsley, M. A. Ultrahigh-temperature ceramic aerogels. *Chemistry of Materials* **2019**, *31*, 3700–3704.

(48) Chao, X.; Yuan, W.; Shi, Q.; Zhu, Z. Improvement of thermal stability of zirconia aerogel by addition of yttrium. *Journal of Sol-Gel Science and Technology* **2016**, *80*, 667–674.

(49) Gao, H.; Zhang, Z.; Shi, Z.; Zhang, J.; Zhi, M.; Hong, Z. Synthesis of high-temperature resistant monolithic zirconia-based aerogel via facile water glass assisted sol–gel method. *Journal of Sol-Gel Science and Technology* **2018**, *85*, 567–573.

(50) Gligor, D.; Baia, M.; Danciu, V. Preparation, physical-chemical and electrochemical characterization of ZrO2 aerogels modified with H3[PW12O40]. *Journal of Optoelectronics and Advanced Materials* **2017**, *19*, 650–657.

(51) Guo, X.; Song, J.; Ren, J.; Yang, F.; Kanamori, K.; Nakanishi, K. Facile preparation of well-defined macroporous yttria-stabilized zirconia monoliths via sol–gel process accompanied by phase separation. *Journal of Porous Materials* **2016**, *23*, 867–875.

(52) Babiarczuk, B.; Lewandowski, D.; Szczurek, A.; Kierzek, K.; Meffert, M.; Gerthsen, D.; Kaleta, J.; Krzak, J. Novel approach of silica-PVA hybrid aerogel synthesis by simultaneous sol-gel process and phase separation. *The Journal of Supercritical Fluids* **2020**, *166*, 104997.

(53) Sert Çok, S.; Koç, F.; Gizli, N. Hydrophobic silica aerogels synthesized in ambient conditions by preserving the pore structure via two-step silylation. *Ceramics International* **2020**, *46*, 27789–27799.

(54) Nguyen, T.; Mai, N.; Minnam Reddy, V.; Jung, J.; Truong, N. Synthesis of silica aerogel particles and its application to thermal insulation paint. *Korean Journal of Chemical Engineering* **2020**, *37*, 1803–1809.

(55) Nah, H.-Y.; Kim, Y.; Kim, T.; Lee, K.-Y.; Parale, V.; Lim, C.-H.; Seo, J.-Y.; Park, H.-H.; Oh, J. Comparisonal studies of surface modification reaction using various sily-

lating agents for silica aerogel. *Journal of Sol-Gel Science and Technology* **2020**, *96*, 346–359.

(56) Luo, W.; Shu, X.; Xu, B.; Liu, Z.; Ou, Z.; Liu, J. Influence of hydrolysis time on properties of SiO2 aerogels prepared by ambient pressure drying. *Arabian Journal for Science and Engineering* **2020**, *46*, 1–8.

(57) Li, Z.; Zhao, S.; Koebel, M.; Malfait, W. Silica aerogels with tailored chemical functionality. *Materials & Design* **2020**, *193*, 108833.

(58) Yujing, W.; Han, J.; Zhai, J.; Yang, D. The Effect of Different Alkaline Catalysts on the Formation of Silica Aerogels Prepared by the Sol–Gel Approach. *J. Ceram. Soc. Jpn.* **2020**, *128*, 395–403.

(59) Yang, X.; Wu, Z.; Chen, H.; Du, Q.; Yu, L.; Zhang, R.; Zhou, Y. A facile preparation of ambient pressure–dried hydrophilic silica aerogels and their application in aqueous dye removal. *Frontiers in Materials* **2020**, *7*.

(60) Ghica, M.; Almeida, C.; Fonseca, M.; Portugal, A.; Durães, L. Optimization of polyamide pulp-reinforced silica aerogel composites for thermal protection systems. *Polymers* **2020**, *12*, 1278.

(61) Vareda, J.; Valente, A.; Durães, L. Silica aerogels/xerogels modified with nitrogen-containing groups for heavy metal adsorption. *Molecules* **2020**, *25*, 2788.

(62) Cai, H.; Jiang, Y.; Feng, J.; Chen, Q.; Zhang, S.; Li, L.; Feng, J. Nanostructure evolution of silica aerogels under rapid heating from 600°C to 1300°C via in-situ TEM observation. *Ceramics International* **2020**, *46*, 12489–12498.

(63) Lermontov, S.; Baranchikov, A.; Sipyagina, N.; Malkova, A.; Kopitsa, G.; Yorov, K.; Ivanova Polezhaeva, O.; Len, A.; Ivanov, V. Is supercritical so critical? The choice of temperature to synthesize SiO2 aerogels. *Russian Journal of Inorganic Chemistry* **2020**, *65*, 255–262.

(64) Parale, V.; Kim, T.; Lee, K.-Y.; Phadtare, V.; Dhavale, R.; Jung, H.-N.-R.; Park, H.-H. Hydrophobic TiO2–SiO2 composite aerogels synthesized via in situ epoxy-ring opening polymerization and sol-gel process for enhanced degradation activity. *Ceramics International* **2019**, *46*.

(65) Yang, H.; Li, C.; Yue, X.; Huo, J.; Ye, F.; Liu, J.; Shi, F.; Ma, J. New BN/SiOC aerogel composites fabricated by the sol-gel method with excellent thermal insulation performance at high temperature. *Materials & Design* **2020**, *185*, 108217.

(66) Zhao, S.; Stojanovic, A.; Angelica, E.; Emery, O.; Rentsch, D.; Pauer, R.; Koebel, M.; Malfait, W. Phase transfer agents facilitate the production of superinsulating silica aerogel powders by simultaneous hydrophobization and solvent- and ion-exchange. *Chemical Engineering Journal* **2019**, *381*, 122421.

(67) Kim, H.; Kim, K.; Kim, H.; Lee, D.; Park, J. Eco-friendly synthesis of water-glass-based silica aerogels via catechol-based modifier. *Nanomaterials* **2020**, *10*, 2406.

(68) Choi, H.; Parale, V. G.; Kim, T.; Choi, Y.-S.; Tae, J.; Park, H.-H. Structural and mechanical properties of hybrid silica aerogel formed using triethoxy(1-phenylethenyl)silane. *Microporous and Mesoporous Materials* **2020**, *298*, 110092.

(69) Wang, L.; Guo, R.; Ren, J.; Song, G.; Chen, G.; Zhou, Z.; Li, Q. Preparation of superhydrophobic and flexible polysiloxane aerogel. *Ceramics International* **2020**, *46*, 10362–10369.

(70) Shi, F.; Liu, J.; Liu, J.; Huang, X.; Hu, S.; Liu, D.; Wang, Y.; Shan, Z. Influences of solvothermal-assisted crystallization process on the microstructure and properties of SiO2-W0.02TiO2.06 composite aerogels synthesized via ambient pressure drying. *Journal of Sol-Gel Science and Technology* **2019**, *92*, 101–115.

(71) Huang, Y.; He, S.; Feng, M.; Dai, H.; Pan, Y.; Cheng, X. Organic solvent-saving prepa-

ration of water glass based aerogel granules under ambient pressure drying. *Journal of Non-Crystalline Solids* **2019**, *521*, 119507.

(72) Gao, H.; Bo, L.; Liu, P.; Chen, D.; Li, A.; Ou, Y.; Dong, C.; Wang, J.; Chen, X.; Hou, C.; Dong, W.; Wang, G. Ambient pressure dried flexible silica aerogel for construction of monolithic shape-stabilized phase change materials. *Solar Energy Materials and Solar Cells* **2019**, *201*, 110122.

(73) Zhang, J.; Kong, Y.; Jiang, X.; Zhong, Y.; Chen, Y.; Shen, X. Synthesis of hydrophobic silica aerogel and its composite using functional precursor. *Journal of Porous Materials* **2020**, *27*, 1–7.

(74) Mandal, C.; Donthula, S.; Rewatkar, P.; Sotiriou-Leventis, C.; Leventis, N. Experimental deconvolution of depressurization from capillary shrinkage during drying of silica wet-gels with SCF CO2 why aerogels shrink? *Journal of Sol-Gel Science and Technology* **2019**, *92*, 662–680.

(75) Stojanovic, A.; Comesaña, S.; Rentsch, D.; Koebel, M.; Malfait, W. Ambient pressure drying of silica aerogels after hydrophobization with mono-, di- and tri-functional silanes and mixtures thereof. *Microporous and Mesoporous Materials* **2019**, *284*, 289–295.

(76) Kong, Y.; Zhang, J.; Zhiyang, Z.; Jiang, X.; Shen, X. Monolithic silicon nitride-based aerogels with large specific surface area and low thermal conductivity. *Ceramics International* **2019**, *45*, 16331–16337.

(77) Chen, F.; Zhang, B.; Cai, W.; Fan, N.; Lu, Y.; Yin, L.; Zhang, Z.; Ning, W.-S. Effect of doping Al on the desulfurization performance of Ag/SiO2-Al2O3 aerogel composite adsorbents. *Industrial & Engineering Chemistry Research* **2019**, *58*, 14918–14928.

(78) Wang, L.; Song, G.; Guo, R.; Qiao, X.; Chen, G.; Zhou, Z.; Li, Q. Enhancing aerogel

mechanical properties with incorporation of POSS. *Ceramics International* **2019**, *45*, 14586–14593.

(79) Mandal, C.; Donthula, S.; Soni, R.; Bertino, M.; Sotiriou-Leventis, C.; Leventis, N. Light scattering and haze in TMOS-co-APTES silica aerogels. *Journal of Sol-Gel Science and Technology* **2019**, *90*, 127–139.

(80) Torres, R.; Vareda, J.; Lamy-Mendes, A.; Durães, L. Effect of different silylation agents on the properties of ambient pressure dried and supercritically dried vinyl-modified silica aerogels. *The Journal of Supercritical Fluids* **2019**, *147*, 81–89.

(81) Wang, L.; Feng, J.; Jiang, Y.; Li, L.; Feng, J. Thermal conductivity of polyvinylpolymethylsiloxane aerogels with high specific surface area. *RSC Advances* **2019**, *9*, 7833–7841.

(82) Guo, X.; Shan, J.; Lei, W.; Ding, R.; Zhang, Y.; Yang, H. Facile synthesis of methylsilsesquioxane aerogels with uniform mesopores by microwave drying. *Polymers* **2019**,

(83) Lamy-Mendes, A.; Girão, A.; Silva, R.; Durães, L. Polysilsesquioxane-based silica aerogel monoliths with embedded CNTs. *Microporous and Mesoporous Materials* **2019**, *288*, 109575.

(84) Zhang, Z.; Wang, X.; Zu, G.; Kanamori, K.; Nakanishi, K.; Shen, J. Resilient, fire-retardant, and mechanically strong polyimide-polyvinylpolymethylsiloxane composite aerogel prepared via stepwise chemical liquid deposition. *Materials & Design* **2019**, *183*, 108096.

(85) F. Al-Sharuee, I. Thermal conductivity performance of silica aerogel after exposition on different heating under ambient pressure. *Baghdad Science Journal* **2019**, *16*, 770–774.

(86) Ban, G.; Song, S.; Lee, H.; Kim, H. T. Effect of acidity levels and feed rate on the porosity of aerogel extracted from rice husk under ambient pressure. *Nanomaterials* **2019**, *9*, 300.

(87) Zhao, Y.; Li, Y. L.; Zhang, R. Silica aerogels having high flexibility and hydrophobicity prepared by sol-gel method. *Ceramics International* **2018**, 21262–21268.

(88) Chen, D.; Wang, X.; Ding, W.; Zou, W.; Zhu, Q.; Shen, J. Silica aerogel monoliths derived from silica hydrosol with various surfactants. *Molecules* **2018**, *23*, 3192.

(89) Liu, S.; Zhang, B.; Bai, Z.; Chen, F.; Xie, F.; Zhou, J.; Lu, Y.; Miao, G.; Jin, J.; Zhang, Z. New Cu2O-SiO2 composite aerogel-like desulfurization adsorbents with different molar ratio of Si/Cu based on π-complexation. *Energy & Fuels* **2018**, *32*, 13004–13014.

(90) Zhu, J.; Ren, H.; Bi, Y. Opacified graphene-doped silica aerogels with controllable thermal conductivity. *Journal of Porous Materials* **2018**, *25*, 1697–1705.

(91) Zhou, T.; Gong, L.; Cheng, X.; Pan, Y.; Li, C.; Zhang, H. Preparation and characterization of silica aerogels from by-product silicon tetrachloride under ambient pressure drying. *Journal of Non-Crystalline Solids* **2018**, *499*, 387–393.

(92) Fei, Z.; Yang, Z.; Chen, G.; Li, K.; Zhao, S.; Su, G. Preparation and characterization of glass fiber/polyimide/SiO2 composite aerogels with high specific surface area. *Journal of Materials Science* **2018**, *53*, 12885–12893.

(93) Xu, H.; Jia, J.; Zhao, S.; Chen, P.; Xia, Q.; Wu, J.; Zhu, P. Hydrophobic TiO2-SiO2 aerogel composites for fast removal of organic pollutants. *ChemistrySelect* **2018**, *3*, 10483–10490.

(94) Li, M.; Jiang, H.; Dong, x. Synthesis and characterization of a xonotlite fibers–silica aerogel composite by ambient pressure drying. *Journal of Porous Materials* **2018**, *25*, 1417–1425.

(95) Lei, C.; Li, J.; Sun, C.; Yang, H.; Xia, T.; Hu, Z.; Zhang, Y. Transparent, elastic and crack-free polymethylsilsesquioxane aerogels prepared by controllable shrinkage of the hydrogels in the aging process. *Microporous and Mesoporous Materials* **2018**, *267*, 107–114.

(96) Maleki, H.; Whitmore, L.; Hüsing, N. Novel multifunctional polymethylsilsesquioxane-silk fibroin aerogel hybrids for environmental and thermal insulation applications. *Journal of Materials Chemistry A* **2018**, *6*, 12598–12612.

(97) Xuan, L.; Li, B.; Li, M.; Hu, W.; Chen, W. Thermal stability of Al-modified silica aerogels through epoxide-assisted sol–gel route followed by ambient pressure drying. *Journal of Sol-Gel Science and Technology* **2018**, *87*, 83–94.

(98) Nah, H.-Y.; Parale, V.; Lee, K.-Y.; Choi, H.; Kim, T.; Lim, C.-H.; Seo, J.-Y.; Ku, Y.; Park, J.-W.; Park, H.-H. Silylation of sodium silicate-based silica aerogel using trimethylethoxysilane as alternative surface modification agent. *Journal of Sol-Gel Science and Technology* **2018**, *87*, 319–330.

(99) Zhou, T.; Cheng, X.; Pan, Y.; Li, C.; Gong, L.; Zhang, H. Mechanical performance and thermal stability of glass fiber reinforced silica aerogel composites based on co-precursor method by freeze drying. *Applied Surface Science* **2017**, *437*, 321–328.

(100) Zu, G.; Kanamori, K.; Shimizu, T.; Zhu, Y.; Maeno, A.; Kaji, H.; Nakanishi, K.; Shen, J. A versatile double cross-linking approach to transparent, machinable, super-compressible, highly bendable aerogel thermal superinsulators. *Chemistry of Materials* **2018**, *30*, 2759–2770.

(101) Piñero, M.; Mesa Diaz, M. d. M.; de los Santos, D.; Reyes Peces, M.; Díaz-Fraile, J.; De la Rosa-Fox, N.; Esquivias, L.; Morales-Florez, V. Reinforced silica-carbon nanotube monolithic aerogels synthesised by rapid controlled gelation. *Journal of Sol-Gel Science and Technology* **2018**, *86*, 391–399.

(102) Mohammadian, M.; Jafarzadeh Kashi, T. S.; Erfan, M.; Soorbaghi, F. P. Synthesis and characterization of silica aerogel as a promising drug carrier system. *Journal of Drug Delivery Science and Technology* **2018**, *44*, 205–212.

(103) Mahani, A.; Motahari, S.; Mohebbi, A. Sol-gel derived flexible silica aerogel as selective adsorbent for water decontamination from crude oil. *Marine Pollution Bulletin* **2017**, *129*, 438–447.

(104) Lei, C.; Hu, Z.; Zhang, Y.; Yang, H.; Li, J.; Hu, S. Tailoring structural and physical properties of polymethylsilsesquioxane aerogels by adjusting NH3·H2O concentration. *Microporous and Mesoporous Materials* **2018**, *258*, 236–243.

(105) Parale, V.; Han, W.; Jung, H.-N.-R.; Lee, K.-Y.; Park, H.-H. Ambient pressure dried tetrapropoxysilane-based silica aerogels with high specific surface area. *Solid State Sciences* **2017**, *75*, 63–70.

(106) Feng, Q.; Chen, K.; Ma, D.; Lin, H.; Liu, Z.; Qin, S.; Luo, Y. Synthesis of high specific surface area silica aerogel from rice husk ash via ambient pressure drying. *Colloids and Surfaces A* **2017**, *539*, 399–406.

(107) Li, T.; Du, A.; Zhang, T.; Ding, W.; Liu, M.; Shen, J.; Zhang, Z.; Zhou, B. Continuous adjustment of fractal dimension of silica aerogels. *Journal of Non-Crystalline Solids* **2018**, *499*, 159–166.

(108) Li, Y.; Du, A.; Shen, J.; Zhang, Z.; Wu, G.; Zhou, B. Temperature dependence of dynamic mechanical behaviors in low density MTMS-derived silica aerogel. *Journal of Porous Materials* **2018**, *25*, 1229–1235.

(109) Nah, H.-Y.; Parale, V.; Jung, H.-N.-R.; Lee, K.-Y.; Lim, C.-H.; Ku, Y.; Park, H.-H. Role of oxalic acid in structural formation of sodium silicate-based silica aerogel by ambient pressure drying. *Journal of Sol-Gel Science and Technology* **2018**, *85*, 302–310.

(110) He, X.; Cheng, X.; Zhang, Y.; Shao, Z. Multiscale structural characterization of methyltriethoxysilane-based silica aerogels. *Journal of Materials Science* **2018**, *53*, 994–1004.

(111) Lermontov, S. A.; Malkova, A. N.; Sipyagina, N. A.; Straumal, E. A.; Baranchikov, A. E.; Ivanov, V. K. Propylene oxide as a new reagent for mixed SiO2-based aerogels preparation. *Journal of Sol-Gel Science and Technology* **2017**, *84*, 377–381.

(112) Lermontov, S.; Malkova, A.; Sipyagina, N.; Yorov, K.; Kopitsa, G.; Baranchikov, A.; Ivanov, V.; Pipich, V.; Székely, N. K. Comparative analysis of the physicochemical characteristics of SiO2 aerogels prepared by drying under subcritical and supercritical conditions. *Inorganic Materials* **2017**, *53*, 1270–1278.

(113) Temel, T.; Karakuzu İkizler, B.; Terzioğlu, P.; Yücel, S.; Elalmış, Y. The effect of process variables on the properties of nanoporous silica aerogels: An approach to prepare silica aerogels from biosilica. *Journal of Sol-Gel Science and Technology* **2017**, *84*, 51–59.

(114) Yiyi, D.; Zhong, M.; Zhang, C.; Liu, W.; Li, N.; Zhang, Z. The relationship between the silica wet-gels relative optical transmittance at 500 nm and structural features of silica aerogels. *Ceramics International* **2017**, *43*, 10668–10672.

(115) Ślosarczyk, A. Synthesis and characterization of silica aerogel-based nanocomposites with carbon fibers and carbon nanotubes in hybrid system. *Journal of Sol-Gel Science and Technology* **2017**, 16–22.

(116) Shalygin, A.; Kozhevnikov, I.; Gerasimov, E.; Andreev, A.; Lapina, O.; Martyanov, O. The impact of Si/Al ratio on properties of aluminosilicate aerogels. *Microporous and Mesoporous Materials* **2017**, *251*, 105–113.

(117) Lei, Y.; Chen, X.; Song, H.; Hu, Z.; Cao, B. Improvement of thermal insulation performance of silica aerogels by Al2O3 powders doping. *Ceramics International* **2017**, *43*, 10799–10804.

(118) Gao, X.; Huang, Y.; Zhang, T.; Wu, Y.; Li, X. Amphiphilic SiO2 hybrid aerogel: An effective absorbent for emulsified wastewater. *Journal of Materials Chemistry A* **2017**, *5*, 12856–12862.

(119) Ehgartner, C.; Grandl, S.; Feinle, A.; Hüsing, N. Flexible organofunctional aerogels. *Dalton Transactions* **2017**, *46*, 8809–8817.

(120) Júlio, M. d. F.; Ilharco, L. M. Ambient pressure hybrid silica monoliths with hexamethyldisilazane: From vitreous hydrophilic xerogels to superhydrophobic aerogels. *ACS Omega* **2017**, *2*, 5060–5070, PMID: 31457783.

(121) He, S.; Chen, X. Flexible silica aerogel based on methyltrimethoxysilane with improved mechanical property. *Journal of Non-Crystalline Solids* **2017**, *463*, 6–11.

(122) Wu, X.; Shao, G.; Liu, S.; Shen, X.; Cui, S.; Chen, X. A new rapid and economical one-step method for preparing SiO2 aerogels using supercritical extraction. *Powder Technology* **2017**, *312*, 1–10.

(123) He, S.; Yang, H.; Chen, X. Facile synthesis of highly porous silica aerogel granules and its burning behavior under radiation. *Journal of Sol-Gel Science and Technology* **2017**, *82*, 407–416.

(124) Li, J.; Lei, Y.; Xu, D. K.; Liu, F.; Li, J.; Sun, A.; Guo, J.; Xu, G. Improved mechanical and thermal insulation properties of monolithic attapulgite nanofiber/silica aerogel composites dried at ambient pressure. *Journal of Sol-Gel Science and Technology* **2017**, *82*, 702–711.

(125) Pan, Y.; He, S.; Gong, L.; Cheng, X.; Li, C.; Li, Z.; Liu, Z.; Zhang, H. Low thermal-conductivity and high thermal stable silica aerogel based on MTMS/water-glass co-precursor prepared by freeze drying. *Materials & Design* **2017**, *113*, 246–253.

(126) Iswar, S.; Malfait, W. J.; Balog, S.; Winnefeld, F.; Lattuada, M.; Koebel, M. M. Effect of aging on silica aerogel properties. *Microporous and Mesoporous Materials* **2017**, *241*, 293–302.

(127) Saeed, S.; Saoud, K.; Bertino, M.; White, L. Fabrication of strong and ultra-lightweight silica-based aerogel materials with tailored properties. *Journal of Porous Materials* **2018**, *25*, 511–520.

(128) Eskandari, N.; Motahari, S.; Atoufi, Z.; Hashemi Motlagh, G.; Najafi, M. Thermal, mechanical, and acoustic properties of silica-aerogel/UPVC composites. *Journal of Applied Polymer Science* **2016**, *134*.

(129) Morales-Florez, V.; Piñero, M.; Braza, V.; Mesa, M.; Esquivias, L.; De la Rosa-Fox, N. Absorption capacity, kinetics and mechanical behaviour in dry and wet states of hydrophobic DEDMS/TEOS-based silica aerogels. *Journal of Sol-Gel Science and Technology* **2017**, *81*, 1–11.

(130) Du, M.-H.; Wei, Q.; Nie, Z.-R.; Cui, S.-P.; Liu, S.-W.; Li, Q.-Y. A rapid and low solvent/silylation agent-consumed synthesis, pore structure and property of silica aerogels from dislodged sludge. *Journal of Sol-Gel Science and Technology* **2017**, *81*, 427–435.

(131) Ren, H.; Zhu, J.; Bi, Y.; Xu, Y.; Zhang, L. One-step fabrication of transparent hydrophobic silica aerogels via in situ surface modification in drying process. *Journal of Sol-Gel Science and Technology* **2016**, *80*, 635–641.

(132) Li, M.; Jiang, H.; Xu, D.; Hai, O.; Zheng, W. Low density and hydrophobic silica aerogels dried under ambient pressure using a new co-precursor method. *Journal of Non-Crystalline Solids* **2016**, *452*, 187–193.

(133) Yorov, K.; Sipyagina, N.; Baranchikov, A.; Lermontov, S.; Borilo, L.; Ivanov, V. SiO2–TiO2 binary aerogels: Synthesis in new supercritical fluids and study of thermal stability. *Russian Journal of Inorganic Chemistry* **2016**, *61*, 1339–1346.

(134) Zhao, S.; Malfait, W. J.; Jeong, E.; Fischer, B.; Zhang, Y.; Xu, H.; Angelica, E.; Risen, W. M.; Suggs, J. W.; Koebel, M. M. Facile one-pot synthesis of mechanically robust biopolymer–silica nanocomposite aerogel by cogelation of silicic acid with citosan in aqueous media. *ACS Sustainable Chemistry & Engineering* **2016**, *4*, 5674–5683.

(135) Sorour, M.; Hani, H.; Bazedi, G.; EL-Rafei, A. Hydrophobic silica aerogels for oil spills clean-up, synthesis, characterization and preliminary performance evaluation. *Journal of Porous Materials* **2016**, *23*, 1401–1409.

(136) Ishihara, A.; Oono, H.; Hashimoto, T.; Nasu, H. Preparation of SiO2 and SiO2–Al2O3 catalysts by gel skeletal reinforcement using hexamethyldisiloxane (HMDS) and acetic anhydride and aluminum tri-sec-butoxide (ASB) systems and elucidation of their catalytic cracking properties as matrices. *Microporous and Mesoporous Materials* **2016**, *233*, 163–170.

(137) Huang, Y.-D.; Gao, X.-D.; Gu, Z.; Li, X.-M. Amino-terminated SiO2 aerogel towards highly-effective lead (II) adsorbent via the ambient drying process. *Journal of Non-Crystalline Solids* **2016**, *443*, 39–46.

(138) Cheng, Y.; Xia, M.; Luo, F.; Li, N.; Guo, C.; Wei, C. Effect of surface modification on physical properties of silica aerogels derived from fly ash acid sludge. *Colloids and Surfaces A* **2016**, *490*, 200–206.

(139) Duan, Y.; Jana, S. C.; Lama, B.; Espe, M. P. Hydrophobic silica aerogels by silylation. *Journal of Non-Crystalline Solids* **2016**, *437*, 26–33.

(140) Liu, S.-W.; Wei, Q.; Cui, S.-P.; Nie, Z.-R.; Du, M.-H.; Li, Q.-Y. Hydrophobic silica

aerogel derived from wheat husk ash by ambient pressure drying. *Journal of Sol-Gel Science and Technology* **2016**, *78*, 60–67.

(141) Perissinotto, A.; Awano, C.; De Vicente, F.; Donatti, D.; Mesquita, A.; Da Silva, L.; Vollet, D. Structure and diffuse-boundary in hydrophobic and sodium dodecyl sulfate-modified silica aerogels. *Microporous and Mesoporous Materials* **2015**, *223*, 196–202.

(142) Bagheri, S.; Mehrpouya, N.; Khosravani, E. The peculiarities of silica aerogel production using azeotropic mixtures. *Journal of Dispersion Science and Technology* **2016**, *37*, 1423–1435.

(143) Wu, X.; Shao, G.; Shen, X.; Cui, S.; Wang, L. Novel Al2O3–SiO2 composite aerogels with high specific surface area at elevated temperatures with different alumina/silica molar ratios prepared by a non-alkoxide sol–gel method. *RSC Advances* **2016**, *6*, 5611–5620.

(144) Zhou, Y.; Schattka, J. H.; Antonietti, M. Room-temperature ionic liquids as template to monolithic mesoporous silica with wormlike pores via a sol-gel nanocasting technique. *Nano Letters* **2004**, *4*, 477–481.

(145) Leventis, N.; Sotiriou-Leventis, C.; Zhang, G.; Rawashdeh, A.-M. M. Nanoengineering strong silica aerogels. *Nano Letters* **2002**, *2*, 957–960.

(146) Peri, J. B. Infrared study of OH and NH2 groups on the surface of a dry silica aerogel. *Journal of Physical Chemistry* **1966**, *70*, 2937–2945.

(147) Randall, J. P.; Meador, M. A. B.; Jana, S. C. Tailoring mechanical properties of aerogels for aerospace applications. *ACS Applied Materials & Interfaces* **2011**, *3*, 613–626, PMID: 21361281.

(148) Dutoit, D.; Schneider, M.; Baiker, A. Titania-silica mixed oxides: I. Influence of sol-gel and drying conditions on structural properties. *Journal of Catalysis* **1995**, *153*, 165–176.

(149) Smirnova, I.; Gurikov, P. Aerogel production: Current status, research directions, and future opportunities. *Journal of Supercritical Fluids* **2018**, *134*, 228–233.

(150) Pierre, A. C.; Pajonk, G. M. Chemistry of aerogels and their applications. *Chemical Reviews* **2002**, *102*, 4243–4266, PMID: 12428989.

(151) Hüsing, N.; Schubert, U. Aerogels—airy materials: Chemistry, structure, and properties. *Angewandte Chemie International Edition* **1998**, *37*, 22–45.

(152) Soleimani Dorcheh, A.; Abbasi, M. H. Silica aerogel; synthesis, properties and characterization. *Journal of Materials Processing Technology* **2008**, *199*, 10–26.

(153) Vukajlovic, J.; Wang, J.; Forbes, I.; Šiller, L. Diamond-doped silica aerogel for solar geoengineering. *Diamond and Related Materials* **2021**, *117*, 108474.

(154) Adhikary, S. K.; Žymantas Rudžionis,; Vaičiukynienė, D. Development of flowable ultra-lightweight concrete using expanded glass aggregate, silica aerogel, and prefabricated plastic bubbles. *Journal of building engineering* **2020**, *31*, 101399.

(155) Wang, Q.; Yu, H.; Zhang, Z.; Zhao, Y.; Wang, H. One-pot synthesis of polymer-reinforced silica aerogels from high internal phase emulsion templates. *Journal of Colloid and Interface Science* **2020**, *573*, 62–70.

(156) Zhao, C.; Li, Y.; Ye, W.; Shen, X.; Yuan, X.; Ma, C.; Cao, Y. Performance regulation of silica aerogel powder synthesized by a two-step sol-gel process with a fast ambient pressure drying route. *Journal of Non-Crystalline Solids* **2021**, *567*, 120923.

(157) Marszewski, M.; King, S.; Galy, T.; Kashanchi, G.; Dashti, A.; Yan, Y.; Li, M.; Butts, D.; Mcneil, P.; Lan, E.; Dunn, B.; Hu, Y.; Tolbert, S.; Pilon, L. Transparent silica aerogel slabs synthesized from nanoparticle colloidal suspensions at near ambient conditions on omniphobic liquid substrates. *Journal of Colloid and Interface Science* **2021**, *606*, 884–897.

(158) Koebel, M.; Rigacci, A.; Achard, P. Aerogel-based thermal superinsulation: An overview. *Journal of Sol-Gel Science and Technology* **2012**, *63*, 315–339.

(159) Cuce, E.; Cuce, P. M.; Wood, C. J.; Riffat, S. B. Toward aerogel based thermal superinsulation in buildings: A comprehensive review. *Renewable and Sustainable Energy Reviews* **2014**, *34*, 273–299.

(160) Thapliyal, P. C.; Singh, K. Aerogels as promising thermal insulating materials: An overview. *Journal of Materials* **2014**, *2014*, 1–10.

(161) Jelle, B. P.; Baetens, R.; Gustavsen, A. Aerogel insulation for building applications. *The Sol-Gel Handbook* **2015**, *3-3*, 1385–1412.

(162) Jones, S. M. Non-silica aerogels as hypervelocity particle capture materials. *Meteoritics and Planetary Science* **2010**, *45*, 91–98.

(163) Lamy-Mendes, A.; Pontinha, A. D. R.; Alves, P.; Santos, P.; Durães, L. Progress in silica aerogel-containing materials for buildings' thermal insulation. *Construction and Building Materials* **2021**, *286*, 122815.

(164) Liu, P.; Gao, H.; Chen, X.; Chen, D.; Lv, J.; Han, M.; Cheng, P.; Wang, G. In situ one-step construction of monolithic silica aerogel-based composite phase change materials for thermal protection. *Composites, Part B* **2020**, *195*, 108072.

(165) Bheekhun, N.; Abu Talib, A. R.; Hassan, M. R. Tailoring aerogel for thermal spray applications in aero-engines: A screening study. *Advances in Materials Science and Engineering* **2018**, *2018*.

(166) Bheekhun, N.; Abu Talib, A. R.; Mustapha, S.; Ibrahim, R.; Hassan, M. R. Towards an aerogel based coating for aerospace applications: reconstituting aerogel particles via spray drying. *IOP Conference Series: Materials Science and Engineering* **2016**, *152*.

(167) Shaid, A.; Wang, L.; Padhye, R.; Bhuyian, M. A. Aerogel nonwoven as reinforcement and batting material for firefighter's protective clothing: a comparative study. *Journal of Sol-Gel Science and Technology* **2018**, *87*, 95–104.

(168) Yang, J.; Li, Y.; Zheng, Y.; Xu, Y.; Zheng, Z.; Chen, X.; Liu, W. Versatile aerogels for sensors. *Small* **2019**, *15*.

(169) Amonette, J.; Matyas, J. Functionalized silica aerogels for gas-phase purification, sensing, and catalysis: A review. *Microporous and Mesoporous Materials* **2017**, *250*, 100–119.

(170) Zheng, Q.; Zhang, H.; Liu, J.; Xiao, L.; Ao, Y.; Li, M. High porosity fluorescent aerogel with new molecular probes for formaldehyde gas sensors. *Microporous and Mesoporous Materials* **2021**, *325*, 111208.

(171) Feinle, A.; Hüsing, N. Mixed metal oxide aerogels from tailor-made precursors. *Journal of Supercritical Fluids* **2015**, *106*, 2–8.

(172) Wicikowska, B.; Nowak, A.; Trzciński, K.; Lisowska-Oleksiak, A. Electrochemical activity of electrode material consisting of porous copper and silica aerogel. *Procedia Engineering* **2014**, *98*, 42–45.

(173) Lee, Y.; Choi, J. W.; Suh, D. J.; Ha, J. M.; Lee, C. H. Ketonization of hexanoic acid to diesel-blendable 6-undecanone on the stable zirconia aerogel catalyst. *Applied Catalysis A: General* **2015**, *506*, 288–293.

(174) Mi, H.-Y.; Jing, X.; Politowicz, A. L.; Chen, E.; Huang, H.-X.; Turng, L.-S. Highly compressible ultra-light anisotropic cellulose/graphene aerogel fabricated by bidirectional freeze drying for selective oil absorption. *Carbon* **2018**, *132*, 199–209.

(175) Sert Çok, S.; Koç, F.; Gizli, N. Lightweight and highly hydrophobic silica aerogels dried in ambient pressure for an efficient oil/organic solvent adsorption. *Journal of Hazardous Materials* **2020**, *408*, 124858.

(176) Chen, D. R.; Chang, X. H.; Jiao, X. L. *The Role of Colloidal Systems in Environmental Protection*; Elsevier B.V., 2014; pp 573–591.

(177) Maleki, H. Recent advances in aerogels for environmental remediation applications: A review. *Chemical Engineering Journal* **2016**, *300*, 98–118.

(178) Kumar, A.; Rana, A.; Sharma, G.; Sharma, S.; Naushad, M.; Mola, G. T.; Dhiman, P.; Stadler, F. J. Aerogels and metal–organic frameworks for environmental remediation and energy production. *Environmental Chemistry Letters* **2018**, *16*, 797–820.

(179) Maleki, H.; Hüsing, N. aerogels as promising materials for environmental remediation - A broad insight into the environmental pollutants removal through adsorption and (photo) catalytic processes. *New Polymer Nanocomposites for Environmental Remediation* **2017**, 389–436.

(180) Cao, N.; Lyu, Q.; Li, J.; Wang, Y.; Yang, B.; Szunerits, S.; Boukherroub, R. Facile synthesis of fluorinated polydopamine/chitosan/reduced graphene oxide composite aerogel for efficient oil/water separation. *Chemical Engineering Journal* **2017**, *326*, 17–28.

(181) Shan, S.; Tang, H.; Zhao, Y.; Wang, W.; Cui, F. Highly porous zirconium-crosslinked graphene oxide/alginate aerogel beads for enhanced phosphate removal. *Chemical Engineering Journal* **2019**, *359*, 779–789.

(182) Yu, Y.; Wu, X.; Fang, J. Superhydrophobic and superoleophilic "sponge-like" aerogels for oil/water separation. *Journal of Materials Science* **2015**, *50*, 5115–5124.

(183) Kim, S. J.; Chase, G.; Jana, S. C. Polymer aerogels for efficient removal of airborne nanoparticles. *Separation and Purification Technology* **2015**, *156*, 803–808.

(184) Simón-Herrero, C.; Peco, N.; Romero, A.; Valverde, J. L.; Sánchez-Silva, L. PVA/nanoclay/graphene oxide aerogels with enhanced sound absorption properties. *Applied Acoustics* **2019**, *156*, 40–45.

(185) Talebi, Z.; Soltani, P.; Habibi, N.; Latifi, F. Silica aerogel/polyester blankets for efficient sound absorption in buildings. *Construction and Building Materials* **2019**, *220*, 76–89.

(186) Ulker, Z.; Erkey, C. An emerging platform for drug delivery: Aerogel based systems. *Journal of Controlled Release* **2014**, *177*, 51–63.

(187) Maleki, H.; Durães, L.; García-González, C. A.; del Gaudio, P.; Portugal, A.; Mahmoudi, M. Synthesis and biomedical applications of aerogels: Possibilities and challenges. *Advances in Colloid and Interface Science* **2016**, *236*, 1–27.

(188) Stergar, J.; Maver, U. Review of aerogel-based materials in biomedical applications. *Journal of Sol-Gel Science and Technology* **2016**, *77*, 738–752.

(189) Jabbari, A.; Moghaddas, J.; Hamishehkar, H.; Jafarizadeh, H. Carboxylic acid decorated silica aerogel nanostructure as drug delivery carrier. *Microporous and Mesoporous Materials* **2021**, *323*, 111220.

(190) Teichner, S. J.; Nicolaon, G. A.; Vicarini, M. A.; Gardes, G. E. Inorganic oxide aerogels. *Advances in Colloid and Interface Science* **1976**, *5*, 245–273.

(191) Peshev, P.; Slavova, V. Preparation of yttria-stabilized zirconia thin films by a sol-gel procedure using alkoxide precursors. *Materials Research Bulletin* **1992**, *27*, 1269–1275.

(192) Gash, A. E.; Tillotson, T. M.; Satcher, J. H.; Hrubesh, L. W.; Simpson, R. L. New sol-gel synthetic route to transition and main-group metal oxide aerogels using inorganic salt precursors. *Journal of Non-Crystalline Solids* **2001**, *285*, 22–28.

(193) Gossard, A.; Toquer, G.; Grandjean, S.; Grandjean, A. Coupling between SAXS and Raman spectroscopy applied to the gelation of colloidal zirconium oxy-hydroxide systems. *Journal of Sol-Gel Science and Technology* **2014**, *71*, 571–579.

(194) Gurav, J. L.; Jung, I. K.; Park, H. H.; Kang, E. S.; Nadargi, D. Y. Silica aerogel: Synthesis and applications. *Journal of Nanomaterials* **2010**, *2010*, 1–11.

(195) Maleki, H.; Durães, L.; Portugal, A. An overview on silica aerogels synthesis and different mechanical reinforcing strategies. *Journal of Non-Crystalline Solids* **2014**, *385*, 55–74.

(196) Haynes, W. M., Ed. *CRC Handbook of Chemistry and Physics*, 92nd ed.; CRC Press: Boca Raton, FL, 2011.

(197) Buckley, A. M.; Greenblatt, M. The preparation and characterisation of silica aerogels and xerogels doped with transition metal species. *Journal of Non-Crystalline Solids* **1992**, *146*, 97–110.

(198) Jones, S. M. Aerogel: Space exploration applications. *Journal of Sol-Gel Science and Technology* **2006**, *40*, 351–357.

(199) Venkateswara Rao, A.; Hegde, N. D.; Hirashima, H. Absorption and desorption of organic liquids in elastic superhydrophobic silica aerogels. *Journal of Colloid and Interface Science* **2007**, *305*, 124–132.

(200) Hamann, T. W.; Martinson, A. B. F.; Elam, J. W.; Pellin, M. J.; Hupp, J. T. Atomic layer deposition of TiO2 on aerogel templates: New photoanodes for dye-sensitized solar cells. *J. Phys. Chem. C* **2008**, *112*, 10303–10307.

(201) Jung, S. B.; Park, S. W.; Yang, J. K.; Park, H. H.; Kim, H. Application of SiO2 aerogel film for interlayer dielectric on GaAs with a barrier of Si3N4. *Thin Solid Films* **2004**, *447-448*, 580–585.

(202) Poco, J. F.; Satcher, J. H.; Hrubesh, L. W. Synthesis of high porosity, monolithic alumina aerogels. *Journal of Non-Crystalline Solids* **2001**, *285*, 57–63.

(203) Zu, G.; Shen, J.; Wei, X.; Ni, X.; Zhang, Z.; Wang, J.; Liu, G. Preparation and characterization of monolithic alumina aerogels. *Journal of Non-Crystalline Solids* **2011**, *357*, 2903–2906.

(204) Patnaik, P. *Handbook of Inorganic Chemicals*, 1st ed.; McGraw-Hill Professional, 2002.

(205) Cao, F.; Ren, L.; Li, X. Synthesis of high strength monolithic alumina aerogels at ambient pressure. *RSC Advances* **2015**, *5*, 18025–18028.

(206) Baumann, T. F.; Gash, A. E.; Chinn, S. C.; Sawvel, A. M.; Maxwell, R. S.; Satcher, J. H. Synthesis of high-surface-area alumina aerogels without the use of alkoxide precursors. *Chemistry of Materials* **2005**, *17*, 395–401.

(207) Simón-Herrero, C.; Romero, A.; Valverde, J. L.; Sánchez-Silva, L. Hydroxyethyl cellulose/alumina-based aerogels as lightweight insulating materials with high mechanical strength. *Journal of Materials Science* **2018**, *53*, 1556–1567.

(208) Al-Yassir, N.; Le Van Mao, R. Thermal stability of alumina aerogel doped with yttrium oxide, used as a catalyst support for the thermocatalytic cracking (TCC) process: An investigation of its textural and structural properties. *Applied Catalysis A: General* **2007**, *317*, 275–283.

(209) Gao, M.; Liu, B.; Zhao, P.; Yi, X.; Shen, X.; Xu, Y. Mechanical strengths and thermal properties of titania-doped alumina aerogels and the application as high-temperature thermal insulator. *Journal of Sol-Gel Science and Technology* **2019**, *91*, 514–522.

(210) Yang, J.; Wang, Q.; Wang, T.; Liang, Y. Facile one-step precursor-to-aerogel synthesis of silica-doped alumina aerogels with high specific surface area at elevated temperatures. *Journal of Porous Materials* **2017**, *24*, 889–897.

(211) Yu, Y.; Peng, K.; Fang, J.; Zhang, R.; Wang, G.; Peng, X. Mechanical and thermal conductive properties of fiber-reinforced silica-alumina aerogels. *International Journal of Applied Ceramic Technology* **2018**, *15*, 1138–1145.

(212) Chen, H.; Sui, X.; Zhou, C.; Wang, C.; Liu, F. Preparation and characterization of monolithic Al2O3SiO2 aerogel. *Journal of the Ceramic Society of Japan* **2016**, *124*, 442–447.

(213) Ebnesajjad, S. Surface Treatment and Bonding of Ceramics. *Surface Treatment of Materials for Adhesive Bonding* **2014**, 283–299.

(214) Wijaya, Y. P.; Suh, D. J.; Jae, J. Production of renewable p-xylene from 2,5-dimethylfuran via Diels-Alder cycloaddition and dehydrative aromatization reactions over silica-alumina aerogel catalysts. *Catalysis Communications* **2015**, *70*, 12–16.

(215) Chatterjee, A.; Basu, J. K.; Jana, A. K. Alumina-silica nano-sorbent from plant fly ash and scrap aluminium foil in removing nickel through adsorption. *Powder Technology* **2019**, *354*, 792–803.

(216) Lee, J. H.; Park, S. J. Recent advances in preparations and applications of carbon aerogels: A review. *Carbon* **2020**, *163*, 1–18.

(217) Hu, L.; He, R.; Lei, H.; Fang, D. Carbon aerogel for insulation applications: A review. *International Journal of Thermophysics* **2019**, *40*.

(218) Kurzweil, P. Capacitors — Electrochemical double-layer capacitors: Carbon materials. *Encyclopedia of Electrochemical Power Sources* **2009**, 634–648.

(219) Guo, F.; Jiang, Y.; Xu, Z.; Xiao, Y.; Fang, B.; Liu, Y.; Gao, W.; Zhao, P.; Wang, H.; Gao, C. Highly stretchable carbon aerogels. *Nature Communications* **2018**, *9*.

(220) Baumann, T. F.; Fox, G. A.; Satcher, J. H.; Yoshizawa, N.; Fu, R.; Dresselhaus, M. S. Synthesis and characterization of copper-doped carbon aerogels. *Langmuir* **2002**, *18*, 7073–7076.

(221) Wohlgemuth, S. A.; White, R. J.; Willinger, M. G.; Titirici, M. M.; Antonietti, M. A one-pot hydrothermal synthesis of sulfur and nitrogen doped carbon aerogels with

enhanced electrocatalytic activity in the oxygen reduction reaction. *Green Chemistry* **2012**, *14*, 1515–1523.

(222) Zhang, S.; Fu, R.; Dingcai, W.; Xu, W.; Ye, Q.; Chen, Z. Preparation and characterization of antibacterial silver-dispersed activated carbon aerogels. *Carbon* **2004**, *42*, 3209–3216.

(223) Zhao, W.; Zhang, H.; Liu, J.; Xu, L.; Wu, H.; Zou, M.; Wang, Q.; He, X.; Li, Y.; Cao, A. Controlled air-etching synthesis of porous-carbon nanotube aerogels with ultrafast charging at 1000 A/g. *Small* **2018**, *14*.

(224) Qiu, B.; Xing, M.; Zhang, J. Mesoporous TiO2 nanocrystals grown in situ on graphene aerogels for high photocatalysis and lithium-ion batteries. *Journal of the American Chemical Society* **2014**, *136*, 5852–5855.

(225) Hu, H.; Zhao, Z.; Gogotsi, Y.; Qiu, J. Compressible carbon nanotube-graphene hybrid aerogels with superhydrophobicity and superoleophilicity for oil sorption. *Environmental Science and Technology Letters* **2014**, *1*, 214–220.

(226) Chen, K. L.; Chiang, A. S.; Tsao, H. K. Preparation of zirconia nanocrystals from concentrated zirconium aqueous solutions. *Journal of Nanoparticle Research* **2001**, *3*, 119–126.

(227) Ranjbar, M.; Yousefi, M.; Lahooti, M.; Malekzadeh, A. Preparation and characterization of tetragonal zirconium oxide nanocrystals from isophthalic acid-zirconium(IV) nanocomposite as a new precursor. *Int. J. Nanosci. Nanotechnol* **2012**, *8*, 191–196.

(228) Lamas, D. G.; Lascalea, G. E.; Juárez, R. E.; Djurado, E.; Pérez, L.; Walsöe De Reca, N. E. Metastable forms of the tetragonal phase in compositionally homogeneous, nanocrystalline zirconia-ceria powders synthesised by gel-combustion. *Journal of Materials Chemistry* **2003**, *13*, 904–910.

(229) Southon, P. D.; Bartlett, J. R.; Woolfrey, J. L.; Ben-Nissan, B. Formation and characterization of an aqueous zirconium hydroxide colloid. *Chemistry of Materials* **2002**, *14*, 4313–4319.

(230) Venugopal, M.; Saravana Kumar, S.; Nissamudeen, K. M.; Padma Kumar, H. Optical and dielectric characterisation of Ceria nanocrystals synthesized by an auto-igniting combustion technique. *Journal of Materials Science: Materials in Electronics* **2016**, *27*, 9496–9502.

(231) Vasylkiv, O.; Sakka, Y. Synthesis and colloidal processing of zirconia nanopowder. *Journal of the American Ceramic Society* **2001**, *84*, 2489–2494.

(232) Livage, J.; Babonneau, F.; Chatry, M.; Coury, L. Sol-gel synthesis and NMR characterization of ceramics. *Ceramics International* **1997**, *23*, 13–18.

(233) Bedilo, A. F.; Klabunde, K. J. Synthesis of high surface area zirconia aerogels using high temperature supercritical drying. *Nanostructured Materials* **1997**, *8*, 119–135.

(234) Sun, Q.; Zhang, Y.; Deng, J.; Chen, S.; Wu, D. A novel preparation process for thermally stable ultrafine tetragonal zirconia aerogel. *Applied Catalysis A: General* **1997**, *152*, L165–L171.

(235) Sui, R.; Rizkalla, A. S.; Charpentier, P. A. Direct synthesis of zirconia aerogel nanoarchitecture in supercritical CO2. *Langmuir* **2006**, *22*, 4390–4396.

(236) Duprez, D.; Rossignol, S. Effect of the preparation method on the properties of zirconia – ceria materials. *Journal of Materials Chemistry* **1999**, *9*, 1615–1620.

(237) Kuo, C. W.; Lee, Y. H.; Hung, I. M.; Wang, M. C.; Wen, S. B.; Fung, K. Z.; Shih, C. J. Crystallization kinetics and growth mechanism of 8 mol% yttria-stabilized zirconia (8YSZ) nano-powders prepared by a sol-gel process. *Journal of Alloys and Compounds* **2008**, *453*, 470–475.

(238) Biver, C.; Pont, C.; Jaworski, L. L. P. Method for preparing a colloidal zirconia solution. 2012.

(239) Ota, I.; Tsuihiji, N. Production method yttrium oxide-stabilized zirconium oxide sol. 2011.

(240) Abdulghani, A. J.; Al-Ogedy, W. M. Preparation and characterization of yttrium oxide nanoparticles at different calcination temperatures from yttrium hydroxide prepared by hydrothermal and hydrothermal microwave methods. *Ogedy Iraqi Journal of Science* **2015**, *56*, 1572–1587.

(241) Chang, Q.; Zhou, J. E.; Wang, Y.; Meng, G. Formation mechanism of zirconia nanoparticles containing pores prepared via sol-gel-hydrothermal method. *Advanced Powder Technology* **2010**, *21*, 425–430.

(242) Wang, Y.; Lin, H.; Xu, W.; Ling, J.; Wang, B.; Wang, K.; Xiong, C.; Zhou, Y. Electrical performance of fine-grained Y-TZP/TiC composites obtained through a hydrothermal-assisted sol-gel process. *Ceramics International* **2020**, *46*, 2033–2040.

(243) Lee, H.-S.; Lim, H. M. Dispersion properties of nano zirconia sols prepared by a hydrothermal method. *Nanoscience and Nanotechnology Letters* **2018**, *10*, 825–829.

(244) Cao, Y.; Hu, J. C.; Hong, Z. S.; Deng, J. F.; Fan, K. N. Characterization of high-surface-area zirconia aerogel synthesized from combined alcohothermal and supercritical fluid drying techniques. *Catalysis Letters* **2002**, *81*, 107–112.

(245) Kurapova, O. Y.; Konakov, V. G. Phase evolution in zirconia based systems. *Reviews on Advanced Materials Science* **2014**, *36*, 177–190.

(246) Gopi, K. R.; Nagarajan, R. Advances in nanoalumina ceramic particle fabrication using sonofragmentation. *IEEE Transactions on Nanotechnology* **2008**, *7*, 532–537.

(247) Guo, J.; Xin, X.; Zhang, X.; Zhang, S. Ultrasonic-induced synthesis of high surface area colloids CeO 2-ZrO2. *Journal of Nanoparticle Research* **2009**, *11*, 737–741.

(248) Yu, J. C.; Zhang, L.; Lin, J. Direct sonochemical preparation of high-surface-area nanoporous ceria and ceria-zirconia solid solutions. *Journal of Colloid and Interface Science* **2003**, *260*, 240–243.

(249) Jodłowski, P. J.; Chlebda, D. K.; Jędrzejczyk, R. J.; Dziedzicka, A.; Kuterasiński, L.; Sitarz, M. Characterisation of well-adhered ZrO2 layers produced on structured reactors using the sonochemical sol–gel method. *Applied Surface Science* **2018**, *427*, 563–574.

(250) Gubanova, N. N.; Baranchikov, A. Y.; Kopitsa, G. P.; Almásy, L.; Angelov, B.; Yapryntsev, A. D.; Rosta, L.; Ivanov, V. K. Combined SANS and SAXS study of the action of ultrasound on the structure of amorphous zirconia gels. *Ultrasonics Sonochemistry* **2015**, *24*, 230–237.

(251) Zhao, Z.; Chen, D.; Jiao, X. Zirconia aerogels with high surface area derived from sols prepared by electrolyzing zirconium oxychloride solution: Comparison of aerogels prepared by freeze-drying and supercritical CO2(l) extraction. *Journal of Physical Chemistry C* **2007**, *111*, 18738–18743.

(252) Wu, Z. G.; Zhao, Y. X.; Xu, L. P.; Liu, D. S. Preparation of zirconia aerogel by heating of alcohol-aqueous salt solution. *Journal of Non-Crystalline Solids* **2003**, *330*, 274–277.

(253) Barrow, S. J.; Tardio, J.; Foger, K.; Bhargava, S. Chemistry of formation of a solid oxide fuel cell electrolyte (yttria stabilized zirconia). **2009**,

(254) Ketzial, J. J.; Nesaraj, S. A. Synthesis of CeO2 nanoparticles by chemical precipitation and the effect of a surfactant on the distribution of particle sizes. *Journal of Ceramic Processing Research* **2011**, *12*, 74–79.

(255) Díaz-Parralejo, A.; MacÍas-García, A.; Sánchez-González, J.; Díaz-Díez, M. Á.; Cuerda-Correa, E. M. A novel strategy for the preparation of yttria-stabilized zirconia powders: Deposition and scratching of thin films obtained by the sol-gel method. *Journal of Non-Crystalline Solids* **2011**, *357*, 1090–1095.

(256) Verma, S.; Amritphale, S. S.; Das, S. Synchronising effect of microwave and cytosine for the synthesis of hybrid homogenised nanosized cerium oxide and cerium oxycarbonate hydrate material. *Journal of Chemical Research* **2016**, *40*, 321–325.

(257) Siddiquey, I. A.; Furusawa, T.; Sato, M.; Bahadur, N. M.; Uddin, M. N.; Suzuki, N. A rapid method for the preparation of silica-coated ZrO2 nanoparticles by microwave irradiation. *Ceramics International* **2011**, *37*, 1755–1760.

(258) Fetter, G.; Bosch, P.; López, T. ZrO2 and Cu/ZrO2 sol-gel synthesis in presence of microwave irradiation. *Journal of Sol-Gel Science and Technology* **2002**, *23*, 199–203.

(259) Baklanova, Y. V.; Denisova, T. A.; Maksimova, L. G.; Tyutyunnik, A. P.; Baklanova, I. V.; Shein, I. R.; Neder, R. B.; Tarakina, N. V. Synthesis and characterisation of new MO(OH)2 (M = Zr, Hf) oxyhydroxides and related Li2MO3 salts. *Dalton Transactions* **2014**, *43*, 2755–2763.

(260) Rezaee, S.; Ranjbar, K. Thermal conductivity of porous Alumina-20 wt% zirconia ceramic composites. *Ceramics International* **2020**, *46*, 16564–16571.

(261) Yang, Z.; Yu, H.; Li, X.; Ding, H.; Ji, H. hyperelastic and hydrophobic silica aerogels with enhanced compressive strength by using VTES/MTMS as precursors. *Journal of Non-Crystalline Solids* **2019**, *525*, 119677.

(262) Yay, B.; Gizli, N. A review on silica aerogels for CO2 capture applications. *Pamukkale University Journal of Engineering Sciences* **2019**, *25*, 907–913.

(263) Kanamori, K.; Aizawa, M.; Nakanishi, K.; Hanada, T. New transparent methylsilsesquioxane aerogels and xerogels with improved mechanical properties. *Advanced Materials* **2007**, *19*, 1589 – 1593.

(264) Holsa, J.; Chateau, C.; Leskela, T.; Leskela, M. Optical study of phase transformations in rare earth oxyhydroxides. *Acta Chemica Scandinavica* **1985**, *39*, 415–421.

(265) Yang, S.; Powell, M.; Kolis, J. W.; Navrotsky, A. Thermochemistry of rare earth oxyhydroxides, REOOH (RE = Eu to Lu). *Journal of Solid State Chemistry* **2020**, *287*, 2–8.

(266) Zhu, D.; Miller, R. A. Development of advanced low conductivity thermal barrier coatings. *International Journal of Applied Ceramic Technology* **2004**, *1*, 86–94.

(267) Angle, J. P.; Wang, Z.; Dames, C.; Mecartney, M. L. Comparison of two-phase thermal conductivity models with experiments on dilute ceramic composites. *Journal of the American Ceramic Society* **2013**, *96*, 2935–2942.

(268) Tsay, C. Y.; Cheng, C. H.; Wang, Y. W. Properties of transparent yttrium oxide dielectric films prepared by sol-gel process. *Ceramics International* **2012**, *38*, 1677–1682.

(269) Liu, J.; Zhao, Z.; Xu, C.; Liu, J. Structure, synthesis, and catalytic properties of nanosize cerium-zirconium-based solid solutions in environmental catalysis. *Chinese Journal of Catalysis* **2019**, *40*, 1438–1487.

(270) Mejri, I.; Younes, M. K.; Ghorbel, A.; Eloy, P.; Gaigneaux, E. M. Characterization and reactivity of aerogel sulfated zirconia-ceria catalyst for n-hexane isomerization. *Journal of Porous Materials* **2010**, *17*, 545–551.

(271) Sun, Y.; Sermon, P. A. Preparation of CaO-, La2O3- and CeO2-doped ZrO2 aerogels by sol-gel methods. *Studies in Surface Science and Catalysis* **1995**, *91*, 471–478.

(272) Montoya, N.; Pardo, P.; Doménech-Carbó, A.; Alarcón, J. Structural stability and electrochemical properties of Gd-doped ZrO2 nanoparticles prepared by sol-gel. *Journal of Sol-Gel Science and Technology* **2014**, *69*, 137–147.

(273) Boyse, R. A.; Ko, E. I. Study of tungsten oxide and sulfate interactions on doubly-doped zirconia aerogels. *Catalysis Letters* **1997**, *49*, 17–23.

(274) Chakhari, S.; Younes, M. K.; Rives, A.; Ghorbel, A. Effect of the doping agent nature on the characteristic and catalytic properties of aerogel zirconia catalysts doped with sulfate groups or heteropolytungstic acid. *Materials Research Bulletin* **2015**, *72*, 35–42.

(275) Siouffi, A. Silica gel-based monoliths prepared by the sol-gel method: Facts and figures. *Journal of Chromatography A* **2003**, *1000*, 801–18.

(276) Gonzalez, R. D.; Lopez, T.; Gomez, R. Sol-gel preparation of supported metal catalysts. *Catalysis Today* **1997**, *35*, 293–317, Sol-gel Preparation of Catalytic Materials.

(277) Kar, M.; Chourasiya, Y.; Maheshwari, R.; Tekade, R. K. *Basic Fundamentals of Drug Delivery*; Elsevier, 2018; pp 29–83.

(278) Fink, J. K. *Petroleum Engineer's Guide to Oil Field Chemicals and Fluids*; Elsevier, 2012; pp 275–293.

(279) Kurajica, S. A brief review on the use of chelation agents in sol-gel synthesis with emphasis on β-diketones and β-ketoesters. *Chemical and Biochemical Engineering Quarterly* **2019**, *33*, 295–301.

(280) Hegde, N.; Rao, A. Effect of processing temperature on gelation and physical properties of low density TEOS based silica aerogels. *Journal of Sol-Gel Science and Technology* **2006**, *38*, 55–61.

(281) Schäfer, H.; Brandt, S.; Milow, B.; Ichilmann, S.; Steinhart, M.; Ratke, L. Zirconia-based aerogels via hydrolysis of salts and alkoxides: The influence of the synthesis procedures on the properties of the aerogels. *Chemistry - An Asian Journal* **2013**, *8*, 2211–2219.

(282) Papet, P.; Le Bars, N.; Baumard, J. F.; Lecomte, A.; Dauger, A. Transparent monolithic zirconia gels: effects of acetylacetone content on gelation. *Journal of Materials Science* **1989**, *24*, 3850–3854.

(283) Gossard, A.; Grasland, F.; Le Goff, X.; Grandjean, A.; Toquer, G. Control of the nanocrystalline zirconia structure through a colloidal sol-gel process. *Solid State Sciences* **2016**, *55*, 21–28.

(284) Schafer, H.; Milow, B.; Ratke, L. Synthesis of inorganic aerogels via rapid gelation using chloride precursors. *RSC Advances* **2013**, *3*, 15263–15272.

(285) Khoo, H. T.; Leow, H. Advancements in the preparation and application of monolithic silica columns for efficient separation in liquid chromatography. *Talanta* **2020**, *224*, 121777.

(286) Esquivel-Castro, T. A.; Ibarra-Alonso, M. C.; Oliva, J.; Martínez-Luévanos, A. Porous aerogel and core/shell nanoparticles for controlled drug delivery: A review. *Materials Science and Engineering C* **2019**, *96*, 915–940.

(287) Leventis, N. Three-dimensional core-shell superstructures: Mechanically strong aerogels. 2007; `https://pubs.acs.org/doi/abs/10.1021/ar600033s`.

(288) Leventis, N.; Vassilaras, P.; Fabrizio, E. F.; Dass, A. Polymer nanoencapsulated rare earth aerogels: Chemically complex but stoichiometrically similar core-shell superstructures with skeletal properties of pure compounds. *Journal of Materials Chemistry* **2007**, *17*, 1502–1508.

(289) Duan, G.; Zhang, C.; Li, A.; Yang, X.; Lu, L.; Wang, X. Preparation and characterization of mesoporous zirconia made by using a poly (methyl methacrylate) template. *Nanoscale Research Letters* **2008**, *3*, 118–122.

(290) Teo, N.; Gu, Z.; Jana, S. C. Polyimide-based aerogel foams, via emulsion-templating. *Polymer* **2018**, *157*, 95–102.

(291) Scherer, G. W. Aging and drying of gels. *Journal of Non-Crystalline Solids* **1988**, *100*, 77–92.

(292) Omranpour, H.; Motahari, S. Effects of processing conditions on silica aerogel during aging: Role of solvent, time and temperature. *Journal of Non-Crystalline Solids* **2013**, *379*, 7–11.

(293) He, F.; Zhao, H.; Qu, X.; Zhang, C.; Qiu, W. Modified aging process for silica aerogel. *Journal of Materials Processing Technology* **2009**, *209*, 1621–1626.

(294) Şahin, I.; Özbakır, Y.; İnönü, Z.; Ulker, Z.; Erkey, C. Kinetics of supercritical drying of gels. *Gels* **2017**, *4*, 3.

(295) Sarawade, P. B.; Kim, J.-K.; Park, J.-K.; Kim, H. Influence of solvent exchange on the physical properties of sodium silicate based aerogel prepared at ambient pressure. *Aerosol and Air Quality Research* **2006**, *6*, 93–105.

(296) Błaszczyński, T.; Ślosarczyk, A.; Morawski, M. Synthesis of silica aerogel by supercritical drying method. *Procedia Engineering* **2013**, *57*, 200–206.

(297) Zheng, S.; Hu, X.; Ibrahim, A. R.; Tang, D.; Tan, Y.; Li, J. Supercritical fluid drying: Classification and applications. *Recent Patents on Chemical Engineering* **2010**, *3*, 230–244.

(298) Bheekhun, N.; Abu Talib, A. R.; Hassan, M. R. Aerogels in aerospace: An overview. *Advances in Materials Science and Engineering* **2013**, 1–18.

(299) Reid, R. C.; Prausnitz, J. M.; Poling, B. E. *The properties of gases and liquids*, 4th ed.; McGraw-Hill: New York, 1987; p 741.

(300) Ebrahimi, A.; Dahrazma, B.; Adelifard, M. Facile and novel ambient pressure drying approach to synthesis and physical characterization of cellulose-based aerogels. *Journal of Porous Materials* **2020**, *27*, 1219–1232.

(301) Lázár, I.; Fábián, I. A continuous extraction and pumpless supercritical CO2 drying system for laboratory-scale aerogel production. *Gels* **2016**, *2*, 26.

(302) Wang, J.; Wei, Y.; He, W.; Zhang, X. A versatile ambient pressure drying approach to synthesize silica-based composite aerogels. *RSC Advances* **2014**, *4*, 51146–51155.

(303) Çok, S. S.; Koç, F.; Balkan, F.; Gizli, N. Exploring a new preparation pathway for the synthesis of silica based xerogels as crack-free monoliths. *Ceramics International* **2019**, *45*, 1616–1626.

(304) Betz, M.; García-González, C. A.; Subrahmanyam, R. P.; Smirnova, I.; Kulozik, U. Preparation of novel whey protein-based aerogels as drug carriers for life science applications. *Journal of Supercritical Fluids* **2012**, *72*, 111–119.

(305) Zhang, H. Introduction to freeze-drying and ice templating. *Ice Templating and Freeze-Drying for Porous Materials and Their Applications* **2018**, 1–27.

(306) Simón-Herrero, C.; Caminero-Huertas, S.; Romero, A.; Valverde, J. L.; Sánchez-Silva, L. Effects of freeze-drying conditions on aerogel properties. *Journal of Materials Science* **2016**, *51*, 8977–8985.

(307) Karamikamkar, S.; Naguib, H.; Park, C. Advances in precursor system for silica-based aerogel production toward improved mechanical properties, customized morphology, and multifunctionality: A review. *Advances in Colloid and Interface Science* **2020**, *276*, 102101.

(308) Chen, Y.; Zhou, L.; Chen, L.; Duan, G.; Mei, C.; Huang, C.; Han, J.; Jiang, S. Anisotropic nanocellulose aerogels with ordered structures fabricated by directional freeze-drying for fast liquid transport. *Cellulose* **2019**, *26*, 6653–6667.

(309) Zhang, H.; Cooper, A. I. Aligned porous structures by directional freezing. *Advanced Materials* **2007**, *19*, 1529–1533.

(310) Du, G.; Zhou, Y.; Tian, X.; Wu, G.; Xi, Y.; Zhao, S. High-performance 3D directional porous LiFePO 4 /C materials synthesized by freeze casting. *Applied Surface Science* **2018**, *453*, 493–501.

(311) Pan, Y.; Cheng, X.; zhou, T.; Gong, L.; Zhang, H. Spray freeze-dried monolithic silica aerogel based on water-glass with thermal superinsulating properties. *Materials Letters* **2018**, *229*, 265–268.

(312) Rodríguez-Dorado, R.; López-Iglesias, C.; García-González, C. A.; Auriemma, G.; Aquino, R. P.; Del Gaudio, P. Design of aerogels, cryogels and xerogels of alginate: Effect of molecular weight, gelation conditions and drying method on particles' micromeritics. *Molecules* **2019**, *24*, 4–6.

(313) Martínez, M.; Arnaudguilhem, C.; Lobinski, R.; Bouyssiere, B.; Caetano, M.; Chirinos, J. Use of xerogels for the elemental analysis of crude oils by laser ablation inductively coupled plasma high resolution mass spectrometry. *Journal of Analytical Atomic Spectrometry* **2012**, *27*, 1007–1011.

(314) Patel, S. B.; Panda, A. P.; Swain, S. K.; Patnaik, T.; Muller, F.; Delpeux-Ouldriane, S.; Duclaux, L.; Dey, R. K. Development of aluminum and zirconium based xerogel for defluoridation of drinking water: Study of material properties, solution kinetics and thermodynamics. *Journal of Environmental Chemical Engineering* **2018**, *6*, 6231–6242.

(315) Ben Nsir, S.; Younes, M. K.; Rives, A.; Ghorbel, A. Characterization and reactivity of zirconia-doped phosphate ion catalyst prepared by sol–gel route and mechanistic study of acetic acid esterification by ethanol. *Journal of Sol-Gel Science and Technology* **2017**, *84*, 349–360.

(316) Krivtsov, I. V.; Ilkaeva, M. V.; Avdin, V. V.; Zherebtsov, D. A. Properties and segregation stability of the composite silica-zirconia xerogels prepared via "acidic" and "basic" precipitation routes. *Journal of Non-Crystalline Solids* **2013**, *362*, 95–100.

(317) Bisson, A.; Rigacci, A.; Lecomte, D.; Rodier, E.; Achard, P. Drying of silica gels to obtain aerogels: Phenomenology and basic techniques. *Drying Technology* **2003**, *21*, 593–628.

(318) Wang, B.; Zhang, W.; Zhang, W.; Mujumdar, A. S.; Huang, L. Progress in drying technology for nanomaterials. *Drying Technology* **2005**, *23*, 7–32.

(319) Dell'Agli, G.; Mascolo, G.; Mascolo, M. C.; Pagliuca, C. Drying effect on thermal behavior and structural modifications of hydrous zirconia gel. *Journal of the American Ceramic Society* **2008**, *91*, 3375–3379.

(320) Castro, R. H.; Gouvêa, D. Sintering and nanostability: The thermodynamic perspective. *Journal of the American Ceramic Society* **2016**, *99*, 1105–1121.

(321) Wu, X.; Li, Z.; Joao, G.; Zhang, Y.; Huang, S.; Liu, Q. Reducing the flammability of hydrophobic silica aerogels by tailored heat treatment. *Journal of Nanoparticle Research* **2020**, *22*.

(322) Woignier, T.; Duffours, L. Densification and strengthening of aerogels by sintering heat treatments or plastic compression. *Gels* **2018**, *4*, 12.

(323) Liu, F.; Wu, J. Morphology study by using scanning electron microscopy. *Education* **2010**, 1781–1792.

(324) Tushar G, R.; Babita R, A. Transmission electron microscopy - An overview. *International Research Journal for Inventions in Pharmaceutical Sciences* **2013**, *1*, 1–7.

(325) Brunauer, S.; Emmett, P. H.; Teller, E. Adsorption of gases in multimolecular layers. *Journal of the American Chemical Society* **1938**, *60*, 309–319.

(326) Barrett, E. P.; Joyner, L. G.; Halenda, P. P. The determination of pore volume and area distributions in porous substances. I. Computations from nitrogen isotherms. *Journal of the American Chemical Society* **1951**, *73*, 373–380.

(327) Reichenauer, G.; Scherer, G. W. Nitrogen sorption in aerogels. *Journal of Non-Crystalline Solids* **2001**, *285*, 167–174.

(328) Brunauer, S.; Deming, L. S.; Deming, W. E.; Teller, E. On a theory of the van der waals adsorption of gases. *Journal of the American Chemical Society* **1940**, *62*, 1723–1732.

(329) Ruckenstein, E.; Nagarajan, R. Critical micelle concentration. A transition point for micellar size distribution. *The Journal of Physical Chemistry* **1975**, *79*, 2622–2626.

(330) Vareda, J. P.; Maximiano, P.; Cunha, L. P.; Ferreira, A. F.; Simões, P. N.; Durães, L. Effect of different types of surfactants on the microstructure of methyltrimethoxysilane-derived silica aerogels: A combined experimental and computational approach. *Journal of Colloid and Interface Science* **2018**, *512*, 64–76.

(331) Walker, R. C.; Stokes, J. L.; Hurwitz, F. I.; Guo, H.; Ferri, J. K. Optimizing surfactant templating of yttria-stabilized zirconia aerogels for high-temperature applications: Effect of cationic surfactant. *Microporous and Mesoporous Materials* **2022**, *330*, 111577.

(332) Yu, Y.; Qiu, H.; Wu, X.; Li, H.; Li, Y.; Sakamoto, Y.; Inoue, Y.; Sakamoto, K.; Terasaki, O.; Che, S. Synthesis and characterization of silica nanotubes with radially oriented mesopores. *Advanced Functional Materials* **2008**, *18*, 541–550.

(333) Olson, N. S.; Hurwitz, F. I.; Guo, H.; Madden, N. J.; Stokes, J. L.; Rogers, R. B.; Krogstad, J. A. Enhanced thermal stability of high yttria concentration YSZ aerogels. *Journal of the American Ceramic Society* **2021**, *104*, 4190–4202.

(334) Rabiei, M.; Palevicius, A.; Monshi, A.; Nasiri, S.; Vilkauskas, A.; Janusas, G. Comparing methods for calculating nano crystal size of natural hydroxyapatite using X-ray diffraction. *Nanomaterials* **2020**, *10*, 1–21.

(335) Huang, S.; Wu, X.; Li, Z.; Shi, L.; Zhang, Y.; Liu, Q. Rapid synthesis and characterization of monolithic ambient pressure dried MTMS aerogels in pure water. *Journal of Porous Materials* **2020**, *27*, 1241–1251.

(336) Li, W.; Han, Y. C.; Zhang, J. L.; Wang, L. X.; Song, J. Thermodynamic modeling of CTAB aggregation in water-ethanol mixed solvents. *Colloid Journal* **2006**, *68*, 304–310.

(337) Das, N. C.; Cao, H.; Kaiser, H.; Warren, G. T.; Gladden, J. R.; Sokol, P. E. Shape and size of highly concentrated micelles in CTAB/NaSal solutions by small angle neutron scattering (SANS). *Langmuir* **2012**, *28*, 11962–11968.

(338) Patel, V.; Dharaiya, N.; Ray, D.; Aswal, V. K.; Bahadur, P. pH controlled size/shape in CTAB micelles with solubilized polar additives: A viscometry, scattering and spectral evaluation. *Colloids and Surfaces A: Physicochemical and Engineering Aspects* **2014**, *455*, 67–75.

(339) Witz, G.; Shklover, V.; Steurer, W.; Bachegowda, S.; Bossmann, H. P. Phase evolution in yttria-stabilized zirconia thermal barrier coatings studied by rietveld refinement of X-ray powder diffraction patterns. *Journal of the American Ceramic Society* **2007**, *90*, 2935–2940.

(340) Rubingh, D. N.; Holland, P. M. In *Cationic Surfactants: Physical Chemistry*, 1st ed.; Rubingh, D. N., Holland, P. M., Eds.; M. Dekker: New York, New York, 1991; p 527.

(341) Kurahashi, M.; Kanamori, K.; Takeda, K.; Kaji, H.; Nakanishi, K. Role of block copolymer surfactant on the pore formation in methylsilsesquioxane aerogel systems. *RSC Advances* **2012**, *2*, 7166–7173.

(342) Baccile, N.; Laurent, G.; Bonhomme, C.; Innocenzi, P.; Babonneau, F. Solid-state NMR characterization of the surfactant-silica interface in templated silicas: Acidic versus basic conditions. *Chemistry of Materials* **2007**, *19*, 1343–1354.

(343) Yu, Y.; Du, F. P.; Yu, J. C.; Zhuang, Y. Y.; Wong, P. K. One-dimensional shape-controlled preparation of porous Cu2O nano-whiskers by using CTAB as a template. *Journal of Solid State Chemistry* **2004**, *177*, 4640–4647.

(344) Huo, W.-L.; Zhang, X.-Y.; Chen, Y.-G.; Lu, Y.-J.; Liu, W.-T.; Xi, X.-Q.; Wang, Y.-L.; Xu, J.; Yang, J.-L. Highly Porous Zirconia Ceramic Foams with Low Thermal Conductivity from Particle-Stabilized Foams. *Journal of the American Ceramic Society* **2016**, *99*, 3512–3515.

(345) Marcolongo, J. P.; Mirenda, M. Thermodynamics of Sodium Dodecyl Sulfate (SDS) Micellization: An Undergraduate Laboratory Experiment. *Journal of Chemical Education* **2011**, *88*, 629–633.

(346) Mukerjee,; Pasupati,; Mysels,; Karol, *Critical micelle concentrations of aqueous surfactant systems*; 1971; pp 1–222.

(347) Thanitwatthanasak, S.; Sagis, L. M.; Chitprasert, P. Pluronic F127/Pluronic P123/vitamin E TPGS mixed micelles for oral delivery of mangiferin and quercetin: Mixture-design optimization, micellization, and solubilization behavior. *Journal of Molecular Liquids* **2019**, *274*, 223–238.

(348) Zhao, D.; Feng, J.; Huo, Q.; Melosh, N.; Fredrickson, G.; Chmelka, B.; Stucky, G. Triblock Copolymer Syntheses of Mesoporous Silica With Periodic 50 to 300 Angstrom Pores. *Science (New York, N.Y.)* **1998**, *279*, 548–52.

(349) Sarawade, P. B.; Shao, G. N.; Quang, D. V.; Kim, H. T. Effect of various structure directing agents on the physicochemical properties of the silica aerogels prepared at an ambient pressure. *Applied Surface Science* **2013**, *287*, 84–90.

(350) Cao, S.; Yao, N.; Yeung, K. Synthesis of freestanding silica and titania-silica aerogels with ordered and disordered mesopores. *Journal of Sol-Gel Science and Technology* **2008**, *46*, 323–333.

(351) He, Z.; Alexandridis, P. Micellization Thermodynamics of Pluronic P123 (EO20PO70EO20) Amphiphilic Block Copolymer in Aqueous Ethylammonium Nitrate (EAN) Solutions. *Polymers* **2017**, *10*, 32.

(352) Hatakeyama-Sato, K.; Umeki, M.; Adachi, H.; Kuwata, N.; Hasegawa, G.; Oyaizu, K. Exploration of organic superionic glassy conductors by process and materials informatics with lossless graph database. *npj Computational Materials* **2022**, *8*.

(353) Hodler, A. E. *White paper: Artificial intelligence & graph technology: Enhancing AI with context & connections*; 2021.

(354) Hodler, A. E. *Artificial intelligence & graph technology: Enhancing AI with context & connections [White Paper]*; 2020; p 11.

(355) Kistler, S. S. Coherent expanded aerogels and jellies. *Nature* **1931**, *127*, 741–741.

(356) Chang, C.-W.; Borne, I.; Lawler, R. M.; Yu, Z.; Jang, S. S.; Lively, R. P.; Sholl, D. S. Accelerating solvent selection for type II porous liquids. *Journal of the American Chemical Society* **2022**, *144*, 4071–4079, PMID: 35170940.

(357) Nie, X.; Kulkarni, A.; Sholl, D. S. Computational prediction of metal organic frameworks suitable for molecular infiltration as a route to development of conductive materials. *The Journal of Physical Chemistry Letters* **2015**, *6*, 1586–1591, PMID: 26263318.

(358) Fang, H.; Kamakoti, P.; Zang, J.; Cundy, S.; Paur, C.; Ravikovitch, P. I.; Sholl, D. S. Prediction of CO2 adsorption properties in zeolites using force fields derived from periodic dispersion-corrected DFT calculations. *The Journal of Physical Chemistry C* **2012**, *116*, 10692–10701.

(359) Demir, H.; Greathouse, J. A.; Staiger, C. L.; Perry IV, J. J.; Allendorf, M. D.; Sholl, D. S. DFT-based force field development for noble gas adsorption in metal organic frameworks. *Journal of Materials Chemistry A* **2015**, *3*, 23539–23548.

(360) Keras: The Python Deep Learning API, https://keras.io/. `https://keras.io/`.

(361) Open-Source Cheminformatics Software, http://www.rdkit.org/. `http://www.rdkit.org/`.

(362) sklearn.preprocessing.OneHotEncoder. `https://scikit-learn.org/stable/modules/generated/sklearn.preprocessing.OneHotEncoder.html`.

(363) Zhang, D.; Dutzer, M. R.; Liang, T.; Fonseca, A. F.; Wu, Y.; Walton, K. S.; Sholl, D. S.; Farmahini, A. H.; Bhatia, S. K.; Sinnott, S. B. Computational investigation on CO2 adsorption in titanium carbide-derived carbons with residual titanium. *Carbon* **2017**, *111*, 741–751.

(364) Kojima, S.; Park, J.; Carter, E. A.; Walton, K. S.; Realff, M. J.; Sholl, D. S.; Yajima, T.; Fujiki, J.; Kawajiri, Y. Discrepancy quantification between experimental and simulated data of CO2 adsorption isotherm using hierarchical bayesian estimation. *Separation and Purification Technology* **2022**, *296*, 121371.

(365) Han, R.; Walton, K. S.; Sholl, D. S. Does chemical engineering research have a reproducibility problem? *Annual Review of Chemical and Biomolecular Engineering* **2019**, *10*, 43–57, PMID: 30916992.

(366) Bingel, L. W.; Walton, K. S.; Sholl, D. S. Experimentally verified alkane adsorption isotherms in nanoporous materials from literature meta-analysis. *Journal of Chemical & Engineering Data* **2022**, *67*, 1757–1764.

(367) Park, J.; Howe, J. D.; Sholl, D. S. How reproducible are isotherm measurements in metal–organic frameworks? *Chemistry of Materials* **2017**, *29*, 10487–10495.

(368) Bingel, L. W.; Chen, A.; Agrawal, M.; Sholl, D. S. Experimentally verified alcohol adsorption isotherms in nanoporous materials from literature meta-analysis. *Journal of Chemical & Engineering Data* **2020**, *65*, 4970–4979.

(369) Agrawal, M.; Han, R.; Herath, D.; Sholl, D. S. Does repeat synthesis in materials chemistry obey a power law? *Proceedings of the National Academy of Sciences* **2020**, *117*, 877–882.

(370) Osterrieth, J. W. M. et al. How reproducible are surface areas calculated from the BET equation? *Advanced Materials* **2022**, *34*, 2201502.

(371) Aegerter, M.; Leventis, N.; Koebel, M. *Aerogels Handbook*; Springer New York, 2011.

Appendix I: Vita

Rebecca Catherine Walker

Education

Graduate

Virginia Commonwealth University (VCU), Richmond, VA — Graduation: December 16th, 2022
Doctor of Philosophy in Chemical and Life Science Engineering — Cumulative GPA: 4.00
Thesis: *Understanding Structure/Process-Property Relationships to Optimize Development Lifecycle in Yttria-Stabilized Zirconia Aerogels for Thermal Management*

Undergraduate

Virginia Commonwealth University (VCU), Richmond, VA — Graduation: May 19th, 2018
Bachelor of Science in Chemical and Life Science Engineering — Concentration: Chemical Engineering
Bachelor of Science in Chemistry — Concentration: Chemical Science
Minor: Mathematics — Cumulative GPA: 4.00

Relevant Experience

NASA AS&ASTAR Fellowship Graduate Researcher *Fall 2018 – Fall 2022*

- Apply information architecture to understand aerogel structure/process-property relationships
- Assess these relationships experimentally through surfactant templating of inorganic aerogels
- Research for 10 weeks each summer at NASA Glenn Research Center in Cleveland, OH
    - ***2022:*** Advancement of proficiency in aerogel synthesis and materials characterization
    - ***2020 & 2021 (Virtual):*** Development of aerogel information architecture
    - ***2019:*** Investigation of chemistries for aerogel synthesis with materials characterization

Interfacial Systems Lab Graduate Researcher, PI: Dr. James Ferri, VCU *Fall 2018 – Fall 2022*

- Formulation of polymer microcapsules used in continuous flow applications
- Surfactant optimization via wetting behavior and surface tension analysis
- Collaboration with other VCU Engineering & Chemistry research labs

Ferri Lab Manager, PI: Dr. James Ferri, VCU *Fall 2019 – Spring 2022*

- Responsible for maintaining compliance of lab safety standards & protocols for lab group of graduate and undergraduate students
- Mentorship & training of undergraduate & graduate student researchers

Polymer Nanomaterials Lab Research Assistant, PI: Dr. Christina Tang, VCU *Spring 2016 - Fall 2018*

- Formulated the self-assembly of dye-loaded polymer nanoparticles
- Electrospun polymer nanofibers, well-suited for producing fibers of large and complex molecules without using high temperatures; Application: Drug Delivery Systems

Teaching Assistant, Algebra & Process Control in Chemical Engineering, VCU *Fall 2015 & Fall 2018*

- Duties included giving a lesson on simulating control systems (Process Control), holding office hours, and grading quizzes, exams, and homework assignments

VCU Senior Design Capstone, Sponsored by ChemTreat & Afton Chemical *Fall 2017 - Spring 2018*

- Employed ChemTreat dual heat-sensitive dye technology to determine the presence of hot spots in gasoline and/or diesel engines
- Worked on a team with other Chemical Engineering seniors and reported to advisors from VCU, ChemTreat, and Afton Chemical

DuPont Power Engineering Intern, Spruance Plant, Richmond, VA *Summer 2017*

- Improved & drafted laboratory procedures used for water treatment
- Modeled filter plant pipe system flow using AFT Fathom software

Honors & Awards

NASA AS&ASTAR (Aeronautics Scholarship & Advanced STEM Training and Research) Fellowship
VCU Scholarships (75% of tuition covered): VCU Dean's Scholarship and Goodwin Endowed Scholarship
Dean's List (Fall 2014, Spring 2015, Fall 2015, Spring 2016, Fall 2016, Spring 2017, Fall 2017, Spring 2018)
Academic Achievement Award, Department of Chemical Engineering, Spring 2018, VCU
Member of Tau Beta Pi, Engineering Honor Society, Inducted Fall 2017, VCU

Skills & Certifications

Lab Techniques: Aerogel Synthesis & Supercritical Drying, Polymer Nanoparticle Self-Assembly, Electrospinning Polymer Nanofibers, Scanning Electron Microscopy (SEM), Chemisorption (BET Method), X-ray Diffraction (XRD), Dynamic Light Scattering (DLS), Gas Chromatography, Spectroscopy (UV-Vis, IR, NMR, Fluorescence), Surface Tension Analysis (Sinterface)
Software: Neo4j, Python, MATLAB, Excel Visual Basic for Applications, MS Excel, LaTeX, R Statistics, JMP

Relevant Courses (as of Spring 2021)

● Intro to Chemical Engineering ● Intro to Programming ● Material Balances ● Energy Balances
● Thermodynamics of Phase Equilibria ● Transport Phenomena I & II ● Chemical Reaction Engineering
● Instrumentation Laboratory ● Unit Operations Laboratory ● Process Control ● Inorganic Chemistry I
● Organic Chemistry with Lab I & II ● Quantitative Analysis with Lab ● Physical Chemistry I & II with Lab
● Graduate Quantitative Analysis ● Graduate Equilibrium Analysis ● Graduate Non-Equilibrium Analysis
● Graduate Chemical Reaction Engineering ● Interfacial Phenomena ● Advanced Topics in Soft Materials
● Complex Chemical Systems Engineering ● Nanoscale Physics ● Advanced Materials Characterization
● Advanced Materials Processing ● Effective Technical Writing

Professional Memberships

American Institute of Chemical Engineers (AIChE), American Society for Gravitational & Space Research (ASGSR), The American Ceramic Society (ACerS), Tau Beta Pi (Engineering Honor Society)

Publications

9. Walker, R. C., Stokes, J. L., Hurwitz, F. I., Guo, H., and Ferri, J. K. (2022) Optimizing surfactant templating of yttria-stabilized zirconia aerogels for high-temperature applications: Effect of cationic surfactant. *Microporous and Mesoporous Materials* doi: 10.1016/j.micromeso.2021.111577
8. Walker, R. C., Potochniak, A. E., Hyer, A. P., and Ferri, J. K. (2021) Zirconia aerogels for thermal management: Review of synthesis, processing, and properties information architecture. *Advances in Colloid and Interface Science* doi: 10.1016/j.cis.2021.102464.
7. Walker, R. C., Hyer, A. P., and Ferri, J. K. (*Under Review*, 2022) Silica aerogel synthesis/process-property predictions by machine learning.
6. Walker, R. C., Penzer, K. E., Stokes, J. L., Hurwitz, F. I., Guo, H., and Ferri, J. K. (*Under Review*, 2022) Optimizing surfactant templating of yttria-stabilized zirconia aerogels: Effect of anionic & nonionic surfactant.
5. Walker, R. C., and Ferri, J. K. (*In preparation*, 2022) Aerogel design principles.
4. Casey, A. H., Walker, R. C., Triplett, G. E. (2021) Microfluidic reaction modeling for evaluating mass transfer of enzymes. Proc. SPIE 11663, *Integrated Sensors for Biological and Neural Sensing*, doi: 10.1117/12.2575999
3. Smith, R. A., Walker, R. C., Levit, S. L., & Tang, C. (2019). Single-Step Self-Assembly and Physical Crosslinking of PEGylated Chitosan Nanoparticles by Tannic Acid. *Polymers, 11*(5), 749. doi: 10.3390/polym11050749
2. Levit, S. L., Walker, R. C., Pham, A. L., & Tang, C. (2019). 3. Polymer-free electrospinning. In N. Horzum, M. Demir, & R. Muñoz-Espí (Eds.), *Green Electrospinning* (pp. 41–68). doi: 10.1515/9783110581393-003
1. Levit, S. L., Walker, R. C., & Tang, C. (2019). Rapid, Single-Step Protein Encapsulation via Flash NanoPrecipitation. *Polymers, 11*(9), 1406. doi: 10.3390/polym11091406

Conferences

Materials Science & Technology Technical Meeting, Oral Presentation, Pittsburgh PA, Fall 2022
Australian Colloid and Surface Science Student Conference, Virtual Presentation, Spring 2022
International Conference and Expo on Advanced Ceramics and Composites, Virtual Presentation, Spring 2021 & Spring 2022
The Adhesion Society Annual Meeting, Oral Presentation, Charleston SC, Spring 2020
American Society for Gravitational and Space Research Meeting, Oral Presentation, Denver CO, Fall 2019
American Institute for Chemical Engineers Student Regional, Poster Session, Princeton NJ, Spring 2018

Leadership & Volunteer Experience

Engineering Graduate Student Association, Co-President, VCU	*2021 - 2022*
Society of Women Engineers (SWE) Mentorship Program, VCU	*2020 - 2022*
Grade Appeal Committee, Graduate Student Member, VCU Engineering	*2020 - 2021*
Engineering Graduate Student Association, Secretary, VCU	*2019 - 2021*
Chemical Engineering Advisory Board, Alumni & Student Member, VCU	*2019 - Present*
Student Outreach Volunteer, VCU Engineering	*2018 - 2022*
Promotion & Tenure Committee, Student Member, VCU Engineering	*2018*
Chemical Engineering Mentorship Program, VCU	*2016 – 2018*
Preschool Sunday School Teacher, Harvest Christian Fellowship	*2017 - Present*
That Dance Thing, Ballroom Dance Teacher and Member of Leadership Team	*2013 - 2018*
Summer Mission Trips to Minsk, Belarus	*2014 & 2015*